INFORMATION TO USERS

This manuscript has been reproduced from the microfilm master. UMI films the text directly from the original or copy submitted. Thus, some thesis and dissertation copies are in typewriter face, while others may be from any type of computer printer.

The quality of this reproduction is dependent upon the quality of the copy submitted. Broken or indistinct print, colored or poor quality illustrations and photographs, print bleedthrough, substandard margins, and improper alignment can adversely affect reproduction.

In the unlikely event that the author did not send UMI a complete manuscript and there are missing pages, these will be noted. Also, if unauthorized copyright material had to be removed, a note will indicate the deletion.

Oversize materials (e.g., maps, drawings, charts) are reproduced by sectioning the original, beginning at the upper left-hand corner and continuing from left to right in equal sections with small overlaps.

Photographs included in the original manuscript have been reproduced xerographically in this copy. Higher quality 6" x 9" black and white photographic prints are available for any photographs or illustrations appearing in this copy for an additional charge. Contact UMI directly to order.

Bell & Howell Information and Learning
300 North Zeeb Road, Ann Arbor, MI 48106-1346 USA

UMI®
800-521-0600

A Generalized Approach for Mechanics of Chip Formation in Steady-State and Dynamic Orthogonal Metal Cutting Using a New Model of Shear Zone With Parallel Boundaries and Its Validation to Cutting-Forces Prediction in Self-Piloting Machining

Mohammed Hayajneh

A Thesis

in

The Department

of

Mechanical Engineering

Presented in Partial Fulfillment of the Requirements for the Degree of Doctor of Philosophy

at

Concordia University

Montreal, Quebec, Canada

August, 1998

ABSTRACT

A Generalized Approach for Mechanics of Chip Formation in Steady-State and Dynamic Orthogonal Metal Cutting Using a New Model of Shear Zone With Parallel Boundaries and Its Validation to Cutting-Forces Prediction in Self-Piloting Machining

Mohammed Hayajneh, Ph.D.
Concordia University, 1998

This study presents a novel approach to the mechanics of chip formation based on a shear zone model with parallel boundaries that has been developed by applying the continuum mechanics to the analysis of the chip formation process. Such a model is formulated without imposing the assumptions commonly made in the single shear or parallel-sided shear zone models.

A steady-state cutting force model has been derived and adapted to orthogonal cutting of a self-piloting drilling. In the formulated model, special attention has been devoted to the thermomechanical state which defines the effect of the temperature on the yield shear stress of the work piece material.

The proposed steady state cutting force model has been extended to formulate a cutting force model to analyze the dynamic behavior of the machining process in orthogonal cutting. The cutting system was modeled using a single degree-of freedom dynamic system where the variations of the cutting forces are represented by their total differentials.

Special attention in this study has been dedicated to experimental verification. The meaningful design, accuracy, precision, and the calibration of the experimental setups are considered in details and several new experimental methodologies are proposed and used.

This study shows the fluctuation of the cutting forces is a result of chip segmentation and not the cause. It also shows the effect of materials and cutting conditions on the cutting signatures that has never been considered as a factor in the known studies on cutting dynamics.

Special attention has been devoted to the chip morphology of the partially and fully deformed chips to verify the proposed model. A quick stop device has been designed to obtain samples of partially formed chip

A new methodology has been proposed to align the machine such that the misalignment between the tool and the workpiece is near zero to make sure that the measured forces are not affected by any other sources. A low cost laser-camera based system has been built to achieve this goal.

To the Memory of My Father

ACKNOWLEDGMENTS

The author would like to express appreciation and gratitude to his technical supervisors, Dr. M. O. M. Osman, Dr. V. Astakhov and Dr. V. Latinovic, who were extremely helpful during the course of this research work. Professor V. Astakhov's efforts were instrumental in the realization of this work. His vision played an important role in this work.

The financial support of the Canadian International Development Agency (CIDA) and the Natural Sciences and Engineering Research Council(NSERC) is gratefully acknowledged.

Special thanks to Dr. Akif Bulgak, the director of the Canadian International Development Agency /Jordan University of Science and Technology/Concordia University (CIDA) project in Canada, and to Mrs. Marie Berryman, the coordinator of the project, who were extremely helpful throughout all stages required for this work.

I would also like to gratefully acknowledge the use of the laboratory facilities of the deep hole machining center, machine tool lab, metallurgy lab, Concordia computer aided vehicle engineering center (CONCAVE), computer-integrated manufacturing (CIM) lab and NC-machining center at Concordia University and metallurgy lab at McGill University.

I am grateful to my mother who is anxiously awaiting the completion of this thesis. I am also grateful to my brothers and sisters for their support during my study.

The most sincere gratitude is to my wife, Manar Bani-Hani, for her caring, encouragement and patience throughout the entirety of this work Without her, it would be impossible to complete this work. I am indebted to my son, Anas, who was born through the course of the research work and I feel guilty because I could not spend enough time with him.

TABLE OF CONTENT

LIST OF FIGURES

CHAPTER 2

CHAPTER 3

CHAPTER 4

CHAPTER 5

CHAPTER 6

CHAPTER 7

CHAPTER 8

CHAPTER 9

LIST OF TABLES

NOMENCLATURE

A	constant
A_s	area of the shear plane
A_α	tool face, i.e., the surface over which the chip flows
a	constant
a	mean uncut chip thickness
a_1	mean cut chip thickness
B	material constant
b	Burgers vector magnitude (*cm*)
b	width of the machined surface; uncut chip width
b_1	chip width
C	machining constant
$C_o(v)$	speed-dependent coefficient which can best be determined from test data
$C_1(v)$ s	speed-dependent coefficient which can best be determined from test data
c_p	specific heat capacity
c_o	distance *OA* (model of chip formation zone with parallel boundaries)
c_v	specific heat capacity at constant volume
E	Young's Modules
F_n	normal force at the tool-chip interface
F_f	frictional force at the tool-chip interface
F_c	force in the cutting direction,
F_t	force normal to the cutting direction
F_s	shear force along the shear plane
F_{ns}	force normal to the shear plane
F_p	plowing force
F_y, F_{yi}	mean tangential force and dynamic tangential force

F_c, F_{ci}	mean cutting force and dynamic cutting force
F_s, F_{si}	mean shear force and dynamic shear force
F_f, F_{fi}	mean friction force and dynamic friction force
f	frequency
$f(.)$	An Arrhenius type function of the temperature.
G	shear modules
H	the intensity of angular deformation
h	shear zone width
h_o	distance OB (model of chip formation zone with parallel boundaries)
J	mechanical equivalent of heat
K	slope of τ_{xAB} vs. σ diagram which can be experimentally determined for each particular material
k	thermal conductivity of the work material
k_1	shear stress in the tool-chip interface zone
l_{ef}	effective length the tool-chip interface
l_c	length of chip
l_f	contact length between the chip and tool
l_p	length of cut
l_s	length of the shear plane
l_{st}	length of the sticking friction region
m	slope of the stress-strain curve
n	parameter characterizing the non-uniform distribution of the tangential velocity in the shear zone.
P	total power consumed in the cutting process
R	resultant tool force
R'	resultant force acting on the chip-tool interface region
r_c	chip thickness ratio or cutting ratio (t/t_1) always < 1
s	feed
s_1, s_2	distances measured along the sliplines.

T	temperature
T_c	average temperature rise of the chip
T_s	temperature rise of material passing through the primary deformation zone
T_o	initial work piece temperature
T_s	temperature in the primary deformation zone
T_f	temperature in the tool-chip interface zone
t	undeformed chip thickness; i.e., the thickness of the layer of material being removed by one cutting edge at the selected point measured normal to the resultant cutting direction
t_1	deformed chip thickness, i.e., the thickness of the chip produced during machining
t_i	dynamic uncut chip thickness
$u_x(y)$	displacement reached y
u^*_x	maximum of the function within the deformation zone.
v	cutting speed i.e., the instantaneous velocity of the primary motion of the selected point on the cutting edge relative to the work piece
v_A, v_B	tangent to the mutual perpendicular sliplines A and B
v_n	normal velocity to the shear plane
v_s	shear velocity
v_x	velocity in x- direction
v_y	velocity in y- direction
v_1	velocity of chip flow
$v_{1\tau}$	component of the chip velocity with respect to the shear zone
v_i	dynamic cutting speed
v_2	the discontinuity of the tangential velocity with respect to the shear zone
v_τ	component of the work piece velocity with respect to the shear zone
$x_1, \dot{x}_1$	displacement of the tool tip and oscillation velocity of the tool tip

$x_2, \dot{x}_2$	displacement at the surface end of the shear zone and oscillation velocity at the surface end of the shear plane
y^*	the value of y at which $u_x(y)$ has the maximum
α, α_i	nominal rake angle of the tool and dynamic rake angle of the tool
β	clearance angle
Γ	proportion of heat in the primary deformation zone
γ	shear strain
$\dot{\gamma}$	shear strain rate
γ_f	final shear strain along the end of the deformation zone
γ_{fa}	failure shear strain
γ_n	helical angle
γ_{EF}	shear strain along EF
Δs_2	thickness of the parallel-sided shear zone
ζ, ζ_i	dynamic compression ratio
ζ_t	chip compression ratio calculated using the length of the chip
θ	angle between resultant cutting force R and the shear plane
λ	mean angle of friction on tool face tool cutting edge inclination
μ	coefficient of friction
ρ	density of work material
σ_{ult}	ultimate tensile stress of work piece material
σ_A	mean compressive stress at A
σ_B	mean compressive stress at B
σ_f	normal stress on the tool face
σ_n	normal stress on the shear plane
σ_y	uniaxial dynamic yield stress
τ_f	shear flow stress on the tool face in sticking region
τ_o	yield shear strength of the work material or shear stress on the shear plane with zero normal stress applied
τ_s	shear stress on shear plane

τ_{sAB}	shear flow stress along *AB*
τ_{sOA}	shear stresses on *OA*
τ_{sOB}	shear stresses on *OB*
τ_{sOD}	shear stresses on *OD*
τ_{sEF}	shear stress along *EF*
τ_{sCD}	shear stresses along *CD*.
φ, φ_i	mean shear angle and dynamic shear angle
φ_p	principal cutting edge
Ω	rotational speed of the work piece
ε	uniaxial (effective) strain
$\dot{\varepsilon}$	uniaxial (effective) strain rate
γ	strain in the shear zone
ω_1	frequency of the tool variation
ω_2	frequency of the work surface slope variation

1

INTRODUCTION

The ultimate objective of the science of metal cutting is the solution of practical problems associated with the efficient and precise removal of metal from workpieces. A properly founded solution of these problems is possible only when the laws governing the cutting process are known. A knowledge of these laws makes it possible to foresee the practical results of the cutting process, and thus to select the optimum cutting conditions for each particular case. Since the knowledge exists in a form of theory, the theory of metal cutting should be advanced.

A vast effort has been dedicated in the past research to develop a suitable theory of metal cutting. But instead of developing predictive theories, which enable prediction of cutting performance such as chip formation, cutting force, tool wear, and surface integrity, theories of descriptive, post-processing nature took over.

Over the last hundred years an extensive study on the machining of metals has been carried out. Most of this focused on the down-to-earth reduction of machining costs and pragmatic approach to the manufacture of parts of acceptable dimensional accuracy and surface quality. Unfortunately, a much smaller volume of research has been devoted to formulating the fundamental mechanisms underlying metal machining process in general, as opposed to seeking case solutions for particular machining problems. The real boom in fundamental metal cutting research, in the 60's, has brought to the field both the recognition of the need for an applicable metal cutting theory as well as the reputation of being extremely complex. Since then the practice of metal cutting has been advanced by costly ways of trial and error while the fundamental research has experienced a slow down after producing huge amounts of data that match the practical results only occasionally.

The modern history of metal cutting began in 1945 when Merchant published his vision of the metal cutting phenomena (Merchant, 1945). As demonstrated by an excellent survey presented by the CIRP working group on chip control (Jawahir and van Luttervelt, 1993), numerous attempts to improve the theory proposed by Merchant failed to improve its predictive ability. As a result, no significant progress has been made and, after 30 years, the theory is still lagging behind the practice. Shaw in his book (1984) summarizes his lifetime experience in the field and concludes that it is next to impossible to predict metal cutting

performance.

Presently industry relies completely upon the empirical data as these are presented by tool and machine tool manufacturers, as well as by professional engineering associations, through handbooks and seminars. Since these recommendations do not result from a common theory behind them, they provide only a good "starting point" thus leaving to the users that, at their own cost, find out the optimal values of cutting parameters for each and every particular case they may encounter. And, for an outside observer with the obscure knowledge in the field, it may appear that the industry is doing very well this way.

At this point one may ask a logical question: "At the present stage of development, do we really need a realistic metal cutting theory?". The answer to this question is given in the recent CIRP working paper (Armarego et al, 1996), the quote of which is as follows: "*A recent survey by a leading tool manufacturer indicates that in the USA the correct cutting tool is selected less than 50% of the time, the tool is used at the rated cutting speed only 58% of the time, and only 38% of the tools are used up to their full tool-life capability. One of the reasons for this poor performance is the lack of the predictive models for machining*" The same has been found in an earlier survey of cutting regime selection on CNC machine tools in the American aircraft industry (Amarego, 1996) showing that selected speeds are far below the optimal economic speeds.

The present study aims to re-evaluate the present models of chip formation (which are in the very cores of the metal cutting theories) in hope to propose a better model of chip formation for steady-state machining.

This work may be thought of as consisting of two logical general parts; theoretical

and experimental parts. The theoretical part comprise the proposed model, an analytical evaluation of the steady-state force model and dynamic force model for wave removing process. The second part concerns with the validating of the proposed model experimentally and comparison of the obtained results with the theoretical values. It includes developing a new experimental methodologies, designing the proper experiment setups and providing the required apparatuses.

The model for steady-state cutting is based on a new velocity diagram proposed by Astakhov and Osman (1996) and Hayajneh et al (1996) contrary to all the present studies on metal cutting which use the Mercant's velocity diagram. It is shown that the use of the Merchant velocity diagram leads to the model of chip formation which is in obvious contradiction with the mathematical theory of plasticity. According to this diagram, the velocity of shearing exceeds the velocity of applied load when a tool with a negative rake angle is used that is in contrary with the principle of mass continuity condition. Using the proposed velocity diagram and the slip-line theory, a new model for chip formation is formulated. A new model to calculate the cutting forces is also proposed. Since cutting experiment is curried out on a deep-hole machine, the model was extended to be applicable for deep-hole drills.

The model for wave-removing process utilizes the basics of the model for steady-state cutting and is used to evaluate the dynamic cutting forces in orthogonal cutting. The cutting system was modeled using a single degree-of freedom dynamic system where the variation of the cutting forces are represented by their total differentials. The influence of temperature on the flow shear stress of workpiece material is accounted

Since cutting experiments are curried out to validate the theory, a special attention was paid to the experimental methodology which includes the conditions of the experiment, the characteristics of the setup used, the cutting regime, etc. It is clear that a slight change in the experimental conditions may lead to a significant error in the obtained results, which, in turn, may lead to wrong conclusion about the validity of the theory.

Among many important characteristics of the experimental setup, the accuracy of the relative position and motion of the tool and the workpiece was of prime concern since it affects the results dramatically. Unfortunately, this parameter has not been reported in the known experimental studies on metal cutting. In the present study, therefore, a special attention was paid to show significance of this accuracy. Since the cutting experiments have been curried out using deep-hole machine, a new method for inspecting machine accuracy has been proposed. It is shown that for deep-hole machines, the misalignment between the tool and workpiece defines the above-mentioned accuracy. The effect of any misalignment on the cutting process has been verified.

Cutting force measurement is an integral part of experimental studies in metal cutting. In the present study two types of such measurement have been carried out:

- measuring the steady-state component of cutting force
- measuring the dynamic component of cutting force.

Metallography of the formed and partially formed chip is an important part of any experimental study in metal cutting. In this work it has been maintained that this kind of experiment makes sense if and only if:

- The initial structure of workpiece material is reported.

- The chip structure is considered at the macro- and micro levels to study, depending on the phenomenon to be investigated, because each phenomenon can be observed at a certain magnification level and requires different preparation techniques of the specimen.
- The structures of the chip and deformation zone are compared with those predicted theoretically to validate the theory used in the analysis.
- A microhardness survey is performed on the structure to reconstruct the distribution of stress and strain undergone by different regions of the chip and deformation zone at the last stage of deformation. The results obtained are compared then with those yielded by the theory.

Unfortunately, the present metallographical studies in metal cutting (as in, Trent, 1991) do not even mentioned these conditions. The present work aims at filling in this gap by proposing a detailed methodology of metallographic experiments in metal cutting.

The objective of this thesis are:

1. Formulation of a new model of chip formation which is not restricted by the most assumptions commonly made to build the single shear plane, flow region and parallel sided shear zone models and capable of relating the cutting forces, tool-workpiece temperature to the cutting speed, feed, tool geometry and properties of the workpiece.
2. Deriving a steady-state cutting force model.
3. Extending the steady-state cutting force model to be applicable for the deep hole machining process.
4. Formulating a dynamic model based on the proposed steady-state cutting force model

to characterize the wave removing cutting process.

5. Validation of the proposed model experimentally.

To achieve this goal the following steps have been performed:

i. Establishing of a new methodology to align the machine such that the misalignment between the tool and the workpiece is near zero to make sure that the measured forces are not affected by any other effects. To test this error effect on the measured forces, the tool has been intentionally misaligned; the misalignment values have been measured using a low-cost laser-camera-based system and the forces have been measured using the Fast Fourier Transformation (FFT) Analyzer for different cutting conditions.

ii. Measurement of the steady-state cutting force components for three different materials and different cutting conditions.

iii. Validating the dynamic force model by measuring the forces for a wavy workpiece for different cutting conditions.

iv. Monitoring and analyzing the chip formation by recoding the cutting force signature using the FFT.

v. Studying the morphology of the formed chip by measuring its structure and micro hardness.

vi. Designing a quick stop device to freeze the process of chip formation and then observing the structure of the partially formed chip.

The outline of the chapters is as follows :

In chapter 2, the literature related to the mechanics of chip formation, chip

morphology, measuring of the cutting forces methodologies ,dynamics of the cutting process, and deep hole machining process is reviewed. It concludes with the objectives of the research.

Chapter 3 presents the mechanics of chip formation using a shear zone model with parallel boundaries. This model has been developed by applying the mechanics of continua to the analysis of the chip formation zone. It concerns with the following aspects -a) analysis the principle of mass conservation in the shear zone in terms of plane slip-line field theory, b) derivation of the equations for velocities and displacements in the defined shear zone and formulation of a new velocity diagram by applying the mechanics of continue, c) examination of the strain and strain rate distribution in the chip forming zone according to the new velocity diagram, d) Studying the deformation process and exploring the texture of the chip formed during orthogonal cutting and e) applying a themomechanical approach to predict the shear stress in the shear zone. According to this model, the shear yield stress is temperature-dependent and decreases at a certain rate with temperature increase. The approach generalizes the effect of temperature on the shear yield stress in the shear zone.

In chapter 4 an analytical formulation of the steady-state cutting force model has been done using the shear zone model with parallel boundaries and the thermomechanical approach. This model was extended to be applicable to deep-hole machining.

Chapter 5 presents formulation of a dynamics cutting force model based on the proposed steady-state cutting force model and characterization o the wave removing process.

Chapter 6 presents a methodology and specially designed setup for the machine misalignment assurance. Also, a new calibration procedure is proposed and discussed.

Chapter 7 presents description of the materials, cutting tools, workpieces, equipments, experimental setups, calibration and analysis procedures used in the experiments of the cutting force and the cutting signature recording.

Chapter 8 presents the procedure of studying the chip morphology. It describe the implementation of the quick stop device which is designed to obtain samples of partially formed chip; then the specimens preparation stages for the metallographic and microhardness tests are detailed. Finally, the microhardness procedure is presented.

Chapter 9 presents the major results. It is showing the effect of misalignment on the steady axial cutting force and torque as well as on the autospectra of the dynamic axial cutting force and torque. It proceeds with a comparison of the experimental and theoretical results of steady-state force in deep hole machining for different cutting tool geometries, workpiece materials and cutting regimes. The simulation results using the dynamic force model for wave removing process are compared with the experimental results. Then, the dynamic axial cutting force and torque signatures are presented. The chapter ends with results of the morphology study.

Chapter 10 contains the conclusions and the recommendations for future work.

2

LITERATURE REVIEW

The references related to the mechanics of chip formation, chip morphology, cutting forces measurement, dynamics of the cutting process, and deep hole machining process are reviewed in this chapter. The reviewed literature is somewhat broad in context, but focused primarily on five main topics :

- The models which deal with the mechanics of chip formation and study of the deformation zones in metal cutting (primary deformation zone and secondary deformation zone).

- The models which deal with the thermomechanical behavior of workpiece material in cutting ,i.e. with the flow shear stress in the primary and secondary deformation zones.
- The dynamics of metal cutting.
- The cutting forces measurements.
- The deep hole machining process in terms of cutting forces measurements.

2.1 MECHANICS OF CHIP FORMATION

The machining of metals has been exercised since the beginning civilization, yet, the mechanics of the process is not fully understood. Most of the development and improvement in machining procedures, until quite recently, have come from trial and error methods and empirical investigation. Machining operations are often considered to be the most important process in manufacturing, and in the last 50 years, a great deal of experimental and theoretical research has been conducted. Researchers in this field have attempted to develop theories of the cutting process which can predict important cutting parameters without the need for empirical formulation.

Metal cutting is often described as a complex process that involves friction, plastic flow and fracture of material under more extreme conditions than normally found in other production processes or in material testing. Among material deformation processes the metal cutting chip formation is unique in many ways. Perhaps the most striking aspect of the deformation is the very high strain rate as large shear strain is imposed in a small deformation zone. Another characteristic of chip formation which sets it apart from other

material processing operations is the relatively unconstrained nature of the process. The cutting tool imposes a displacement on one face of the work material while the other surfaces are free. The proportion of the free surface is large. The result of these circumstances is a peculiar deformation process in which significant heating takes places and a large change in stress state occurs over short distance.

Although a considerable amount of effort has been devoted to the analysis of the metal cutting problem in the last hundred years, the mechanics of the chip formation process is still far from clear. Jawahir and van Luttervelt (1993) presented an excellent and thorough review of numerous approaches previously taken by investigators in the field. The number of approach used so far reveals complexity of the problem of modeling chip formation. Moreover, each author attempted to change something within the shear-model in the hope to obtain a better agreement of theory with cutting experiments.

The art of metal cutting is ancient. The historical development and early published works are reviewed in detail by Ernst (1951), Finnie (1956) and DeVries (1970).

In 1851, a French investigator Cocquillent was first involved into the investigation on mechanics of cutting process. He studied various materials such as iron, brass, stone and other materials in drilling operation to find out the work required to remove given volume of material. Several other researchers in the cutting mechanics and chip formation in the past were Joessel, Tresca, and Reuleaux in France, Timme, Zvorykin and Briks in Russia, Mallock in England. Taylor in the United States- made his contribution in the area of tool wear and tool life (Armarego and Brown, 1969; Finnie, 1956).

Most of the analytical research in metal cutting have been done since the mid forty's.

Merchant (1944; 1945) assumed that a continuous type of chip is formed by a shearing process on a single plane extending from the cutting edge to the work surface ahead of the tool. This plane was termed "shear plane" and the angle it makes with the surface generated was called shear angle and designated by φ.

Lee and Shaffer (1951) applied the theory of plasticity for an ideally rigid-plastic material to the continuous chip formation. Two essential aspects of their consideration are of importance. Firstly, they considered the state of stress of the chip through which forces exerted by the tool transmitted to the shear plane. Secondly, the shear plane was considered as a line in a two-dimensional cut along which the tangential component of velocity is discontinued and this is in agreement with the mathematical theory of plasticity

Eggleston et al (1959) made extensive experimental studies on orthogonal cutting using steel, aluminum alloys and alpha-brass. They concluded that the angle between the resultant force and the shear plane is not unique for any given material.

Kobayashi et al (1960) and Kobayashi and Thomsen (1959) experimentally predicted that the shearing stress on the shear plane for steel and other alloys is approximately constant. This prediction contradicts Merchant's assumption of a variable shear stress in his modified theory.

Kececioglu (1960; 1958) studied experimentally the effects of shear size, compressive stress and shear strain on mean shear flow stress in metal cutting. He observed that the shear zone size generally decreases as the rake angle and the speed increase and as the depth of cut decreases. The compressive stress decreases as the rake angle and the depth of cut increase and as the speed of cut decreases. The shear strain decreases as the rake

angle, the depth of cut and the speed of cut increase. In his conclusions he pointed out that the strain, strain rate, size of shear zone, the normal compressive stress, temperature and the shear flow stress are functionally related.

Albrecht (1960a; 1960b) emphasized the importance of ploughing in the metal cutting process. He established an experimental method to measure the ploughing force. His analysis suggested that the ploughing process has an effect on chip curling and residual stresses in the work material.

Usui and Hoshii (1963) proposed slip-line field solution. In their analysis it was assumed that Coulomb's law for dry sliding friction does not hold.

Kudo (1965) proposed slip-line solution for two dimensional steady state machining. His solution is the same as the one proposed by Lee and Shaffer, except that the slip-lines are curved to give a curling chip.

Bitans and Brown (1965) investigated the deformation of wax work pieces for various cutting conditions. They observed a large plastic shear zone that becomes thicker at smaller rake angles. They also found that plastic flow occurs near the rake face and the clearance face of the tool.

Hsu (1966) studied the normal and shear stress distributions on the face of the cutting tool. He discussed the presence of a ploughing force in the metal cutting process and suggested that its magnitude remains constant for different depths of cut and chip-tool contact lengths. From cutting tests he calculated the average normal stress σ_m and shear stress τ_m for different contact length ratios and found that the variation of τ_m and σ_m are independent of the depth of cut.

Thomsen (1966) studied the shear zone in metal cutting. After careful examination of a large number of chip roots he concluded that it is difficult to determine the precise points at which plastic deformation starts and ceases.

Goriani and Kobayashi (1967) studied the strain and strain rate distributions in steady state orthogonal cutting of *SAE 1113-B* steel. They estimated the maximum shear strain rate to be approximately equal to 1550 per second. A mean shear strain rate of 10^3 to 10^6 per second is estimated by Shaw (1950) and of 10^4 to 10^5 per second by Kececioglu (1960). They concluded that the determination of shear zone thickness is critical in estimating the average strain rate.

Spaans (1971) measured the forces acting on a tool near the cutting edge. He noted that the existence of a built-up layer or built-up edge is an important factor concerning the magnitude of the extra forces near the cutting edge. He also developed equations to determine the shape of the streamlines in the deformation zone based on constant strain rate and flow stress in the plastic zone.

Roth and Oxley (1972) proposed a slip-line field for a strain hardening material from experimental results.

Liu and Barash (1976) studied the sub-layer of a surface generated by the chip removal process. Their study concludes that the apparent strain energy, the maximum residual stress and the maximum strain hardening index are approximately proportional to the shear plane length or indirectly proportional to the cutting ratio for a given depth of cut.

Dewhurst (1978) considered a model for the machining process where the chip emerges from the deformation zone with a significant angular velocity. One of the

conclusions from his analysis is that the machining process is not uniquely defined for any set of steady state machining conditions.

Yamamoto et al (1979) analyzed the stress distribution on the tool-chip contact surface for a transient cutting process of orthogonal cutting by a photo-elastic experimental method in which lead plates were cut with an epoxy resin tool. The following are observed: for a positive rake ($\alpha > 0$) the shear stress on the rake face remains constant for a certain distance and drops to zero rapidly after that, while for negative rake ($\alpha < 0$), the shear stress is zero at the cutting tip of the tool and increases to a maximum along the tool, and maintains this maximum for a certain range before it drops to zero. In both cases, the normal stress is maximum at the cutting tip of the tool and decreases gradually toward the chip separation point.

Wright et al (1979) proposed that at the chip tool interface in machining some of the interface regions experience full seizure whereas others experience sliding. The proportion of seized areas as to real area of contact A_r is given by $K = A_s/A_r$. The constant K which varies from 0 to 1 depends on factors such as material purity, tool material and preparation, cutting time, cutting speed, rake angle, lubrication and machine stability.

Doyle et al (1979) used a transparent sapphire cutting tool to study directly the frictional interactions occurring at the chip-tool interface in continuous chip formation. They concluded that the contact length between the chip and the cutting tool may be divided into three regions. In the first region the relative movement is observed at the interface. In the second region the evaporated thin films on the tool were removed suggesting chip sliding. In third region the fresh chip is exposed continually to the environment which leads to

increased adhesion and friction and is evidenced by the gross transfer of chip material to the tool face.

Childs (1980) considered the effect of elastic contact between chip and tool which occurs beyond the plastically stressed contact region during chip formation in metal cutting. The main assumption in his analysis is that the shear stress is constant over the plastic contact between chip and tool and decreases parabolically over the elastic contact. The ratio of the shear stress to the normal stress on the rake face is constant over the elastic contact region. It turns out, however, that the velocity on the elastic contact region is not compatible with the holograph of the plastic zone that produces a curled chip.

Horne et al (1981) studied experimentally the built-up edge formation in aluminum, brass and steel using transparent sapphire cutting tools. They observed that the nature of flow around the cutting edge causes a natural stagnant point around which very high shear strains are produced. They proposed that pure materials do not exhibit a built-up edge because they can withstand high strains; but in alloys such high strains lead to shear failures that cause internal separation and built-up-edge.

Wright (1981) studied the frictional interactions at the chip-tool interface in machining lead, aluminum, copper, iron, and nickel over a range of cutting speeds and times. He used steel, cemented carbide and transparent sapphire cutting tools; the last allowing the interface to be observed directly. His results confirmed Doyle et al (1979) findings that there is less transfer of work material immediately behind the cutting edge (the first region) than at some distance from the edge (second region).

Ramalingam et al (1981) applied plane strain plasticity theory to metal cutting

problems. By considering a plastic circular arc free boundary that connects the work material with the chip they obtained the plastic zone boundaries in closed form. This was then compared with the experimental results of Roth and Oxley (1972). The conclusion was that the observed deformation can not be accounted for with ideal plasticity formulation. However, in their studies the velocity requirements were not satisfied. Besides, the calculated plastic region is not extended towards the tool face. They only compared the calculated shape of the plastic zone with the part of the plastic region near the free surface that was suggested by Roth and Oxley. But, by considering velocity discontinuities in their solution they could have matched the experimental observation satisfactorily.

Wright (1982) presented an upper round type analysis for predicting the shear plane angle in machining, using the work material strain-hardening characteristics. In this analysis, friction on the rake face and the high strain rates and temperatures that arise in practice are neglected.

Wright et al (1982) studied the role of chip-tool friction on the value of the shear plane angle in machining. The conclusion was that the friction model was not fully predictive and he suggested that the original frictionless model (Wright, 1982) is a good approximation and is a useful technique as it stands, especially for softer metals.

Bagchi (1983) criticized Wright's model by pointing out that except for *AISI 1113* steel the comparison between the experimental and the predicted values are not close. He suggested modifying Wright's model by adding an empirical factor.

The following is a review for important models which tackle the mechanics of chip formation.

2.1.1 ShearPlane Model

The most widely used model is the one proposed by Ernst and Merchant (1941) and Merchant (1944; 1945). In this model it is assumed that chip formation is accomplished by the shearing of material over an inclined single imaginary plane extending from the cutting edge to the work surface ahead of the tool. This plane was termed "shear plane" and the angle it makes with the surface generated was designated as φ. This shear plane *AB* in Figure 2.1 across which the work velocity v is instantaneously changed to the chip velocity v_1. This requires a discontinuity (jump) in the tangential component of velocity across *AB* equal to v_s as shown by the velocity diagram in Figure 2.1.

The drawbacks of this model are, as analyzed by Zorev, (1966), the presence of a single shear plane *AB* and the absence of a smooth connection between the external surface of the cut layer of metal and the chip (point *A*), which is contrary to experimental evidence that one plastic zone is not one shear plane. Rather, it consists of a large number of slip surfaces over which plastic shearing takes place successively. As stated in (Okushima and Hitomi, 1961) such cutting mechanism, based on simple shear along a single shear plane, contains the following conflicts: a) a moving metal particle must attain an infinite acceleration when it passes across the shear plane, changing its position from the work region to the chip region, b) an infinite stress gradient exists on the shear plane, c) the rate of strain is extremely large compared with that in static material tests, and d) extremely large strain is produced abruptly on the shear plane, and the relationship between stress and strain in cutting does not agree with that in static material tests.

Also the shear plane model was severely criticized by Oxley (1989) and Palmer and

Oxley (1959). It was pointed out that the assumption of a single shear plane and the associated constant normal stress along this plane were dependent on another assumption, namely, that the flow stress of the work material does not not vary during the deformation. Merchant (1945) found that his model agreed well with experimental results obtained when cutting synthetic plastic but agreed poorly with experimental results obtained for steel machined with a centered carbide tool. In Ernst and Merchant's first analysis (1944) , the following assumptions were made (Shaw, 1984): a) the shear stress is a maximum in the direction of the shear plane, b) the coefficient of friction is independent of the shear angle, c) the resultant force R is independent of the shear angle, d) the tool tip is sharp and no rubbing occurs between the tool and work piece, e) the deformation is two-dimensional, i.e., no side spread, f) the stress on the shear plane is uniformly distributed, g) the resultant force R on the chip applied at the shear plane is equal, opposite and collinear to the force R' applied to the chip at the tool-chip interface.

From these conditions a force diagram as shown in Figure 2.2 was constructed and the following relations can be concluded :

$$\begin{aligned} F_c &= R\cos(\lambda-\alpha) \\ F_t &= R\sin(\lambda-\alpha) \\ F_f &= R\sin(\lambda) \\ F_n &= R\cos(\lambda) \\ \theta &= \varphi+\lambda-\alpha \\ \tau_{sAB} &= \frac{R\cos(\varphi+\lambda-\alpha)\sin\varphi}{tb} \end{aligned} \qquad (2.1)$$

in which, F_c and F_t are the forces in the cutting direction and normal to this direction respectively , F_f and F_n are the frictional and normal forces at the tool-chip interface, F_s is the shear force along AB, τ_{sAB} is the shear flow stress along AB, t is the undeformed chip

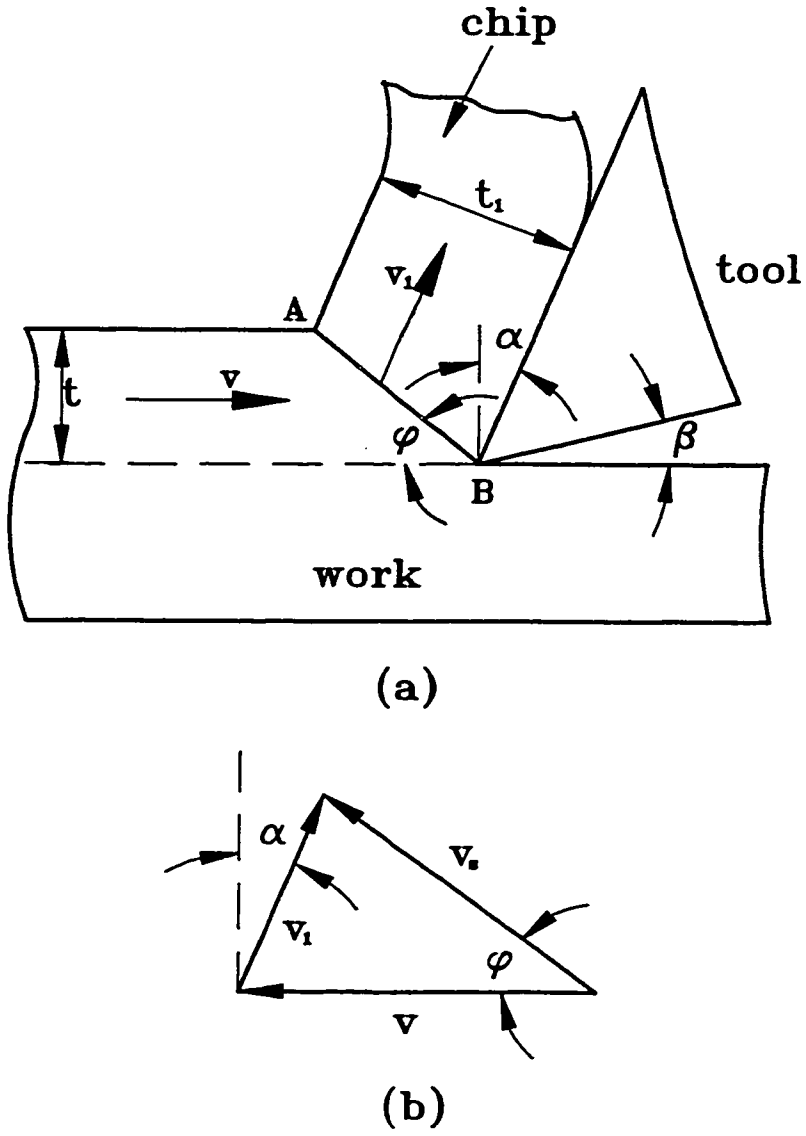

Figure 2.1: Shear plane model (a): the model (b) the velocity diagram (Ernst and Merchant, 1941; Merchant, 1944 ; Merchant, 1945).

thickness, b is the width of cut measured along the cutting edge, α is the rake angle, φ is the shear angle, θ is the angle made by resultant R with AB and λ is the mean angle of friction used to describe the frictional condition at the tool-chip interface. From the Equations (2.1) the cutting forces may be determined, provided the shear stress τ_{sAB}, friction angle λ and the shear angle φ are known. Merchant considered that τ_{sAB} would have the yield shear strength for the work material and that λ would have the usual value for dry sliding friction.

Ernst and Merchant (1941) proposed that the shear plane would take such a position that the shear stress τ_{sAB} would be a maximum. They expressed the shear stress in terms of the tool rake angle α, the friction angle between chip and tool rake face λ and shear angle φ and differentiated τ_{sAB} in equation (2.1) with respect to shear angle φ and equating the resulting expression to zero. This led to the result

$$\varphi = 45 - \frac{\lambda}{2} + \frac{\alpha}{2} \tag{2.2}$$

Merchant (1945) presented a different derivation that led to equation (2.2) such that the total power consumed P in the cutting process would be minimum . An expression for the total power P consumed in the chip formation can be written as

$$P = F_c v = \tau_{sAB} t b v \frac{\cos(\lambda - \alpha)}{\sin\varphi \cos(\varphi + \lambda - \alpha)} \tag{2.3}$$

An expression identical to equation (2.2) can be obtained when P is differentiated with respect to φ considering λ and τ_{sAB} to be independent of φ.

Upon finding equation (2.2) to be in poor agreement with experimental data, Merchant (1945) presented a different approach, and a different set of assumptions were

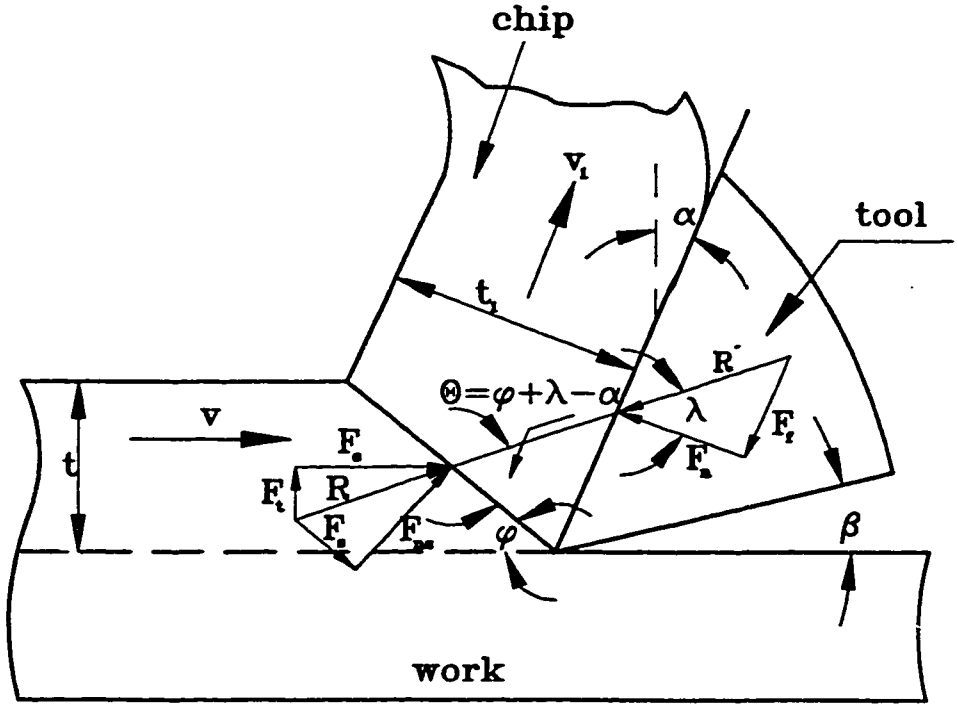

Figure 2.2: Forces associated with the shear plane model (Ernst and Merchant, 1941; Merchant, 1944 ; Merchant, 1945).

made:- a) the angle φ is such that the total power is a minimum, b) the friction angle λ is independent of the shear angle φ, c) the shear stress τ_{sAB} on the shear plane is independent of the shear angle φ, and d) the yield shear stress τ_{sAB} of the metal is increased linearly by the presence of a normal compressive stress σ on the shear plane according to the following equation

$$\tau_{sAB} = \tau_o + K\sigma \tag{2.4}$$

where K is the slope of τ_{sAB} vs. σ diagram which can be experimentally determined for each particular material. There is no clear physical reason why item (a) should be true. Many examples may be found in nature in which non conservative processes, such as that of metal cutting, clearly occur in such a manner that the energy consumed is not a minimum. However, according to the formentioned assumptions, and from Figure 2.2, it can be seen that

$$\sigma = \tau_{sAB}\tan(\varphi+\lambda-\alpha) \tag{2.5}$$

Substituting equation (2.5) into equation (2.4), we have

$$\tau_{sAB} = \frac{\tau_o}{1-K\tan(\varphi+\lambda-\alpha)} \tag{2.6}$$

When this is substituted into equation (2.3) the following equation can be obtained

$$P = \frac{\tau_o t b v \cos(\lambda-\alpha)}{[1-K\tan(\varphi+\lambda-\alpha)][\sin\varphi\cos(\varphi+\lambda-\alpha)]} \tag{2.7}$$

When P is differentiated with respect to φ and equating the resulting expression to zero with τ_o and λ considered independent of φ, the following equation can be obtained

$$\varphi = \frac{\cot^{-1}K}{2} - \frac{\lambda}{2} + \frac{\alpha}{2} \tag{2.8}$$

Merchant called the quantity $\cot^{-1}K$ the machining constant C. Allowing C to be an adjustable parameter which varies from one material to another, the above expression would yield a good approximation of the φ values to the experimental observations. But the magnitude of C is impossible to be real in some cases (Oxley, 1989).

2.1.2 Slip-line Field Theory

The theory of Lee and Shaffer (1951) was the result of an attempt to apply the plasticity theory to the problem of orthogonal metal cutting. In dealing with problems using the plasticity theory, it is necessary to make certain assumptions regarding the behavior of the work material under stress as follows:

1. The material is rigid plastic, which means that the elastic strain is negligible during deformation and that once the yield point is exceeded, deformation takes place at constant stress.
2. The behavior of the material is independent of the rate of deformation.
3. The effect of temperature increase during deformation is neglected.
4. The inertia effect resulting from acceleration of the material during deformation is neglected.

These assumptions have led to useful solutions of many problems in plasticity.

In the solution of a problem in plasticity, the construction of a slip line field is necessary; this field consists of two orthogonal families of lines (called slip lines), indicating,

at each point in the plastic zone, the two orthogonal directions of maximum shear stress. The slip-line field proposed by Lee and Shaffer for the orthogonal cutting of a continuous chip is shown in Figure 2.3. It can be seen that Lee and Shaffer have employed the idealized shear-plane model of cutting, where all the deformation takes place in a plane extending from the tool cutting edge to the point of intersection of the free surfaces of the work and chip. This transmission of forces results in the triangular plastic zone *ABC*, where no deformation occurs but the material is stressed to its yield point. Thus, the maximum shear stress throughout this zone is τ_s, the shear stress on the shear plane, and the two directions of this maximum shear stress are indicated by the two orthogonal sets of straight lines (slip lines).

If the boundaries of this triangular zone are considered, it is clear that the shear plane *AB* must give the direction of one set of slip lines since the maximum shear stress must occur along the shear plane. Also, since no forces act on the chip after it has passed through the boundary *AC*, no stresses can be transmitted across this boundary. Thus, *AC* can be regarded as a free surface, and since the directions of maximum shear stress always meet a free surface at $\pi/4$, the angle *CAB* is equal to $\pi/4$. Finally, assuming that the stresses acting at the chip-tool interface are uniform, the principal stresses at the boundary *BC* will meet this boundary at angles λ and $(\lambda+\pi/2)$ (where λ is given by $\tan^{-1}(F_f/F_n)$ and is the mean chip-tool friction angle).

From Figure 2.3, it can be written

$$\varphi+\lambda-\frac{\pi}{4}-\alpha = \frac{\pi}{2} \tag{2.9}$$

that is

$$\varphi = \frac{\pi}{4} + \alpha - \lambda \qquad (2.10)$$

Lee and Shaffer (1951) realized that equation (2.10) does not hold for all possible values of λ and α, namely for high tool friction and small or negative rake angles. They postulated that under such conditions, a build-up of material occurred at the nose of the tool. However, to support this point a second solution was presented for the new geometry where a built-up edge is present on the tool face.

The theories outlined above were compared with the results of independently conducted experiments (Pugh, 1958). It can be seen that neither of these theories approach is in agreement with any of the experimental relationships for the various materials tested.

2.1.3 Thick-Zone Models

To eliminate the conflicts in the conventional cutting theory based upon the shear process along single plane many models were proposed by Okushima and Hitomi (1961), Kececioglu (1958; 1960), Stevenson and Oxley (1970), Fenton and Oxley (1970) and others. These models can be classified into two types the flow region model and the parallel-sided model. In these models the single shear plane model is open up to get ride of the conflicts in the shear plane model.

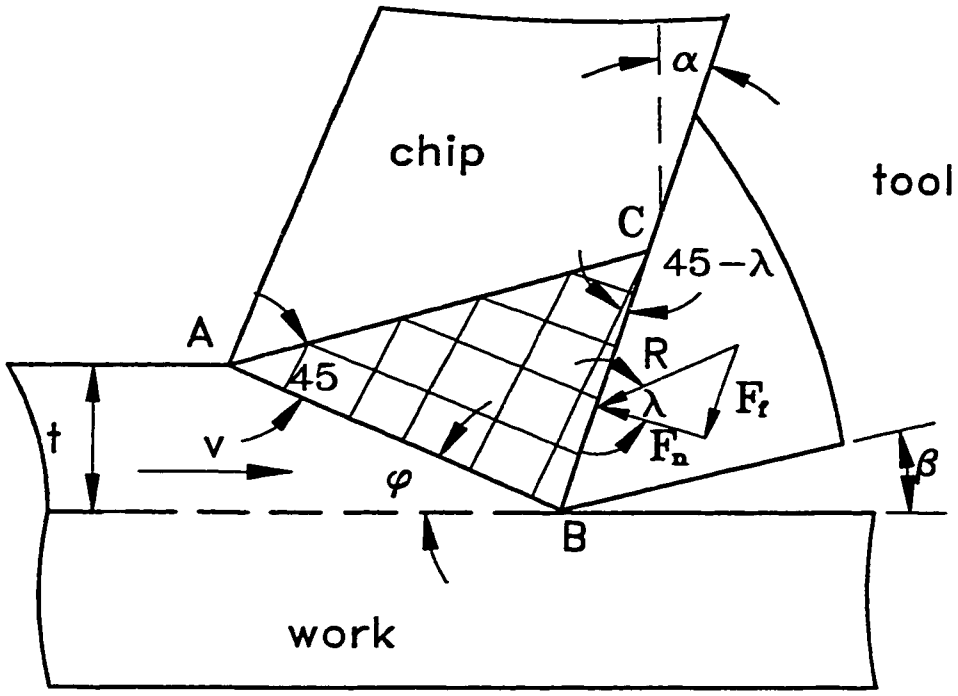

Figure 2.3: Lee and Shaffer's slip-line field for orthogonal cutting (Lee and Shaffer, 1951).

2.1.3.1 Flow region models

Okushima and Hitomi (1961) suggested the scheme shown in Figure 2.4. They suggested that there is a fairly large transitional zone *AOB* for plastic deformation of metal be taken into consideration between the rigid of work piece and the plastic region of steady chip. In this model the material was assumed to be ideally plastic and the shear stresses on *OA*, *OB* and *OD* were considered equal to the yield shear strength τ_o. Thus,

$$\tau_{sOA} = \tau_{sOB} = \tau_{sOD} = \tau_o \tag{2.11}$$

From Figure 2.4, it can be concluded that

$$\tau_{sOA} = \frac{R\sin\varphi_1\cos(\varphi_1-\alpha+\lambda)}{tb} \quad , \tag{2.12}$$

$$\tau_{sOB} = \frac{R\cos(\varphi_2-\alpha)\cos(\varphi_2-\alpha+\lambda)}{bt_1} \tag{2.13}$$

and

$$\tau_{sOD} = \frac{R\sin\lambda}{bl_f} \tag{2.14}$$

where l_f is the tool-chip contact length. From Equations (2.12), (2.13), and (2.14) , the angle φ_1 and φ_2 can be expressed by

$$\varphi_1 = \frac{\eta_1}{2}-\frac{\lambda}{2}+\frac{\alpha}{2} \tag{2.15}$$

and

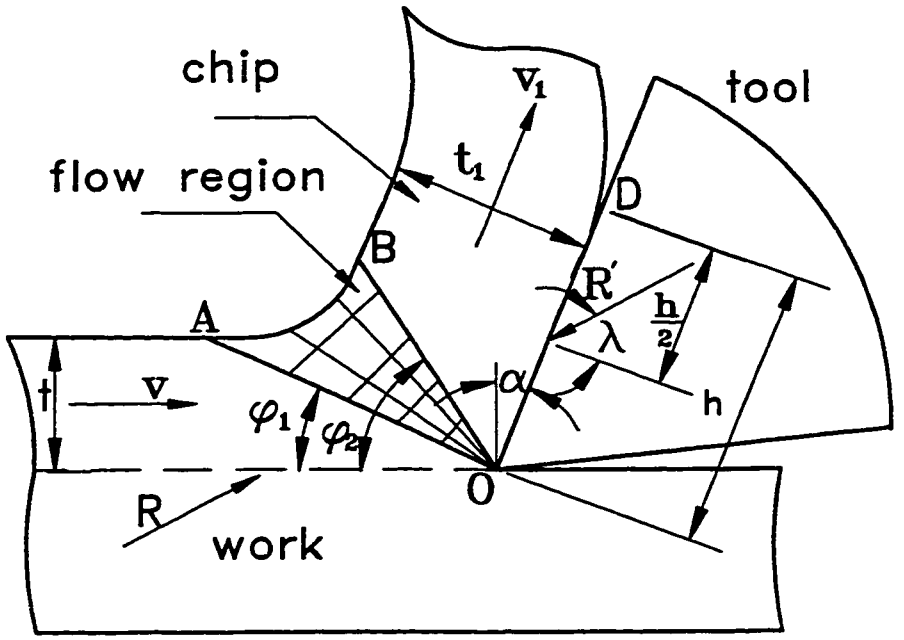

Figure 2.4: Deformation model assumed by Okushima and Hitomi (1966).

$$\varphi_2 = \frac{\eta_2}{2} - \frac{\lambda}{2} + \frac{\alpha}{2} \tag{2.16}$$

where

$$\eta_1 = \sin^{-1}\left[\frac{2t}{l_f}\sin\lambda + \sin(\lambda-\alpha)\right] \tag{2.17}$$

$$\eta_2 = \cos^{-1}\left[\frac{2t_1}{l_f}\sin\lambda - \cos\lambda\right] \tag{2.18}$$

The thickness of the deformation zone can be represented by φ, so that

$$\varphi = \varphi_2 - \varphi_1 = \frac{\alpha}{2} - \frac{\eta_1}{2} + \frac{\eta_2}{2} \tag{2.19}$$

Experiments on a lead work piece showed that φ was always positive, suggesting that the analysis yielded sound results. It was also declared that the shear strain was much lower than that in the shear plane model, a result which led Okushima and Hitomi to conclude that their model was more reasonable. However, this model is criticized by Kobayashi and Thomsen in the discussion of their work because it is not possible to construct a slip-line field satisfying equilibrium and continuity for the constructed sector where each of the radial lines is at the same time one of the maximum shear direction. Also point "*O*" in this model, causes the same conflicts as in the shear plane model. This model also neglected effect of the temperature produced during the cutting process.

2.1.3.2 Parallel-sided shear zone model

To get ride of the discontinuity in the velocity and to account for the effect of the strain-hardening properties on the hydrostatic stress distribution in the chip formation zone the parallel-sided shear zone model has been introduced by Oxley and his co-workers (Stevenson and Oxley, 1970; Fenton and Oxley, 1970) as shown in Figure (2.5). In this model (parallel-sided shear zone model) , the shear plane *AB* of the shear plane model shown in Figure. 2.1 is just open up so that the boundary *CD* between the shear zone and work piece and the boundary *EF* between the shear zone and chip are parallel to and equidistant from *AB*. It is easy to realize that the there is no difference between shear plane model and parallel-sided shear zone model except that shear plane *AB* in shear plane model is open up to become of a finite thickness instead of zero thickness as in the shear plane model.

The following assumptions were made to construct the parallel-sided shear zone model:-

1. Plane strain deformation. This means that there is no side flow.
2. Steady state conditions.
3. Perfectly sharp tool edge.
4. The shear plane *AB* in this model is assumed to open up so that the work velocity v is assumed to change to the chip velocity v_1. in the shear zone along smooth geometrically identical streamlines with no discontinuities in velocity.
5. The overall geometry of the shear zone in parallel-sided model is assumed to be the same geometry in the shear plane model with *AB* and φ in this model geometrically equivalent to the shear plane and shear angle.

6. The force polygon of the shear plane model remains the same in the parallel-sided shear zone model.

7. The overall change in velocity in the parallel-sided model is assumed to be the same velocity diagram as in the shear plane model.

8. The shear strain-rate is assumed to be constant through the shear zone.

9. The effect of temperature is neglected.

10. The shear stress τ_s is assumed to be constant along *AB*.

11. According to the slipline field theory the variation in hydrostatic (mean compressive) stress along *AB* is linear with $\sigma_A > \sigma_B$.

12. This model assumes that *AB* would bend to meet the free surface at the required angle $\pi/4$ in the region where it still could be taken as parallel to the cutting direction and assuming that the angle that has to be turned through to meet this condition $(\pi/4 - \varphi)$ occurs within negligible distance.

13. Linear stress-strain relation is assumed such that $\Delta\tau_s = m\,\gamma_{EF}$ where m is the slope of the stress-strain curve.

14. Half of the resulted shear strain is assumed to occur at *AB*.

15. The ratio of the shear zone length to its thickness $(l_s / \Delta s_2)$ is found experimentally to have a value between 6 and 15 and with an average a value of 10.5.

16. In the parallel-side shear zone model λ is considered the mean friction angle as the tool-chip interface parameter in the same way as for the shear plane model solutions, i.e. λ would have the usual value as for dry sliding friction.

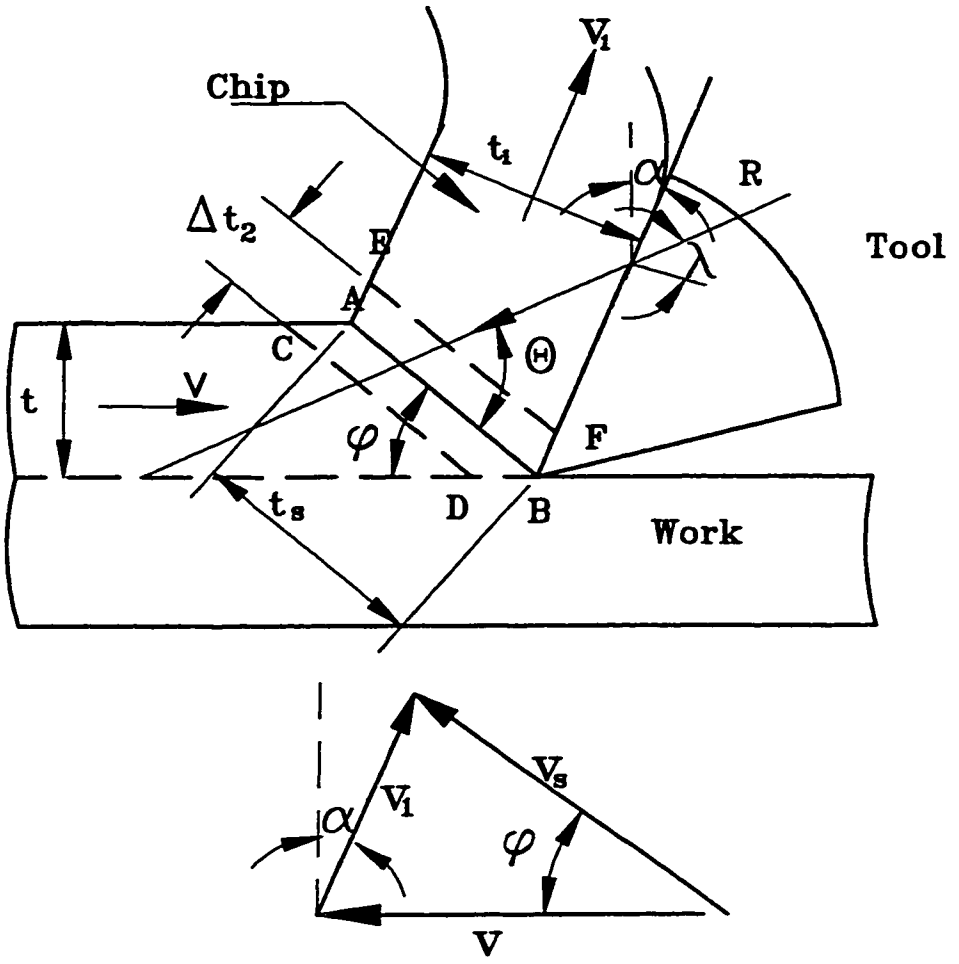

Figure 2.5: Parallel-sided shear zone model (Oxley and Welsh, 1963).

The parallel-sided shear zone theory assumes constant velocity in the shear zone; this means that the shear strain rate is constant throughout the shear zone. This strain-rate can be given as :

$$\dot{\gamma} = \frac{v_s}{\Delta s_2} \tag{2.20}$$

where, v_s is the shear velocity which is equal in magnitude to the velocity discontinuity of the shear plane model, and Δs_2 is the thickness of the shear zone. Early experimental work at low cutting speed revealed that the ratio of length to the mean thickness of the shear zone ($l_s/\Delta s_2$) had a value between 6 and 15 for a range of work materials and cutting speed, but for high cutting speed there are no information about that ration (Oxley, 1989). According to the assumptions (9), and (10), the stress equilibrium equations referred to slip-lines becomes :-

$$d\sigma = \frac{d\tau_s}{ds_2}\, ds_1 \tag{2.21}$$

where s_1 and s_2 are distances measured along the slip-lines.

For the assumed model ($d\tau_s/ds_2$) can be replaced by the finite difference ($\Delta\tau/\Delta s_2$) as follow

$$\frac{d\tau_s}{ds_2} = \frac{\Delta\tau_s}{\Delta s_2} = \frac{\tau_{sEF} - \tau_{sCD}}{\Delta s_2} \tag{2.22}$$

Applying equation (2.21) between A and B gives

$$\sigma_A - \sigma_B = \frac{\Delta\tau_s}{\Delta s_2}\, l_s \tag{2.23}$$

in which, σ is the hydrostatic stress, σ_A and σ_B are the hydrostatic stresses at A and B, l_s is the length of AB and τ_{sEF}, and τ_{sCD} are the shear stresses along EF and CD. Therefore, the normal force F_{ns} acting on AB can be calculated as :-

$$F_{ns} = \frac{\sigma_A + \sigma_B}{2} l_s b \tag{2.24}$$

where b is the uncut chip width. The shear force on AB can be obtained from the following equation:

$$F_s = \tau_{sAB} l_s b \tag{2.25}$$

If the angle made by the resultant force R with AB is θ as shown in Fig. (2.6) , and by using equation (2.23) then

$$\tan\theta = \frac{F_{ns}}{F_s} = \frac{\sigma_A+\sigma_B}{2\tau_{sAB}} = \frac{\sigma_A}{\tau_{sAB}} - \frac{\Delta\tau_s}{2\tau_{sAB}} \frac{l_s}{\Delta s_2} \tag{2.26}$$

According to the assumption (12), the following equation can be written

$$\frac{\sigma_A}{\tau_{sAB}} = 1 + 2\left(\frac{\pi}{4}-\varphi\right) \tag{2.27}$$

Substituting for σ_A into equation (2.26), it can be concluded that

$$\tan\theta = 1 + 2\left(\frac{\pi}{4} - \varphi\right) - \frac{\Delta\tau_s}{2\tau_{sAB}} \frac{l_s}{\Delta s_2} \tag{2.28}$$

θ can be expressed in term of the shear angle φ , the mean friction angle λ, and the rake angle α by

$$\theta = \varphi+\lambda-\alpha \tag{2.29}$$

Oxley and Welsh (1963) related the change in the yield shear stress $\Delta\tau_s$ in the parallel-sided shear zone by assuming a linear stress-strain relation (assumption (13))

$$\Delta\tau_s = m\gamma_{EF} \tag{2.30}$$

where m is the slope of the stress-strain curve and γ_{EF} is the shear strain along EF. γ_{EF} can be found by multiplying the time taken for a particle of material to pass through the shear zone by the strain-rate in the shear zone (equation (2.20)), that is

$$\gamma_{EF} = \frac{\Delta s_2}{v_n}\frac{v_s}{\Delta s_2} \tag{2.31}$$

where v_n is the velocity normal to AB. However, some useful relationships between velocities can be obtained from the velocity diagram in Figure 2.5, namely

$$\begin{aligned} v_1 &= \frac{v\sin\varphi}{\cos(\varphi-\alpha)} \\ v_s &= \frac{v\cos\varphi}{\cos(\varphi-\alpha)} \\ v_n &= v\sin\varphi \end{aligned} \tag{2.32}$$

Substituting for v_s and v_n from Equations (2.32) into equation (2.31) yields

$$\gamma_{EF} = \frac{\cos\alpha}{\sin\varphi\cos(\varphi-\alpha)} \tag{2.33}$$

Using the assumption (14), that half of this strain will have occurred at AB then

$$\tau_{sAB} = \tau_o + \frac{1}{2}m\gamma_{EF} \tag{2.34}$$

where τ_o is the yield shear strength of the work piece. Substituting Equations (2.29), (2.30), (2.33) and (2.34) into (2.28), the following equation has been obtained:

$$\tan(\varphi+\lambda-\alpha) = 1+2\left(\frac{\pi}{4}-\varphi\right)-\left(\frac{m\cos\alpha}{2\tau_o\sin P\varphi os(\varphi-\alpha)+m\cos\alpha}\right)\left(\frac{t}{\sin\varphi\Delta s_2}\right) \quad (2.35)$$

Now, for given values of α, λ, and t, it is possible to determine φ from equation (2.35) by trail and error if a appropriate values of τ_o, m and the thickness of the shear zone Δs_2 are known. the shear angle φ can be used together with the corresponding values of τ_{sAB} to calculate the cutting forces from equation (2.1).

This model as shown has been constructed using 16 assumptions, some of them are questionable such as the assumption that half of the resulted shear strain occurred at AB, the neglecting of the temperature, and assumption of constant shear strain-rate.

2.2 THERMOMECHANICAL BEHAVIOR OF WORKPIECE MATERIAL IN CUTTING

The goal of metal cutting research is to develop methods of predicting the quality and cost of a machined work piece without physically machining it. If this can be done reliably, a wider variety of potential process conditions can be evaluated easier than currently possible through trail-and-error experimentation, leading to more efficient process and tooling design (Lee and Kapoor, 1986; Steed, 1987). A basic requirements for achieving this goal is a reliable method for predicting cutting forces for arbitrary process conditions. Almost all quantities which affect the quality and cost of the machined work piece such as, tolerance, tool life, and power consumption , depend on cutting forces either directly or indirectly. Since the flow shear stress τ_s is the main parameter affecting the energy requirement and the cutting forces in the machining, the estimation of this stress and its change during plastic

deformation remains one of the principal goals in the theory of chip formation. Investigators in the metal cutting field have attempted to develop an analytical means for the cutting process which gives a clear understanding of the mechanism involved and enables a prediction of the cutting forces without a need for exhaustive empirical testing. In this review the flow shear stress τ_s that occurs at the shear zone in metal cutting is considered.

The well known Merchant's force model (Figure 2.2) is the only model accepted in practically all known publications on metal cutting (Merchant, 1945; Zorev, 1966; Shaw, 1984: Oxley, 1989). The core of the model includes determination of the shear force component F_s of the resultant cutting force as follows:

$$F_S = \tau_{sAB} \frac{t\ b}{\sin\ \varphi} \tag{2.36}$$

where τ_{sAB} is the shear flow stress along the shear plane AB; t is the uncut chip thickness; b is the width of cut; φ is the shear angle.

Although many studies on metal cutting have been attempted to derive theoretically or obtain experimentally the flow shear stress, this is still one of the most controversial issues in the field. There are several principal questions concerning the flow shear stress of workpiece material in cutting: Could the stress-strain relations obtained in the standard tensile (compressive) test be used in metal cutting? Would the stress in the deformation zone stop growing or even start decreasing (an idealistic idea which stands behind so called high-speed machining (King, 1985)) in case of large strains such as those in metal cutting? Is the flow shear stress affected by high strain rates (10^4 - 10^8 higher than in the standard tensile test) and high temperatures occurring in cutting? Practically all serious studies done on

metal cutting contain the direct or indirect answers to these questions.

The approaches that tackle the characteristics of the flow shear stress in the shear zone can be classified into three categories :

1. Those approaches that consider the flow shear stress in the shear zone equal to the yield shear strength of the work piece. Some of these approaches consider the effects of the shear strain rate and the temperature on the flow shear stress but these effects are considered to be canceling each other.
2. Those approaches that consider the effects of strain hardening only, or the effect of strain hardening and shear strain rate on the flow shear stress together.
3. Those approaches that consider the effects of strain hardening, shear strain rate, and the effect of temperature on the flow shear stress.

The first effort in this direction was by Ernst and Merchant (1941) who offered an analysis for the cutting force based on the shear plane model. They assumed that the flow shear stress τ_{sAB} on the shear plane is constant and equals to the yield shear strength τ_o .

Merchant (1945) found that this theory agreed well with experimental results obtained when cutting synthetic plastics but poorly with experimental results obtained for steel machined with a centered carbide tool. By reconsidering the assumptions on which that theory has been established, Merchant (1945) derived the following equation:

$$\tau_{sAB} = \frac{\tau_o}{1 - K\tan(\varphi + \lambda - \alpha)} \tag{2.37}$$

which resulted from the equation:

$$\tau_{sAB} = \tau_o + K\sigma \tag{2.38}$$

indicating that the flow shear stress τ_{sAB} on the shear plane increase linearly with the increase in the normal stress, σ, on the shear plane; where K is the slope of τ_s vs. σ diagram experimentally determined for each particular material, φ is the shear angle, α is the rake angle, and λ is the mean friction angle. This equation agreed with the work of Bridgman (1937; 1943), where , in experiments on polycrystal line, the flow shear stress τ_s was shown to be dependent on the normal stress σ on the shear plane .

Shaw and Finnie (1955) suggested that the small size of the deformation region may influence the flow shear stress value. This follows from the theory of size effect for single crystals which is based on the concept that at small sizes the probability of finding dislocation sources is reduced and hence the flow shear stress of a work piece rises.

Kececioglu (1960; 1958) studied the effects of the shear size, compressive stress, and shear strain in metal cutting on the flow shear stress and he introduced the following expression for the flow shear stress in the shear zone

$$\tau_s = \tau_o + (\frac{E}{\Delta s_2}) + F\sigma + G\gamma \qquad (2.39)$$

where τ_o is the yield shear strength of the work piece, σ the compressive stress acting on the shear plane, γ the shear strain undergone by the chip during its formation, Δs_2 the thickness of the shear zone E, F, and G are material constants.

Okushima and Hitomi (1961) developed the flow region concept. The flow region AOB is a transitional deformation zone which exists between the rigid region of the work and the plastic region of steady chip as shown in Figure 2.4 in which the stress must be at the yield level. Hence, according to Okushima, and Hitomi model the flow shear stress τ_s (τ_{sOA},

τ_{sOB}) on both boundary lines equals the yield shear strength (τ_o) of the work piece material.

To explain the increase in the flow shear stress τ_s in the primary shear deformation zone during machining , it has been suggested by a number of researchers that strain hardening plays an important role in determining the flow shear stress τ_s in metal cutting (Shaw and Finnie, 1955; Oxley, 1961) and Oxley (1989) suggested the following relation for the flow shear stress τ_{sAB} on the shear plane *AB* shown in Figure 2.5

$$\tau_{sAB} = \tau_o + \frac{1}{2} m \gamma_f \tag{2.40}$$

where τ_o is the yield shear strength of the work piece, *m* the slope of the plastic stress-strain curve at the corresponding mean shear strain rate in the primary shear deformation zone, which can be experimentally determined for each particular material, and γ_f is the final strain along the end of the deformation zone *EF* shown in Figure 2.5 which can be expressed as

$$\gamma_f = \frac{\cos\alpha}{\sin\varphi\cos(\varphi-\alpha)} \tag{2.41}$$

Von Turkovich (1970), obtained the behavior of the flow shear stress τ_s by considering the process of plastic deformation from the viewpoint of dislocation theory. The theory was developed for high strain rate processes and very large strains.

Klamecki and Kim (1988) developed a model for the flow shear stress τ_s in the primary shear deformation zone that take into account the effect of temperature *T* and strain associated with the chip formation γ , and the flow shear stress prior to the plastic deformation τ_o, which can expressed as :-

$$\tau_s = \tau_o + a\gamma^m - bT^n \tag{2.42}$$

where a, b, m, and n are coefficients to be obtained through experiments. However, no specific solution was given foryielding work material stress/strain behavior shown by the previous equation, and in reaching a solution, that equation requires four additional experimentally obtained coefficients : a, b, m, and n, which need to be determined through lengthy, expensive and very often inaccurate experimental procedure.

Klamecki and Kim (1988) studied the effects of the stress state transition from plane stress at the work piece surface to plane strain in the central region of the chip formation zone. In their model they expressed the flow shear stress τ_s in terms of the yield shear stress τ_o of the work material, strain γ and temperature T using the following expression:

$$\tau_s = \tau_o + K\gamma^n - AT \tag{2.43}$$

The strains and temperatures used in this expression are the local values calculated in the finite element simulation. Changes in the material behavior are specified by constants K, n, and A.

To apply these approaches it is necessary to do many experiments in order to determine the involved constants. Some of these experiments are lengthy, expensive and often inaccurate. This means that there is a need to develop approach enabling us to predict the flow shear stress in the shear zone without doing additional experiments, or with fewer number of experiments.

2.3 DYNAMICS OF THE CUTTING PROCESS

A metal cutting system essentially comprises the cutting process and the tool layout. The cutting process involves the removal of metal in form of chips from the workpiece by the action of the cutting tool which is coupled to the machine structure through different elastic elements. Thus, the tool traces a uniform path relative to the workpiece. Normally, any small vibration caused by occasional disturbances, such as inhomogeneity of the work material, the runout and misalignment of the workpiece, would be damped out by the structure of the cutting system. Sometimes, however, the disturbances are maintained and the system becomes unstable and the relative periodic displacement between the tool and the workpiece may build up to a large amplitude. This relative periodic motion between the cutting tool and the workpiece is known as chatter (Armarego, 1969).

Chatter imposes an undesirable limit on machine tool performance because it can imped the maintaining of the work surface finish and also it has adverse effect on part dimensional accuracy and the cutting tool life.

Machine tool dynamics against chatter vibration is a challenging subject of metal cutting research not only because of the level of physical complexity involved but also because of its role as the limiting factor in machining productivity. A large number of investigation in machining chatter have been undertaken in the last forty years in order to predict the dynamic behavior of the cutting process. Even though significant progress in approaching this goal has been made, the basic problem of establishing a universal force relationship with respect to the dynamic variables in metal cutting apparently has not been solved.

Studying the wave-removing process which comprises moving the cutting tool in a straight line while the surface to be cut oscillates has a big advantages in knowing the mechanism of the chatter.

Kobayashi and Shabaik (1964), using a photographic technique, which gave a direct observation of the shear angle variation, confirmed that the shear angle changes with the slope relative to the top surface of the uncut chip thickness.

Kobayshi and Kawata (1967) studied the effect of curvature of work surface on metal cutting and concluded that when the work surface has a curvature, the cutting characteristics differ from that in a planning operation. It was concluded that the effects of curvature must be taken into account when a work piece with a diameter less than 50 mm is machined. In the analysis of metal cutting process, a commonly assumed model is one in which the tool makes a linear motion. However, there are many processes such as turning, boring and drilling, in which the tool or the work makes a circular motion. In these cases the work surface has a certain curvature. When the curvature is convex, the process may be called an external cutting whereas it may be called an internal cutting in a concave case.

When the free surface of the uncut chip has a sinusoidal shape, it loses its harmonic character after passing through the shear zone. This led Albrecht (1962) to conclude that the accompanying shear angle variation must be essentially of the saw-tooth type. However, Das (1965) showed that a distorted cut chip profile in no way proves the presence of a shear angle variation. Even with a constant shear angle, a symmetrical uncut chip profile becomes unsymmetrical after passing through the Shear zone.

Das and Tobias (1967) developed a mathematical model which shows the connection

between the static and dynamic cutting coefficients. Three cases of dynamic cutting are considered: wave cutting, wave removing and wave-on-wave cutting. This model is based on the assumption that under dynamic conditions the orientation of the shear plane remains unaffected by a variation of chip thickness, provided this fluctuates relatively fast.

Rubenstein (1972) analyzed the influence of tool oscillation during a planning operation. A fundamental assumption made at the outset is that only those phenomena which have been observed to occur in steady-state cutting occur in dynamic cutting. The influence of tool motion is shown to be compounded of two parts, namely, tool motion alters the geometry of the cutting process and affects the magnitude of some of the cutting stresses by altering the strain and the strain rate to which material passing below the tool is subject. The resulting equations for the force components along and normal to the steady-state cutting direction are non-linear, and are expressed in terms of the stress-strain and stress-strain rate equations of the work piece material.

Nigm and Sadek (1977a) investigated experimentally the dynamic response of the shear plane and the variation of the dynamic cutting coefficients at various values of feed, cutting speed, rake angle, clearance angle, frequency, and amplitude of chip thickness modulation. This investigation showed that the shear plane responds to the dynamic variations in the cutting conditions and that its angular oscillation is not in phase with the chip thickness modulation. Moreover, the dynamic cutting coefficients are not in phase with the chip thickness modulation. In both wave generation and wave removal, the magnitude and phase of the dynamic cutting coefficients and shear plane oscillation are found to be function of the cutting conditions. However, the clearance angle has no effect on these

parameters. In reference to the dynamic cutting coefficients it has been concluded that while the tangential coefficient is not affected by the amplitude of chip thickness modulation, the thrust coefficient is slightly affected. The experimental results of this investigation showed also that there is no difference between the DC components of the shear angle and the cutting forces obtained under steady-state cutting.

Nigm et al (1977a) presented a dimensional analysis of the orthogonal steady state metal cutting process. This yielded explicit mathematical expressions for the chip thickness ratio, the force ratio and the termination of the built-up edge in terms of the rake angle, the feed and the cutting speed. The functions derived were found to be independent of the cutting conditions, for a particular combination of work and tool materials, characterized by a set of coefficients. The validity was tested experimentally and by reference to observed results obtained by previous investigators and a good correlation was observed in all case. The expressions derived, with the experimentally determined machining stress, permit the predication of the cutting forces over a wide range of cutting conditions from a limited number of machining tests.

Nigm et al (1977b) presented a mathematical model for determination of the dynamic cutting coefficients from steady state data. In other word, the physical relationships estblished in steady-state cutting can be applied to dynamic cutting as well, if the amplitude of vibration is relatively small. This theory is based on a non-dimensional analysis of the steady state orthogonal cutting process. It takes into consideration the oscillations of the shear plane response to dynamic variations of the cutting parameters. The model was verified, directly with dynamic cutting tests for the wave cutting and the wave removal, in

which the variations or the shear plane and those of the cutting force coefficients were measured. Indirect verification was achieved by reference to the work of previous investigators concerned with dynamic cutting and the stability of the cutting process.

Wu and Liu (1985a; 1985b) developed a mathematical model of machining chatter through an analytical approach in order to predict dynamic cutting force from steady-state cutting tests. The model is derived from a pseudo-static geometric configuration of the cutting process by taking into account the fact that the mean friction coefficient fluctuates dynamically responding to variation of the relative speed on the chip tool interface. The force functions through this derivation can be used to explain all three basic mechanics associated with chatter vibration of all the three cases namely, velocity dependent, regenerative, and mode coupling effects.

Ahn et al (1985) presented a new approach to the identification of the cutting process dynamics in the form of a transfer function derived from the finite difference equation model.

Wu (1986) presented a new method of modeling the angular oscillation in dynamic orthogonal cutting. The system governing equations were derived based on the work-hardening slip-line field theory in cutting mechanics by taking into account the changes of stress conditions on both the shear plane and the tool-chip interface.

Fujii et al (1986a) investigated the whirling vibration of the drill in the beginning of the drilling operation experimentally. Special attention is paid to how vibration develops as the drill proceeds into the work piece. Three types of drills with different web thicknesses were used, and the characteristics and cause of the vibration were discussed. Whirling vibration, which has an elliptical orbit, is a self-exited vibration accompanied by a phase lag

with respect to the revolution of the work piece. The vibration energy is provided by the regenerative effect at the major cutting edge, while the chisel edge acts to dampen the vibration.

Fujii et al (1986b) examined the influence of widely varied point angles, relief angles, and helix angles on whirling vibration of drill point geometry at the major cutting edge. The influence of the flank surface configuration of the major cutting edge was studied in particular. Based on the obtained results, an attempt was made to obtain useful parameters by which the initiation boundary of whirling could be predicted.

Marui et al (1988a) observed the primary and the regenerative chatter vibrations occurring in a spindle-workpiece system, and clarified the effects of the vibratory characteristics of the system and cutting conditions on the chatter vibration.

Marui et al (1988b) measured the effect of the dynamic variations of cutting depth, cutting velocity, and rake angle on the cutting force acting in the dynamic state of a lathe spindle-workpiece system by unique experiments. The phase lag between the dynamic cutting force and vibration displacement is clarified under various cutting conditions. The dynamic cutting force is measured when the cutting velocity and the rake angle were dynamically changed, and the results were represented as the cutting velocity coefficients and the rake angle coefficients. Based on these results, the energy supplied by the dynamic cutting force was obtained and the mechanism by which the chatter vibration occurred was discussed.

Marui et al (1988c) treated chatter vibration occurring in the spindle-workpiece system of a lathe theoretically, considering the phase lag of cutting force and chatter marks.

As a result, it was clarified that the chatter vibration is mainly induced by the phase lag of cutting force (primary chatter) and by the phase lag of chatter marks in successive cutting (regenerative chatter). The dynamic variations of the cutting velocity and rake angle made the spindle-workpiece system more unstable under vibration. The effect of cutting velocity variation was more remarkable than that of rake angle in both types of chatter. Chatter vibration could effectively be suppressed by increasing the damping capacity of the system.

Wu (1989; 1988) introduced a new concept to develop a comprehensive cutting force model for analyzing the dynamic behavior of the machining process. The model was derived based on the principles of the cutting mechanics, and it takes into account the fluctuation of the mean coefficient of frictional on the tool-chip interface as well as the variations of the normal hydrostatic pressure distribution and the shear flow stress along the primary plastic deformation zone. The model has been tested through computer simulation for orthogonal wave-removing processes by reference to an existing experimental evidence.

2.4 MEASUREMENT OF CUTTING FORCES

To place the analysis of the metal cutting process on a qualitative and quantitative basis, certain investigation must be made before, during, and after the cutting (Shaw, 1984). The number of observations that can be attained during the cutting process is rather limited. One among of those is the determination of the cutting forces.

An understanding of the forces in machining process is necessary since they are related to such things as tool wear, vibrations, accuracy, power consumption, process planning, and computer aided manufacture. Since force magnitudes can be determined by

variety of techniques, it is important to know the methodology of measurement to ensure the correct results. This is extremely important when certain aspects of a new model have to be examined knowing that results are used to judge the theory. Therefore, it would be logical to expect methodological research work on the cutting force measurement in order to introduce and establish a certain kind of standard for such measurements to ensure their repeatability and reliability..

In the cutting force measurement practice, it has been long recognized that although each dynamometer must be specially designed to meet specific requirements, certain design criteria are general and well discussed by Zorev (1966) and Shaw (1984). Unfortunately, the resent books on metal cutting ignore this significant aspect though they present the results of studies including cutting forces (Oxley, 1989; Trent, 1991; Stephenson and Agapiou, 1997). To support this point, a number of examples were reported:

Zhang and Kapoor (1987) used a strain gages on the boring bar to detect the cutting force signals through a Weston bridge amplifier. Nothing is mentioned how they did this.

Thangaraj and Wright (1988) used a Kistler piezoelectric platform dynamometer to measure the downward thrust force exerted by the drill. They did not mention about the measurement calibration procedure.

Lee et al (1989) measured cutting forces with a Kistler piezo-electric dynamometer type 9263A. The force signals were recorded on a chart-recorder for the static component stored on a multi-channel magnetic recorder for the analysis of the dynamic component. The tape-recorded signals were subsequently run on the spectrum analyzer using the Fast Fourier Transform function to obtain frequency spectrum.

Strenkowski and Moon (1990) measured the cutting forces using three axis dynamometer. Nothing is reported about the type of the used load washer and the calibration procedure.

Elbestawi et al (1991) used table dynamometer to measure the two in-plane components of the cutting force by means of four piezo-electric charge transducers, two of each of the x- and y-directions. The forces acting on the dynamometer were collected synchronously and averaged in the time domain. Approximately 20 s of actual machining runs were recorded in each test.

Lin et al (1992) measured the cutting forces using a dynamometer. They have not indicated what the type of the used dynamometer and how it was calibrated.

Song (1995) used a Kistler piezoelectric dynamometer to measure the axial and tangential cutting forces. In his work he discussed the accuracy, the reliability of the measured parameters though he has not mentioned any kind of calibration.

Stevenson and Stephenson (1995) adapted a piezo-electric three-axis dynamometer to measure the forces and the force signals were recorded on a data tape recorder and displayed on a digital oscilloscope. All data reported were in time domain.

As it is seen from above examples, no researcher even mentioned the calibration of the set-up for the force measurement, no one considered possible errors in the recording of force signals caused by the cut-off frequency of the recorder, no one reported the sampling rate, cut-off frequency,..etc.

Strain-gage-based transducers have never been entirely successful in metal cutting dynamometry. One reason is the high rigidity of the tool system which does not allow for

enough strain to be induced for the measurements. Also, the difficult conditions around the cutting edge can not accommodate the application of strain gages in the close vicinity. This necessitate the use of complex measuring setups, as an integral part of the machine, with intermediate elements whose dynamic contribution is difficult to compensate for.

A new era in the cutting force dynamometry started when piezo-electric transducers became available. However, a high sensitivity of such transducers was unusual for metal cutting researchers. Instead of one simple signal (recording) from a dynamometer which could be easily analyzed using a static calibration curve, they started getting an assemble of signals reflecting even small dynamic unevenness of the machine, fixtures, cutting tool, auxiliary components together with the environmental noise. To process signals from these dynamometers, researchers had to use new experimental methodologies, never used before in metal cutting experiments, like, for example, Fast Fourier Transform Analyzer (FFT). Moreover, they had to control the theory behind the new instruments, since machine tools in general are far from being the simple linear systems.

Another thing that has never been really recognized is that machine tools as dynamic systems exist only during machining. The reason for this would be that only after the cutting forces have been applied to take up many clearances in the assembly, thus introducing friction etc., as well as the questionable support at the cutting tool, the dynamic system has been established. This calls for costly real-time measurements with extensive use of triggering facilities. Unfortunately, not rarely both the static and the dynamic calibration were performed on a stationary machine tool without cutting. Numerous reported work suffered from the same mistake of calibrating one system while using a completely different

one, in terms of dynamics, when testing. This practice is still common today (Adolfsson and Stahl, 1995; El-Wardany et al, 1996)

To represent signals in the frequency domain, new functions have been introduced, among them most common being power spectral density function (Bendat and Piersol,1980; Bendat and Piersol,1971). This function describes the general frequency composition of the acquired signal in terms of spectral density of its mean square value.

However, the power spectral density function has become the most abused statistical function in the dynamics of metal cutting. The trouble comes from the misunderstanding of the word "power" that has been kept here only for historical reasons. In the theory of stochastic processes, this word means that the function standing under integral is squared so that the power spectral density function shows the rate of change of mean square value with frequency. In metal cutting dynamics, particularly in the cutting force measurement, this word was thought of as reflecting the mechanical power. As a result, the power spectral density function was assigned dimensions as g^2 /Hz, or even W/Hz, instead of N^2 /Hz and $(Nm)^2$ /Hz when measuring forces and torques (Osman and Sankar, 1972; Sankar and Osman, 1975; Chandrachekhar, Osman, and Sankar, 1985; Frazao et al, 1986). Moreover, the number of Hz to scale the axes was never related to the instrument setup. Such a wrong resulted in a conclusion that the cutting process is fully stochastic in nature. Obviously, this conclusion is in contradiction with the whole metal cutting practice which desperately needs a appropriate dynamic force measurements to improve the quality and efficiency of machining.

2.5 DEEP HOLE MACHINING PROCESS

Since the deep hole machining process has been selected to perform the required experiments as a typical orthogonal cutting, it is necessary to give a description of this process. Deep hole machining is known to be one of the most complex of all hole making operations, wherein the individual drilling processes are classified by the types of tools they use. The choice of a specific drilling process for any particular application, starts with the requirements of the hole-diameter, depth, macro- and micro errors of geometry and must include not only the production volume, but also the specific types of drilling equipment available. The sub-category of "deep-hole drilling" includes gun drilling, BTA drilling, and trepanning. One of the main features of this type of machining is that the tool holding structure is relatively slim and this adversely affects the cutting tool life, the accuracy of the finished hole, and the entire dynamical behavior of the machine tool.

At this stage it would be appropriate to give a short summary of previous work in the area of deep-hole machining. The review has not covered all the work in detail but the intention is to include fully only the work that can be or has been declared to be related, by any means, to the analyzing and measuring the cutting forces in deep hole machining.

The meticulous research began in the late 60's to develop a number of good works, most of them done by Griffiths (United Kingdom) and German authors, These works presented first dynamometry considerations in deep hole machining. Subsequent work moved the emphasis towards the dynamics, with the intention to make possible the use of higher feeds with slenderer shanks and boring bars.

Griffths (1973a; 1973b) adopted a dynamometer consisting of a thin wall tube to

which strain gauges were bonded to measure the mean value of static thrust and torque.

Pfleghar (1977) introduced the whole line of research which tried to model design criteria for securing static stability of the self-guided tools. He introduced a comprehensive analysis of forces acting on a multi-insert BTA tool. He explained the role of the supporting pads in balancing the cutting forces and featured the need for meaningful location of the supporting pads to insure stability in the presence of the dynamic component of the resultant cutting force. He showed, experimentally with gun drills, that the location of the supporting pads is related to the drift of the tool to oversize or undersize the holes. He measured the cutting and the burnishing forces using simple strain-gage based transducers to estimate stability.

Sakuma et al (1980a; 1980b) measured the torque and thrust using a dynamic strain meter and a direct recording electro-magnetic oscillograph by two a cross type strain gauge roset bonded on the periphery of the boring bar near its mounting holder.

Del Taglia and Tani (1982) proposed a method for measuring all the three components of forces in boring using a combination of a dynamo metric table and an angular position transducer. The dynamo metric table measures the axial component of the cutting force and the angular position transducer gives the radial and tangential force.

Sun, et al (1982) introduced a piezo-electric shank type dynamometer and have used it to measure the cutting forces in turning operation. Here the piezo-electric quartz three component transducer is placed in an oval opening of the tool shank to reduce the cross-correlation.

Chandrashekhar (1984) took an impractical approach towards the dynamics of a

deep-hole machine tool. When examining the dynamic model of a machine tool, he set up with many springs and dashpots to close up with the boring bar and unclear boundary conditions. With a view of the machine tool as a stochastic system, he presented a stream of analytical expressions with often missing nomenclature thus making it impossible for a reader to follow. A little measurement that was attempted resulted in frequency spectra with wrong dimensions.

Sakuma et al (1981) investigated runout in deep holes drilled under different misalignment conditions. The runout was measured on holes drilled with a misaligned guide bushing, They did not provide any information about the effect of the misalignment on the cutting forces.

As seen from the above review, the condition of the used machine has never been even mentioned especially the misalignment condition which yields discrepancy between the results reported by Griffith(1982, 1978), Chandarcheckar(1984), and Sakuma et al (1980a; 1980b; 1981). The misalignment between boring bar and the workpiece change the location of the tool and the contact points and this will lead to change the rake angle and flank angle. This lead to a large effect on the cutting forces, dynamics of the cutting process, the tool wear which result in changing the whole picture.

2.6 RESEARCH OBJECTIVES

In view of the above, the ultimate objectives of this investigation are:

1. Proposing a new model of chip formation which is not limited by the most assumptions usually build in the single shear plane, flow region and parallel sided

shear zone models and in the same time capable of relating the cutting forces, tool-workpiece and temperature to the cutting speed, feed, tool geometry and properties of the workpiece material. The proposed model involves the development of the shear zone model with parallel boundaries. This model have been developed by applying the continuum mechanics to the analysis of the chip formation zone.

2. Studying a thermomechanical approach to predict the shear stress in the shear zone. According to this model, the yield shear stress in the shear zone is temperature-dependent and decrease at a definite rate as temperature increases. This approach generalizes the effect of temperature on the yield shear stress in the shear zone.

3. Providing an analytical formulation of a tool cutting force system, examining the characteristics of the cutting process and deriving a steady-state force model using the shear zone model with parallel boundaries.

4. Extending the steady-state cutting forces model to be applicable for the deep hole machining process.

5. Deriving a dynamic model based on the proposed steady-state cutting force model to characterize the wave removing cutting process.

6. Verifying the proposed models experimentally. To achieve this goal the following steps have been performed:-

   a. Proposing a new methodology to align the machine such that the misalignment between the tool and the workpiece is near zero to make sure that the measured forces are not affected by misalignment. To quantify the effect of misalignment on the cutting forces, the tool

has been deliberately misaligned where the misalignment values have been measured using a low cost laser-camera based system and the forces have been measured using the Fast Fourier Transformation (FFT) Analyzer.

b. Validating steady-state cutting force model by measuring the forces for three different materials and different cutting conditions.

c. Validating the dynamic force model by measuring the forces for a wavy workpiece for different cutting conditions.

d. Monitoring and investigating the chip formation by measuring the cutting forces signature using the FFT

e. Studying the morphology of the formed chip by investigation its structure and micro hardness distributions..

f. Designing a quick stop device to freeze the process of the chip formation then investigating the structure of the partially formed chip.

3

MECHANICS OF CHIP FORMATION USING SHEAR ZONE MODEL WITH PARALLEL BOUNDARIES

The proposed approach involves the development of the shear zone model with parallel boundaries, as well as the analysis of the basic relationship of metal cutting (Hayajneh et al, 1996). The concept of the shear zone with parallel boundaries has been proposed many years ago(Kececloglu, 1960, Oxley and Welsh, 1963) and a strong experimental evidence of such a shape is provided by Spaans (1972). However, it was assumed that both the shear stress and the normal stress are constant within the deformation zone limits that evidently is in contradiction with mechanics of materials (Dieter, 1986).

3.1 ANALYSIS OF THE CONTINUITY CONDITION

The proposed model is shown in Figures 3.1a , 3.2a, and 3.3a for different rake angles, where the tool is single-point that is characterized by the rake angle α and intensive shear action is created on the metal ahead of the tool as a result of the applied force. A cut of layer t turns into a chip of thickness t_1 as a result of shear action in a narrow zone that runs from the cutting edge of the tool to the work piece-chip free surface. This zone is designated by the region *ABCD* with parallel boundaries occurring at a shear angle φ. In terms of plane strain slip-line field theory, the continuity condition can be written as follows (Keceloglu, 1960; Johnson et al, 1982).

$$\frac{\partial v_x}{\partial x}+\frac{\partial v_y}{\partial y}=0 \tag{3.1}$$

This condition can be simplified by using the known fact that the upper boundary of the shear zone is a slip-line. It is known that for velocities v_A and v_B, tangent to the mutual perpendicular slip-lines A and B as shown in Figure 3.4, the Geiringer equations are valid (Fredental and Geiringer, 1962):

$$dv_A - v_B d\varphi_A = 0 \tag{3.2}$$

$$dv_B + v_A d\varphi_B = 0 \tag{3.3}$$

Since the upper boundary of the shear zone is straight line, $d\varphi_A = 0$. Then, equation (3.2) becomes

$$dv_A = 0 \rightarrow v_A = constant \tag{3.4}$$

Hence, the velocity along a straight slip-line is constant and this leads to

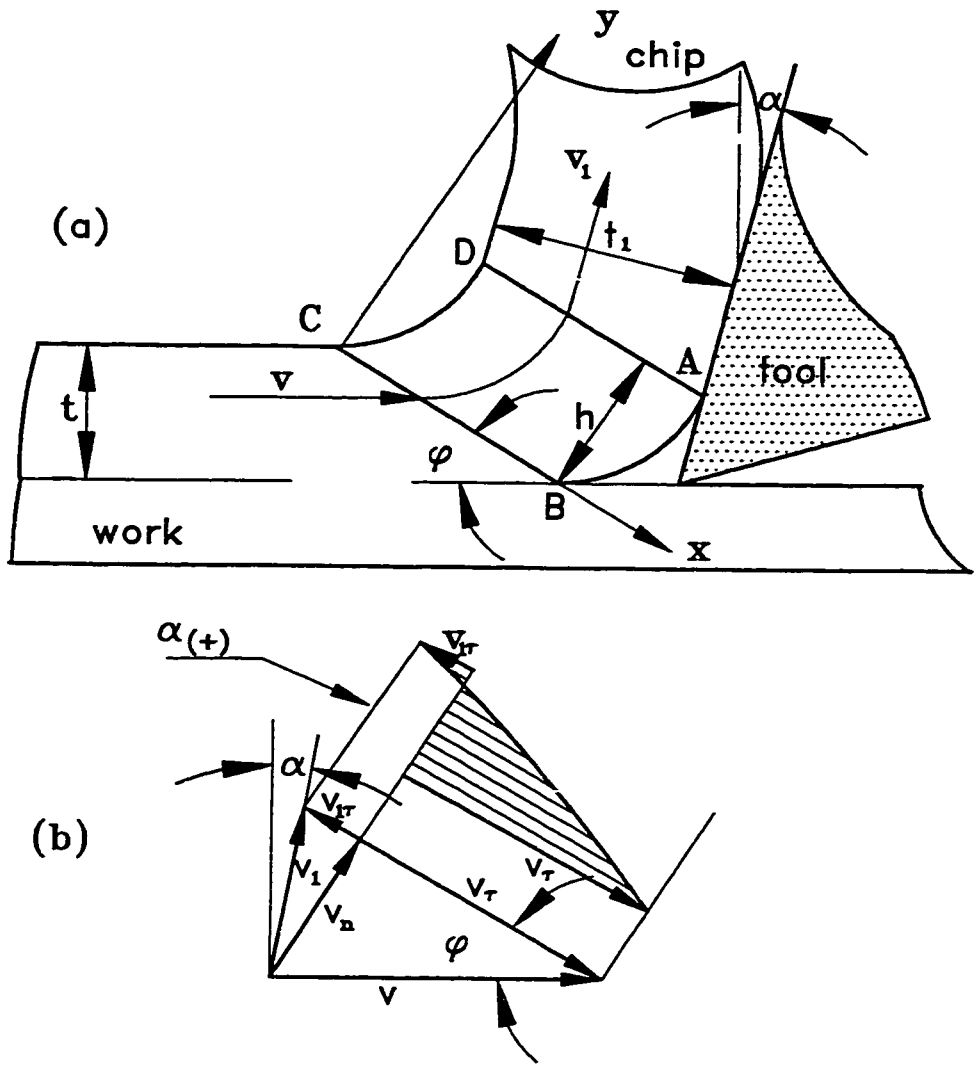

Figure 3.1: Parallel boundaries shear zone model for a positive rake angle: (a) the model (b) the velocity diagram.

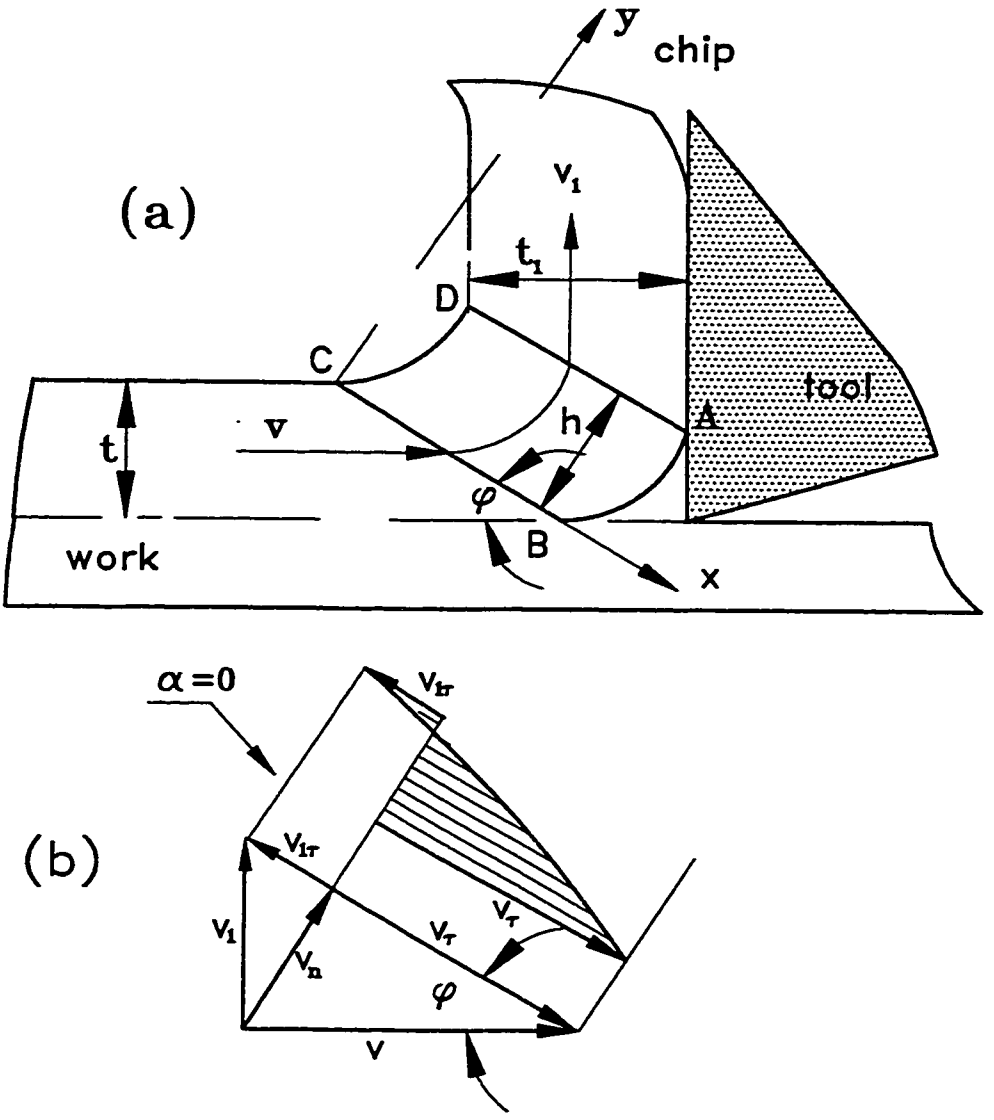

Figure 3.2: Parallel boundaries shear zone model for zero rake angle: (a) the model (b) the velocity diagram.

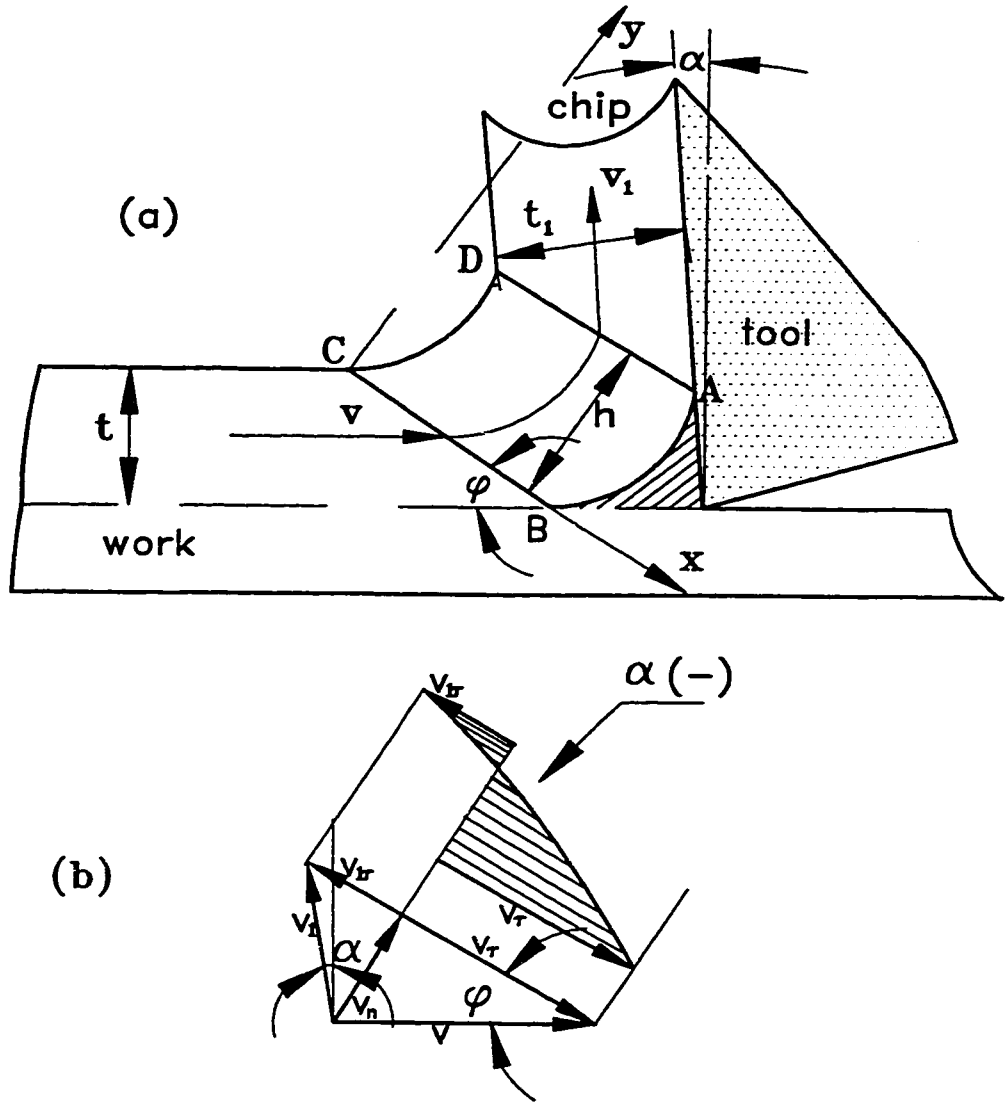

Figure 3.3: Parallel boundaries shear zone model for a negative rake angle: (a) the model (b) the velocity diagram.

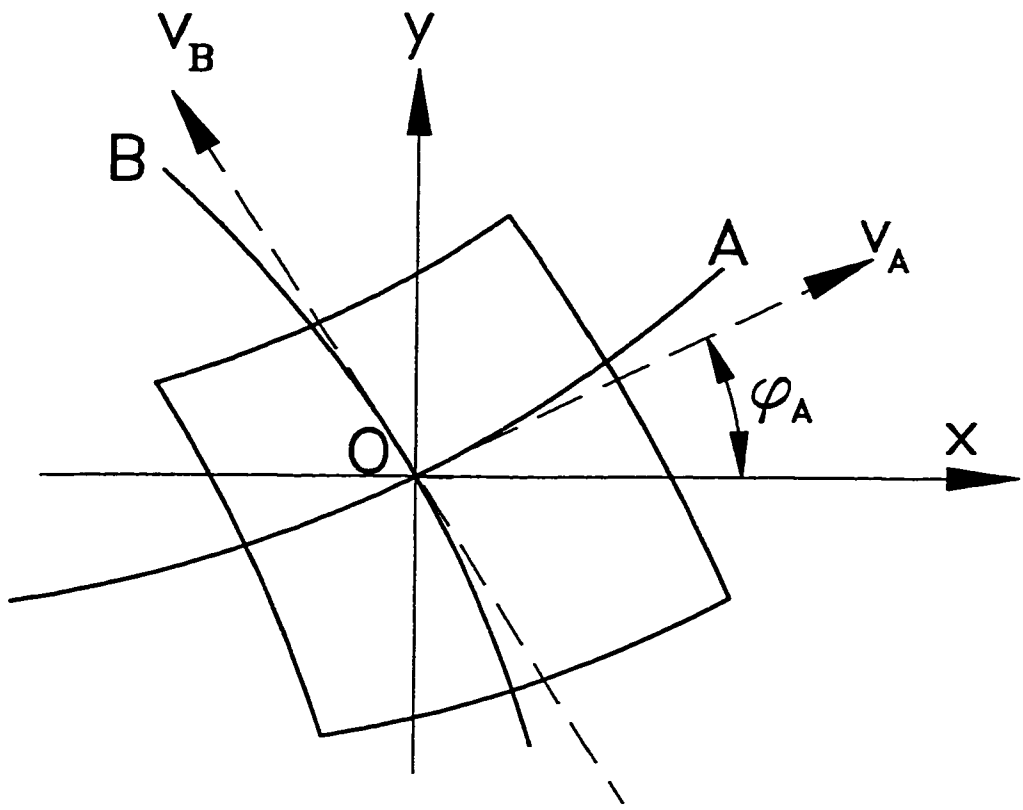

Figure 3.4: Location of the tangent velocities relative to the slip-lines.

$$\frac{\partial v_x}{\partial x}=0 \tag{3.5}$$

and equation (3.1) becomes

$$\frac{\partial v_y}{\partial y}=0 \rightarrow v_y=constant \rightarrow proj._y v=proj._y v_1 \tag{3.6}$$

Since v_y= constant, then from equation (3.3) it can be concluded that $dv_B = 0$. Therefore, the following equation can be written

$$d\varphi_B=0 \rightarrow \varphi_B=constant \tag{3.7}$$

Hence, the second family of the slip-lines is a set of straight lines. Due to the orthogonality of the slip-lines, the second deformation zone with parallel slip-lines is attached to the straight upper boundary. The condition (3.6) can be rewritten in the following form

$$v\sin\varphi=v_1\cos(\varphi-\alpha) \tag{3.8}$$

The ratio of velocities v and v_1, or the ratio of the length of cut L_p and the chip length L_c are known as the chip compression ratio ζ which can be written as (Zorev, 1966):

$$\frac{v}{v_1}=\frac{v\Delta t}{v_1\Delta t}=\frac{L_p}{L_c}=\zeta=\frac{\cos(\varphi-\alpha)}{\sin\varphi} \tag{3.9}$$

Therefore, this well-known equation is another form of the continuity condition. However, this equation shows the ways by which the chip compression ratio can be determined experimentally (Zorev, 1966; Astakhov, 1983). It follows from previous considerations that equation (3.9) is still valid for any accepted shape of the shear zone with a straight upper boundary. This non-dimensional parameter (a compression ratio) is widely

used in metal cutting studies but it should be emphasized here that the chip compression ratio approach is valid not only for conditions of two-dimensional machining but also for three-dimensional machining too and that the compression ratio does not depend on the shape of the cross-section of the chip.

3.2 PERMISSIBLE VELOCITIES AND DISPLACEMENTS IN THE SHEAR ZONE

According to the continuity condition (3.6), the boundary conditions for the tangential and normal velocity components (Figures 3.1b, 3.2b, and 3.3b) are:

$$v_x=\begin{pmatrix} v_\tau = v\cos\varphi\ , & y=0 \\ v_{1\tau}=-v_1\sin(\varphi-\alpha)\ , & y=h \end{pmatrix} \qquad (3.10)$$

$$v_y=v_n=v\sin\varphi$$

The component of the work piece velocity v_τ and the component of chip velocity $v_{1\tau}$ with respect to the shear zone can have either the same or the opposite direction according to the shear angle φ and the rake angle α. The difference between the velocities v_τ and $v_{1\tau}$ defines the discontinuity v_2 of the tangential velocity v_x with respect to the shear zone:

$$v_2=v_\tau-v_{1\tau}=v\frac{\cos\alpha}{\cos(\varphi-\alpha)} \qquad (3.11)$$

The discontinuity v_2 of the tangential velocity v_x during the transformation of a deformed fragment from the work piece into the chip should be considered as an inherent feature of the shear plane model in the cutting process. In practice, the shear zone has a certain width h in which the continuous transformation of the velocity v_x from v_τ to $v_{1\tau}$ takes place. Thus, this transformation should be approximated by the suitable continuous

transition curve justifying the boundary conditions (3.10) as shown in Figures 3.1b, 3.2b, and 3.3b. Since the slip-lines are straight lines, the velocity v_x depends on the y coordinate only. The law governing this dependence is unknown. However, using the experimental data and existing experience (Kececloglu, 1960; Poletica, 1976; Trent, 1991; Bobrov, 1984; Scrutton, 1968; The, 1975), the curve $v_x(y)$ can be approximated by the following analytical function:

$$v_x(y)=v_\tau-v_2\left(\frac{y}{h}\right)^n \tag{3.12}$$

where n is a parameter characterizing the non-uniform distribution of the tangential velocity in the shear zone.

The effect of n on velocity ratio v_x/v_n is shown in Figures (3.5), (3.6), and (3.7) for different chip compression ratios. These figures reveal that the shear zone is composed of two regions. The first region is termed as the "wide region" where the tangential velocity v_x changes at a small rate. The second region is termed as the "narrow region " where the tangential velocity v_x changes at a high rate. Also, it can be seen that as n increases, the "wide region" becomes larger and the " narrow region" becomes smaller. This conclusion is in a good agreement with the results of the study of coordinate grid deformation (Poletica, 1976; Bobrov, 1984). The narrow region where a significant change of the tangential velocity takes place may be thought as the region of the discontinuity of this velocity. This model plays a principal role in the foregoing analysis because both the state of stress and the state of strain and the resistance of the work material to cutting in this " narrow region" are very specific.

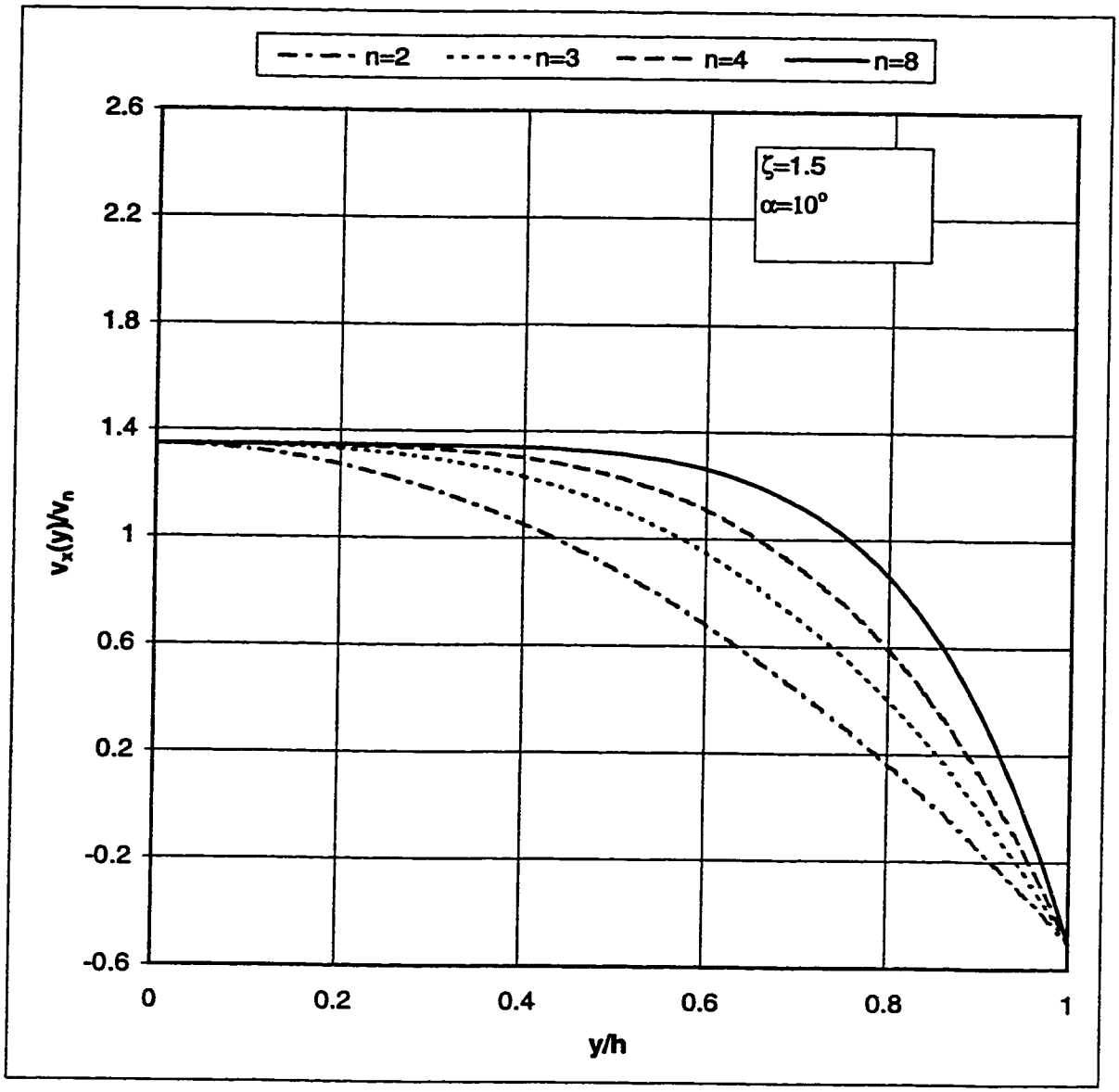

Figure 3.5: Effect of n on the velocity ratio $v_x(y)/v_n$ for $\alpha=10^\circ$ and $\zeta=1.5$.

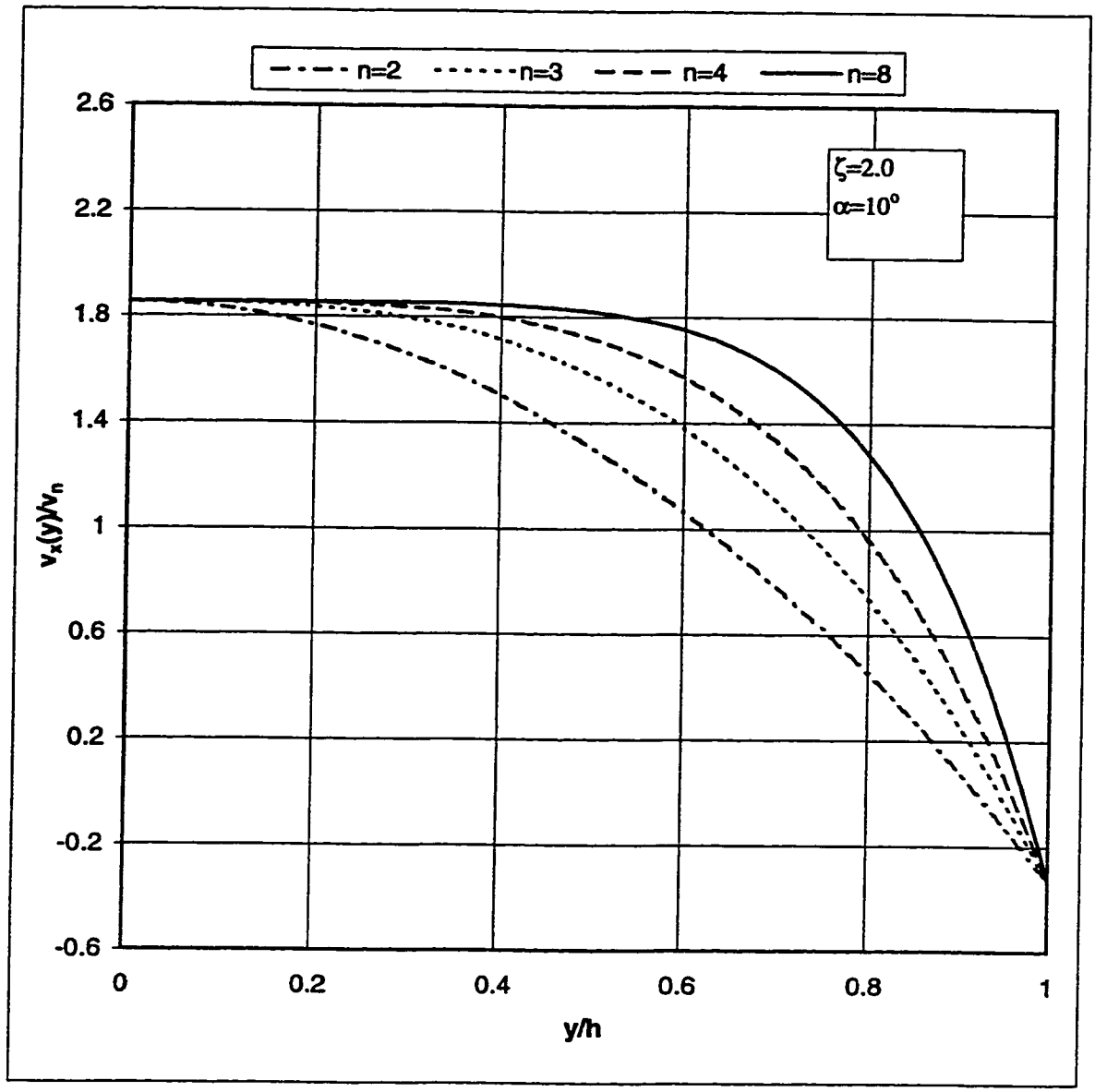

Figure 3.6: Effect of n on the velocity ratio $v_x(y)/v_n$ for $\alpha=10^\circ$ and $\zeta=2.0$.

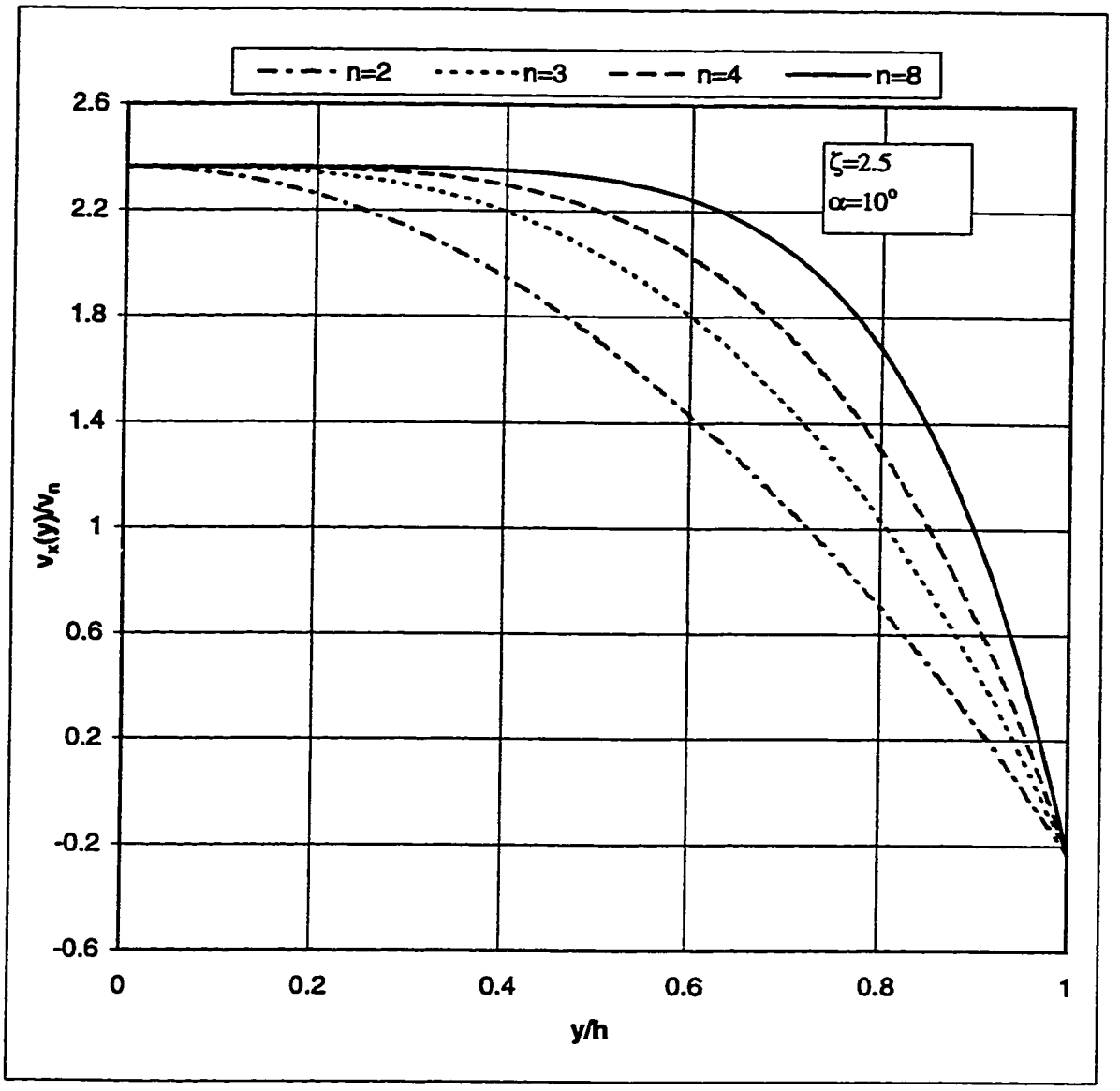

Figure 3.7: Effect of n on the velocity ratio $v_x(y)/v_n$ for $\alpha=10^\circ$ and $\zeta=2.5$.

Integration of equation (3.12) gives the displacement $u_x(y)$ reached at y as:

$$u_x(y)=\int_0^{y/v_n} v_x(\frac{y}{v_n})d(\frac{y}{v_n})=\frac{v_\tau}{v_n}y-\frac{v_2}{v_n}\frac{h}{n+1}\left(\frac{y}{h}\right)^{n+1} \tag{3.13}$$

The velocity $v_{1\tau}$ and the velocity v_τ have opposite direction because the shear angle φ is usually larger than the rake angle γ. Therefore, as shown in Figure 3.8, the function $u_x(y)$ has the maximum (y^*, u^*_x) within the deformation zone. By increasing n, this maximum is shifting closer to the upper boundary.

Function $u_x(y)$ defines the streamlines in the deformation zone bounded by parallel boundaries. Thus, it describes the transition line *CDE* between the free surface of the work piece and the chip as shown in Figure 3.8. The tangents to *CDE* at their intersection points with the lower and upper boundaries are collinear with the velocity v and the velocity v_1.

It is known that the streamlines in the deformation zone are equidistant lines (Zorev, 1966; Poletica, 1976). Therefore, to justify the continuity condition, the zone *OAB* of heavy deformation should be attached to the rake surface as shown in Figure 3.8. This zone is separated from the deformation zone by the streamline line *AB*, from the workpiece by the line *OB* (h_0)and from the rake surface by the line *OA* (c_0).

To calculate lengths of *OA* and *OB*, consider the equations for tangents *CF* and *EF*:

$$x_{CF}=y\cot\varphi \tag{3.14}$$

$$x_{EF}=u_x(h)-(y-h)\tan(\varphi-\alpha) \tag{3.15}$$

From the tangents intersection at point F which has the coordinate y_F, it can be written:

$$u_x(h)=[\cot\varphi+\tan(\varphi-\alpha)]y_F-h\tan(\varphi-\alpha) \tag{3.16}$$

it follows from equations (3.14-3.16):

$$\frac{y_F}{h}=\frac{v_\tau}{v_2}+\frac{1}{n-1}\tan(\varphi-\alpha)=\frac{\cot\varphi}{\gamma}+\tan(\varphi-\alpha)-\frac{1}{n-1}= \tan(\varphi-\alpha)\left(1-\frac{1}{\gamma}\right)+1-\frac{1}{n+1} \tag{3.17}$$

where γ is the shear strain.

In particular case $\alpha \approx \varphi$ for a large rake angle, equation (3.17) can be further simplified:

$$\frac{y_F}{h}\Big|_{\varphi=\alpha}=1-\frac{1}{n+1} \tag{3.18}$$

It follows from equation (3.18) that with increasing n the shear plane approaches the upper boundary of the deformation zone. At that point, the shape of the transition curve changes dramatically as shown in Figure 3.9. For large n, a major part of this curve coincides with the tangent at the initial point C. This phenomenon can be considered as the reduction of the transition curve length. From observations of the free surface of the workpiece and chip, it follows that, the change of the transition curve shape and position of the shear plane with increasing n corresponds to the increase in the cutting speed.

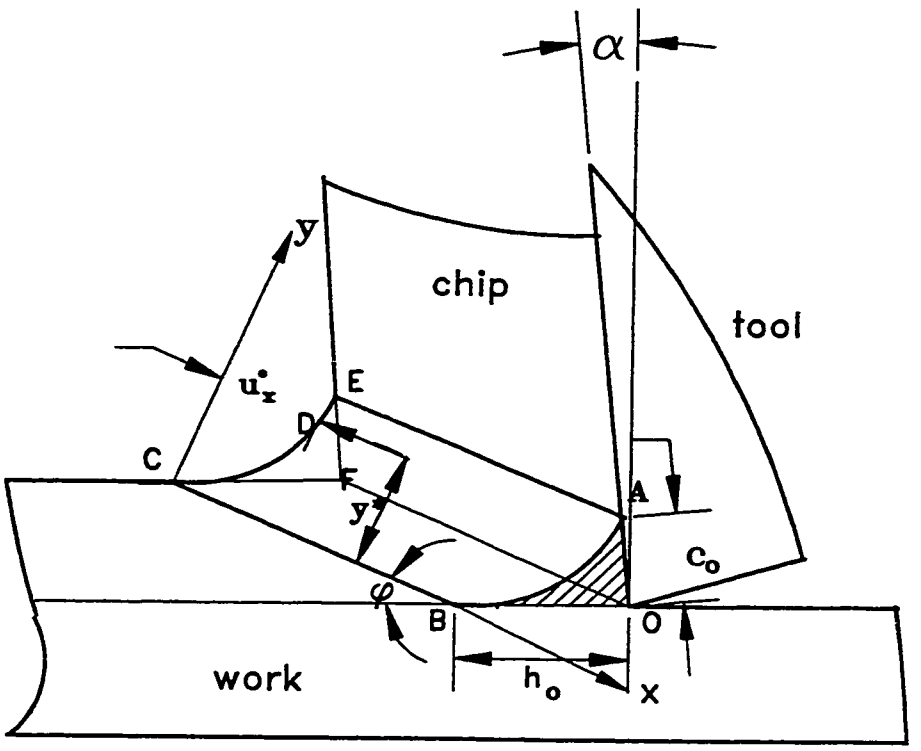

Figure 3.8: A model of a chip formation zone with parallel boundaries.

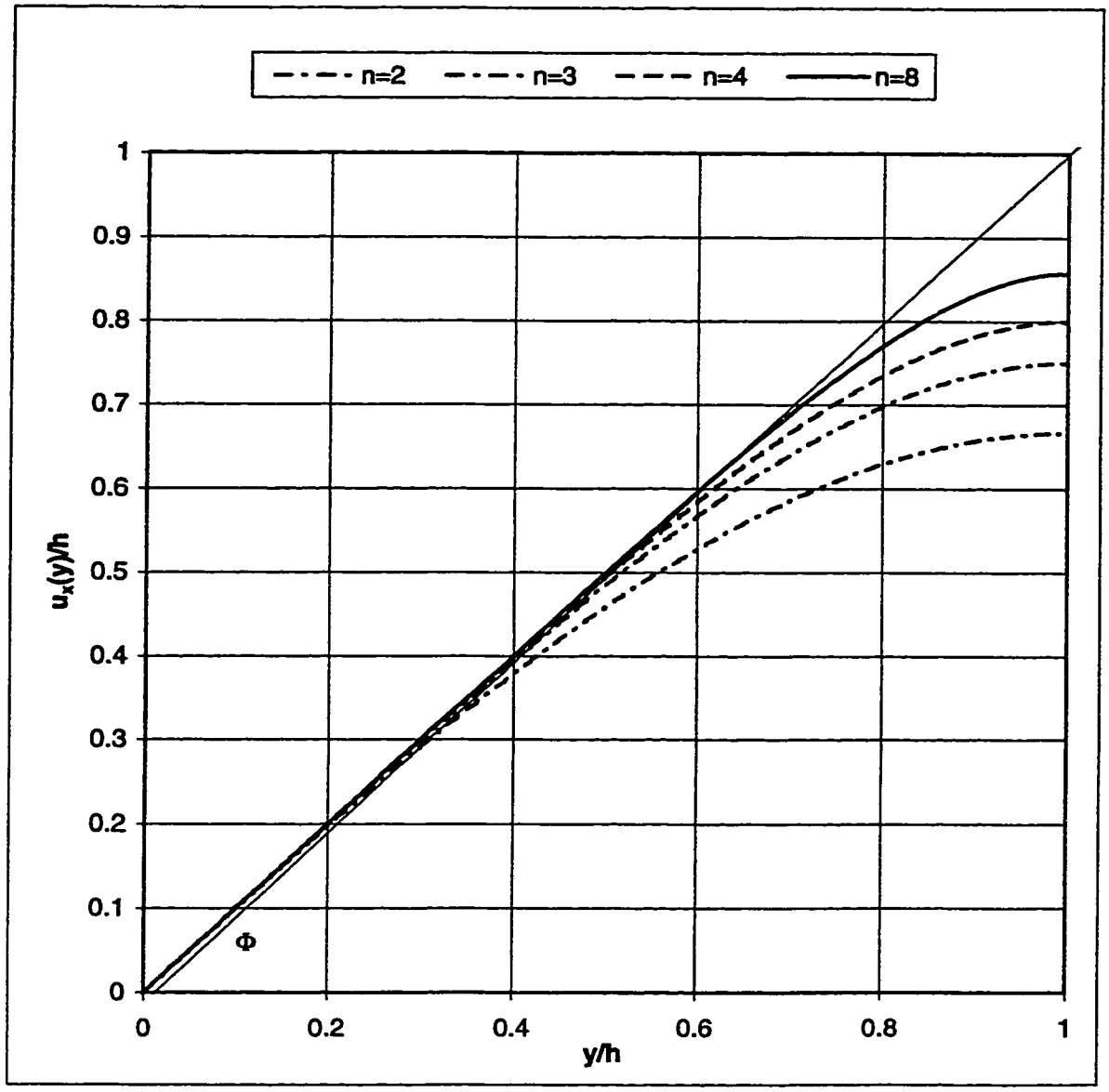

Figure 3.9: Transition curves for different n.

Also, it can be deduced from Figure 3.8 that

$$c_0=\frac{h-y_F}{\cos(\varphi-\alpha)};\ \frac{c_0}{h}=\frac{1}{\cos(\varphi-\alpha)}\left(1-\frac{y_F}{h}\right)\approx\frac{1}{n+1} \tag{3.19}$$

and

$$h_0=\frac{y_F}{\sin\varphi};\ \frac{h_0}{h}=\frac{1}{\sin\varphi}\frac{y_F}{h}\approx\frac{1}{\sin\varphi}\left(1-\frac{1}{n+1}\right) \tag{3.20}$$

Taking into account that $h/t \approx 0.3 \ldots 0.5$ and $\sin\varphi$ changes within the same limits, the following approximations for c_0 and h_0 can be obtained

$$h_0\approx t \tag{3.21}$$

,

$$c_0\approx 0.1t \tag{3.22}$$

The region $OB = h_0$ plays the same role in the cutting theory as the wear-land on the flank surface. Therefore, this region should be taken into consideration in the calculation of temperatures and forces on the flank surface. The region OA on the rake surface reduces the actual contact tool-chip length. For small a this region does not play any significant role and can be ignored. However, when a becomes larger, this region plays a significant role in the mechanics of metal cutting because it causes the formation of the built-up edge (BUE).

3.3 DISTRIBUTION OF DEFORMATION IN THE CHIP FORMATION ZONE

In studying the deformation in metal cutting the main attention is usually paid to the deformation rate which takes place in the shear zone. The rate of deformation is closely related to the displacement and the velocities. To calculate the deformation rate a number of different approaches and formulas were proposed (Boothroyd and Knight, 1989). The known approaches are based on the known velocity diagram (Merchant, 1945) which has to be corrected as shown previously. Therefore, the deformation rate for the model of deformation zone with parallel boundaries requires additional study.

In many studies of metal cutting, the deformation in the chip formation zone is characterized by the shear strain calculated as:

$$\gamma=\frac{v_2}{v_n}=\frac{\cos\alpha}{\cos(\varphi-\alpha)\sin\varphi}=\frac{\zeta^2-2\zeta\sin\alpha+1}{\zeta\cos\alpha} \qquad (3.23)$$

The reported derivation of this formula is not strict enough (Rozenberg, 1956). The study of deformation using the grid method refutes the assumption that the deformation in the shear zone is a simple shear (Bhattacharyya and Ham, 1969). According to experimental data, the deformation in metal cutting is a complex deformation which cannot be characterized by the simple shear strain.

Under accepted model of deformation shown in Figures 3.1, 3.2, and 3.3, the tensor of infinitely small increments of deformations can be represented by only two (which are equal due to the symmetry of the tensor) non-zero shear strain components.

The other two components of that tensor are equal to zero, that is

$$d\varepsilon_{xx}=\frac{\partial}{\partial x}(du_x)=0$$
$$d\dot{\varepsilon}_{xx}=\frac{\partial}{\partial x}(dv_x)=0 \tag{3.24}$$

and

$$d\varepsilon_{yy}=\frac{\partial}{\partial y}(du_y)=0$$
$$d\dot{\varepsilon}_{yy}=\frac{\partial}{\partial y}(dv_y)=0 \tag{3.25}$$

Since the normal velocity v_n is constant across the shear zone and the slip-lines are straight, the displacement increment along the x-coordinate depends only on y-coordinate.

Since $d\varepsilon_{xx}$ and $d\varepsilon_{yy}$ are equal to zero, the corresponding components of final deformation are also equal to zero. Therefore, the maximum shear strain rate can be expressed as

$$\dot{\gamma}_{max}=\frac{dv_x}{dy}+\frac{dv_y}{dx}=v\frac{\cos\alpha}{\cos(\varphi-\alpha)}\frac{n}{h}\left(\frac{y}{h}\right)^{n-1} \tag{3.26}$$

To calculate the engineering shear strain, consider the displacements in the deformation zone with the parallel boundaries shown in Figure 3.10. The x-coordinate coincides with the direction of shearing and the y-coordinate is in the direction of v_n. In this coordinate system, the displacement $u_x(y)$ becomes:

$$u_x(y)=\frac{v_\tau}{v_n}y-\frac{v_2}{v_n}\frac{h}{n+1}\left(\frac{y}{h}\right)^{n+1} \tag{3.27}$$

According to the theory of deformation, an infinitely small increment of angular

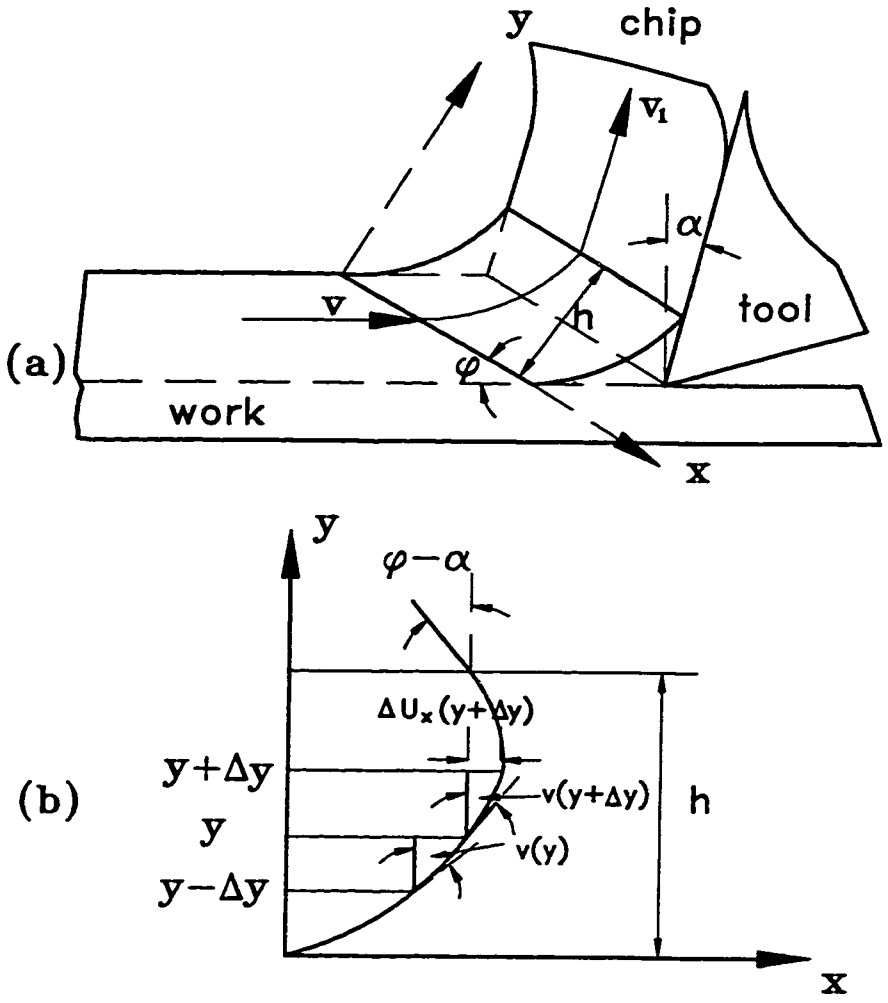

Figure 3.10: (a) The model of the chip formation zone and (b) the trajectory of a particle in this zone.

deformation can be defined as the sum of partial strain increments along the x and y coordinates (Fredental and Geiringer, 1962):

$$d\gamma_{xy}=\frac{\partial}{\partial y}[du_x(y)]=\frac{d}{dy}[du_x(y)]=\frac{n\,v_2}{h\,v_n}\left(\frac{y}{h}\right)^{n-1}dy \tag{3.28}$$

The shear strain $\gamma(y)$ in the chip formation zone may be obtained by the integration of equation (3.28) which gives:

$$\gamma(y)=\int_0^y\frac{n\,v_2}{h\,v_n}\left(\frac{y}{h}\right)^{n-1}dy=\frac{v_2}{v_n}\left(\frac{y}{h}\right)^{n} \tag{3.29}$$

The final engineering shear strain $\gamma(h)$, when $y = h$, coincides with the strain defined by equation (3.23) which is commonly used in practice and can be written in the following form:

$$\gamma(h)=\frac{v_2}{v_n}=\frac{\cos\alpha}{\cos(\varphi-\alpha)\sin\varphi} \tag{3.30}$$

It follows from equation (3.30) that the final engineering shear strain $\gamma(h)$ (when the deformation of work material is considered in the zone with parallel boundaries) does not depend neither on the width of the zone h, nor on n, but is entirely defined by the values of the velocity break v_2 and of the normal velocity v_n. Since $\gamma(h)$ does not depend on n, it can be concluded that equation (3.29) is also valid for the model with single shear plane, which can be considered as a limiting case of the model with parallel boundaries when $n \to 0$. Figure 3.11 reveals the function (3.29) as well as the experimental results obtained in cutting of copper with small cutting speeds (Kufarev,1970). The comparison between the calculated and experimental results shows that the experimental results can be well approximated by

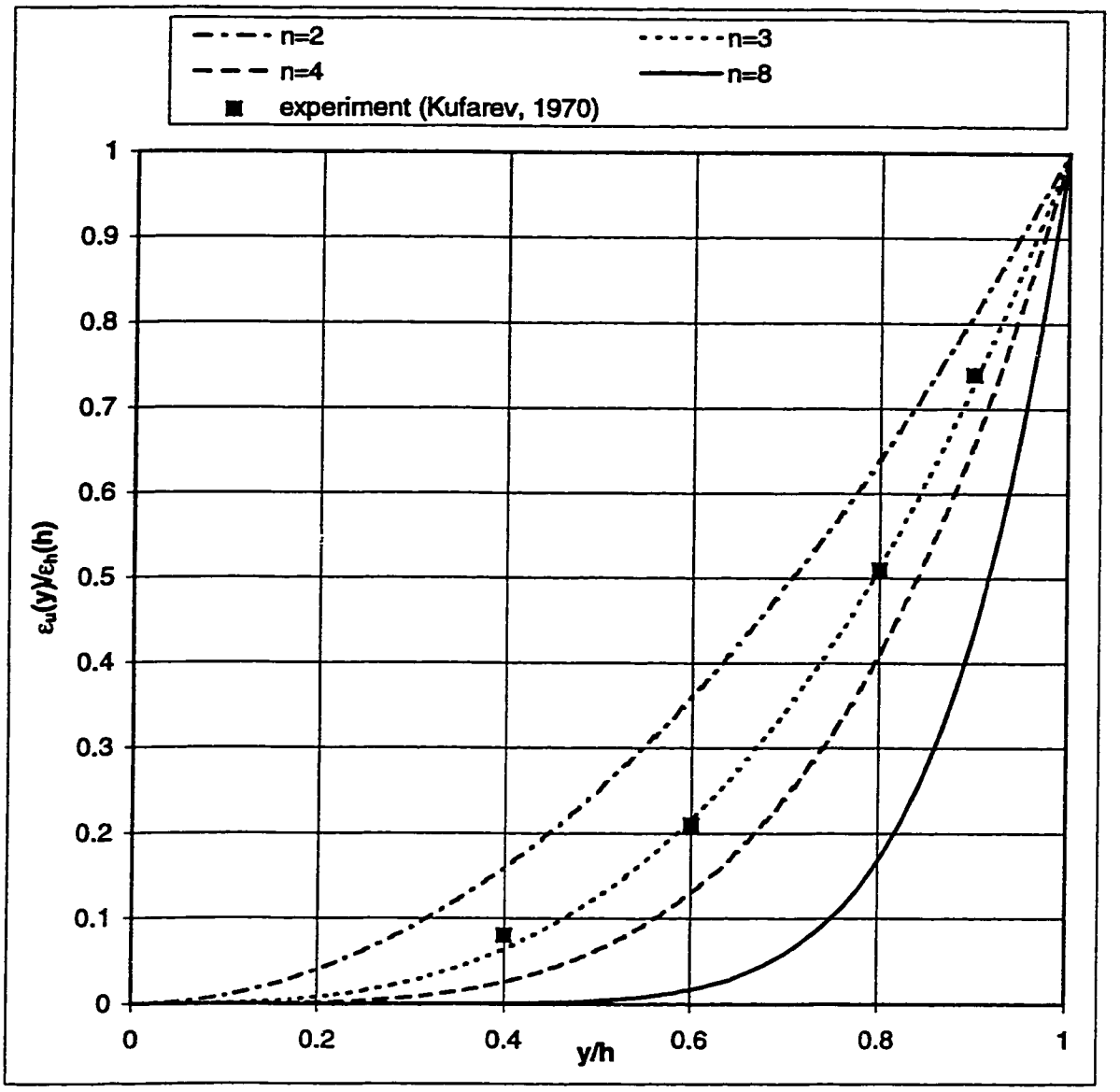

Figure 3.11: Distribution of the true shear strain along the width of the shear zone.

function (3.29) when n=3.

As it follows from Figure 3.11, a major part of the plastic deformation takes place in the closed neighborhood of the upper boundary of the deformation zone. The increase in cutting speed increases this tendency.

The conditional separation of the deformation zone into two parts as mentioned before, assumes that conditional boundary exists between "wide" and "narrow" parts of this zone. The position of this boundary should be estimated quantitatively. Such an estimation requires a certain idealization of a real cutting process. The objective of this idealization is to define the resistance of the work material to cutting. Because the yield shear stress in cutting is correlated to the mechanical characteristics in tensile tests, the value of engineering strain, which is equal to the intensity of angular deformation in a tensile test at the instant of necking initiation, is taken as a criterion of separation between "wide" and "narrow" parts of the deformation zone. This criterion is already used by a number of investigators for the comparison of cutting and tensile tests.

When the elastic part of deformation is not considered, the failure shear strain γ_{fa} and failure strain ε_{fa} relationship may be taken as a criterion to define the boundary separated "wide" and "narrow" parts of the deformation zone:

$$\gamma_{fa} = \sqrt{3}\ln(1+\varepsilon_{fa}) \tag{3.31}$$

For the typical cutting conditions the final average strain $\gamma(h)$=2.5, and ε_{fa}=0.2. Therefore, as the first approximation, the deformation in the wide zone for the typical practical conditions is as large as 10-15% of the final strain. With an increase in the rake angle α and the failure strain of the work piece material, the part of deformation, which takes

place in the wide zone, is growing.

Assuming for particular case $\gamma_{fa}/\gamma(h)=0.12$ and using equation (3.29), the ratio h_1/h (h_1 is the size of the zone of the main deformations) as a function of n may be found as shown in Figure 3.12 :

$$\frac{h_1}{h}=1-\frac{y}{h}=1-\left(\frac{\gamma_{fa}}{\gamma(h)}\right)^{\frac{1}{n}} \tag{3.32}$$

Examination of Figure 3.12 shows that with increasing n the size of h_1 becomes smaller. The same tendency was observed with increase in the cutting speed. Changing the cutting speed from 0.3 to 3 m/s leads to the reduction of the deformation zone by half. In a conclusion, it can be stated that, for practical conditions of machining of steels by the carbide tools, the value of n =4-8 is a good approximation. The shear strain rate and its distribution in the deformation zone play a vital role in metal cutting studies. This rate can be calculated as :

$$\dot{\gamma}(y)=\frac{d\gamma(y)}{dy}\frac{dy}{dt}=\frac{v_2}{h}n\left(\frac{y}{h}\right)^{n-1} \tag{3.33}$$

where $y=v_n t$.

Taking the width of the deformation zone, h, approximately equal to the half of uncut chip thickness, t, it can be concluded that, for the typical cutting conditions, the term v_2/h is of the order of 10^4 sec^{-1} as shown in Figure 3.13 (in logarithmic scale) shows the distribution of the strain rate in the deformation zone for different n. It can be seen that the strain rate at the border of the preliminary and final deformation zone reaches high values 10^4 sec^{-1} but almost, does not depend on n when n = 4-8. Therefore, it is not necessary

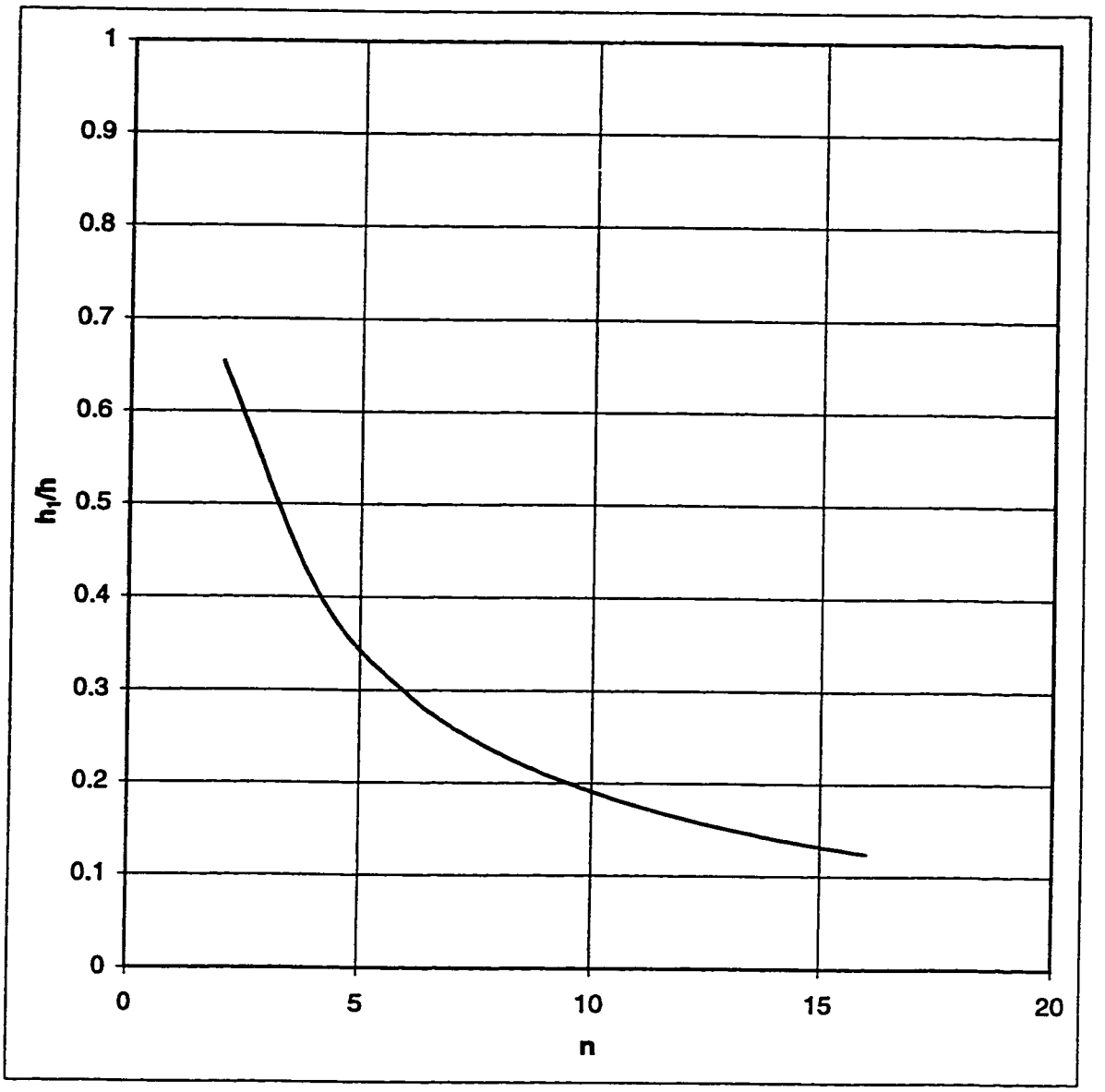

Figure 3.12: h_1/h vs. n under $\varepsilon^*/\varepsilon_u$ =0.12.

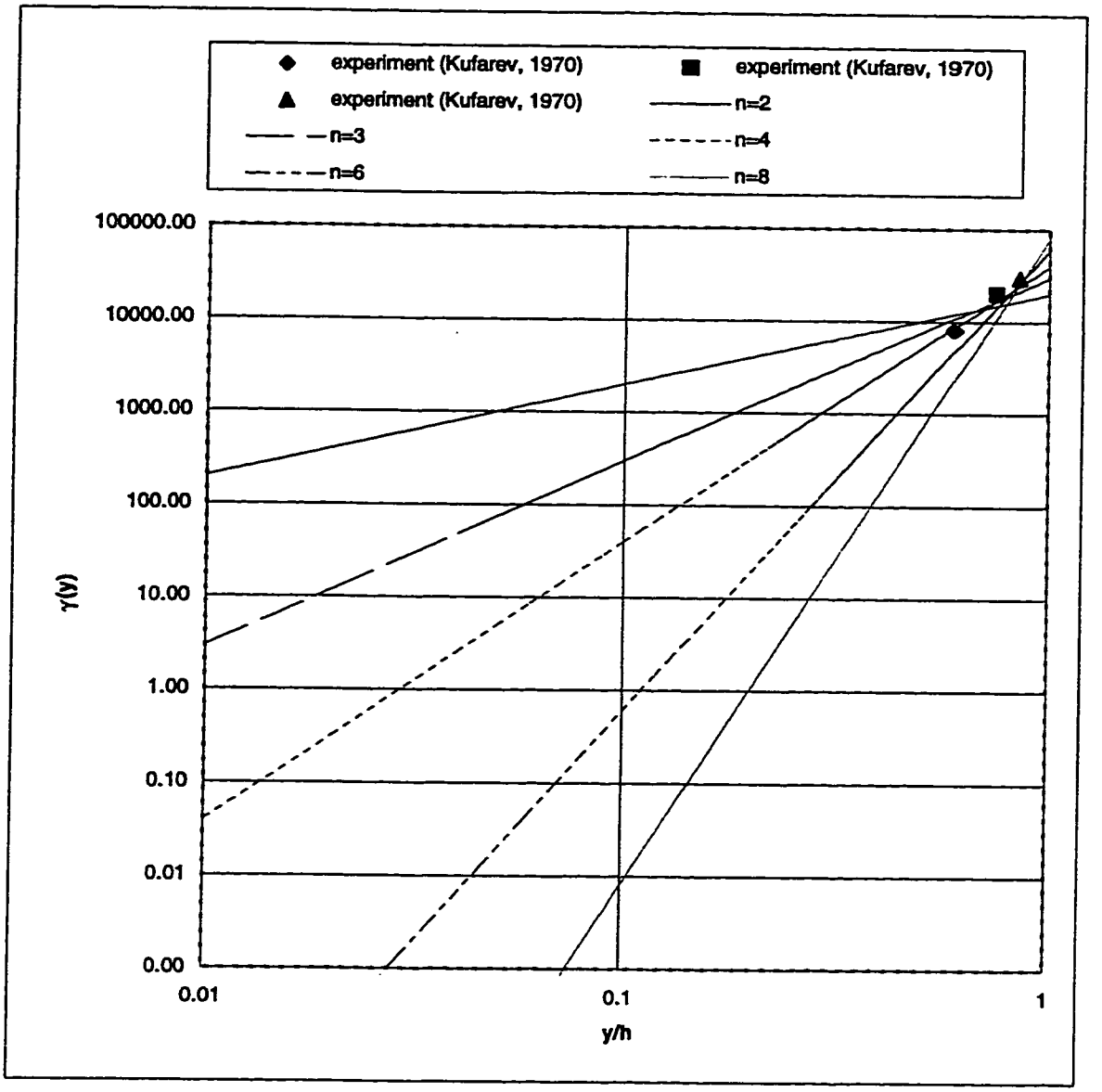

Figure 3.13: Distribution of the deformation rate in the deformation zone under $v_2/h=10^4$ s^{-1} and different n. The points correspond to the deformation rate at the border of the primary and final deformation.

to measure the values of n experimentally. The strain rate $\dot{\gamma}_{fa}$ at the border of the wide and final approximation zone is

$$\dot{\gamma}_{fa}=\frac{v_2}{h}n\left(\frac{\gamma_{fa}}{\gamma(h)}\right)^{\frac{n-1}{n}}\approx(0.8-1.2)\frac{v_2}{h} \tag{3.34}$$

It can be seen from equation (3.34) that for the practically reasonable regimes, both the values of v_2/h and the failure strain rate are of the same order.

The strain rate reaches its maximum value when it approaches the upper border of the deformation zone and it reaches

$$\dot{\gamma}(h)=\frac{v_2}{h}n \tag{3.35}$$

It follows from equation (3.35) that when $h\to 0$, the strain rate $\dot{\gamma}(h)\to\infty$. This model corresponds to one shear plane model and, to a big surprise, is not contradict with the mechanics of materials because, even under this extreme conditions, the inertia stress remains relatively small.

3.4 THERMOMECHANICAL MODEL FOR THE SHEAR STRESS IN THE PRIMARY AND SECONDARY SHEAR ZONES

The thermomechanical model of the work piece material resistance to cutting was first proposed by Kushnir (1982) and modified by Astakhov (1994). According to the thermomechanical model, the flow shear stress of the workpiece material is temperature-dependant and decreases at a defined rate as temperature increases. Summarized

to measure the values of n experimentally. The strain rate $\dot{\gamma}_{fa}$ at the border of the wide and final approximation zone is

$$\dot{\gamma}_{fa}=\frac{v_2}{h}n\left(\frac{\gamma_{fa}}{\gamma(h)}\right)^{\frac{n-1}{n}}\approx(0.8-1.2)\frac{v_2}{h} \tag{3.34}$$

It can be seen from equation (3.34) that for the practically reasonable regimes, both the values of v_2/h and the failure strain rate are of the same order.

The strain rate reaches its maximum value when it approaches the upper border of the deformation zone and it reaches

$$\dot{\gamma}(h)=\frac{v_2}{h}n \tag{3.35}$$

It follows from equation (3.35) that when $h\to 0$, the strain rate $\dot{\gamma}(h)\to\infty$. This model corresponds to one shear plane model and, to a big surprise, is not contradict with the mechanics of materials because, even under this extreme conditions, the inertia stress remains relatively small.

3.4 THERMOMECHANICAL MODEL FOR THE SHEAR STRESS IN THE PRIMARY AND SECONDARY SHEAR ZONES

The thermomechanical model of the work piece material resistance to cutting was first proposed by Kushnir (1982) and modified by Astakhov (1994). According to the thermomechanical model, the flow shear stress of the workpiece material is temperature-dependant and decreases at a defined rate as temperature increases. Summarized

the experimental data for a wide range of the workpiece materials shown in Figure 3.17, reveals that this rate is a constant. The basic relationship of this model can be presented in the following form:

$$\tau=\sigma_{ult}(1-.0005T) \tag{3.36}$$

where τ is the yield shear stress of the workpiece in the shear zone (Mpa), σ_{ult} is the ultimate tensile strength of work piece material *(Mpa)* and T is the temperature in centigrade (C°). Analysis of reported studying temperature in metal cutting (Boothroyd, 1963; Kushner, 1982; Boothroyd and Knight, 1989; Oxley, 1989; Astakhov, 1992) shows that the average temperature in the shear zone, can be predicted by :

$$T_s=\frac{\sigma_{ult}\gamma}{\rho c_p} \tag{3.37}$$

where c_p is the specific heat capacity of the workpiece material and ρ the density of the workpiece material.

Substituting equation (3.37) into equation (3.36), the following equation can be obtained

$$\tau_s = \sigma_{ult}\left(1-0.0005\frac{\sigma_{ult}\dfrac{\cos\alpha}{\sin\varphi\cos(\varphi-\alpha)}}{c_v}\right) \tag{3.38}$$

The average temperature along the plastic part of the tool-chip interface, T_f, can be defined as (Kushner, 1982):

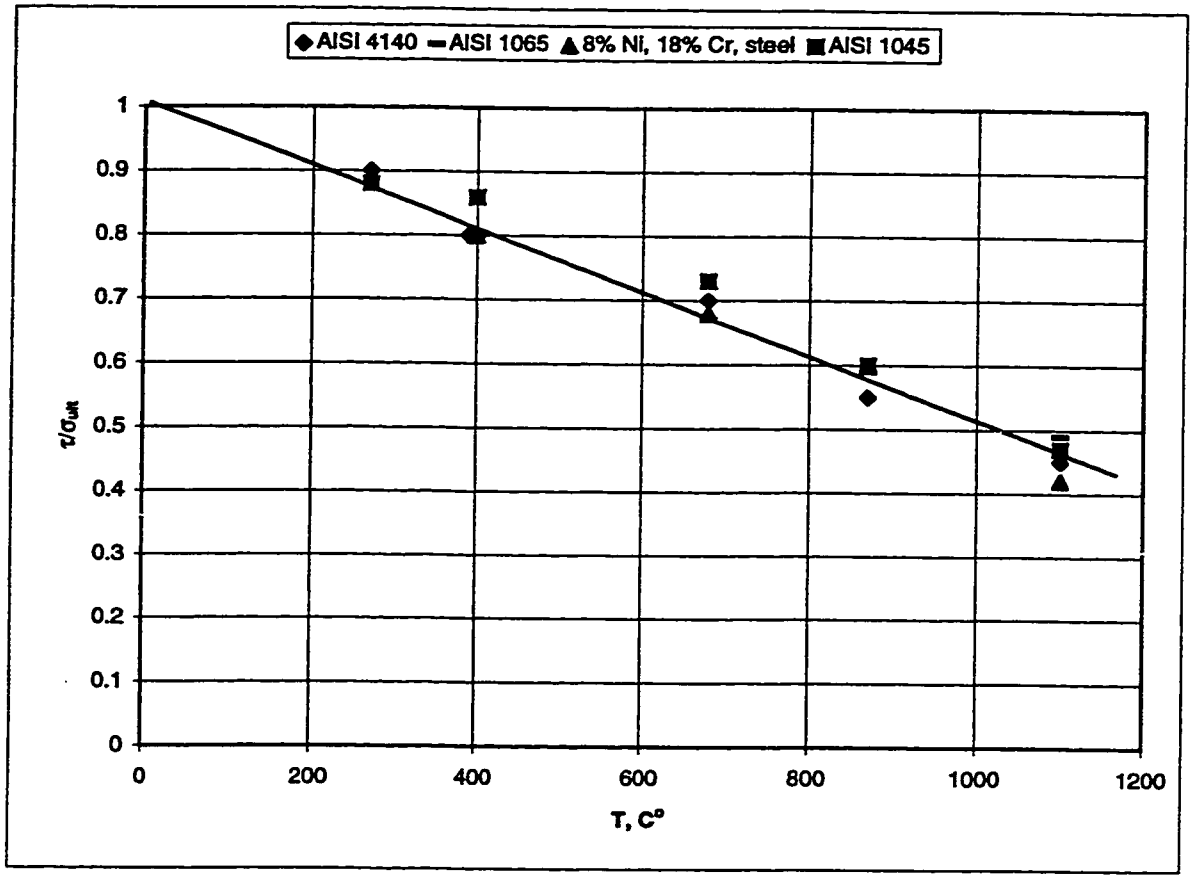

Figure 3.14: Effect of temperature on the ratio τ/σ_{ult} (Kushner, 1982).

$$T_f = 79\left(\frac{\tau_s}{100c_p}\right)^{.8}\left(\frac{l_{st}}{t\zeta}\right)^{.4}(Pe)^{.4} \tag{3.39}$$

where l_{st} is the length of the plastic part of the tool-chip contact length (m), ζ is the chip compression ratio, t is the uncut chip thickness (m) and Pe is the Peclet number which can be defined as follow:-

$$Pe = \frac{vt}{w} \tag{3.40}$$

where v is the cutting speed (m/s), t is the uncut chip thickness (m) and w is the thermal diffusiticity of the workpiece material (m^2/s). By substituting equation (3.40) into equation (3.39), it can be obtained:

$$T_f = 79\left(\frac{\tau_s}{100c_p}\right)^{0.8}\left(\frac{l_{st}}{t\zeta}\right)^{0.4}\left(\frac{vt}{w}\right)^{0.4} \tag{3.41}$$

3.5 SUMMARY

The shear zone model with parallel boundaries has been chosen as a model for mechanics of cutting and cutting force determination. The analysis leads to the following conclusions:

1. Two families of straight slip-lines constitute the deformation zone in metal cutting: one family is parallel and another is perpendicular to the straight upper boundary of this zone.
2. The well-known equation for the chip compression ratio is another form of the

continuity condition. This equation is valid for any shape of shear zone with a straight upper boundary.

3. The discontinuity of the tangential velocity (the component of the cutting speed which is parallel to the boundary of the shear zone) during the transformation of a deformed fragment from the work piece into the chip is an attribute of the shear plane model phenomenon in the cutting process. In practice, the shear zone always has a certain width, within which the continuous transformation of the velocity takes place. Therefore, the acceleration, strain and strain-rate in the shear zone with parallel boundaries are not uniformly distributed as thought before. The final true shear strain does not depends upon neither the zone's width, nor the exponent of non-uniform strain distribution of strain, but is entirely defined by the values of the discontinuity of the tangential velocity and normal velocity. Therefore, the shear plane model may be considered as a limiting case of the shear zone model with parallel boundaries.

4. Thermomechanical model of the work-material resistance to cutting defines the ratio of the yield shear stress (in the shear zone and in the plastic zone on the tool rake) to the ultimate tensile strength and it is a linear function of cutting temperature.

5. Based on this, shear zone a model for cutting force components is suggested as will be seen in the next chapter. To avoid the determination of friction angle, computation of the tangential force acting on the tool face is proposed.

4

STEADY-STATE CUTTING FORCE MODEL BASED ON THE SHEAR ZONE MODEL WITH PARALLEL BOUNDARIES AND ITS APPLICATION TO THE BTA PROCESS.

This chapter comprises the analytical evaluation of the steady-state force model which has been derived using the model of shear zone with parallel boundaries. Then this model has been applied to the deep hole machining process as typical orthogonal..

4.1 STEADY-STATE CUTTING FORCE MODEL

Theoretical determination of the cutting forces is one of the main concerns in metal cutting. The cutting force components acting along the corresponding axes, namely the cutting force F_c and the thrust force F_t can be determined from the following equation:

$$F_c = \frac{F_s \cos\alpha + F_f \sin\varphi}{\cos(\varphi - \alpha)}$$
$$F_t = \frac{F_f \cos\varphi - F_s \sin\alpha}{\cos(\varphi - \alpha)} \qquad (4.1)$$

where F_s is the shear force along the shear zone boundaries, F_f is the tangential force on the rake face, φ is the shear angle, and α is the rake angle. To calculate these components it is necessary to know shear force F_s in the shear zone and the tangential force F_f on the rake face. The shear force F_s can be calculated as:

$$F_s = \tau_s \frac{tb}{\sin\varphi} \qquad (4.2)$$

where τ_s is the shear flow stress in the shear zone; b is the width of cut; t is the uncut chip thickness; and φ is the shear angle.

It is also known that the shear flow stress of the workpiece material is temperature dependent and it decreases at a constant rate with temperature (Dieter, 1986). It has been shown by Kushner (1982) that for a vast variety of steels, the shear flow stress may be related to the ultimate tensile strength in terms of temperature as follows:

$$\tau = \sigma_{ult} (1 - 0.0005T) \qquad (4.3)$$

where τ is the shear flow stress of the workpiece material (Mpa), σ_{ult} is ultimate tensile strength of the workpiece material (Mpa) at 20 C^o and T is the temperature (C^o).

The temperature in the shear zone , T_s, can be defined as (Oxley 1989):

$$T_s = \frac{\sigma_{ult}\gamma}{c_v} \qquad (4.4)$$

where c_v is the specific heat capacity at constant volume of deformed material and γ is the final shear strain which is known to be (Merchant, 1945):

$$\gamma = \frac{\cos\alpha}{\sin\varphi\cos(\varphi-\alpha)} \tag{4.5}$$

Substituting equation (4.5) into equation (4.4) one may obtain:

$$T_s = \frac{\sigma_{ult}\dfrac{\cos\alpha}{\sin\varphi\cos(\varphi-\alpha)}}{c_v} \tag{4.6}$$

Substituting equation (4.6) into equation (4.3):

$$\tau_s = \sigma_{ult}\left(1-0.0005\frac{\sigma_{ult}\dfrac{\cos\alpha}{\sin\varphi\cos(\varphi-\alpha)}}{c_v}\right) \tag{4.7}$$

Substituting equation (4.7) into equation (4.2):

$$F_s = \sigma_{ult} t b\left(1-0.0005\frac{\sigma_{ult}\dfrac{\cos\alpha}{\sin\varphi\cos(\varphi-\alpha)}}{c_v}\right)\frac{1}{\sin\varphi} \tag{4.8}$$

The tangential force F_f acting along the tool-chip interface can be obtained as (Zorev, 1966)

$$F_f = \tau_f\, b\, l_{ef} \tag{4.9}$$

here l_{ef} is the effective length of the tool-chip interface and τ_f is the shear flow stress along the chip-tool interface which can be obtained from the thermomechanical model knowing

the tool-chip interface temperature as

$$\tau_f = \sigma_{ult}(1-0.0005T_f) \tag{4.10}$$

where T_f is the tool-chip interface temperature (Kushner, 1982)

$$T_f = 79\left(\frac{\tau_s}{100\rho c_p}\right)^{0.8}\left(\frac{l_{st}}{\zeta t}\right)^{0.4}(Pe)^{0.4} \tag{4.11}$$

where l_{st} is the length of the plastic part of the tool-chip interface and Pe is the peclet number which can be written as

$$Pe = \frac{vt}{w} \tag{4.12}$$

where w is the diffusity of the workpiece material which can be written as

$$w = \frac{k}{\rho c_p} \tag{4.13}$$

where k is the thermal conductivity of the workpiece material,

However, the experimental work done by Astakhov (1994; 1983) shows that the full tool-chip interface length l_f, the effective length l_{ef} and the length of the plastic part of the tool-chip interface l_{st} can be written in terms of chip compression ratio ζ as follow:

$$\begin{aligned} l_f &= t\ \zeta^{1.5} \\ l_{ef} &= \frac{2}{3}\ l_f = \frac{2}{3}\ t\ \zeta^{1.5} \\ l_{st} &= \frac{3}{4}\ l_{ef} = \frac{3}{4}\frac{2}{3}\ l_f = \frac{1}{2}\ t\ \zeta^{1.5} \end{aligned} \tag{4.14}$$

The shear flow stress in the tool-chip interface can be calculated as

$$\tau_f = \sigma_{ult}\left[1-0.00395\left(\frac{\sigma_{ult}}{100c_v}-0.0005\frac{\sigma_{ult}^2}{100c_v^2}\frac{\cos\alpha}{\sin\varphi\cos(\varphi-\alpha)}\right)^{0.8}\left(\frac{l_{st}v}{\zeta w}\right)^{0.4}\right] \qquad (4.15)$$

here, l_{st} is the length of the plastic part of the tool-chip interface, w is the thermal diffuseness of workpiece material and ζ is the chip compression ratio.

Substituting equation (4.15) into equation (4.9) the tangential force F_f along the tool-chip interface can be written as

$$F_f = \sigma_{ult} b l_{ef}\left[1-0.00395\left(\frac{\sigma_{ult}}{100c_v}-0.0005\frac{\sigma_{ult}^2}{100c_v^2}\frac{\cos\alpha}{\sin\varphi\cos(\varphi-\alpha)}\right)^{0.8}\left(\frac{l_{st}v}{\zeta w}\right)^{0.4}\right] \qquad (4.16)$$

Knowing the shear force F_s and F_f, the cutting force F_c and the tangential force F_t can be obtained from the following equation:

$$\begin{aligned} F_s &= F_c\cos\varphi - F_t\sin\varphi \\ F_f &= F_c\sin\alpha + F_t\cos\alpha \end{aligned} \qquad (4.17)$$

4.2 CUTTING FORCE COMPONENTS IN BTA MACHINING USING THE SHEAR ZONE WITH PARALLEL BOUNDARIES

The BTA method basically utilizes single or multi cutting edge tool with an internal chip removal. The cutting edge geometry is important because it defines the model for metal cutting, cutting force distribution, chip formation, cutting edges wear, and the surface accuracy of the hole produced.

4.2.1 Cutting Force Components

Based on the tool geometry and due to the fact that the velocity of cutting is perpendicular to the cutting edges, the deep-hole machining operation may be considered as an orthogonal machining operation. The resultant cutting force is commonly resolved into three components (Latinovic, 1978):

1. The tangential contributing component F_t parallel to the cutting velocity vector.
2. The radial component F_r along the radius of the tool.
3. The axial component F_a along the axis of the tool.

The formulation of the steady state cutting force equations requires evidence on the nature of the deformation zone. A complete force system in the deep-hole machining operation is specified by the axial, tangential, radial force components and the point of application of the resultant force. This system will be modified by shifting the force to the axis of the tool. But such a shift of the three forces leads to an introduction of a torque acting along the axis of the boring bar-cutting tool system. Therefore to specify the *BTA* deep hole machining operation not only are the axial, radial and tangential forces to be evaluated, but also an expression for torque is to be obtained.

For the purpose of evaluating the total cutting force, the entire cutting edge can be considered as being made up of small increments of cutting edge "*dr*" and then summing up the contributions due to these over a radius of hole.

The force system on an incremental of the cutting profile is shown in Figure 4.1. Since the cutting velocity at each increment is at right angles to the cutting profile the machining is an orthogonal operation and the cutting force at each section can t be described.

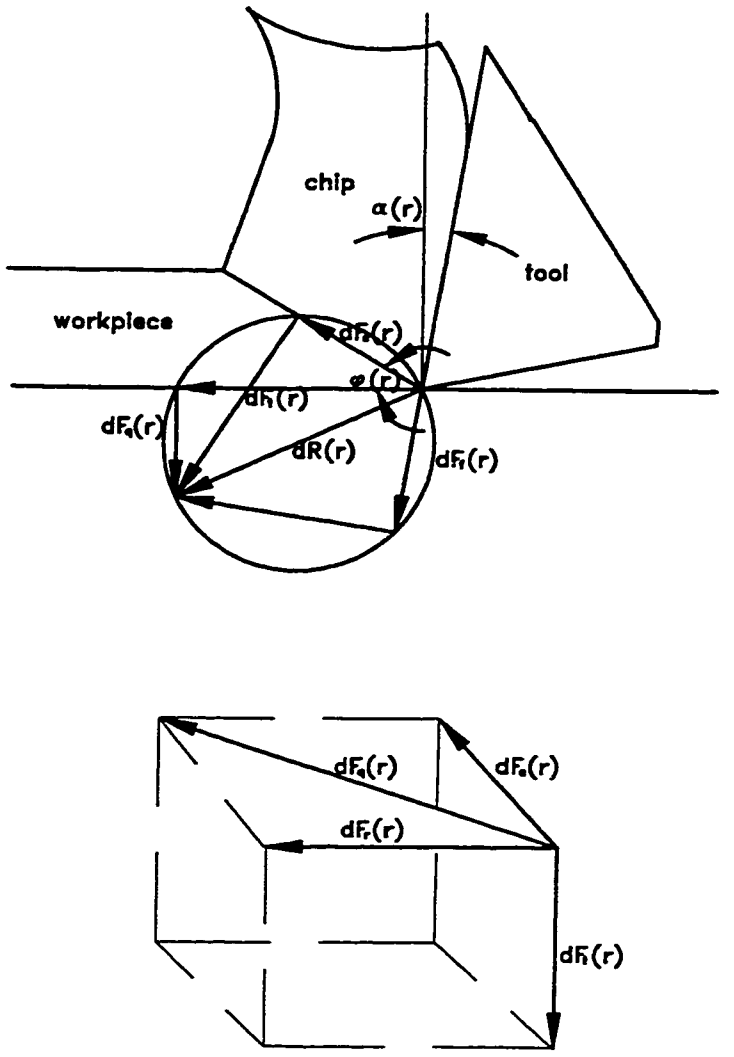

Figure 4.1: Cutting force representation at a distance *r* from the center of the cutting tool.

The shear flow stress at distance r can be defined using the thermo mechanical model as

$$\tau_s(r) = \sigma_{ult}(1-0.0005\,T_s(r)) \tag{4.18}$$

where $T_s(r)$ is the temperature in the shear zone which can be defined as (Oxley, 1989)

$$T_s(r) = \frac{\sigma_{ult}\gamma(r)}{\rho c_p} \tag{4.19}$$

where $\gamma(r)$ is the shear strain in the shear zone at distance r and ρc_p is the heat capacity of the workpiece material. The shear strain $\gamma(r)$ can be written as

$$\gamma(r) = \frac{\cos\alpha(r)}{\sin\varphi(r)\cos(\varphi(r)-\alpha(r))} \tag{4.20}$$

where $\alpha(r)$ and $\varphi(r)$ are the rake and shear angles at radius r, respectively.

Substituting equation (4.19) into equation (4.18)

$$\tau_s(r) = \sigma_{ult}\left(1-.0005\frac{\sigma_{ult}\gamma(r)}{\rho c_p}\right) \tag{4.21}$$

The relationship between the shear angle $\varphi(r)$ and the rake angle $\alpha(r)$ and the chip compression ratio $\zeta(r)$ at certain point can be written as

$$\varphi(r)=\tan^{-1}\left(\frac{\cos\alpha(r)}{\zeta(r)-\sin\alpha(r)}\right) \tag{4.22}$$

It is well known that the shear angle $\varphi(r)$ depends upon the velocity of the machining $v(r)$, the feed t, the rake angle $\alpha(r)$, cutting tool, workpiece material, and cutting fluid. Mathematically it can be expressed in the following form:

$$\zeta(r) = f_1(v(r), t, \alpha(r), \textit{cutting tool material, workpiece material}) \tag{4.23}$$

As it was suggested (Nigm and Sadek, 1977), the following equation for chip compression ratio $\zeta(r)$ can be written

$$\zeta(r) = \frac{1}{e\sin\alpha(r) + (1 - f\sin\alpha(r))\left(g + \frac{h}{(4\times10^4 t)^k} \ln\left(\frac{40t(200v(r))^n}{q} \right) \right)} \tag{4.24}$$

where e, f, g, h, k, n and q are constants, t is the undeformed chip thickness (m) and $v(r)$ is the cutting speed (m/s).

The shear flow stress at the chip-tool interface at distance r can be written as

$$\tau_f(r) = \sigma_{ult}(1 - 0.0005 T_f(r)) \tag{4.25}$$

where $T_f(r)$ is the tool-chip interface at distance r from the center of rotation which can be written as

$$T_f(r) = 79\left(\frac{\tau_s(r)}{100\rho c_p} \right)^{0.8} \left(\frac{l_{st}(r)}{\zeta(r)t} \right)^{0.4} (Pe(r))^{0.4} \tag{4.26}$$

where $Pe(r)$ is the peclet number at distance r which can be written as

$$Pe(r) = \frac{\rho c_p v(r) t}{k} \tag{4.27}$$

and $l_{st}(r)$ is the length of the plastic part of the tool-chip interface. Using equation (4.14) the full tool-chip interface length l_f, the effective length l_{ef} and the length of the plastic part of the tool-chip interface l_{st} at a distance r from the axis of the cutting tool can be written as

$$
\begin{aligned}
l_f(r) &= t\zeta(r)^{1.5} \\
l_{ef}(r) &= \frac{2}{3} l_f(r) = \frac{2}{3} t\zeta(r)^{1.5} \\
l_{st}(r) &= \frac{3}{4} l_{ef(r)} = \frac{3}{4}\frac{2}{3} l_f(r) = \frac{1}{2} t\zeta(r)^{1.5}
\end{aligned}
\tag{4.28}
$$

The shear force on an incremental thickness dr of the cutting profile at distance r can be written as

$$
dF_s(r) = \tau_s(r) \frac{t}{\sin\varphi(r)} dr \tag{4.29}
$$

which can be written as

$$
\begin{aligned}
dF_s(r) &= H_s(r) dr \\
H_s(r) &= \tau_s(r) \frac{t}{\sin\varphi(r)}
\end{aligned}
\tag{4.30}
$$

Also the tangential force $F_f(r)$ on the rake face at distance r can be written as

$$
F_f(r) = \tau_f(r) l_{ef}(r) dr \tag{4.31}
$$

which can be written as

$$
\begin{aligned}
dF_f(r) &= H_f(r) dr \\
H_f(r) &= \tau_f(r) l_{ef}(r)
\end{aligned}
\tag{4.32}
$$

Knowing the shear force $F_s(r)$ and the tangential friction force $F_f(r)$, the cutting forcees on an incremental thickness as shown in Figure 4.1 can be obtained from the following equations

$$
\begin{aligned}
dF_s(r) &= dF_t(r)\cos\varphi(r) - dF_q(r)\sin\varphi(r) \\
dF_f(r) &= dF_t(r)\cos\alpha(r) + dF_q(r)\cos\alpha(r)
\end{aligned}
\tag{4.33}
$$

Hence

$$dF_t(r) = \frac{H_s(r)(r)\cos\alpha(r)+H_f(r)\sin\varphi(r)}{\cos(\varphi(r)-\alpha(r))}dr$$
$$dF_q(r) = \frac{H_f(r)\cos\varphi(r)-H_s(r)\sin\alpha(r)}{\cos(\varphi(r)-\alpha(r))}dr \quad (4.34)$$

From the geometry of the cutting edge, the expression for the radial and axial components of the cutting force in the region under consideration can be written as

$$dF_r(r) = dF_q(r)\sin\varkappa(r)$$
$$dF_a(r) = dF_q(r)\cos\varkappa(r) \quad (4.35)$$

where $\varkappa(r)$ is the approach angle of the cutting edge at distance r.

The tangential, radial and axial forces can be written in the following form

$$dF_t(r) = \frac{H_s(r)\cos\alpha(r)+H_f(r)\sin\varphi(r)}{\cos(\varphi(r)-\alpha(r))}dr$$
$$dF_r(r) = \frac{H_f(r)\cos\varphi(r)-H_s(r)\sin\alpha(r)}{\cos(\varphi(r)-\alpha(r))}\sin\varkappa(r)dr \quad (4.36)$$
$$dF_a(r) = \frac{H_f(r)\cos\varphi(r)-H_s(r)\sin\alpha(r)}{\cos(\varphi(r)-\alpha(r))}\cos\varkappa(r)dr$$

which can be rewritten as

$$dF_t(r) = \Lambda(r)dr$$
$$dF_r(r) = M(r)\sin\varkappa(r)dr \quad (4.37)$$
$$dF_a(r) = M(r)\cos\varkappa(r)dr$$

where

$$\Lambda(r) = \frac{H_s(r)\cos\alpha(r)+H_f(r)\sin\varphi(r)}{\cos(\varphi(r)-\alpha(r))}$$
$$M(r) = \frac{H_f(r)\cos\varphi(r)-H_s(r)\sin\alpha(r)}{\cos(\varphi(r)-\alpha(r))} \quad (4.38)$$

A complete specification for any rotating tool requires an expression for the torque acting on the cutting edge. The torque on a given section can be written as

$$dT(r) = r dF_t(r) \tag{4.39}$$

which can be written as

$$dT(r) = \Lambda(r) r\, dr \tag{4.40}$$

The forces and torque consist of two components, the steady and the dynamic components, that is

$$\begin{aligned} F_t(r) &= F_{tm}(r)+\Delta F_t(r) \\ F_r(r) &= F_{rm}(r)+\Delta F_r(r) \\ F_a(r) &= F_{am}(r)+\Delta F_a(r) \\ T(r) &= T_m(r)+\Delta T(r) \end{aligned} \tag{4.41}$$

where $F_{tm}(r)$, $F_{rm}(r)$ and $F_{rm}(r)$ are the steady forces on the incremental thickness at distance r, $\Delta F_t(r)$, $\Delta F_r(r)$ and $\Delta F_a(r)$ are the dynamic components of these forces, $T_m(r)$ is the steady torque component and $\Delta T(r)$ is the dynamic components of the torque.

The steady components of the tangential, radial and axial forces over the entire cutting edge can be written as

$$\begin{aligned} F_{tm} &= \int_{\text{section } i=1} \Lambda(r)dr + \int_{\text{section } i=2} \Lambda(r)dr + \ldots\ldots \int_{\text{section } i=n} \Lambda(r)dr \\ F_{rm} &= \int_{\text{section } i=1} \mathrm{M}(r)\sin\varkappa(r)dr + \int_{\text{section } i=2} \mathrm{M}(r)\sin\varkappa(r)dr + \ldots\ldots \int_{\text{section } i=n} \mathrm{M}(r)\sin\varkappa(r)dr \\ F_{am} &= \int_{\text{section } i=1} \mathrm{M}(r)\cos\varkappa(r)dr + \int_{\text{section } i=2} \mathrm{M}(r)\cos\varkappa(r)dr + \ldots\ldots \int_{\text{section } i=n} \mathrm{M}(r)\cos\varkappa(r)dr \\ T_m &= \int_{\text{section } i=1} \Lambda(r)rdr + \int_{\text{section } i=2} \Lambda(r)rdr + \ldots\ldots \int_{\text{section } i=n} \Lambda(r)rdr \end{aligned} \tag{4.42}$$

where n is the number of the sections over the diameter of the tool as seen Figure 4.2 (Latinovic, 1978).

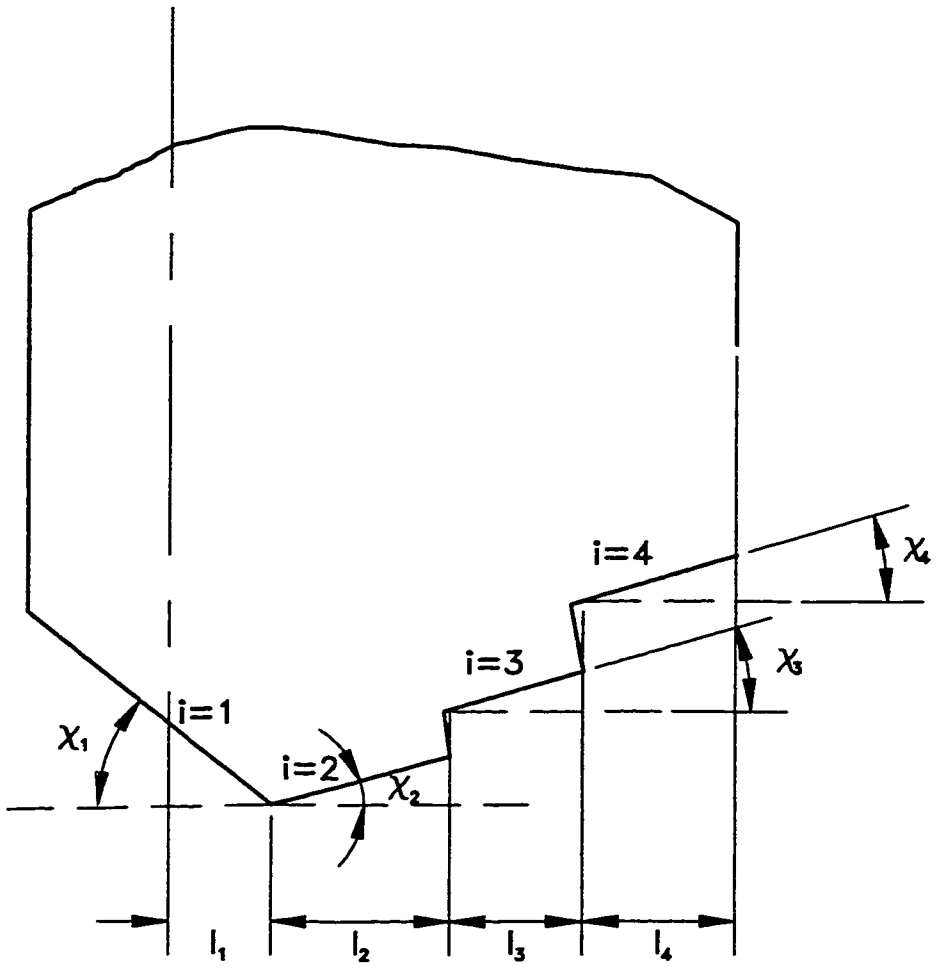

Figure 4.2: Section of the BTA cutting profile.

4.2.2 Computer Simulations

Four series of testing programs were curried out to assess the effects of the cutting tool geometry, feed, cutting speed, and workpiece material on the steady state cutting forces. A Fortran program has been written to simulate the formulated model. The results of this simulation together with the obtained experimntal results are presented in chapter nine.

5

AN ANALYTICAL EVALUATION OF THE CUTTING FORCES IN ORTHOGONAL CUTTING USING THE DYNAMIC MODEL OF SHEAR ZONE WITH PARALLEL BOUNDARIES

This chapter present an evaluation of the dynamic forces in orthogonal cutting using the shear zone model with parallel boundaries (Hayajneh et al, 1997a, 1997 b). The cutting system was modeled using a single degree-of freedom dynamic system where the variations of the cutting forces are represented by their total differentials. The influence of temperature on the shear flow stress of workpiece material is accounted. The experimental verification of the proposed model was performed using a two-component piezoelectric dynamometer and applying the rotating cutting tool-stationary workpiece method.

5.1 INTRODUCTION

In order to study the chatter, it is important to distinguish the sources of vibrations. Basically, the machining vibrations are usually classified into the following four main categories (Nigm et al, 1977):

1. Free vibration which may be initiated by some impact or shock. This vibration usually decays under the damping action of the machine tool.
2. Forced vibration caused by a source other than cutting. This may be initiated by unbalance in the machine-tool drive. Knowing the source of these forced vibrations, they can be prevented by redesign of the machine tool structure.
3. Forced vibration initiated by the inherent periodicity in the cutting process such that the built-up edge and discontinuity of the chip.
4. Self-excited vibration. This type is classified into a regenerative and a non-regenerative chatter. The regenerative effect is caused by the superposition of successive cuts, where the tool removes a wavy surface generated in the previous pass. The non-regenerative vibration is maintained by cutting force fluctuations that are induced by the cutting tool-workpiece relative displacement of periodic nature.

In order to understand the mechanisms leading to the chatter, it is essential to know how the cutting forces vary with variation of cutting conditions and tool-workpiece relative motion. The cutting forces depend on a large number of cutting system parameters which make the formulation of an analytical dynamic cutting force model a rather difficult task. Many techniques have been developed over the past 50 years for machine tool-cutting process identification. The general approach of these techniques is to assume that the cutting

forces are an approximate linear function of relative tool-workpiece position and velocity (Peters et al, 1971). The coefficients of this function, known as dynamic force coefficients, are the induced stiffness and the damping. Traditionally, the dynamic force functions are assumed to be linear expressions in terms of a number of time-dependent variables, which include the inner and outer modulations of the uncut chip thickness and their first time derivatives. The coefficients of these variation terms may be determined through experimental or analytical technique. The experimental technique is to develop an experimental method for direct measurement of the transfer function between the cutting force and the variables in the modulation of the uncut chip thickness (Peter et al, 1971). The experimental method is highly empirical and requires a very sophisticated test apparatus and analysis procedures.

The promising way of formulating a proper dynamic cutting force is using the mechanics of chip formation (Nigm et al, 1977; Das and Tobias, 1967; Rubenstein, 1972). However, the models for chip formation used so far for this purpose are not in good agreement with the results of experiments. For example, Wu and Liu (1985a, 1985b) and Wu (1986; 1988; 1989) developed a dynamic cutting force model using the single shear plane model for orthogonal cutting which exhibits serious shortcomings (Astakov and Osman, 1996; Oxley, 1989). Therefore, it is reasonable to suggest that a new model of chip formation which is in better agreements with the experiments should be used.

Astakhov and Osman (1996) proposed a model of chip formation with parallel boundaries which appears to be free from many of the known contradictions associated with the other reported models. It would be logical to incorporate it into the dynamic analysis

of the cutting forces. This is one of the main objectives of the work.

5.2 DYNAMIC MODEL OF SHEAR ZONE WITH PARALLEL BOUNDARIES

5. 2.1 General Force Model

In the present study, the real machining system is approximated with a single degree-of-freedom dynamic system shown in Figure 5.1. In this figure, a flexible cutting tool, vibrating normal to the cutting direction, is set to remove a layer of work material with a wavy top surface produced during previous cuts. The cutting speed, the mean uncut chip thickness, and the rake angle are preset to be v, t , and α, respectively. The coordinate system, illustrated in Figure 5.1, is described as follows:

- the x-axis is normal to the direction of the cutting speed and this axis will be referred to as the vibration axis;
- the y-axis is perpendicular to the x-axis as shown in Figure 5.1.

At any instant, the tool tip has the displacement x_1 along the vibration axis, while the surface end of the shear plane has the displacement x_2 relative to its equilibrium position, as shown in Figure (5.1). The oscillation velocities of the tool tip and the surface end of the shear plane are denoted by $\dot{x_1}$ and $\dot{x_2}$, respectively.

It is known (Merchant, 1945) that for steady-state machining the cutting forces are determined only by an invariable cutting configuration. Once that configuration is known, the cutting force components acting along the corresponding axes, namely the tangential F_y and the radial F_x cutting force (Figure 5.1) can be determined as follows

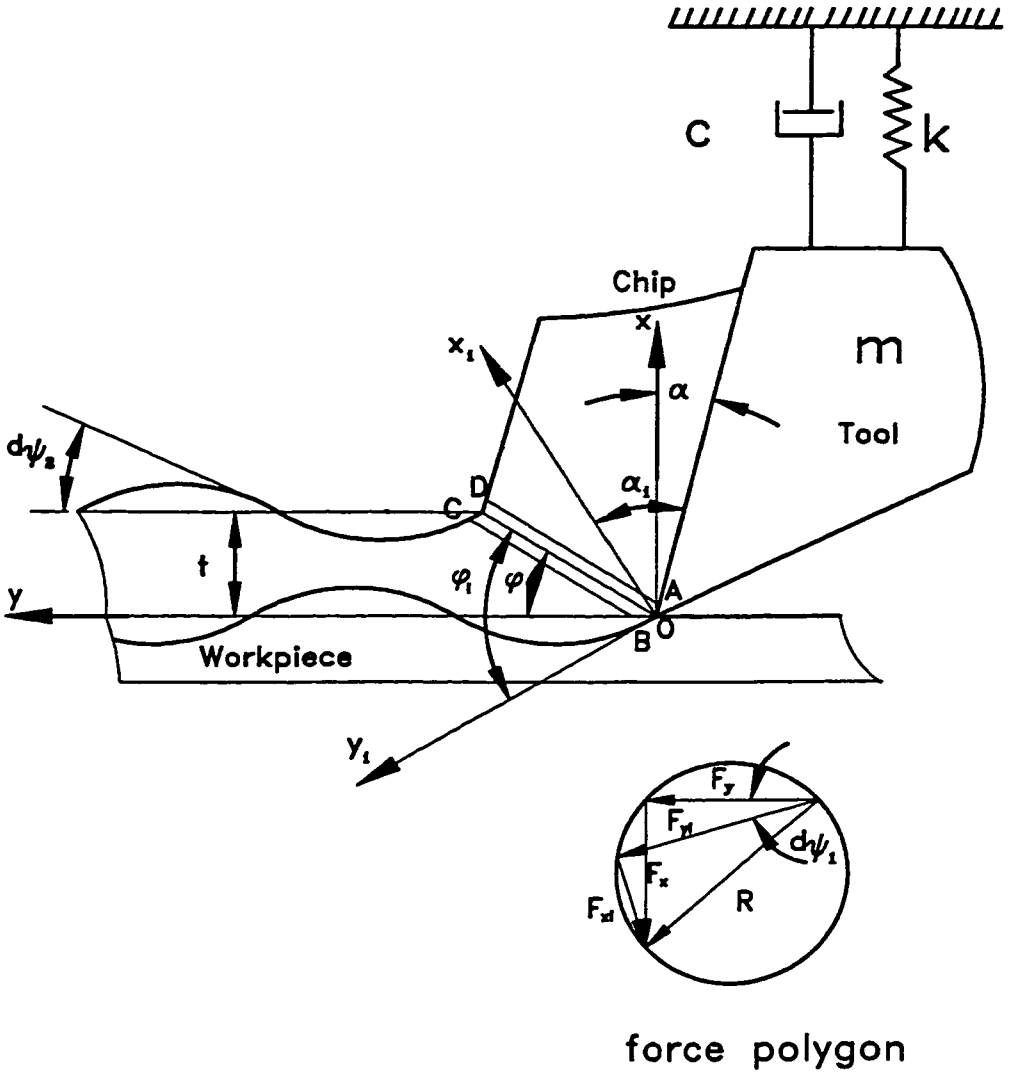

Figure 5.1: A model of shear zone with parallel boundaries as applied to evaluate the dynamic cutting force.

$$F_y = \frac{F_s \cos\alpha + F_f \sin\varphi}{\cos(\varphi - \alpha)}$$
$$F_x = \frac{F_f \cos\varphi - F_s \sin\alpha}{\cos(\varphi - \alpha)} \qquad (5.1)$$

where F_s is the shear force along the shear zone boundaries, F_f is the tangential force on the rake face and φ is the shear angle.

Since in the present study the configuration of the cutting system is considered to be variable then the dynamic values of these forces should be considered as functions of the corresponding dynamic cutting parameters such as shear force, shear angle, and rake angle which are denoted as F_{fi}, F_{si}, φ_i, and α_i, respectively. Therefore, a general force model may be represented in the following form:

$$F_{yi} = \frac{F_{si} \cos\alpha_i + F_{fi} \sin\varphi_i}{\cos(\varphi_i - \alpha_i)}$$
$$F_{xi} = \frac{F_{fi} \cos\varphi_i - F_{si} \sin\alpha_i}{\cos(\varphi_i - \alpha_i)} \qquad (5.2)$$

The dynamic value of each model's component may be represented by the the sum of its steady-state value and its incremental variation as follows:

$$\begin{aligned} F_{yi} &= F_y + dF_y \\ F_{xi} &= F_x + dF_x \\ F_{si} &= F_s + dF_s \\ F_{fi} &= F_f + dF_f \\ \alpha_i &= \alpha + d\alpha \\ \varphi_i &= \varphi + d\varphi \end{aligned} \qquad (5.3)$$

5.2.2 Determination of the Cutting Force Components

The incremental variations of the cutting forces F_y and F_x may be represented by

their total differentials. Using equation (5.2) and neglecting the terms of high orders, one may obtain these incremental variations in the following form

$$\begin{aligned} dF_y &= g_1 dF_s + g_2 dF_f + g_3 d\varphi + g_4 d\alpha \\ dF_x &= e_1 dF_s + e_2 dF_f + e_3 d\varphi + e_4 d\alpha \end{aligned} \tag{5.4}$$

where the coefficients of equation (5.4) are

$$\begin{aligned} g_1 &= \frac{\cos\alpha}{\cos(\varphi-\alpha)} \\ g_2 &= \frac{\sin\varphi}{\cos(\varphi-\alpha)} \\ g_3 &= \frac{F_f\cos\varphi\cos(\varphi-\alpha)+(F_s\cos\alpha+F_f\sin\varphi)\sin(\varphi-\alpha)}{\cos^2(\varphi-\alpha)} \\ g_4 &= \frac{-F_s\sin\alpha\cos(\varphi-\alpha)+(F_s\cos\alpha+F_f\sin\varphi)\sin(\varphi-\alpha)}{\cos^2(\varphi-\alpha)} \end{aligned} \tag{5.5}$$

and

$$\begin{aligned} e_1 &= -\frac{\sin\alpha}{\cos(\varphi-\alpha)} \\ e_2 &= \frac{\cos\varphi}{\cos(\varphi-\alpha)} \\ e_3 &= \frac{-F_f\sin\varphi\cos(\varphi-\alpha)+(F_f\cos\varphi-F_s\sin\alpha)\sin(\varphi-\alpha)}{\cos^2(\varphi-\alpha)} \\ e_4 &= \frac{-F_s\cos\alpha\cos(\varphi-\alpha)+(F_f\cos\varphi-F_s\sin\alpha)\sin(\varphi-\alpha)}{\cos^2(\varphi-\alpha)} \end{aligned} \tag{5.6}$$

It is known (Merchant, 1945) that the shearing force F_s is calculated as:

$$F_s = \tau_s \frac{t\,b}{\sin\varphi} \tag{5.7}$$

where τ_s is the shear flow stress in the shear zone; b is the width of cut; t is the uncut chip

thickness; and φ is the shear angle.

The incremental variation of the shearing force F_s may be represented by its total differential. Using equation (4.8) and neglecting the terms of high orders, one may obtain:

$$dF_s = n_1 dt + n_2 d\varphi + n_3 d\alpha \tag{5.8}$$

where the coefficients n_1, n_2 and n_3 are calculated as

$$\begin{aligned}
n_1 &= \sigma_{ult} b \left[\frac{1}{\sin\varphi} - 0.0005 \frac{\sigma_{ult}}{c_v} \frac{\cos\alpha}{\sin^2\varphi\cos(\varphi-\alpha)} \right] \\
n_2 &= \sigma_{ult} t b \left[-\frac{\cos\varphi}{\sin^2\varphi} + 0.0005 \frac{\sigma_{ult}}{c_v} \frac{\cos\alpha(-\sin^2\varphi\sin(\varphi-\alpha)+2\sin\varphi\cos\varphi\cos(\varphi-\alpha))}{\sin^4\varphi\cos^2(\varphi-\alpha)} \right] \\
n_3 &= \sigma_{ult} t b \left[0.0005 \frac{\sigma_{ult}}{c_v} \frac{\sin^2\varphi\cos(\varphi-\alpha)\sin\alpha - \cos\alpha\sin^2\varphi\sin(\varphi-\alpha)}{\sin^4\varphi\cos^2(\varphi-\alpha)} \right]
\end{aligned} \tag{5.9}$$

The incremental variation of the tangential force F_f may be represented by its total differential. Using equation (4.16) and neglecting the terms of high orders, one may obtain:

$$dF_f = m_1 dt + m_2 d\zeta + m_3 dv + m_4 d\varphi + m_5 d\alpha \tag{5.10}$$

where m_1 , m_2, m_3, m_4 and m_5 are

$$m_1 = C_1\left[\zeta^{1.5} - 1.4C_2\frac{t^{2.5}\zeta^{4.25}v}{2w}\left(C_3 - C_4\frac{\cos\alpha}{\sin\varphi\cos(\varphi-\alpha)}\right)^{0.8}\left(\frac{t^{3.5}\zeta^{4.25}v}{2w}\right)^{-0.6}\right]$$

$$m_2 = C_1\left[1.5t\zeta^{0.5} - C_2 * \frac{17}{10}\frac{t^{3.5}\zeta^{3.25}v}{2w}\left(C_3 - C_4\frac{\cos\alpha}{\sin\varphi\cos(\varphi-\alpha)}\right)^{0.8}\left(\frac{t^{3.5}\zeta^{4.25}v}{2w}\right)^{-0.6}\right]$$

$$m_3 = C_1\left[-C_2\frac{t^{3.5}\zeta^{4.25}}{2w}\left(C_3 - C_4\frac{\cos\alpha}{\sin\varphi\cos(\varphi-\alpha)}\right)^{0.8}\left(\frac{t^{3.5}\zeta^{4.25}v}{2w}\right)^{-0.6}\right] \qquad \textbf{(5.11)}$$

$$m_4 = C_1\left[-.8C_2C_4\frac{\cos\alpha\cos(2\varphi-\alpha)}{\sin^2\varphi\cos^2(\varphi-\alpha)}\left(C_3 - C_4\frac{\cos\alpha}{\sin\varphi\cos(\varphi-\alpha)}\right)^{-0.2}\left(\frac{t^{3.5}\zeta^{4.25}v}{2w}\right)^{0.4}\right]$$

$$m_5 = C_1\left[0.8C_2C_4\frac{\sin(\varphi-2\alpha)}{\sin\varphi\cos^2(\varphi-\alpha)}\left(C_3 - C_4\frac{\cos\alpha}{\sin\varphi\cos(\varphi-\alpha)}\right)^{-0.2}\left(\frac{t^{3.5}\zeta^{4.25}v}{2w}\right)^{0.4}\right]$$

5.2.3 Influence of Incremental Variations of the Shear Angle

The model of shear zone with parallel boundaries utilizes the Merchant's expression for the shear angle φ (Merchant, 1945):

$$\varphi = \tan^{-1}\left(\frac{\cos\alpha}{\zeta - \sin\alpha}\right) \qquad \textbf{(5.12)}$$

Here, the chip compression ratio and rake angle are constant. However, this is not the case in the present consideration. Therefore, dynamic variations of these parameters should be considered.

The incremental variation of the shear angle may be represented by its total differential in the following form:

$$d\varphi = \frac{\partial\varphi}{\partial\zeta}d\zeta + \frac{\partial\varphi}{\partial\alpha}d\alpha + \frac{\partial\varphi}{\partial\alpha}d\psi \qquad \textbf{(5.13)}$$

As can be seen, equation (5.13) contains three terms instead of two as might be expected from equation (5.12). We may explain this as follows. The angle ψ represent the angle between the free surface of the workpiece and the y-direction. Since in the steady-state consideration this angle is zero, it does not appear in equation (5.12). In the dynamic consideration, however, this angle plays an important role. In wave cutting , the dynamic direction of cutting is at an angle $d\psi_1$ with the direction against which the rake angle of the tool is measured that increases the rake angle. In wave removing, the opposite is the case so that $d\psi_2$ decreases the rake. In actual practice, a certain combination of the above two types (wave cutting and wave removing) is the case. Therefore, the static rake angle is modified by the incremental variation of angle ψ. This incremental variation can be represented as:

$$d\psi = d\psi_1 + d\psi_2 \tag{5.14}$$

Bearing in mind the foregoing consideration, one may express equation (5.13) as follows:

$$d\varphi = s_1 d\zeta + s_2 d\alpha + s_2 d\psi \tag{5.15}$$

where s_1 and s_2 are

$$s_1 = \frac{-\cos\alpha}{(\zeta-\sin\alpha)^2\left[1+\left(\frac{\cos\alpha}{\zeta-\sin\alpha}\right)^2\right]}$$
$$s_2 = \frac{1-\zeta\sin\alpha}{(\zeta-\sin\alpha)^2\left[1+\left(\frac{\cos\alpha}{\zeta-\sin\alpha}\right)^2\right]} \tag{5.16}$$

The compression ratio ζ can be written as (Nigm et al, 1977):

$$\zeta = \frac{1}{e\sin\alpha + (1 - f\sin\alpha)\left[g + \frac{h}{(4\times10^4 t)^p}\ln\left(\frac{40t(200v)^n}{q}\right)\right]} \tag{5.17}$$

where e, f, g, h, p, n and q are constants, t is the undeformed chip thickness (m) and v is the cutting speed (m/s).

As might be expected, the chip compression ratio varies with other cutting parameters (Astakhov and Osman, 1996; Nigm and Sadek, 1977). The incremental variation of the compression ratio ζ can be represented by its total differential in the following form:

$$d\zeta = \frac{\partial\zeta}{\partial t}dt + \frac{\partial\zeta}{\partial v}dv + \frac{\partial\zeta}{\partial\alpha}d\alpha \tag{5.18}$$

which can be simplified as

$$d\zeta = l_1 dt + l_2 dv + l_3 d\alpha \tag{5.19}$$

where l_1, l_2 and l_3 are

$$l_1 = \frac{-(1-f\sin\alpha)\left[\dfrac{h}{t(4\times10^4 t)^k}+\dfrac{-kh}{(4\times10^4 t)^{k+1}}\ln\left(\dfrac{40t(200v)^n}{q}\right)\right]}{\left[e\sin\alpha+(1-f\sin\alpha)\left[g+\dfrac{h}{(4\times10^4 t)^k}\ln\left(\dfrac{40t(200v)^n}{q}\right)\right]\right]^2}$$

$$l_2 = \frac{-(1-f\sin\alpha)\left[\dfrac{h}{(4\times10^4 t)^k}\left(\dfrac{n}{v}\right)\right]}{\left[e\sin\alpha+(1-f\sin\alpha)\left[g+\dfrac{h}{(4\times10^4 t)^k}\ln\left(\dfrac{40t(200v)^n}{q}\right)\right]\right]^2} \qquad \textbf{(5.20)}$$

$$l_3 = \frac{-\left[e\cos\alpha+(1-f\cos\alpha)\left[g+\dfrac{h}{(4\times10^4 t)^k}\ln\left(\dfrac{40t(200v)^n}{q}\right)\right]\right]}{\left[e\sin\alpha+(1-f\sin\alpha)\left[g+\dfrac{h}{(4\times10^4 t)^k}\ln\left(\dfrac{40t(200v)^n}{q}\right)\right]\right]^2}$$

Substituting equation (5.19) into equation (5.15), one may obtain:

$$d\varphi = s_1 l_1 dt + s_1 l_2 dv + (s_1 l_3 + s_2) d\alpha + s_2 d\psi \qquad \textbf{(5.21)}$$

The incremental variation of the shearing force is obtained by substituting equations (5.19) and (5.21) into equation (5.10)

$$dF_f = P_1 dt + P_2 dv + P_3 d\alpha + P_4 d\psi \qquad \textbf{(5.22)}$$

where P_1 , P_2, P_3 and P_4 are

$$\begin{aligned} P_1 &= m_1 + m_2 l_1 + m_4 s_1 l_1 \\ P_2 &= m_2 l_2 + m_3 + m_4 s_1 l_2 \\ P_3 &= m_4 s_1 l_3 + m_4 s_2 + m_2 l_3 + m_5 \\ P_4 &= m_4 s_2 \end{aligned} \qquad \textbf{(5.23)}$$

Similarly, substituting equation (5.21) into equation (5.8), one may get

$$dF_s = T_1 dt + T_2 dv + T_3 d\alpha + T_4 d\psi \qquad \textbf{(5.24)}$$

where T_1, T_2, T_3 and T_4 are

$$
\begin{aligned}
T_1 &= n_1 + n_2 s_1 l_1 \\
T_2 &= n_2 s_1 l_2 \\
T_3 &= n_2 s_1 l_3 + n_2 s_2 + n_3 \\
T_4 &= n_2 s_2
\end{aligned}
\tag{5.25}
$$

Finally, the incremental variations of the cutting force's coordinate components are obtained by substituting equations (5.21), (5.22) and (5.24) into equation (5.4):

$$
dF_y = A_{ty}dt + A_{vy}dv + A_{\alpha y}d\alpha + A_{\psi y}d\psi \tag{5.26}
$$

where A_{ty}, A_{vy} , $A_{\alpha y}$, $A_{\psi y}$ are

$$
\begin{aligned}
A_{ty} &= g_1 T_1 + g_2 P_1 + g_3 s_1 l_1 \\
A_{vy} &= g_1 T_2 + g_2 P_2 + g_3 s_1 l_2 \\
A_{\alpha} y &= g_1 T_3 + g_2 P_3 + g_3 s_1 l_3 + g_3 s_2 + g_4 \\
A_{\psi y} &= g_1 T_4 + g_2 P_4 + g_3 s_2
\end{aligned}
\tag{5.27}
$$

and

$$
dF_x = A_{tx}dt + A_{vx}dv + A_{\alpha x}d\alpha + A_{\psi x}d\psi \tag{5.28}
$$

where A_{tx}, A_{vx} , $A_{\alpha x}$, $A_{\psi x}$ are

$$
\begin{aligned}
A_{tx} &= e_1 T_1 + e_2 P_1 + e_3 s_1 l_1 \\
A_{vx} &= e_1 T_2 + e_2 P_2 + e_3 s_1 l_2 \\
A_{\alpha} x &= e_1 T_3 + e_2 P_3 + e_3 s_1 l_3 + e_3 s_2 + e_4 \\
A_{\psi x} &= e_1 T_4 + e_2 P_4 + e_3 s_2
\end{aligned}
\tag{5.29}
$$

5.2.4 Interpretation of The Incremental Variations in Terms of Cutting Process Parameters

If the motion of the lower chip boundary is designated by $\dot{x_1}$, and the motion of the upper chip boundary is designated by $\dot{x_2}$, then the variation of the cutting parameters are

given by

$$
\begin{aligned}
d\alpha &= \frac{\dot{x}_1}{v} \\
d\psi &= \frac{\dot{x}_1 - \dot{x}_2}{v} \\
dt &= x_1 - x_2 + \varepsilon\frac{\dot{x}_1}{v} \\
dv &= \frac{\dot{x}_1^{\,2}}{2v}
\end{aligned}
\tag{5.30}
$$

where ε is the geometric lead of the free end of the shear zone relatively to its end on the tool cutting edge. Simple analysis of the model in Figure. (5.1) shows that:

$$\varepsilon = t\cot\varphi \tag{5.31}$$

Substituting equation (5.30) and (5.44) into equations (5.26) and (5.28), one may obtain:

$$dF_y = A_{ty}\left(x_1 - x_2 + t\cot\varphi\frac{\dot{x}_1}{v}\right) + A_{vy}\left(\frac{\dot{x}_1^{\,2}}{2v}\right) + A_{\alpha y}\left(\frac{\dot{x}_1}{v}\right) + A_{\psi y}\left(\frac{\dot{x}_1 - \dot{x}_2}{v}\right) \tag{5.32}$$

and

$$dF_x = A_{tx}\left(x_1 - x_2 + t\cot\varphi\frac{\dot{x}_1}{v}\right) + A_{vx}\left(\frac{\dot{x}_1^{\,2}}{2v}\right) + A_{\alpha x}\left(\frac{\dot{x}_1}{v}\right) + A_{\psi x}\left(\frac{\dot{x}_1 - \dot{x}_2}{v}\right) \tag{5.33}$$

5.2.5 Equations of Motion

Multiple observations and measurements of the profile of the surface of cut show that x_1 and x_2 may be assumed to be harmonic functions having corresponding frequencies ω_1 and ω_2, that is

$$
\begin{aligned}
x_1 &= X_1 \cos\omega_1 T \\
x_2 &= X_2 \cos\omega_2 T \\
\dot{x}_1 &= -X_1 \omega_1 \sin\omega_1 T \\
\dot{x}_2 &= X_2 \omega_2 \sin\omega_2 T
\end{aligned}
\tag{5.34}
$$

where ω_1, ω_2 are defined by the chosen cutting regime and the diameter of the workpiece if the chip formation process is stable (Astakhov et al, 1977).

5.2.6 Proposed Model for the Cutting Force Evaluation

The proposed model for the cutting force evaluation is obtained by substituting equation (5.34) into equations (5.32) and (5.33) and by substituting the result into equation (5.3):

$$
\begin{aligned}
F_{yi} = F_y + dF_y = F_y + A_{by}\left(X_1 \cos\omega_1 T - X_2 \cos\omega_2 T - t\cot\varphi \frac{X_1 \omega_1 \sin\omega_1 T}{v} \right) + \\
A_{vy}\left(\frac{X_1{}^2 \omega^2{}_1 \sin^2 \omega_1 T}{2v} \right) + A_{\alpha y}\left(\frac{-X_1 \omega_1 \sin\omega_1 T}{v} \right) + \\
A_{\psi y}\left(\frac{-X_1 \omega_1 \sin\omega_1 T + X_2 \omega_2 \sin\omega_2 T}{v} \right)
\end{aligned}
\tag{5.35}
$$

and

$$
\begin{aligned}
F_{xi} = F_x + dF_x = F_x + A_{bx}\left(X_1 \cos\omega_1 T - X_2 \cos\omega_2 T - t\cot\varphi \frac{X_1 \omega_1 \sin\omega_1 T}{v} \right) + \\
A_{vx}\left(\frac{X_1{}^2 \omega^2{}_1 \sin^2 \omega_1 T}{2v} \right) + A_{\alpha x}\left(\frac{-X_1 \omega_1 \sin\omega_1 T}{v} \right) + \\
A_{\psi x}\left(\frac{-X_1 \omega_1 \sin\omega_1 T + X_2 \omega_2 \sin\omega_2 T}{v} \right)
\end{aligned}
\tag{5.36}
$$

5.2.7 Computer Simulations

Four series of testing programs were carried out to assess the effects of the cutting feed, cutting speed, rake angle and frequency of the waves on the work surface on the dynamic force components F_x and F_y. T able 5.1 presents the cutting conditions and Table 5.2 presents the cutting regimes used in the simulations. A Fortran program has been written to simulate formulated model. In chapter nine, the results of the simulation has been presented together with the experimental results.

Table 5.1. Cutting conditions for the simulation study

Workpiece material	Hot finished mild steel 0.25% C
Cutting tool	Carbide inserts (rake angles 0, 5, 10 degree)
Width of cut	3.5 mm
Work surface	Sinusoidal wave form of 0.05 mm amplitude
Tool vibration	Sinusoidal wave form of 0.05 mm amplitude
Cutting method	Orthogonal dry cutting
Clearance angle	10 degree

Table 5.2. Cutting parameters for the simulation study

	Series 1	Series 2	Series 3	Series 4
Objective: effect of	feed	speed	rake angle	frequency
Feed (mm/rev)	0.075-0.300	0.19	0.19	0.19
Speed (m/min)	140	60-240	140	140
Rake angle (deg.)	5	5	0-10	5
Frequency (Hz)	120	120	120	60-300

6

MISALIGNMENT ASSURANCE

As suggested in chapters 1 and 2, the relative position and motion between the tool and workpiece may affect both the steady-state and dynamic cutting forces dramatically. So that it become difficult to distinguish between the cutting signature due to the dynamic response of the cutting process and that due to the noise originating from the inaccuracy in the position of the workpiece relative to the cutting tool. Nevertheless, the accuracy of the workpiece rotation has never been a factor in cutting force studies. A great scatter in the reported results on the cutting force measurements may be partially explained by the mentioned inaccuracy. This becomes particularly important if a new model of chip formation has to be verified by experiments and, in doing so, the results of predicted and measured cutting forces have to be compared.

Since in the present study the experiments on the cutting force determination have been carried out using deep-hole machining and their results were compared with

experiments, the discussed problem becomes even more significant because in deep-hole machining the problem of the relative location of the workpiece and the tool can be solved only by proper setting of the machine component.

In deep-hole machining, the relative location of the tool and the workpiece is defined by the relative location of the axes of rotation of the tool, workpiece and starting bush as shown in Figure 6.1.

The problem may become so severe such that many researches, analyzing the signal from the force dynamometer in deep-hole machining, concluded that the cutting force and the process itself have stochastic nature (Osman and Chandrashekhar, 1984). Such a conclusion has no physical justifications since there is no randomly changing components in the machining system. The property of the tool (its geometry and tool material) does not change significantly during the process, the machining regime is maintained with reasonable accuracy, the mechanical properties of the workpiece may change no more then 2-3%. Therefore, this simple consideration shows that the noisy signal may give false impression not only about the magnitude of the cutting force but also about its frequency composition and even its nature.

This chapter presents the proposed methodology and the specially designed setup for misalignment assurance. The chapter begins with a general description of the various components of the deep hole drilling machine which have been used in the designed setup. Then, the principal elements of this setup and overall configuration of the measuring system have been detailed of. Next, a newly-developed calibration procedure is presented.

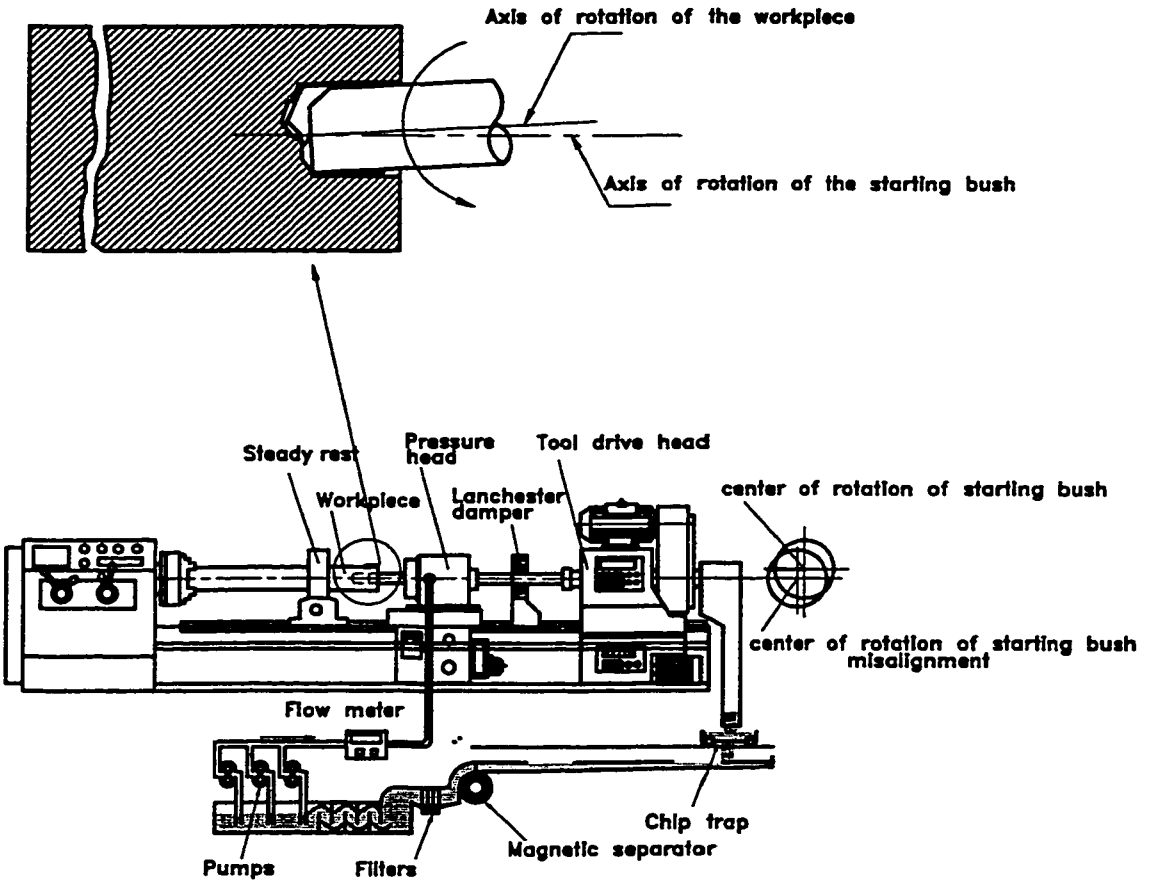

Figure 6.1: Misalignment between the axis of rotation of spindle nose and the axis of starting bush.

6.1 THE DEEP HOLE DRILLING MACHINE

The machine used in this investigation is 30HP Schaerer HPD 631 lathe retrofitted for deep-hole drilling as shown in Figure 6.2. To obtain variable feed drive and speed control, the drive unit motor was replaced with 15 KW variable speed AC motor and the feed motor was replaced with 5 KW variable speed AC motor. The motors are individually controlled by AC invertors. The AC invertors are designed to provide required Volts/Hertz ratio, allowing the AC motors to run at their optimum efficiency. The control section of the AC inventors consists of a control board with a 16-bit microprocessor and keypad interface with an 8-bit microprocessor.

The following is a description for main components of the deep-hole machine used in the experiments.

(A) Cutting Tool Drive Unit: The drive unit consists of two variable speed motors that controls the feed and the rotating speed of the boring bar-tool assembly. The primary rotational motion is applied to the boring bar and the feed motion is applied to the the drive unit sliding along the ways of the machine bed. The boring bar-tool assembly is clamped onto the drive unit spindle. The spindle is mounted on high-precision bearings to minimize its runout and end play.

(B) Pressure Head : The pressure head is used to provide :

- Cutting fluid supply to the drill
- Initial support to the tool by means of the starting bush mounted in the pressure head
- Support and centering for the workpiece by means of a chamfered reception plate installed on high-precision bearings mounted in the pressure head.

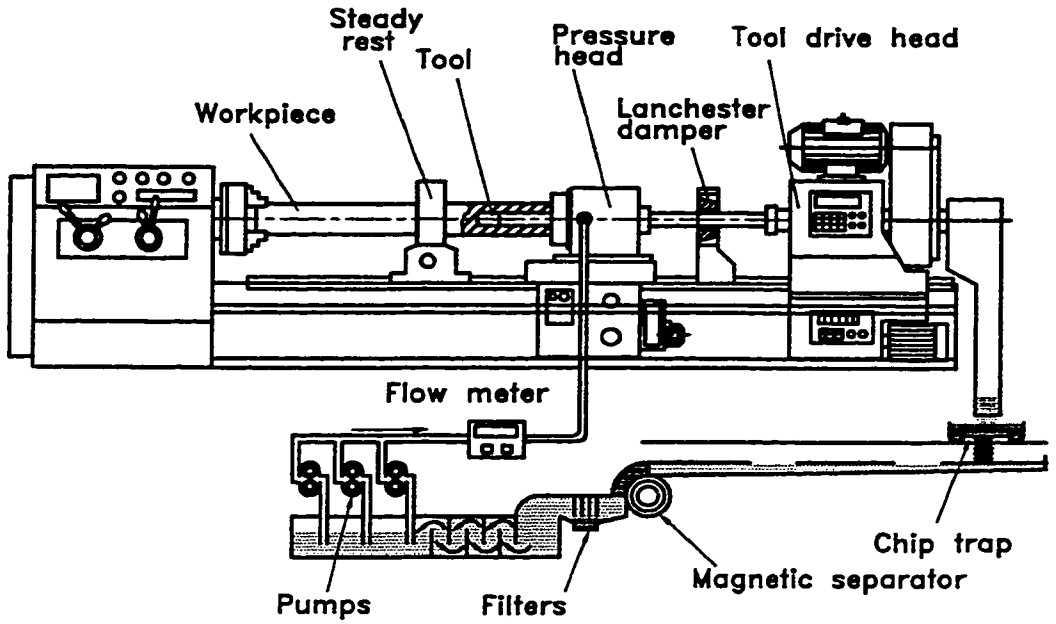

Figure 6.2: Deep-hole drilling machine.

The pressure head can be moved along the machine bed to accommodate workpieces of different lengths. The motion of the pressure head is provided by means of a split nut and lead screw connected to the feed drive. During machining the pressure head is locked at its position ensuring that no leakage occurs at the workpiece-pressure-head reception plate interface.

(C) Workpiece Drive Unit: The machine is designed with possibility to rotate the workpiece. However, in the designed setup, the rotation tool-stationary workpiece scheme has been used.

6.2 MISALIGNMENT MEASUREMENT SETUP

The schematic arrangement of the experimental setup on the deep-hole machine is shown in Figure 6.3. A photograph of the experimental setup is shown in Figure 6.4. A laser-based measurement system has been developed to measure the misalignment between the axis of rotation of spindle nose and the axis of starting bush of the deep hole machine. A reference laser beam has been generated by a laser tube, which is held the chuck of the machine using a special case. The laser beam is captured by a photo sensor camera having a capture video card. The output images are sent to image precessing software capable to track the laser beam position by processing these images. The output from the image processing software represent the position of the centroid of the laser beam on the photo sensor in a certain position along the axis of rotation of the machine. The misalignments have been calculated by comparing the average centroid of the of the images which have been captured when the photo sensor camera and starting bush axes coincide and when the camera and nose spindle axis coincide (Figure 6.5). To align the machine, these centroid must be

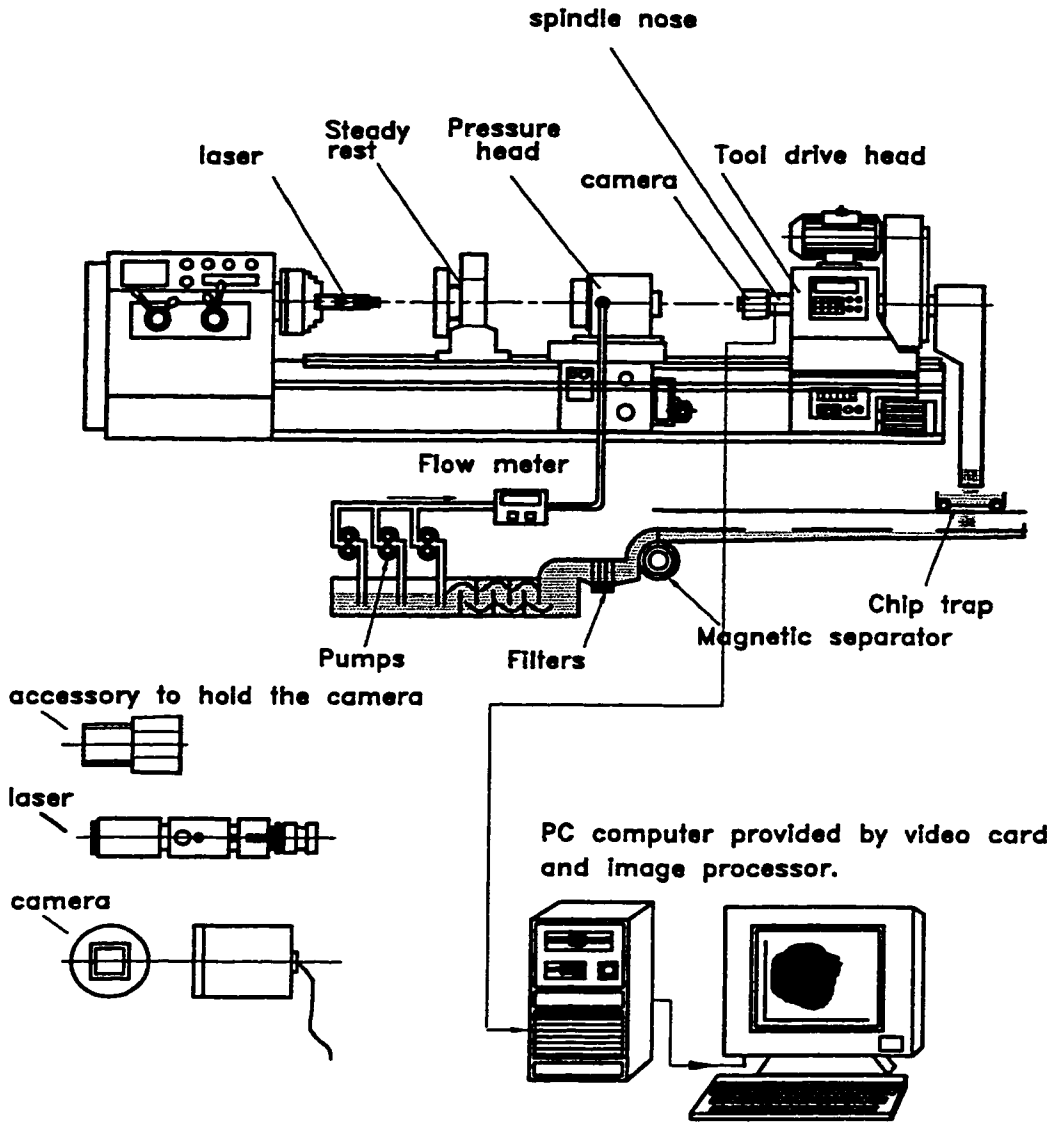

Figure 6.3: The schematic arrangement of the experimental setup.

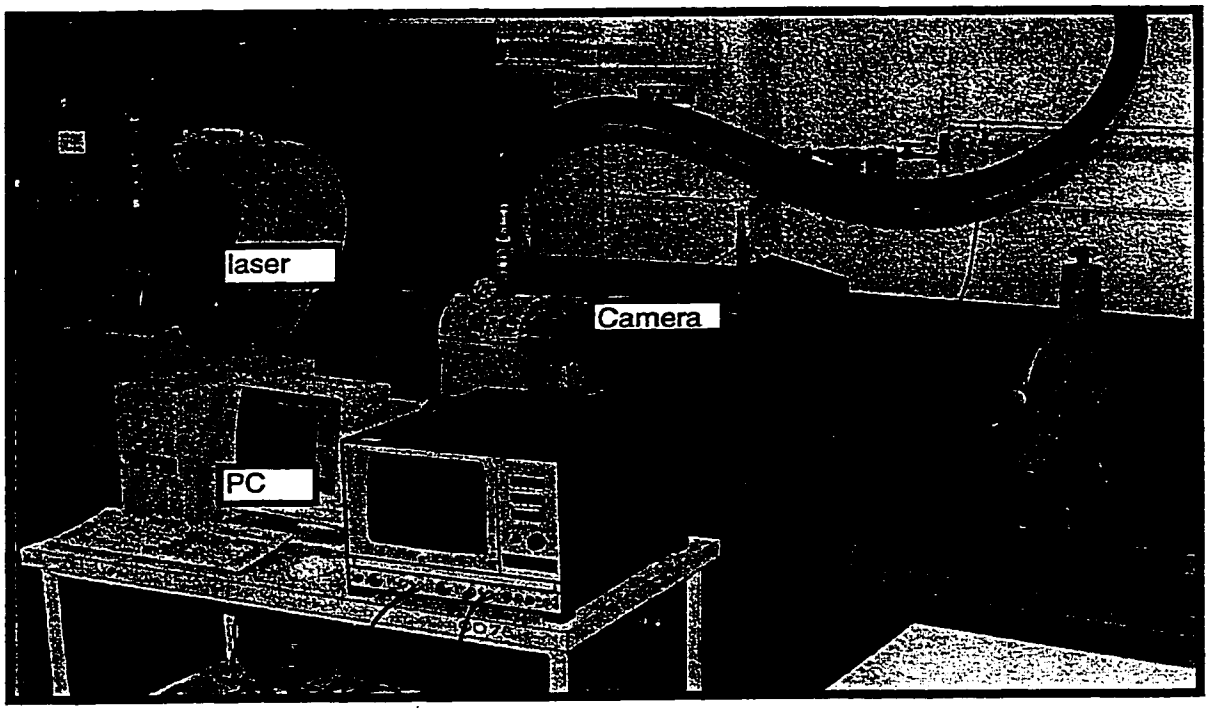

Figure 6.4: A photograph of the experimental setup for misalignment measurement.

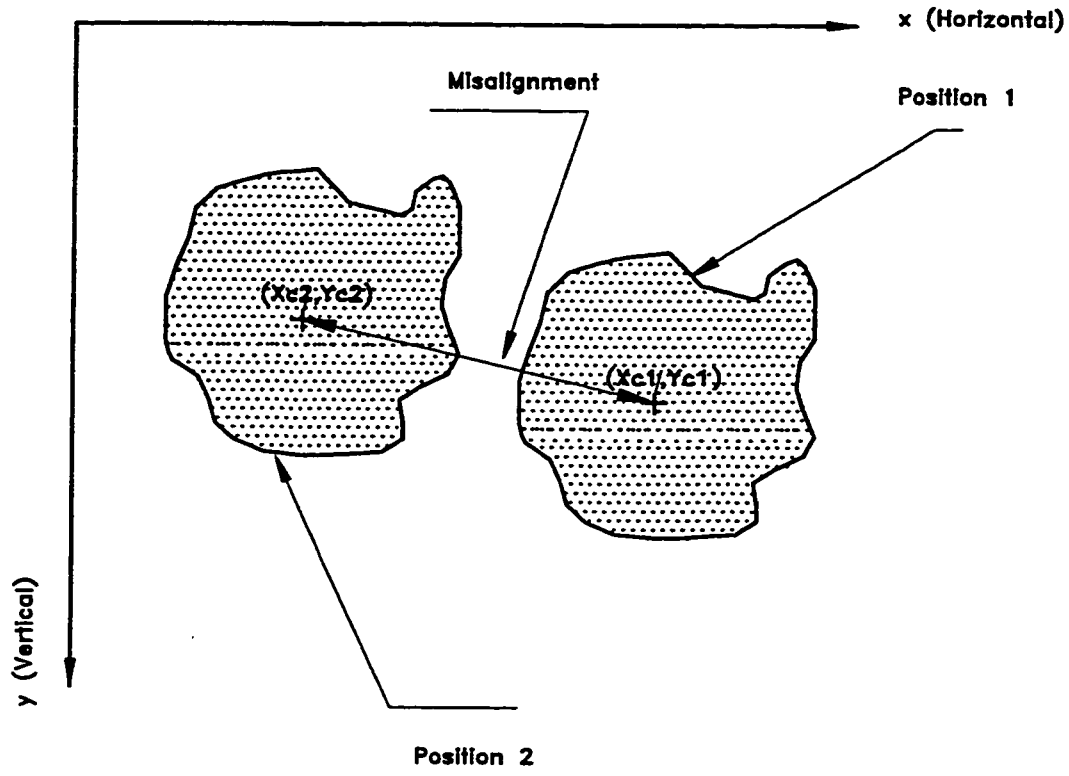

Figure 6.5: The principle of the misalignment measurements.

brought to coincide with the zero reference point. The zero reference point was established on the axis of the cylindrical camera housing within a reasonable tolerance (0.5 micrometer). A special accessory has been designed to hold the photo sensor camera in different position along the axis of rotation of the machine. To study the effect of misalignment, the starting bush was intentionally misaligned by moving the pressure head over the carriage using the lead screw of the cross slide.

The principal elements of this setup (Figure 6.6) are as follow:

1. Laser (LTT4H Adjustable Alignment Tool, Emerging Technologies Inc., Laseraim tool division, Little Rock, AR, USA) : This laser project a laser beam visible as a "dot" of laser light on distant surfaces. The laser beam is projected in perfectly straight line from the laser referred as the tool. This beam is used as a straight reference line over the entire length of the beam. The tool have adjustable focus feature which allows to control the laser dot size on a surface located perpendicular to the beam (referred to as the screen). This adjustment allows the use of the smallest possible dot size at specific distance thus facilitates more accurate measurements. Since the focus adjustment is also linear, a change in the focus will not affect the units X and Y alignment. In practical terms it means that the smallest possible dot size may be used at a close distance from the tool and then, when the screen in placed further, the tool may be re-focused again to the smallest possible dot keeping the centroid of these two dots on the same plane.
2. A photo-sensor digital camera Pulinx TM7 has been used as the screen. This camera contains high resolution interline transfer ½ `` CCD (charge-coupled device). The camera was requested from the manufacturer to be of super mini size that allows it

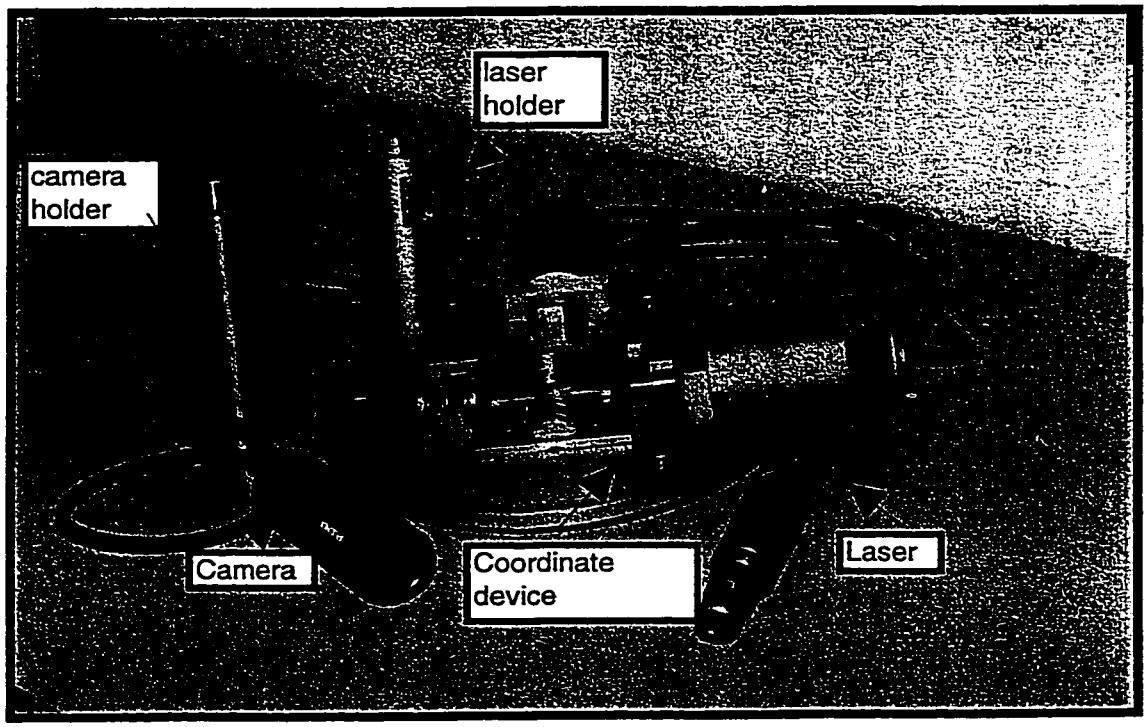

Figure 6.6: Photograph of the principal elements of misalignment setup.

accurate and convenient mounting within the setup.

3. A special case to hold the laser in the chuck as depicted in Figure 6.7.

4. A special case to mount the camera in different positions along the machine bad. This case , as shown in Figure 6.8, was precisely manufactured to achieve: a) to match the cone in the starting bushing liner, b) to match the diameter of the camera, and c) to match the outer diameter of the spindle nose. Figure 6.9 shows a picture of these accessories.

5. Video capture card : This card is a single-slot, accelerated, 24 bit-per-pixel, true-color, designed to capture and display high quality video images. The card provides the complete set of camera control function required for capturing high quality images. The card is also supported with a fully comprehensive software that allows fully exploitation of the hardware architecture. Captured images are saved as BMP or TIFF files.

6. Image processing software (Matrox Inspector, Version 2.0) : The images captured by the camera were precessed to find the centroid of the images. This centroid represent the center of rotation of the boring bar. A typical example of the captured images and the processed images along with the results of the processing is shown in Figure 6.10.

6.3 CALIBRATION OF THE SYSTEM

To ensure the repeatability and reproducibility of the proposed technique, a special care has been paid to the calibration of the proposed system.

The first step in the calibration procedure is to align the laser beam to be parallel with the case of the laser. This provides a laser beam parallel to the laser case at any distance and

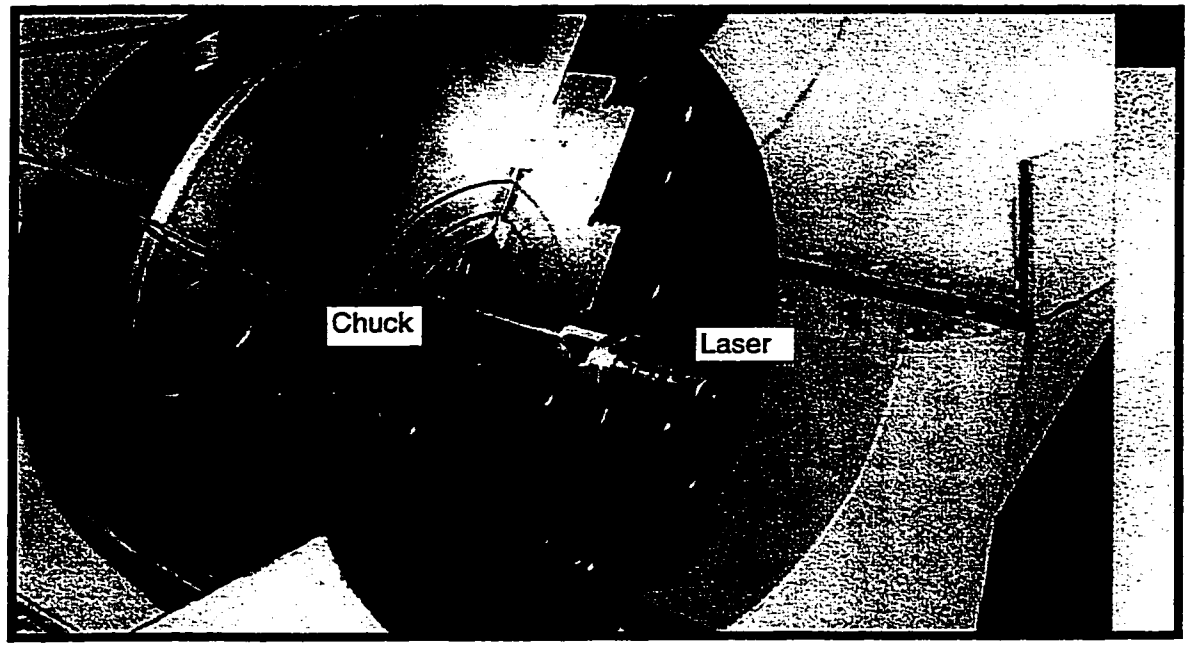

Figure 6.7: Laser holder.

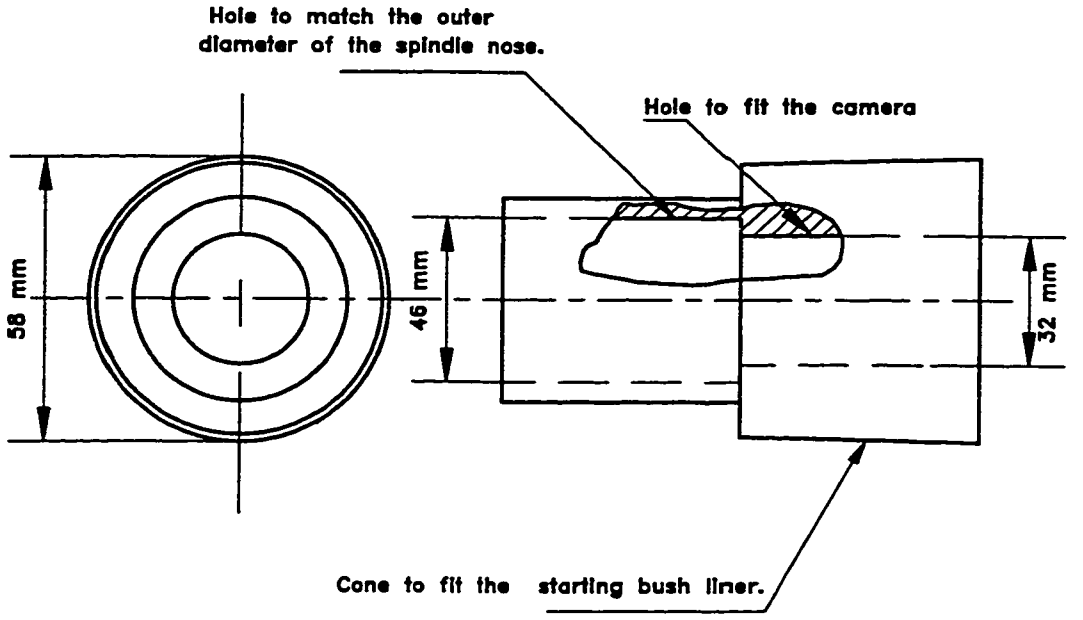

Figure 6.8: Accessory to mount the camera in different positions.

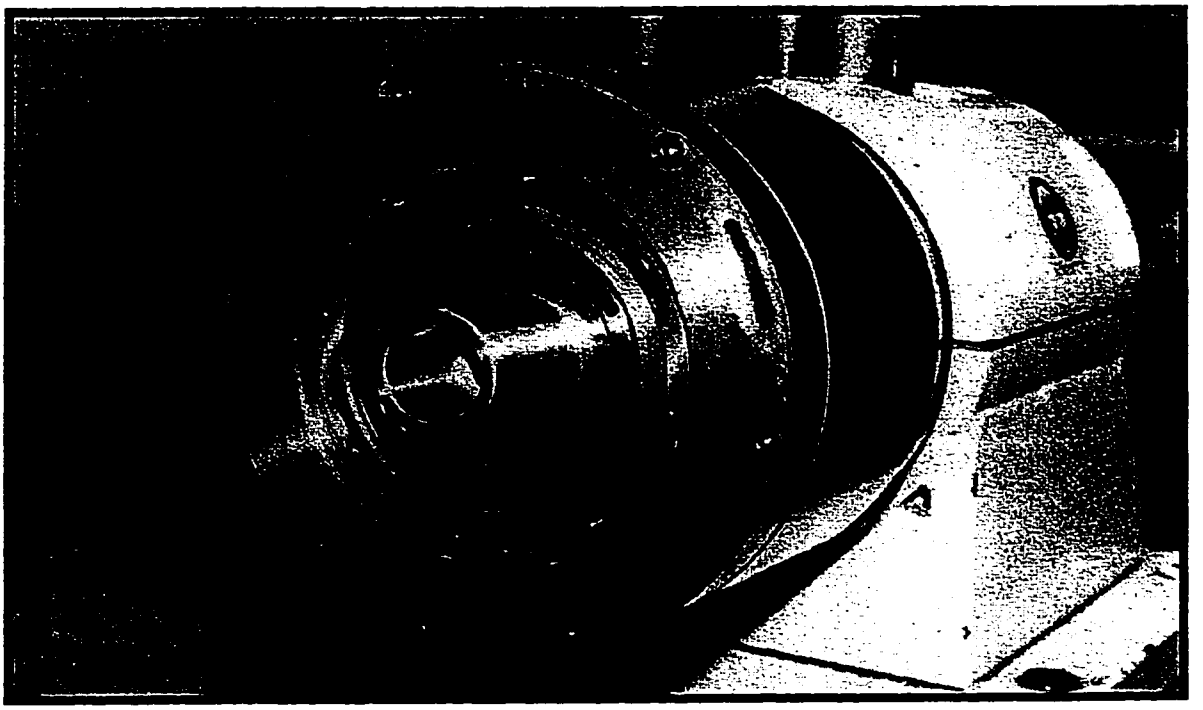

Figure 6.9: A photograph of the accessory for mounting the camera in different positions

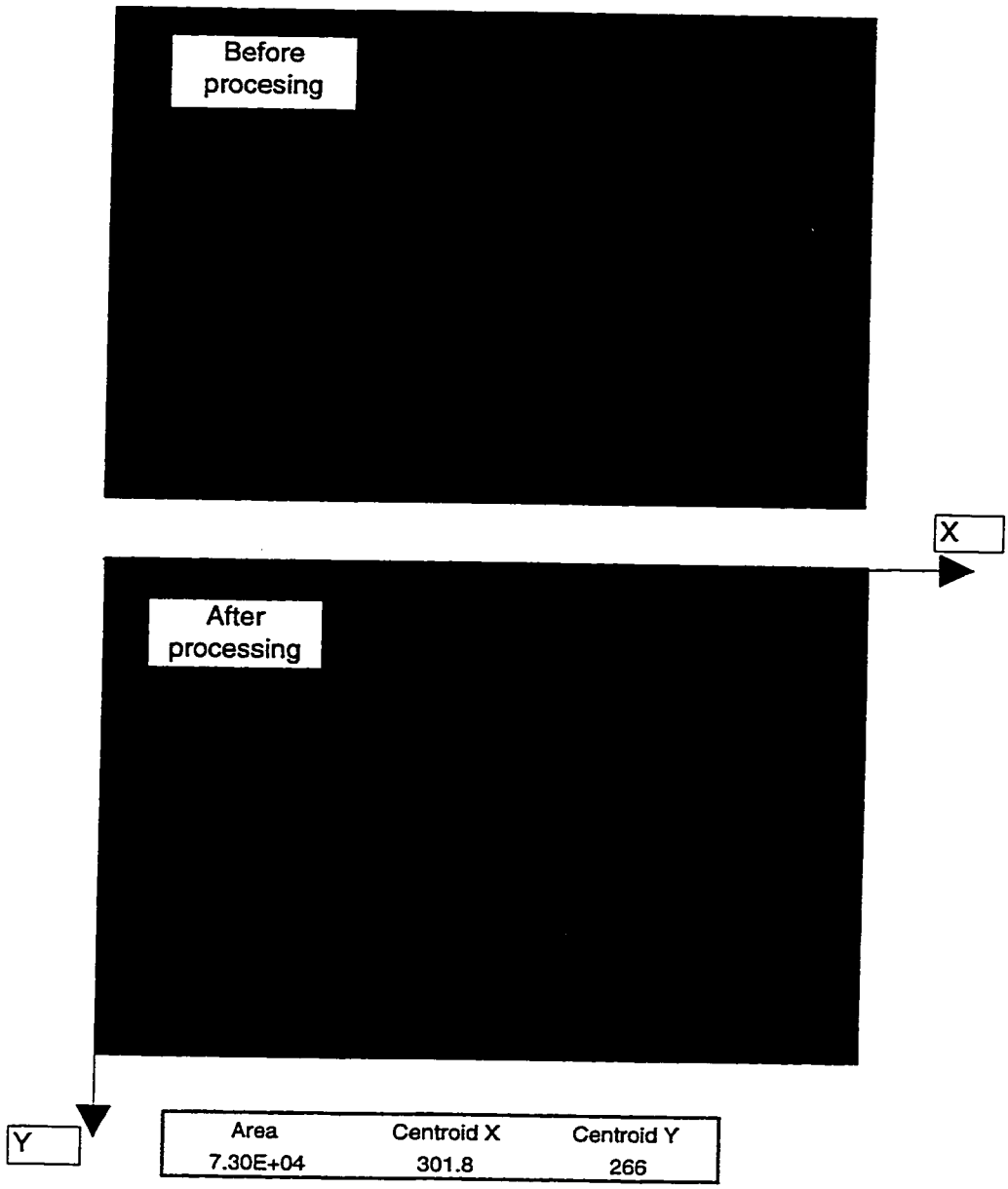

Figure 6.10: An example of the captured image, and the results of the image processing.

can be used as a reference over the entire length of the beam. To align the laser, a V-block has been used. The following nine-steps procedure has been developed and recommended:

1. Project the laser beam onto a screen placed approximately 20 meters away.
2. Rotate the case until the switch is in the straight up 12 o'clock position.
3. Mark the exact center of the laser dots over the distant surface.
4. Rotate the tool 180 degrees so that the switch is straight down in the 6 o'clock position.
5. Mark the exact center of the laser dots again.
6. Draw a line connecting the marks.
7. Measure the length of the line and mark the center point between the two marks.
8. Adjust the tool using the X and Y micrometer heads until the center of the laser dot covers the center point between the two marks.
9. Check the result by rotating the tool on V-block. The projected dot image should turn on itself. The center of the dot should remain in the same position. If the center of the dot moves or the dot draws a circular pattern when rotated, the alignment procedures should be repeated again until center of the dot remains in a constant position when the tool is rolled.

The second step is to check that the tool coincides with the axis of the chuck. To do this, the following steps have to be executed:

1. Hold the laser case in the chuck of the machine.
2. Focus the beam on the screen to shoot the smallest possible dot.
3. Rotate the chuck by hand.
4. Mark the circle produced by the dot.

5. Find the center of this circle.

6. Adjust the laser using the X and Y micrometer heads and bring the dot to the center of the circle until the dot does not move when rotating the chuck and the projected dot image turns on itself.

The third step is to calibrate the laser-camera-image processor system. To do this, a coordinate device has been designed as shown in Figs. 6.11 and 6.12. The setup of the calibration is shown in Figure 6.13 and pictured in Figure 6.14. The camera has been mounted on the coordinate device and was displaced in the X- and Y- directions by the micrometer heads. The images produced by the laser beam have been captured and processed by the image processing. The results of the image processing have been compared with the actual displacements of the coordinate device. Figures 6.15 shows the calibration curves for the system. It can be seen that an excellent agreement between the actual and the measured value was achieved.

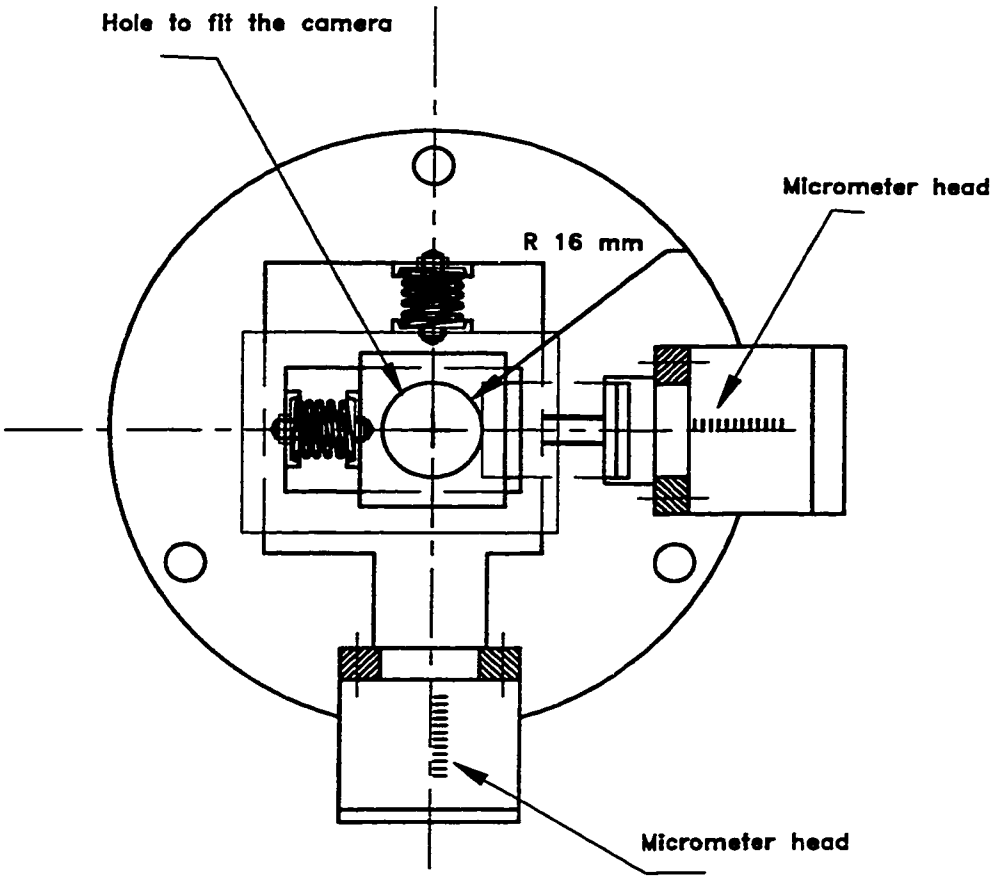

Figure 6.11: A systematic drawing of the coordinate device.

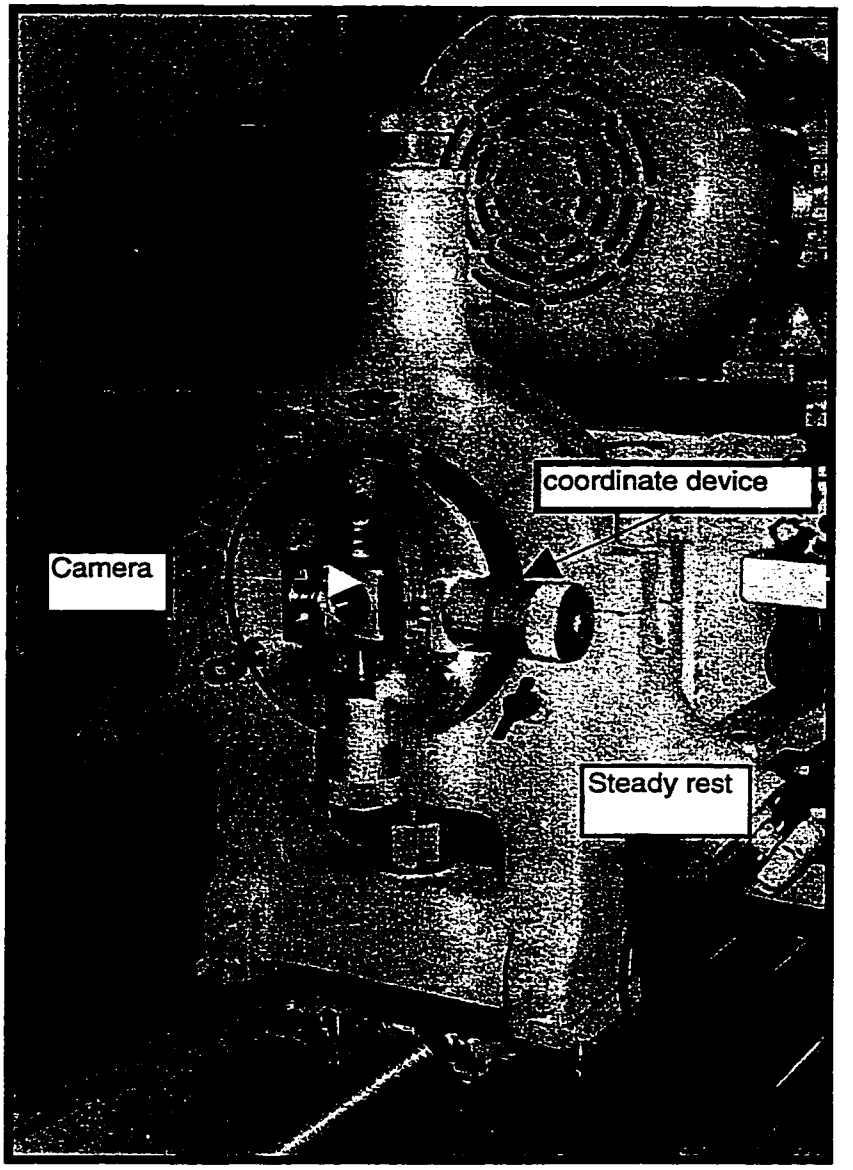

Figure 6.12: A photograph of the coordinate device.

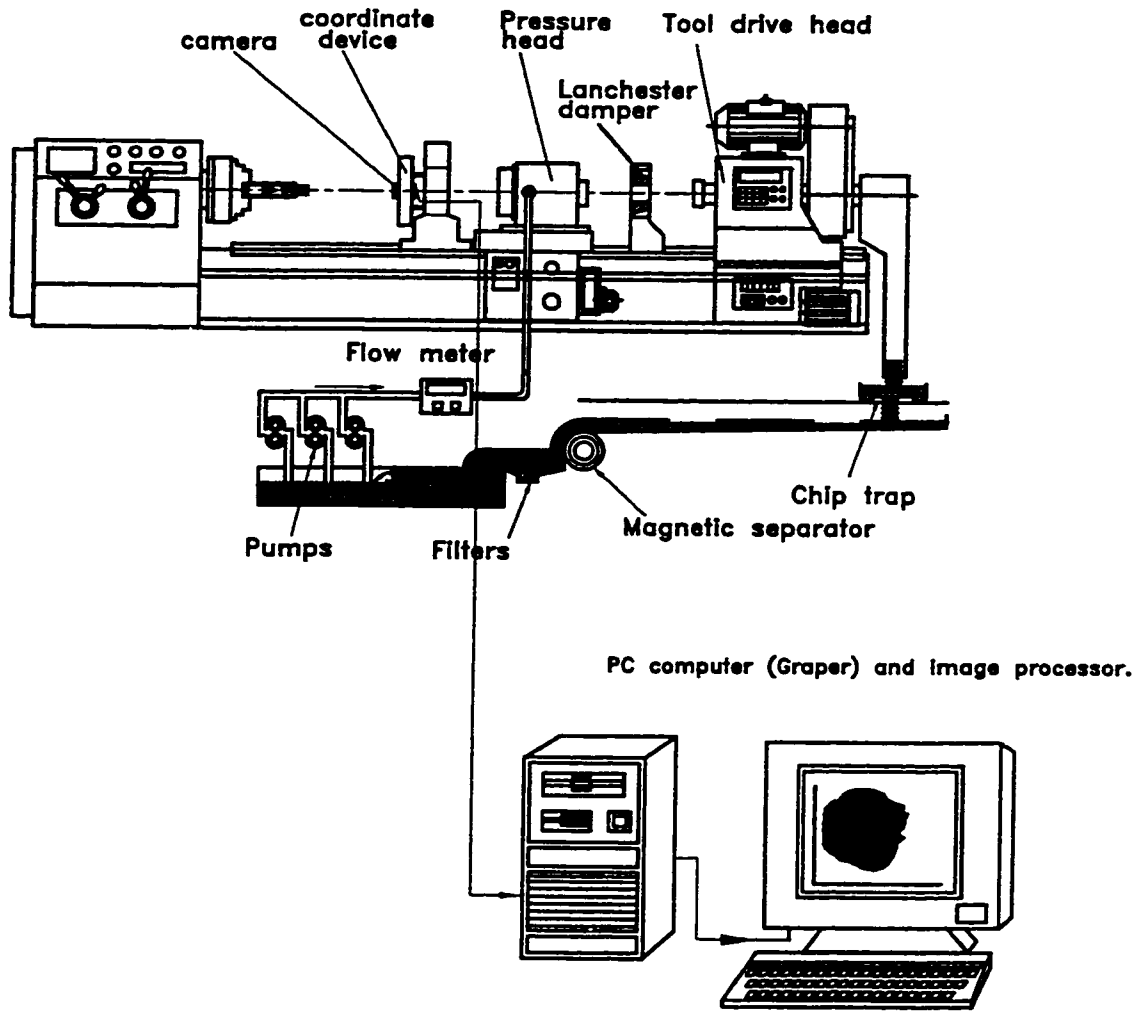

Figure 6.13: The calibration setup.

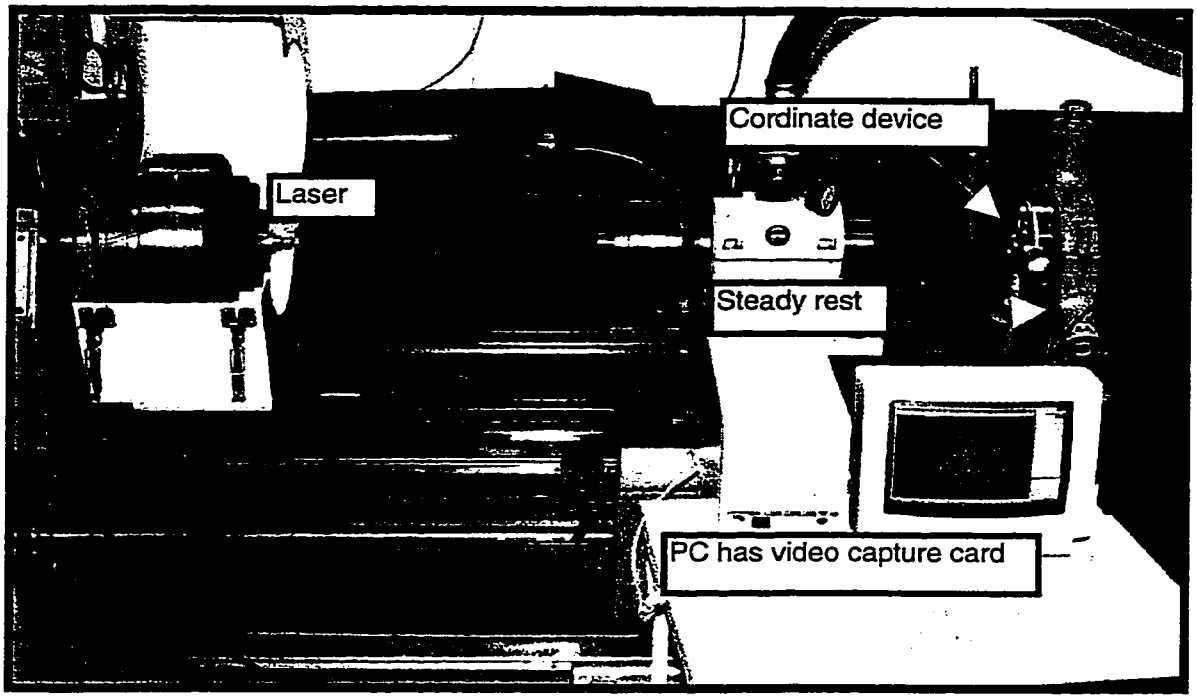

Figure 6.14: Photograph of the calibration setup.

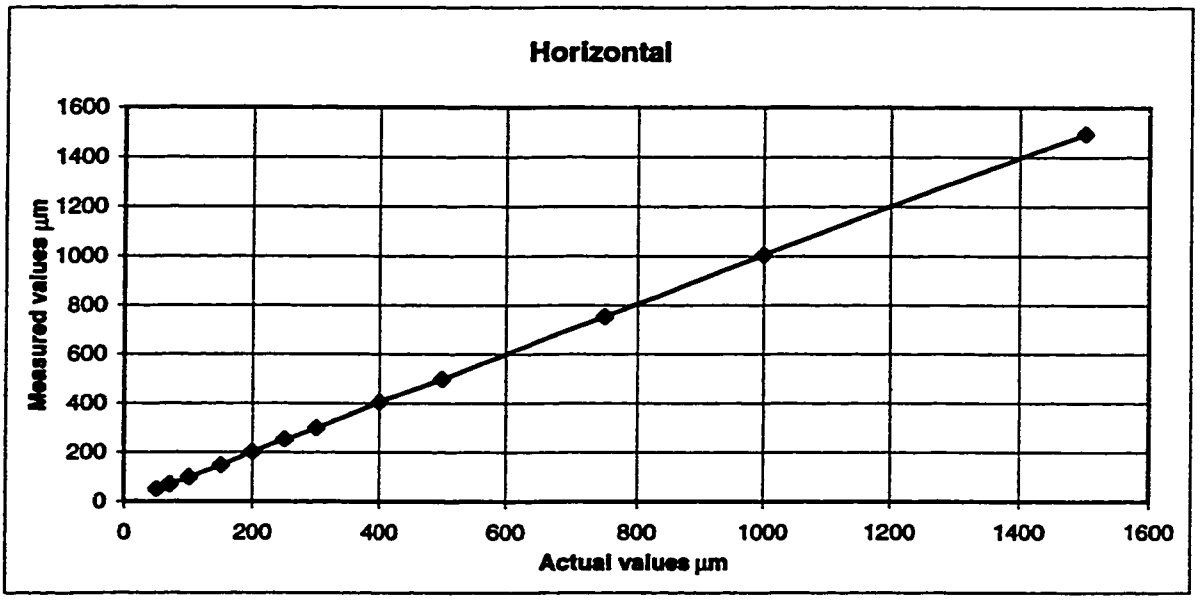

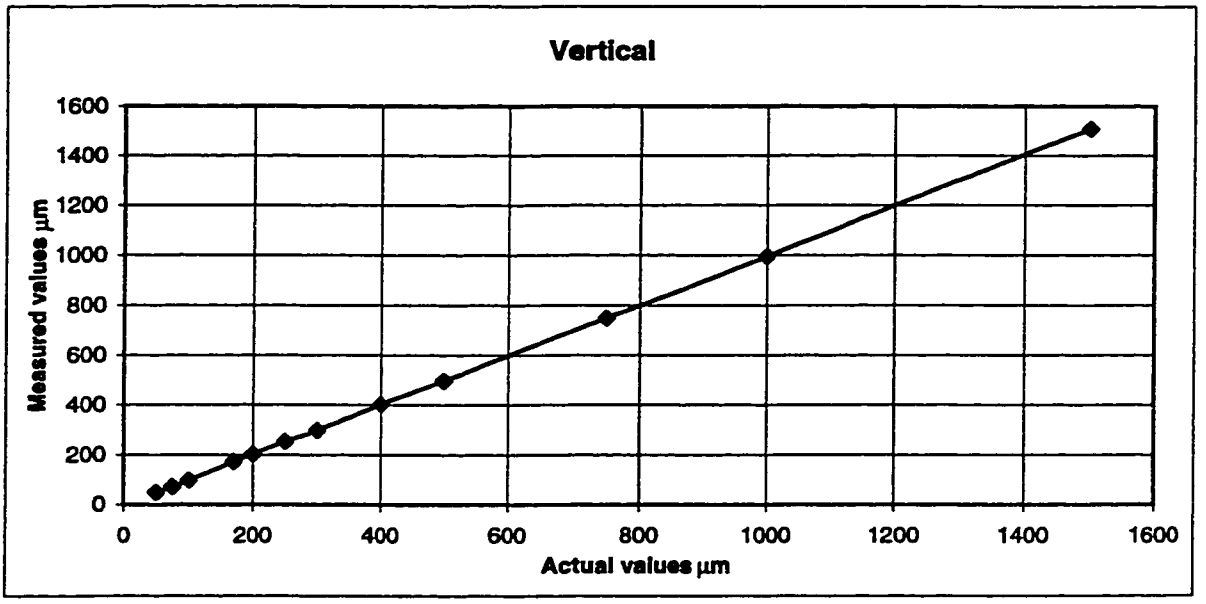

Figure 6.15: Calibration of the proposed misalignment measuring system in the horizontal and vertical directions.

7

CUTTING FORCE MEASUREMENTS AND RESPONSE OF THE DYNAMIC CUTTING PROCESS

As pointed out in Chapters 1 and 2, experimental verifications are required to validate the proposed models in terms of the steady-state, dynamic cutting forces and the dynamic response of the cutting process. In doing so, four types of experiments included cutting force measurements have been carried out:

1. Investigation the effect of misalignment on the steady-state and dynamic cutting force and torque.

2. Measuring the steady-state cutting force for three different materials using two types of cutting tools under different cutting regimes.

3. Measuring the dynamic cutting force for wave removing process.

4. Investigation and monitoring of the dynamic response of the chip formation by measuring the cutting force and torque signatures.

This chapter presents full descriptions for the materials, cutting tools, workpiece, equipments, experimental setups, calibrations and analysis procedures used to perform the required experiments.

7.1 WORKPIECE MATERIALS

Four types of workpiece material, representing four major groups of materials used in industry, were selected to the study:

1. AISI 1025 HR ASTM A576 RD.

2. AISI 1045 HR ASTM A576 RD.

3. AISI 4340 HR ANN RD ASTM 322 91.

4. AISI 303 ANN CF RD ASTM A582 93.

Tables 7.1, 7.2, 7.3 and 7.4 show the chemical compositions of the selected materials. The composition, and the element limits for these materials had been chosen according to the requirements of standard *ANSI/ASME B94.55M-1985* and were requested from the steel dealer.

Table 7.1: Description of AISI 1025 STEEL.

Description : 1025 HR Specification: ASTM A576									
CHEMICAL ANALYSIS									
0.26	0.52	0.004	0.02	0.20	0.10	0.03	0.03	0.019	0.0
0.006	0.002	0.006							

Table 7.2: Description of AISI 1045 STEEL.

Description : 1045 HR A576 RD Specification: ASTM A576									
CHEMICAL ANALYSIS									
0.470	0.83	0.007	0.019	0.29	0.14	0.03	0.03	0.025	0.0
0.008	0.002	0.009							

Table 7.3: Description of AISI 4340 STEEL.

Description : 4340 HR ANN RD Specification: ASTM A322 91									
CHEMICAL ANALYSIS									
0.402	0.09	0.024	.0007	.0013	0.72	1.82	0.003	0.001	0.006
0.87	0.005	0.012	0.023	0.25	0.005	0.26	0.008	.0002	

Table 7.4: Description of AISI 303 STEEL.

Description : 303 ANN CF RD Specification: ASTM A582 93									
CHEMICAL ANALYSIS									
0.07	1.93	0.38	0.326	.038	17.46	8.45	0.24	0.43	0.04

7.2 WORKPIECE TYPES

Three types of workpiece specimens were used :

1. Test specimens of 37.5 mm diameter and of 600 mm length. These specimens were welded with flanges which, in turn, were clamped to the dynamometer. Six samples from AISA 1045, AISA 4340 and AISA 303 materials were prepared (Figure 7.1).
2. Test samples of 37.5 mm diameter and of 600 mm length made from AISI 1025 steel. These samples were welded with flanges which in turns were clamped to the dynamometer. The outer surface of these workpieces has been waved using CNC machine to obtain sinusoidal wave of 0.05 mm amplitude.

7.3 CUTTING TOOLS

Two types of machining process have been used in the experiments, namely, turning and deep-hole drilling. Consequently, two different types of cutting tools have been utilized:

(A) Cutting Tools for the Turning Process : A special tool holder and indexable carbide inserts were used. The inserts were grinded with different rake angles. Tool material was carbide C-6. The inserts used were ground with a zero nominal cutting edge radius which were controlled using a computer-controlled optical corporator (Mitutoy PH 350). The actual radius did not exceed values of 0.015 mm.

(B) Cutting Tools for Deep-Hole Drilling Process : Two commonly tools have been used in this process, single cutting edge BTAH (American Heller design) and partioned cutting edge BTAS (Sandvik design) drills as shown in Figures 7.2 and 7.3 respectively. Figure 7.4 pictured these cutting tools.

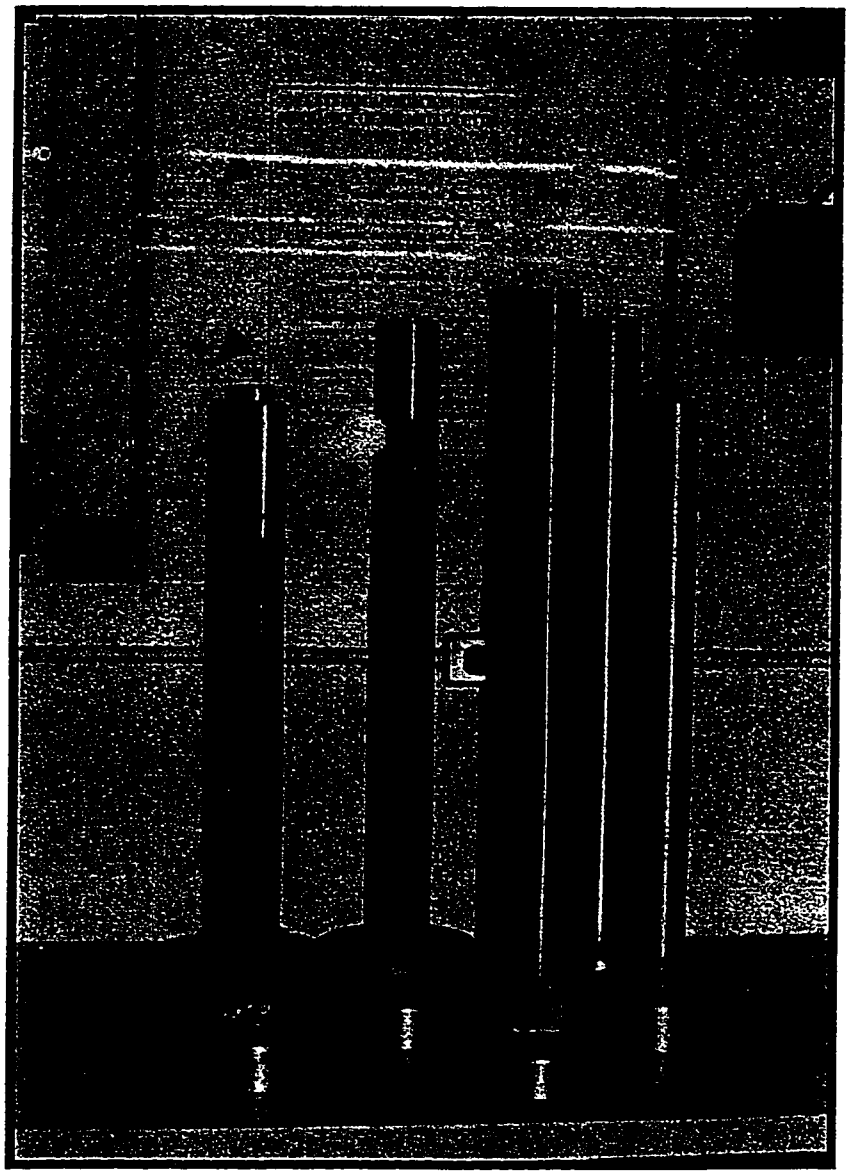

Figure 7.1: A photograph of the workpieces used.

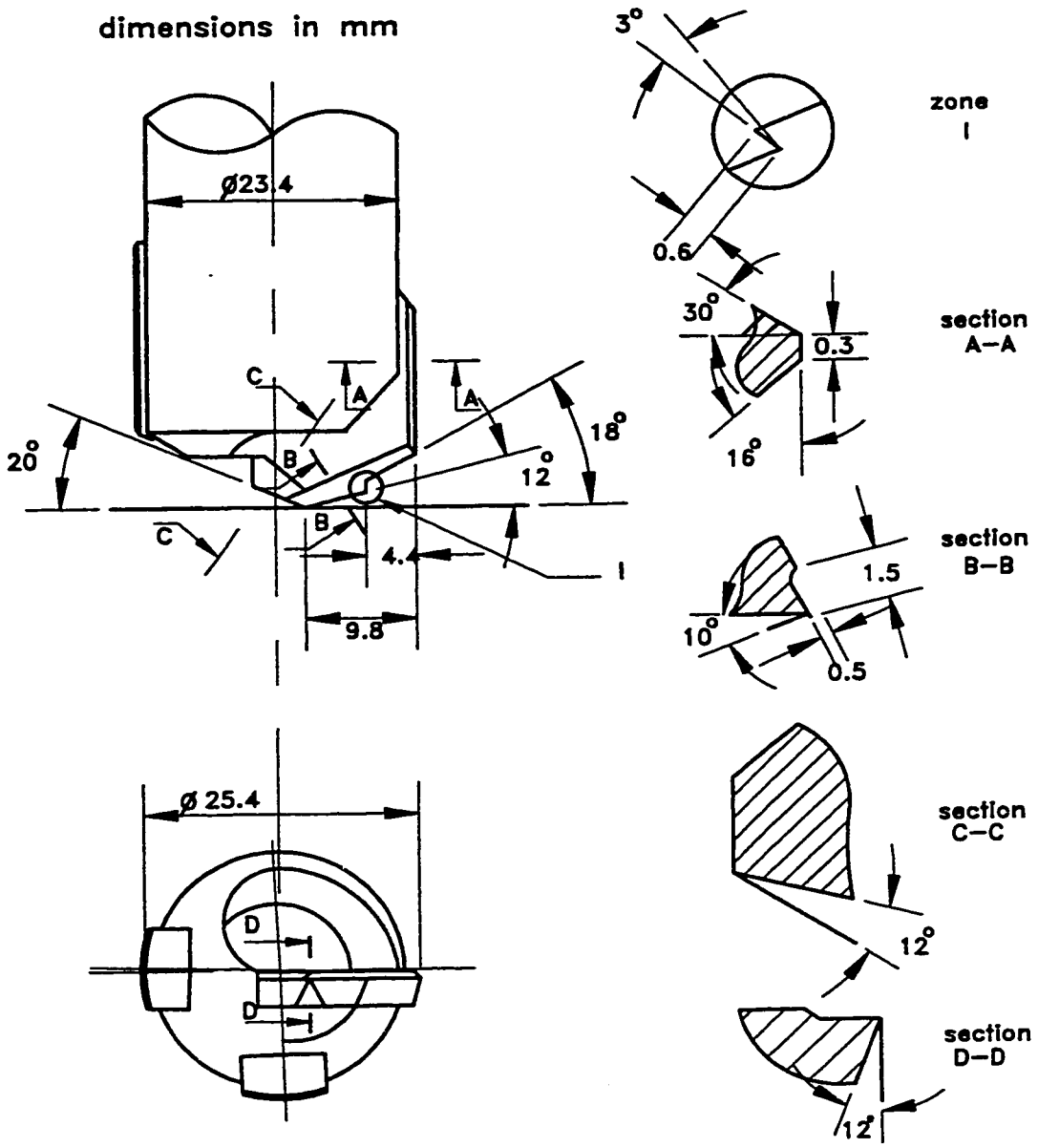

Figure 7.2: BTAH tools of single cutting edge (American Heller design).

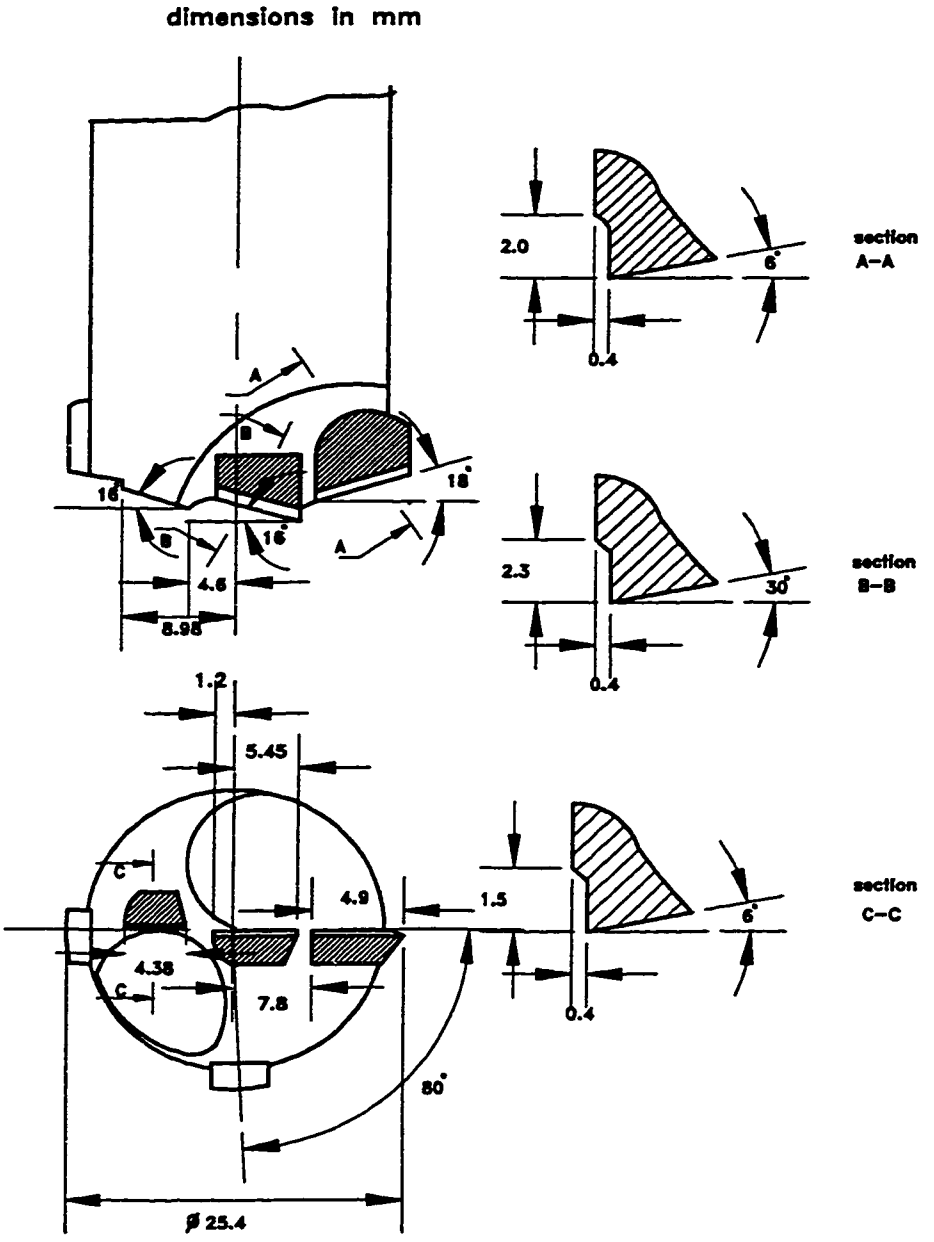

Figure 7.3: BTAS tools of partioned cutting edges (Sandvik design).

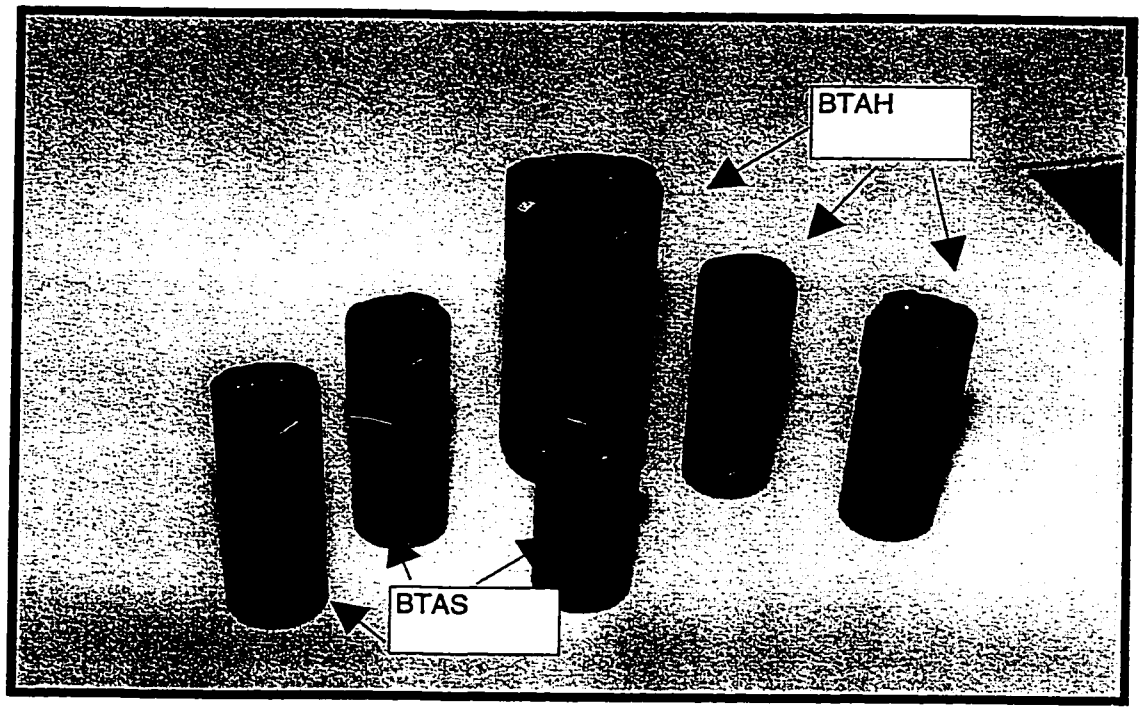

Figure 7.4: A photograph of the cutting tools used.

7.4 CUTTING FORCES MEASUREMENT SETUP

The setup for measuring the static and dynamic cutting forces consists of the following sub-systems as shown in Figures 7.5 and 7.6 and pictured in Figure 7.7 :

1. Deep-hole drilling machine (described in the previous chapter).
2. Dynamometer : The dynamometer shown in Figure 7.8 (pictured in Figure 7.9) has been designed to insert a 2-component load washer, Kistler Type 9065 according to the standard specified by the supplier (Kistler) (Figure 7.10). As recommended, the load washer was pre-loaded to 120 KN to measure the cutting force over a range from -20 to +20 KN and the cutting torque over a range from -200 to +200 Nm. Table 7.5 presents the technical data of the load washer used in the experiments..
3. Charge preamplifiers: Two charge preamplifiers (Kistler model 5004) have been used to convert the output of the load washer into voltage and feed it to the FFT analyzer.
4. Dual-channel Fast Fourier Transformation (FFT) spectrum analyzer (B&K Analyzer Type 2032) : The data acquisition was performed by means of the FFT Spectrum Analyzer using functions in both time and frequency domain. Figure 7.11 shows the main functions of this analyzer. The FFT unit is provided with low-pass filters which cut off at 25600 Hz, (the antialiasing filters), and with additional filters which cut off at 6400 Hz. During the measurements, both sets of filters have been used at frequencies below 6400 Hz, since this give extra dynamic range, and avoid effects due to the transducer resonances.
5. User interface between the FFT and PC to control the measurements.

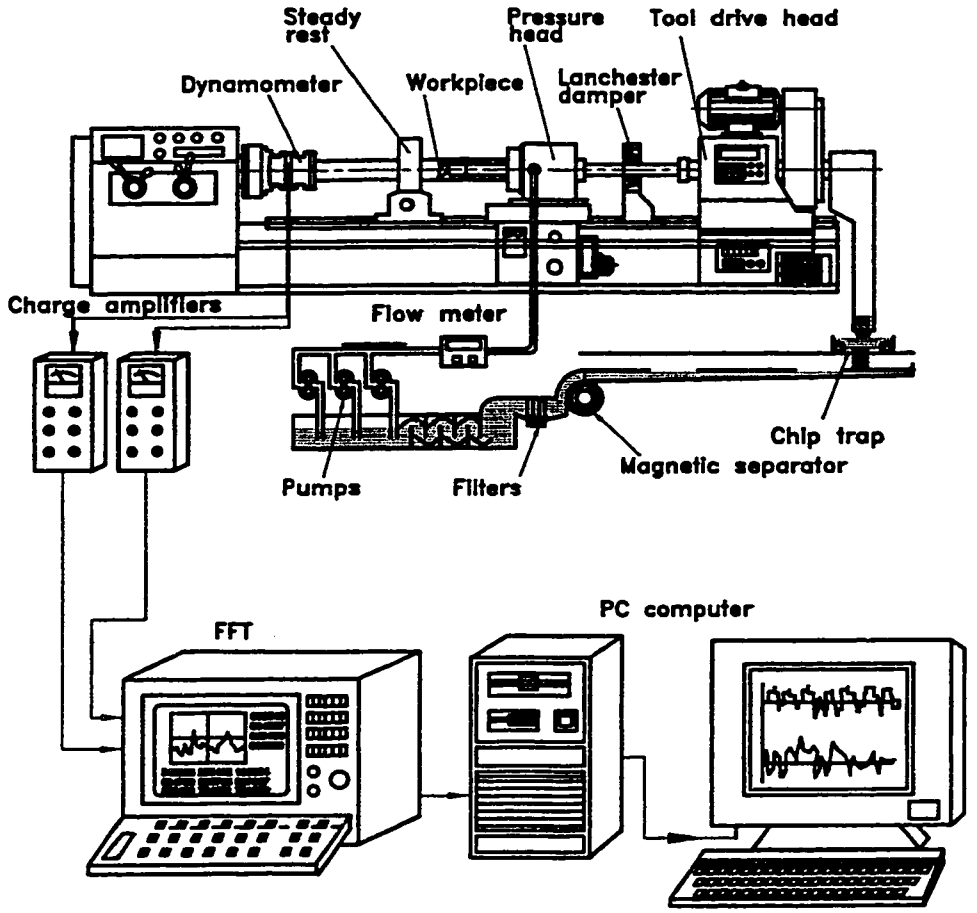

Figure 7.5: Set up for measuring the cutting forces in drilling.

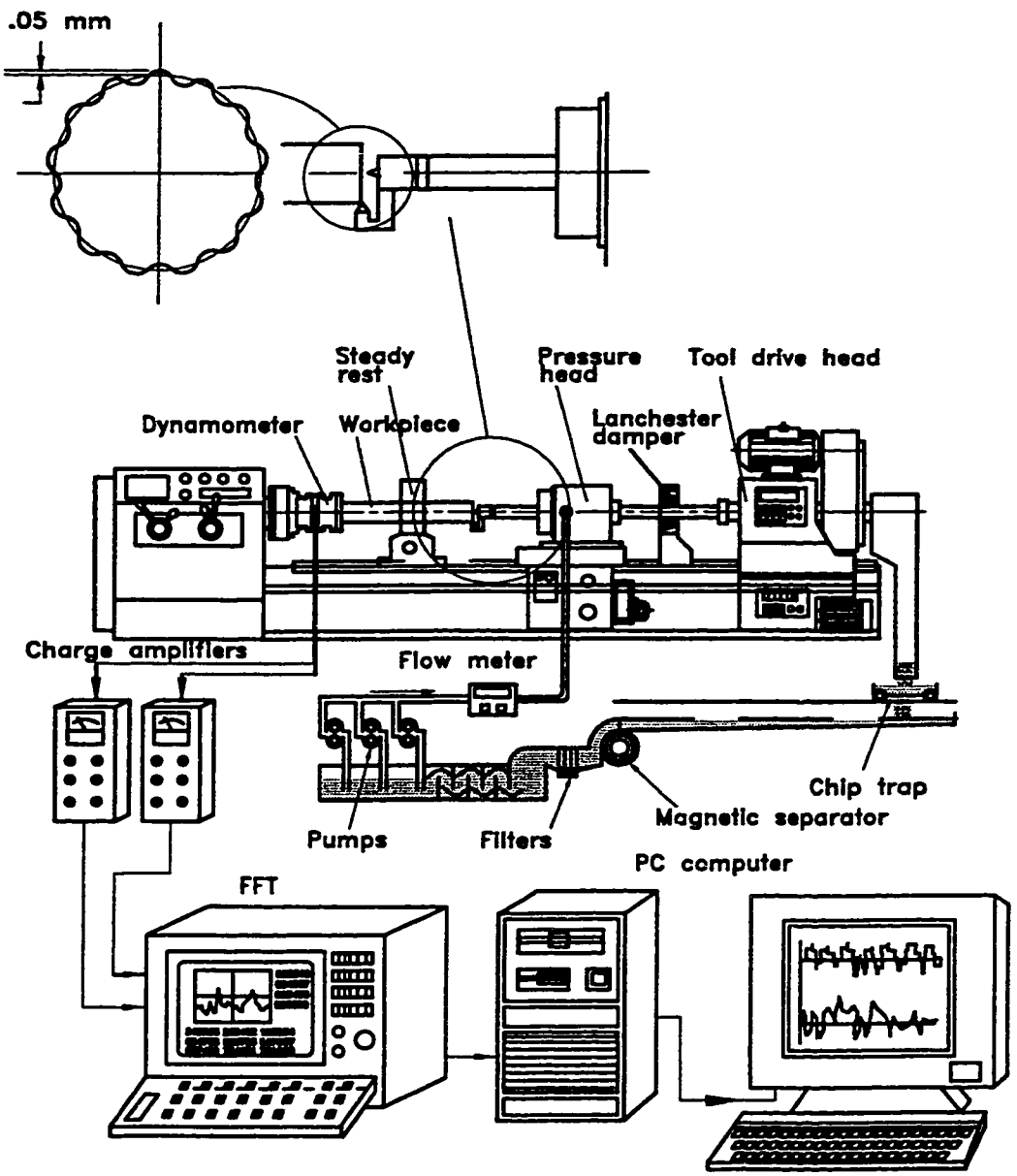

Figure 7.6: Set up for measuring the dynamic cutting forces in wave-removing cutting process.

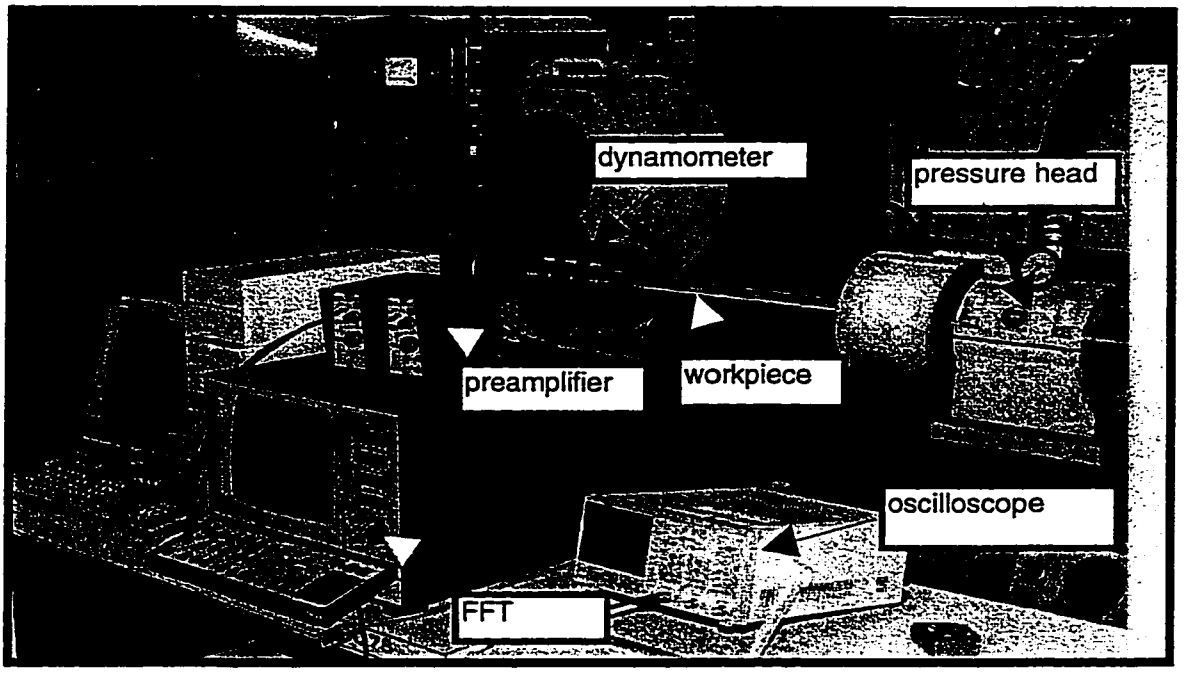

Figure 7.7: A photograph of the set up for measuring the steady-state and dynamic cutting forces.

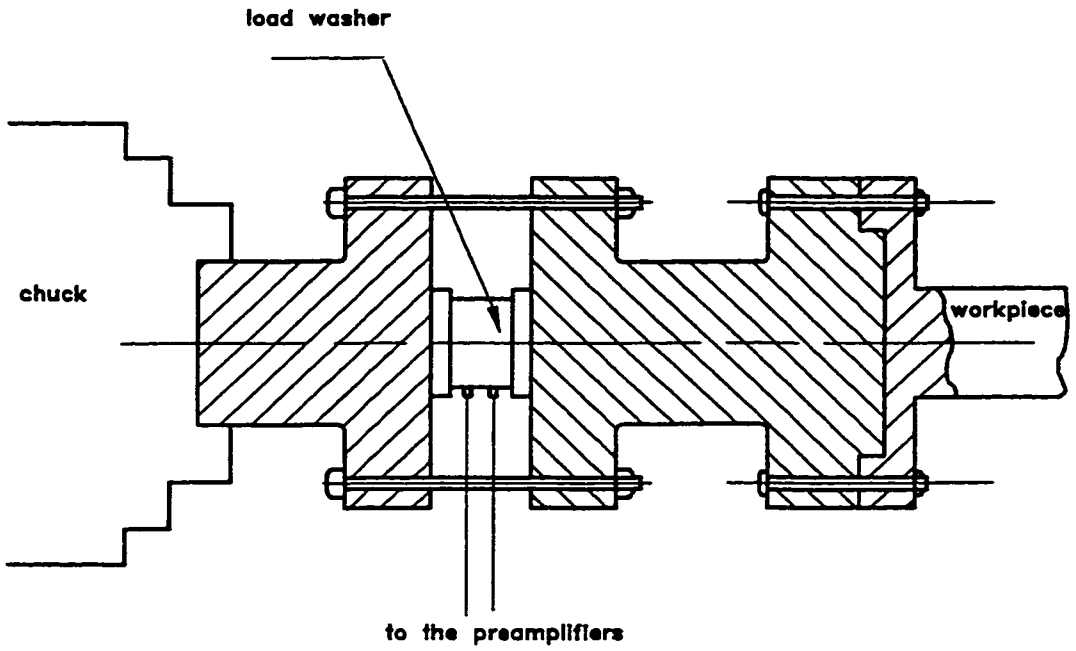

Figure 7.8: Dynamometer.

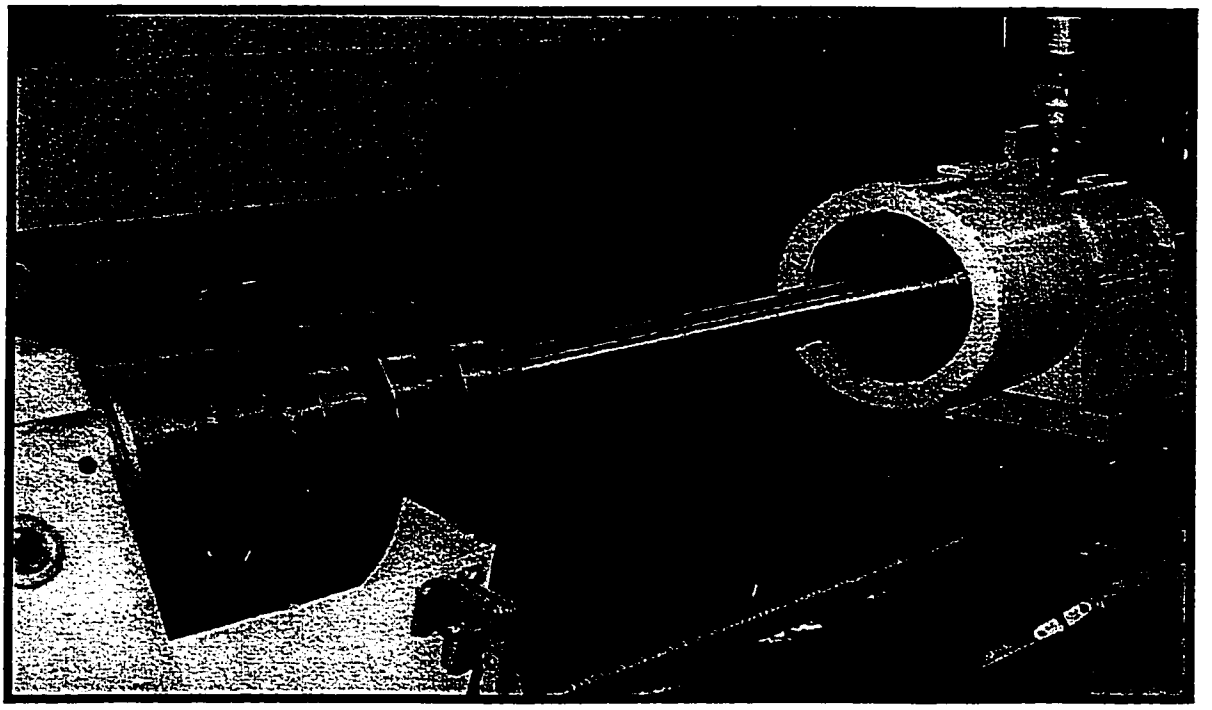

Figure 7.9: A photograph of the dynamometer.

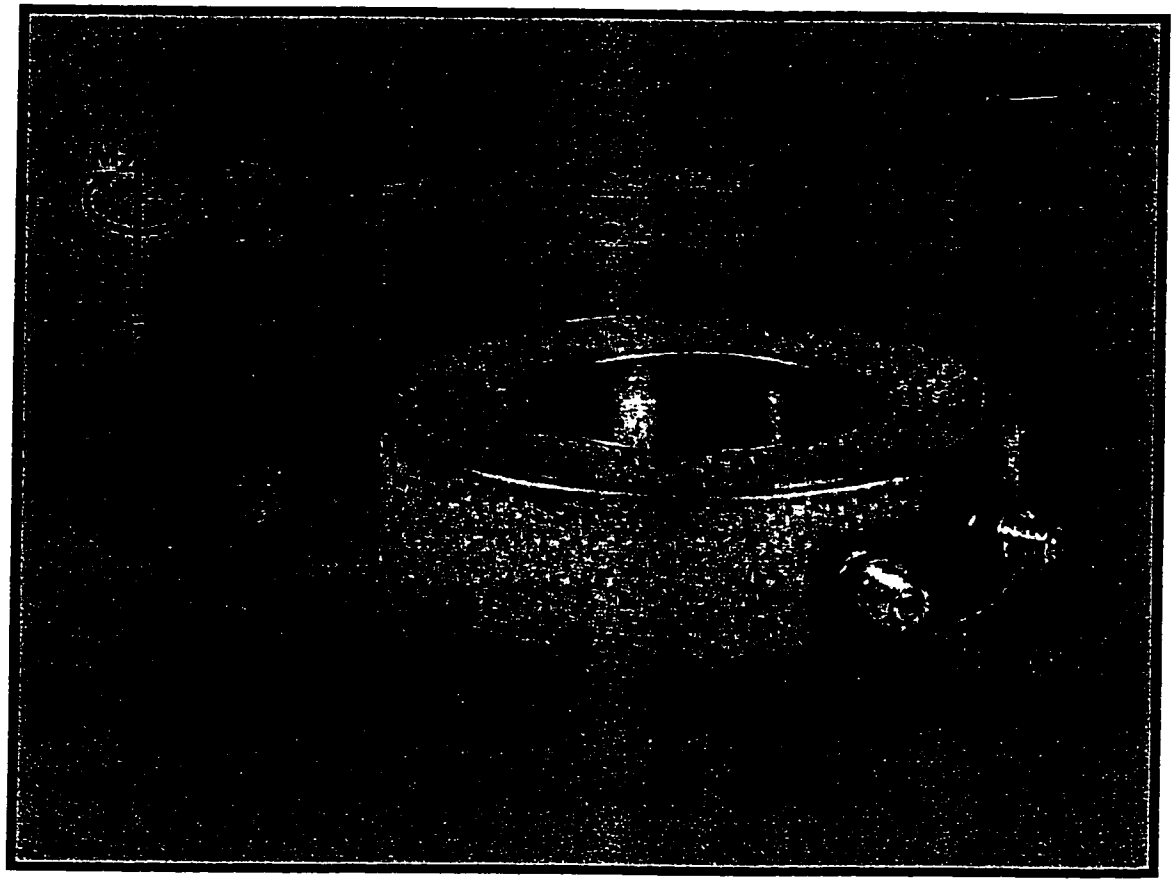

Figure 7.10: Kistler 9065 load washer.

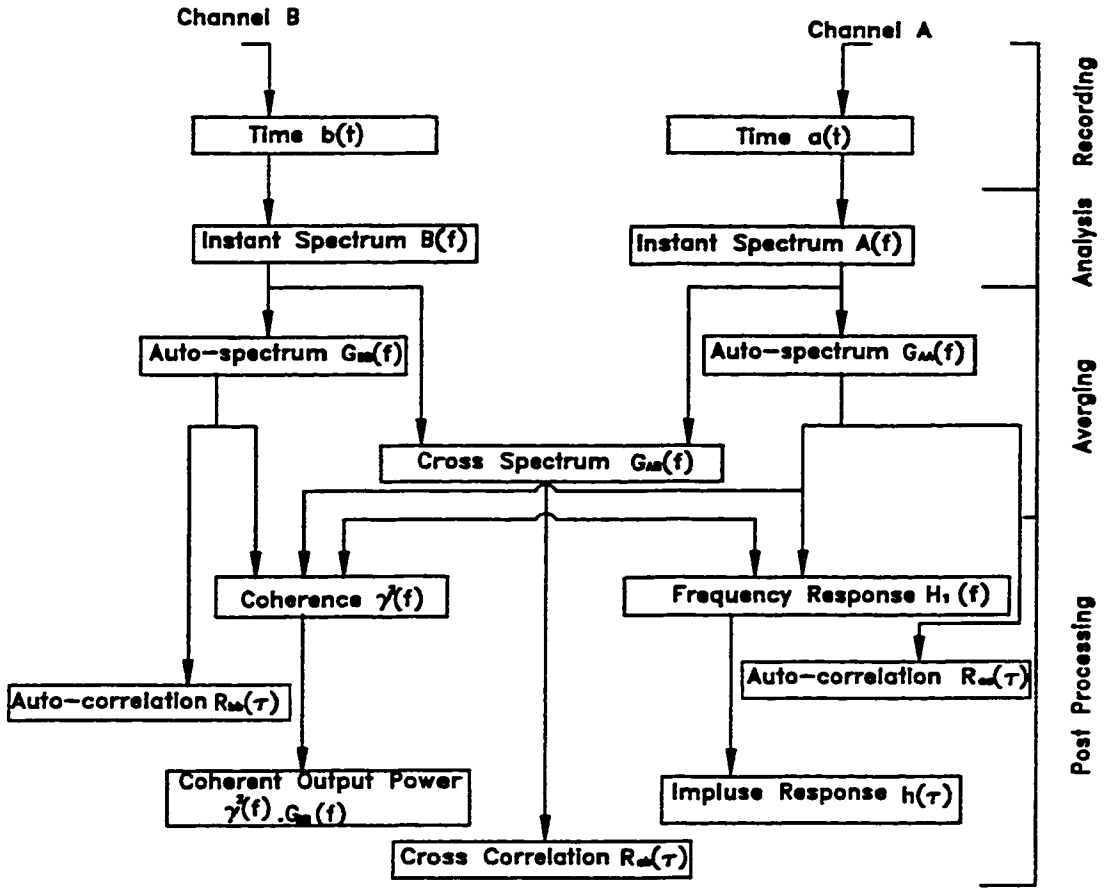

Figure 7.11: Main functions of FFT analyzer.

Table 7.5: Kistler 9065 technical data

Range F_z	± 20 kN
Range M_z	±200 N.m
Sensitivity F_z	-1.8 pC/N
Sensitivity M_z	-1.6 pC/N.cm
Crosstalk $F_z \rightarrow M_z$	±0.02 N.cm/N
Crosstalk $M_z \rightarrow F_z$	±0.01 N/N.cm
Natural Frequency	40kHz

7.5 MAIN FUNCTIONS OF FFT

This section presents a brief description of the main FFT functions which were used in the current study to calibrate the experiment setups and to perform the system and signals analyses.

(A) Frequency Response Functions

The main objective of system analysis is to investigate the input-output relationships. A dual-channel Fast Fourier Transform FFT analysis of the input and output of a system permits the calculation of functions which describe its dynamic behavior. These functions, which are the Impulse Response Function IRF, $h(\tau)$, and the Frequency Response Function FRF, $H(f)$, are related via the Fourier transform and contain the same information about the system in two different formats referred as time domain and frequency domain. If the system input signal is $A(t)$ and output signal is $B(t)$ then the Fourier transform of $A(t)$ and $B(t)$ are designated as $A(f)$ and $B(f)$, respectively. In the frequency domain there is a simple

relationship between the input and output given by:

$$B(f) = H(f) \cdot A(f) \tag{7.1}$$

from which it is easy to derive the FRF, $H(f)$.

A dual-channel measurement can be considered to be a simultaneous measurement of the cross-spectrum between the signals in the two channels, and of the autospectrum of each of the two channels. All other functions such as FRF and coherence are derived from these three spectra (Randall, 1987).

(B) Autospectra and Cross-spectra

The autospectrum $G_{AA}(f)$ defined as the mean square of the Fourier spectrum, can be defined through $A(f)$ as:

$$G_{AA}(f) = \overline{A^*(f) \cdot A(f)} \tag{7.2}$$

In this equation the over line denotes an averaged value and the asterisk a complex conjugate. The autospectrum is real and positive because of the complex squaring, whereas the Fourier spectrum is complex. Expressed in different terms, one could say that the autospectrum has zero phase. The cross-spectrum is defined in a similar way (Randall, 1987).

$$G_{AB}(f) = \overline{A^*(f) \cdot B(f)} \tag{7.3}$$

$G_{AB}(f)$ is complex and thus contains a phase, which is the phase between the output and the input of the system under test. This can be verified as follows. Since the input signal may be represented as

$$A(f) = |A(f)| \cdot e^{i\varphi_A(f)} \tag{7.4}$$

and output signal as

$$B(f) = |B(f)| \cdot e^{i\varphi_B(f)} \tag{7.5}$$

i.e. they are the two complex Fourier spectra in the polar coordinates.

The complex conjugate of the input is:

$$A*(f) = |A(f)| \cdot e^{-i\varphi_A(f)} \tag{7.6}$$

Thus the cross-spectrum is calculated as:

$$G_{AB}(f) = |A(f)| \cdot |B(f)| e^{i\varphi_B(f) - i\varphi_A(f)} \tag{7.7}$$

where the phase of the cross-spectrum:

$$\varphi_{BA}(f) = \varphi_B(f) - \varphi_A(f) \tag{7.8}$$

is the phase difference between the output and the input of the system.

Rearranging Equation (7.1), the FRF is defined as:

$$H(f) = \frac{B(f)}{A(f)} \tag{7.9}$$

Since the dual-channel FFT analyzer produces three fundamental spectra, $G_{AA}(f)$, $G_{BB}(f)$ and $G_{AB}(f)$, these spectra must be used for the calculations. As an example, multiply both the numerator and the denominator by the complex conjugate of $A(f)$ and then average both of them:

$$H(f) = \frac{\overline{A^*(f) \cdot B(f)}}{\overline{A^*(f) \cdot A(f)}} = \frac{G_{AB}}{G_{AA}} = H_1(f) \tag{7.10}$$

This produces the H_1 estimator.

Similarly,

$$H_2(f) = \frac{G_{BB}}{G_{BA}} \tag{7.11}$$

and

$$H_3(f) = \sqrt{H_1(f) \cdot H_2(f)} = \frac{G_{BB}}{G_{AA}} \cdot \frac{G_{AB}}{|G_{AA}|} \tag{7.12}$$

H_1, H_2 and H_3 represent three methods of presenting the FRF. It can be seen from the formulae that H_1 is the best estimator when there is an output noise problem since G_{BB} is not used in the calculation. In similar way H_2 is preferable if there is an input noise. H_3 is a compromise between H_1 , and H_2 estimators.

(C) Coherence Function

Consider two signals $A(t)$ and $B(t)$. Their coherence function is defined as

$$\gamma^2(f) = \frac{|G_{AB}(f)|^2}{G_A(f)G_B(f)} = \frac{H_1(f)}{H_2(f)} \quad 0 \le \gamma^2(f) \le 1 \tag{7.13}$$

where $G_A(f)$, $G_B(f)$ are the respective autospectra of $A(t)$ and $B(t)$, and $G_{AB}(f)$ is the cross-spectrum between $A(t)$ and $B(t)$. It follows that:

1. If $A(t)$ and $B(t)$ are completely uncorrelated so that $G_{AB}(f)=0$ for all the frequency f, then the coherence function $\gamma^2(f)=0$ for all f.
2. If $A(t)$ and $B(t)$ are completely correlated, then the coherence function $\gamma^2(f)=1$ for all f.
3. Otherwise, $0 \le \gamma^2(f) \le 1$ for all f. In actual practice, the coherence function is greater

than but less than unity as one or more of the following main conditions exist (Bendat and Piersol, 1980):

a. the output $B(t)$ is due to other inputs besides $A(t)$ for an $A(t)$ input-$B(t)$ output system;

b. extraneous noise is present in the measurements;

c. resolution bias errors are present in the spectral estimation;

d. the system relating $B(t)$ and $A(t)$ is nonlinear.

Low coherence function express the degree of linear relationship between $A(f)$ and $B(f)$. Low coherence can be due to either difficult or bad measurements.

7.6 CALIBRATION

To check and validate the measurements, the setup was calibrated statically and dynamically:

(A) Static Calibration: The objective of the static calibration is to establish a relation between the measured and the actual values of the forces to be measured, a static calibration has been performed. In spite of the fact that the piezoelectric transducers are generally used to sense dynamic quantities, the static calibration is possible because of the high insulation resistance of the load washer, and because of the high input impedance provided by the charge amplifier. Thus, for any value of the load, less than the maximum value, in both the axial and torque direction, the time duration of the signal is sufficiently large enough to permit the reading on a digital voltmeter. The static calibration of the dynamometer has been carried out by applying various loads of known magnitudes, measuring the output of the

dynamometer, and establishing a graphical relation between the measured quantities and the applied forces. In calibration of the dynamometer along the axial direction, a known load was applied using a vertical loading machine (Figure 7.12). During the measurement, the charge preamplifiers were set to "long", so that the time constant of the system becomes large, and the rate of decay of charge during the static measurement is reduced. This minimizes considerably the error introduced in static calibration. The load was incrementally increased from zero to 10 KN and readings were recorded. The output from the torque channel was also recorded to estimate the cross coupling between the channels. Similar readings were recorded during the unloading cycle. The static calibration of the dynamometer along the torque direction has been carried out by applying a pure torque of known value (Figure 7.13). A bar was attached symmetrically on the chuck. Dead weights were introduced at the free ends of this bar. So, the resultant torque introduced equals the moment arm times the load. Similar to the calibration procedure described above, the charge preamplifiers were set to "long" so that the error introduced in static calibration is a minimum. The load was increased gradually from zero to about 90 N and the voltage readings were recorded. The output from the axial force channel was also recorded to estimate the influence of the torque on the axial force. Similar voltage readings were recorded during an unloading sequence. The static calibration of the dynamometer enables the determination of a relation between the charge developed and the magnitude of the axial force and torque. Figure 7.14a shows the results of the static calibration along the axial direction where figure 7.14b shows the results of the static calibration along the torque direction.

(B) Dynamic Calibration: A dynamic calibration of the dynamometer-workpiece-machine

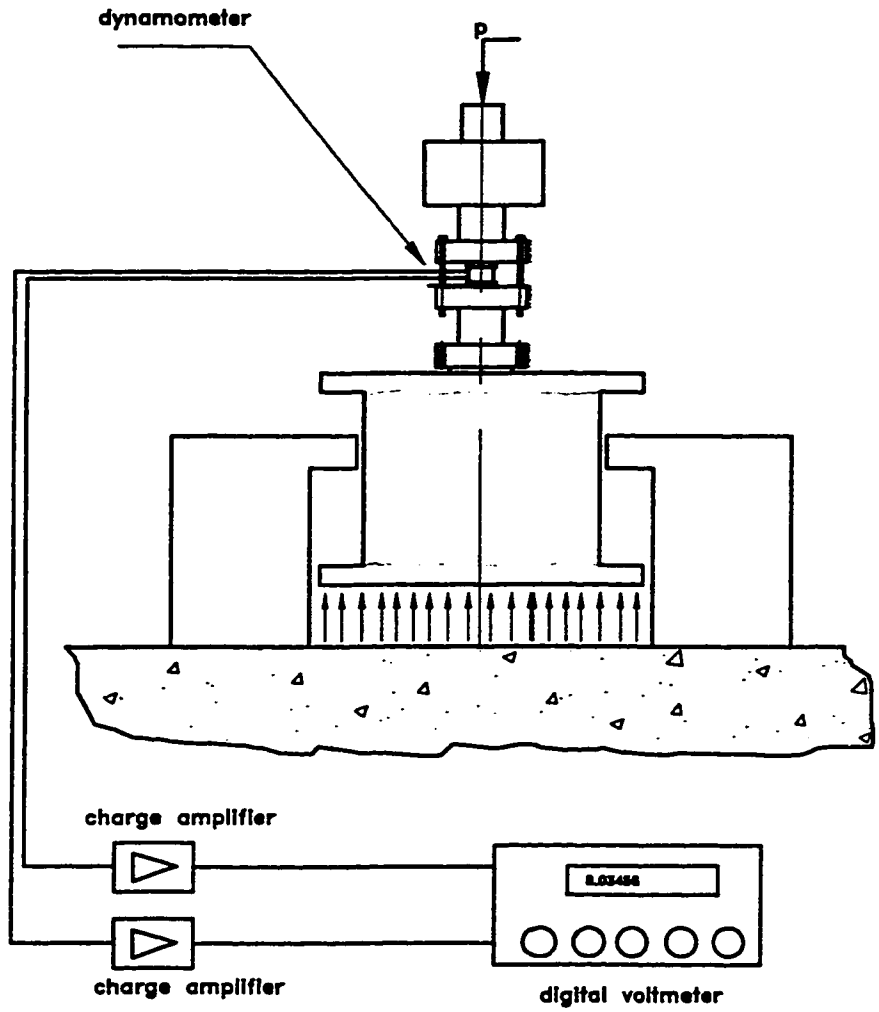

Figure 7.12: Setup of the static calibration of the dynamometer along the axial direction.

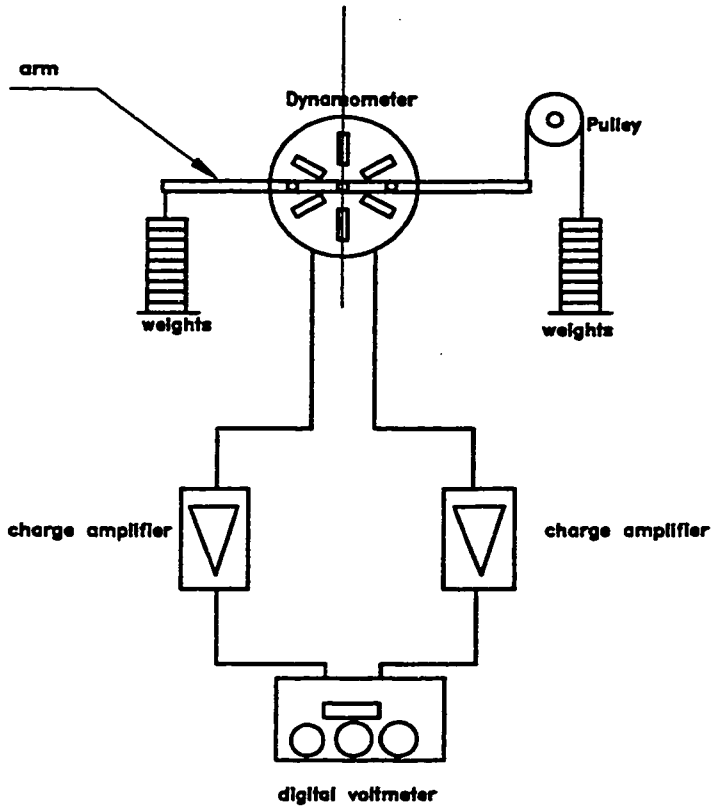

Figure 7.13: Setup of the static calibration of the dynamometer along the torque direction.

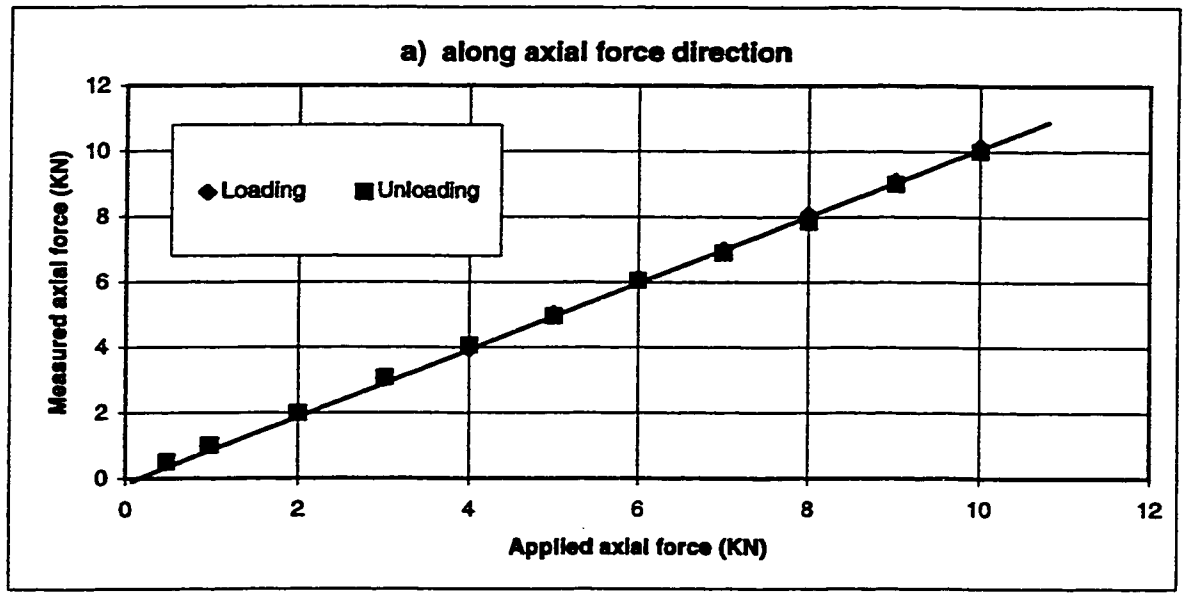

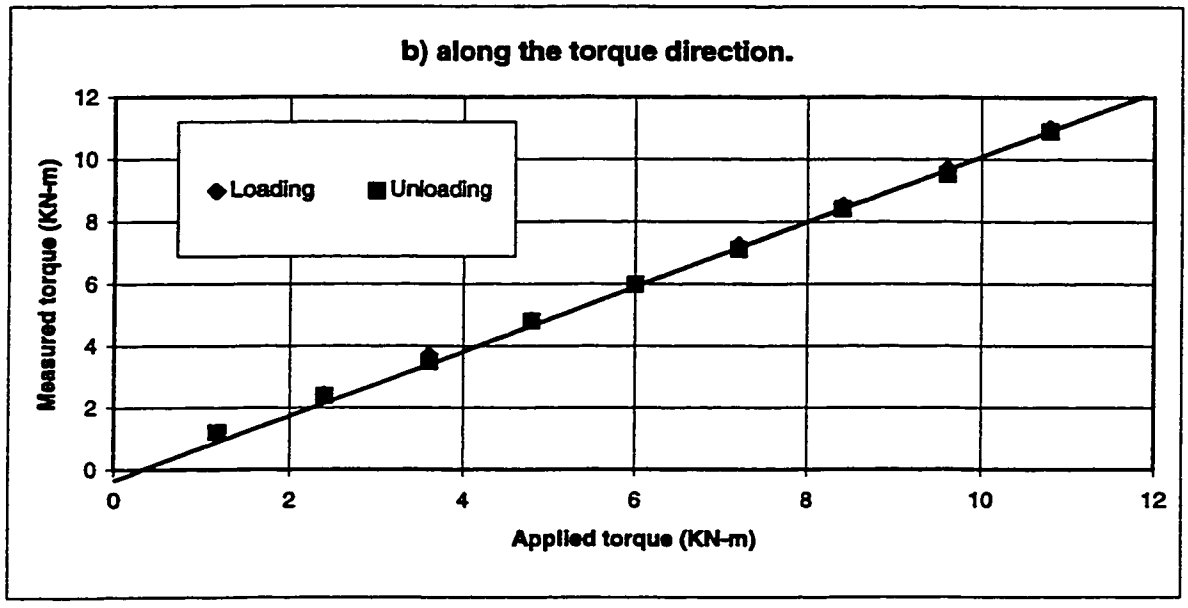

Figure 7.14: Results of the static calibration a) along the axial direction and b) along the torque direction.

tool system has been carried out to:

1. Avoid measuring the vibration of the tool instead of the force fluctuations.
2. Determine the frequency band, over which the dynamometer can be used for reliable measurements.
3. Determine the resonant frequencies of the system so as to make sure that the response of the cutting process is not in the neighborhood of the dynamometer resonant frequencies.
4. Determine the range of frequencies of the cutting forces which could be measured accurately without distortion.

A hammer B&K 8203 with a built-in cell has been used to supply an impulse excitation to machine dynamometer-workpiece system while the FFT has been used to resolve the signals coming out from the hammer and the load washer. The frequency response function (FRF), $H_i(f)$, of the machine dynamometer-workpiece system was determined in order to find out the frequency band in which the FRF function remains constant. This frequency band determines the range of frequencies of the resultant force system, which can be measured without the introduction of any signal distortion due to the system nonlinearities. The experiment to determine the frequency response function was performed with the workpiece fixed to the dynamometer. Figure 7.15a shows that the FRF (direct correlation) was very close to unity in the frequency range of 0-1100 Hz where Figure 7.15b that the FRF (cross-correlation) has a constant value of 0.02 in the in the same range. The FRF determination of the machine dynamometer-workpiece system when the input force is along the torque direction was carried out using the same experimental set up

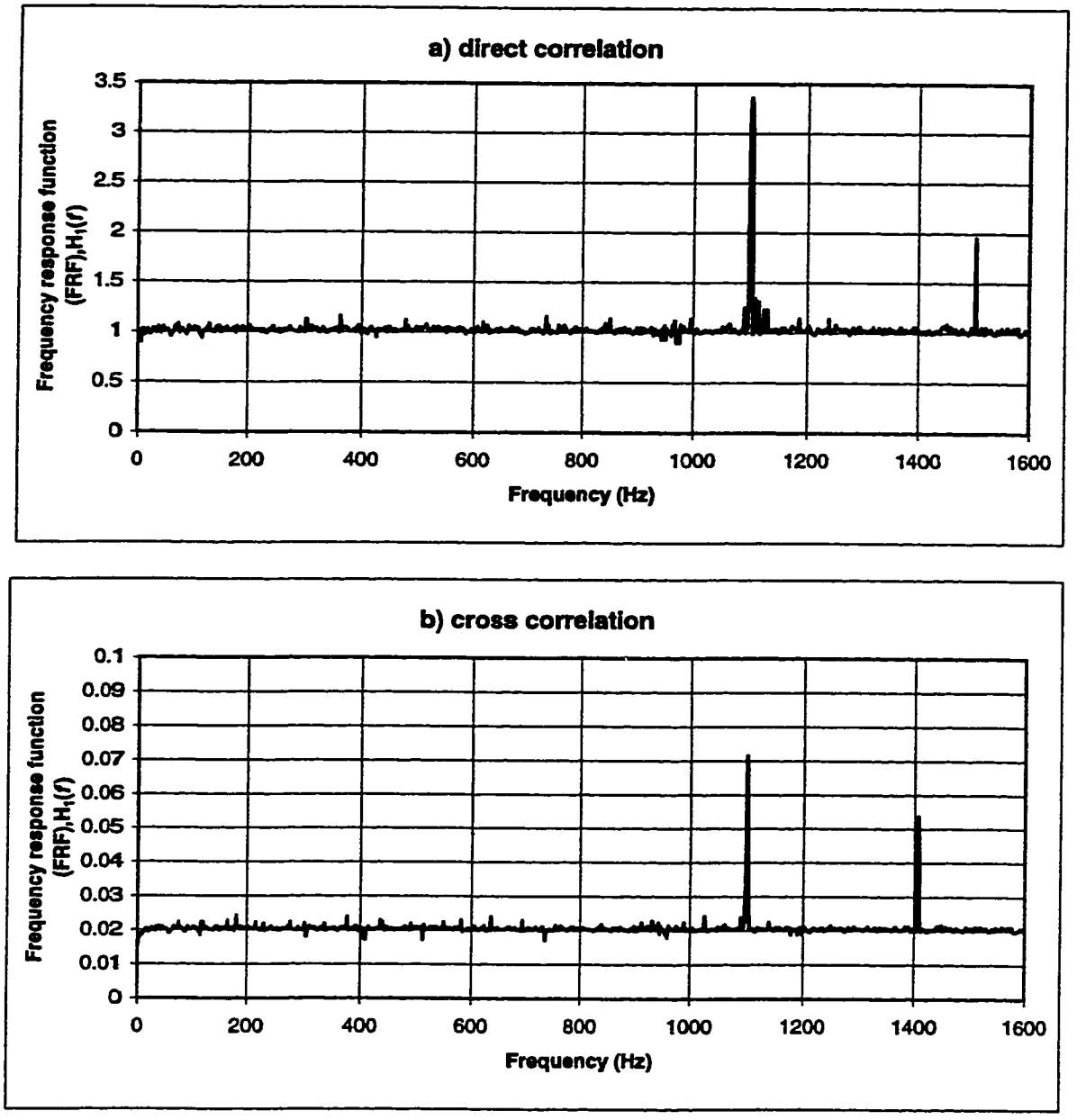

Figure 7.15: Frequency response function FRF when the input is along the axial force direction: a) direct correlation and b) cross correlation.

used to perform the static calibration for the torque. A similar calibration procedure, to the one described previously, was carried out. The results showed that the FRF is unity in the frequency range of 0-1070 Hz as shown in Figure 7.16a. The cross correlation plots show that the FRF has a constant value of 0.01 in the frequency range 0-1100 Hz as shown in Figure 7.16b.

(C) Examining the Validity of the Measurements: The validity of the measurements have been checked by calculating the coherence function $\gamma^2(f)$ for the measured spectrums as shown in Figs. 7.17a and 7.17b. The coherence gives a measure of the degree of linear dependence between any two signals over the frequency axis. It is calculated from the two autospectra and the cross spectrum. As seen from these figures, this function is close to unity that conform the linear independency of the measurements.

7.7 MEASUREMENTS

To obtain as complete as it is possible information about the dynamics of the machine tool used in the experiment and its effect on the cutting force measurement, a system and signal analyses have been accomplished. In these analysis, the Fast Fourier Transform (FFT) unit has been used to define the system autospectra over a frequency range and facilitate the interpretation of the results.

7.7.1 System Analysis

A hammer (B&K 8203) with a built-in cell has been used to supply an impulse excitation to the boring bar mounted on the machine while the accelerometer (KD-2350) has

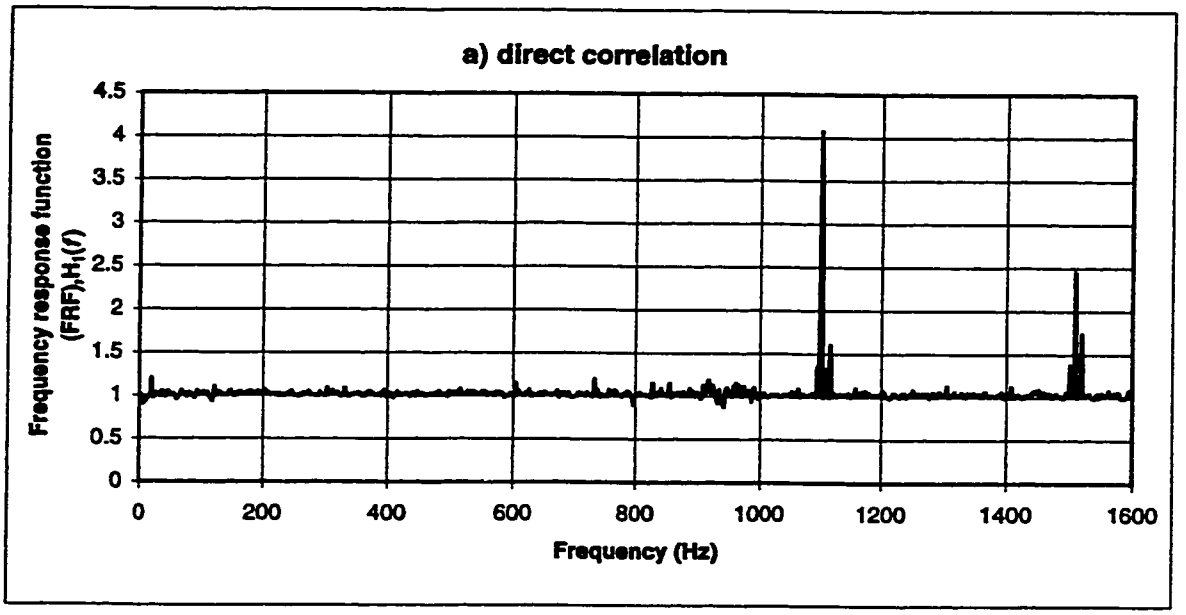

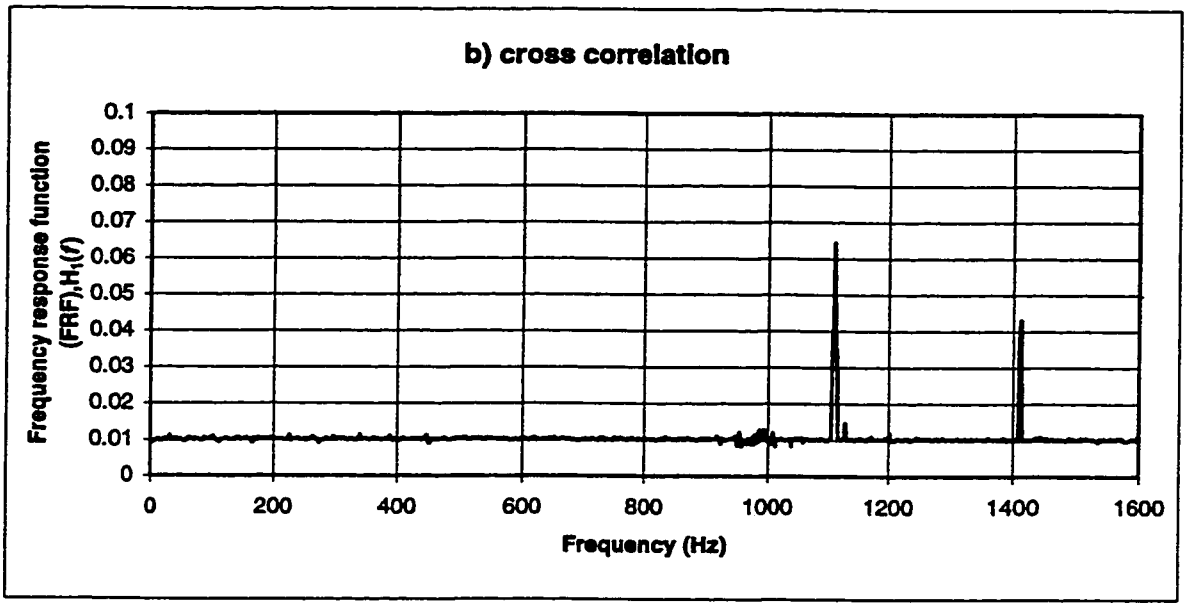

Figure 7.16: Frequency response function FRF when the input is along the torque direction: a) direct correlation and b) (cross correlation).

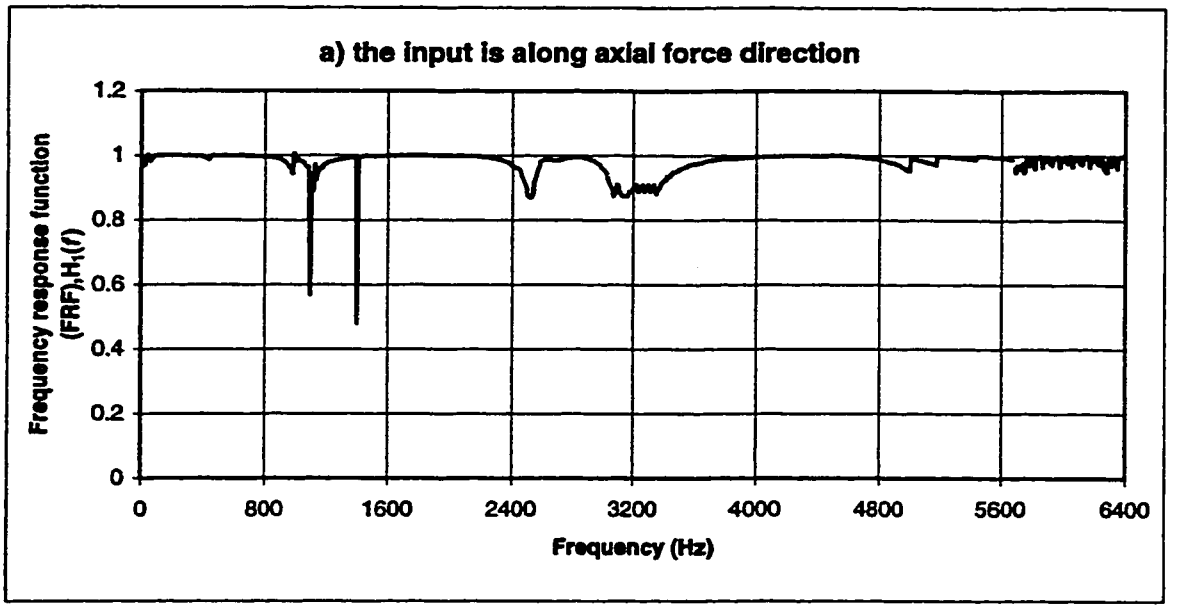

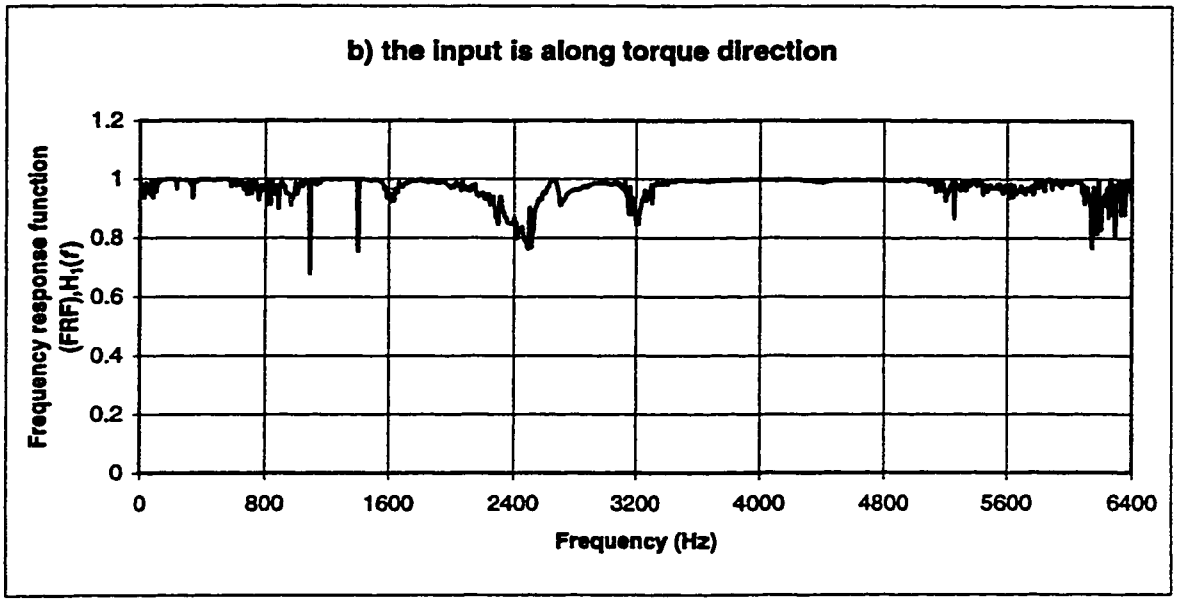

Figure 7.17: Coherence of the dynamometer signal vs. hammer signal when the input is along a) axial force and b) torque directions.

been used to measure the response and the FFT has been used to resolve the signals coming out from the hammer and the accelerometer as shown in Figure 7.18. To perform the system analysis, the whole chain including both the transducers with allied pre-amplifiers and the FFT analyzer has been calibrated to ensure the accurate frequency response function (FRF) measurements. First, the autospectrum of the input channel (hammer) has been obtained to ensure that the hammer is capable of providing enough energy over the frequency range of interest. Since the response is a transient function, the autospectrum has been scaled to show the energy spectral density of the signal (ESD). When equipped with a metal tip, the hammer has provided a uniform input over a broad frequency range from 0Hz to 6.4kHz as shown in Figure 7.19a. Here, a drop of less than 20dB has been allowed complying with the common recommendation for resonance measurements (Randall, 1987) which is in good agreement with the obtained results. The whole measurement chain including both transducers with allied preamplifiers and the FFT analyzer has been calibrated by hammering a known mass (1.0 kg). By checking on the value of the frequency response function (FRF), the setup has been calibrated for the correct ratio to ensure the accurate FRF measurements as shown in Figure 7.19b.

7.7.2 Signal Analysis

A signal analysis would be the logical choice to start the study of the dynamics of the cutting process because this analysis offers the advantages of actual results since the measurements are carried out under real operation conditions.

The first step in the analysis is knowing the type of the obtained signal because the

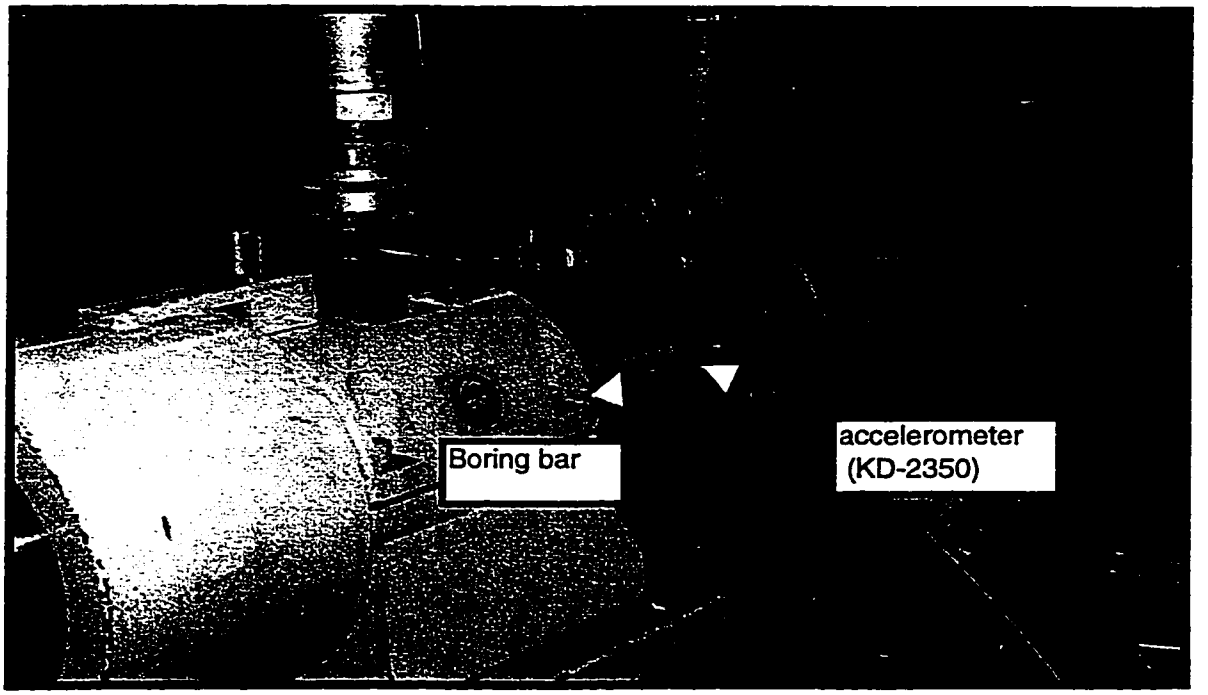

Figure 7.18: A photograph of the set up for performing the system analysis.

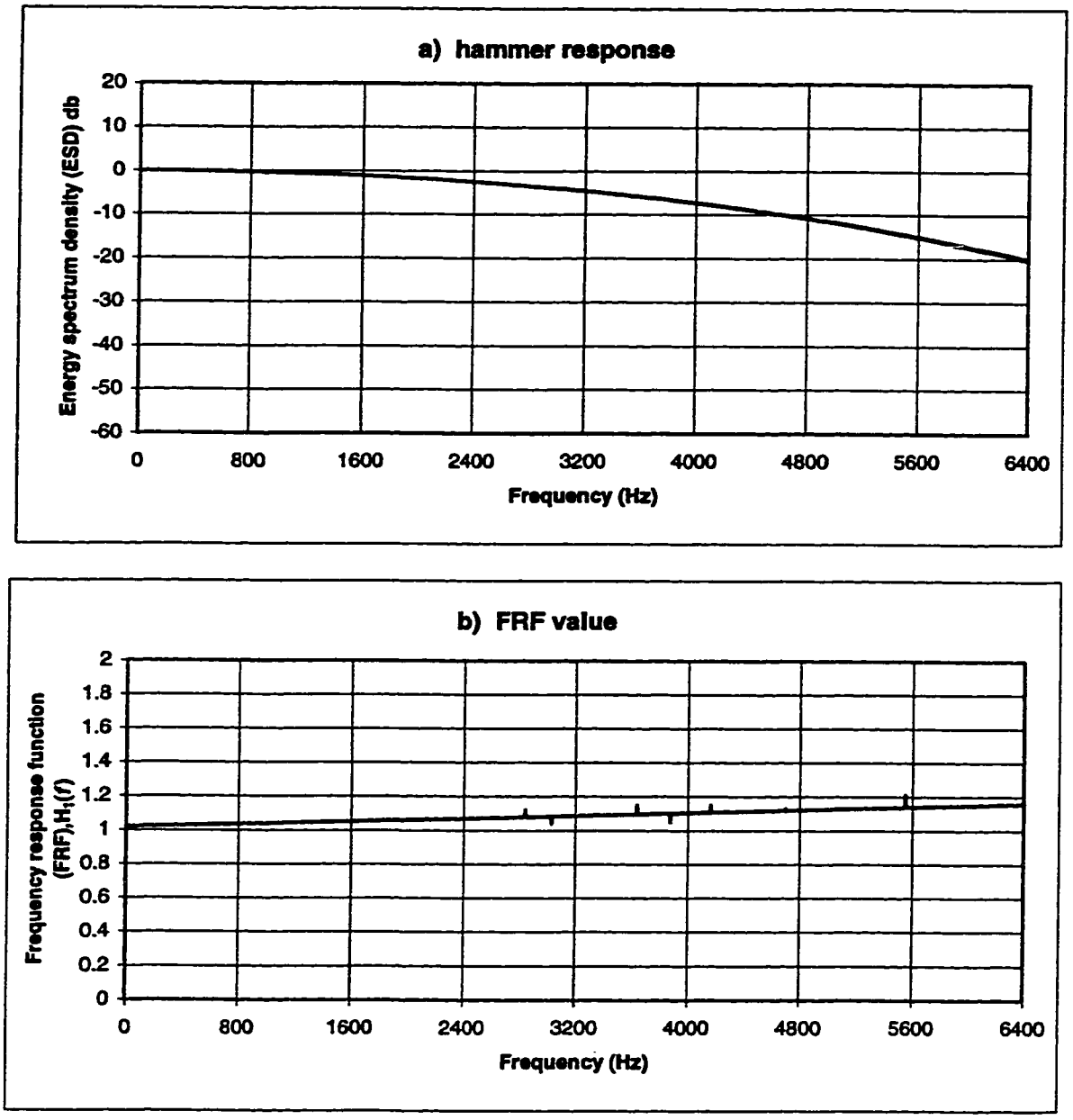

Figure 7.19: Calibration of the hammer for the frequency responses function (FRF) measurements a) hammer response and b) FRF value.

type of the signal to be analyzed has an influence on the type of the analysis to be carried out and also on the choice of the analysis parameters.

However, the most fundamental division of the signals is into stationary and non-stationary signals (Randall, 1987). Stationary signals are those whose average properties do not vary with time and are thus independent of the particular sample record used to determine them. This applies to both deterministic and random signals, but in particular in the later case it is important to realize that the results obtained from different records are not necessarily identical. Non-stationary signals are those whose average properties vary with time and are dependent on the particular sample record. It may be roughly divided into continuous non-stationary signals and transient signals which may be defined as those which start and finish at zero. Transient signals are treated and analyzed as a whole, whereas a continuous non-stationary signal will normally be analyzed in short sections, each of which will often be quasi-stationary. Figure 7.20 shows two autospectra of the axial cutting force which have been acquired simultaneously but scaled using two different measures i.e. the root mean square value of the signal (RMS) and the power spectral density (PSD). The record reveals the discrete form of the spectra thus confirming that the signal is stationary deterministic as one would expect from a mechanical system featuring rotating components. The figure shows that, for the analysis bandwidth sufficiently narrow to separate all individual components, the use of RMS format is fully justified. The only reason for using the PSD format as a more complex measure normalizing the " power " with respect to the analysis bandwidth could be that, for random signals, the RMS value for each frequency is zero since an infinite number of frequencies are present and the total power is finite. The obtained

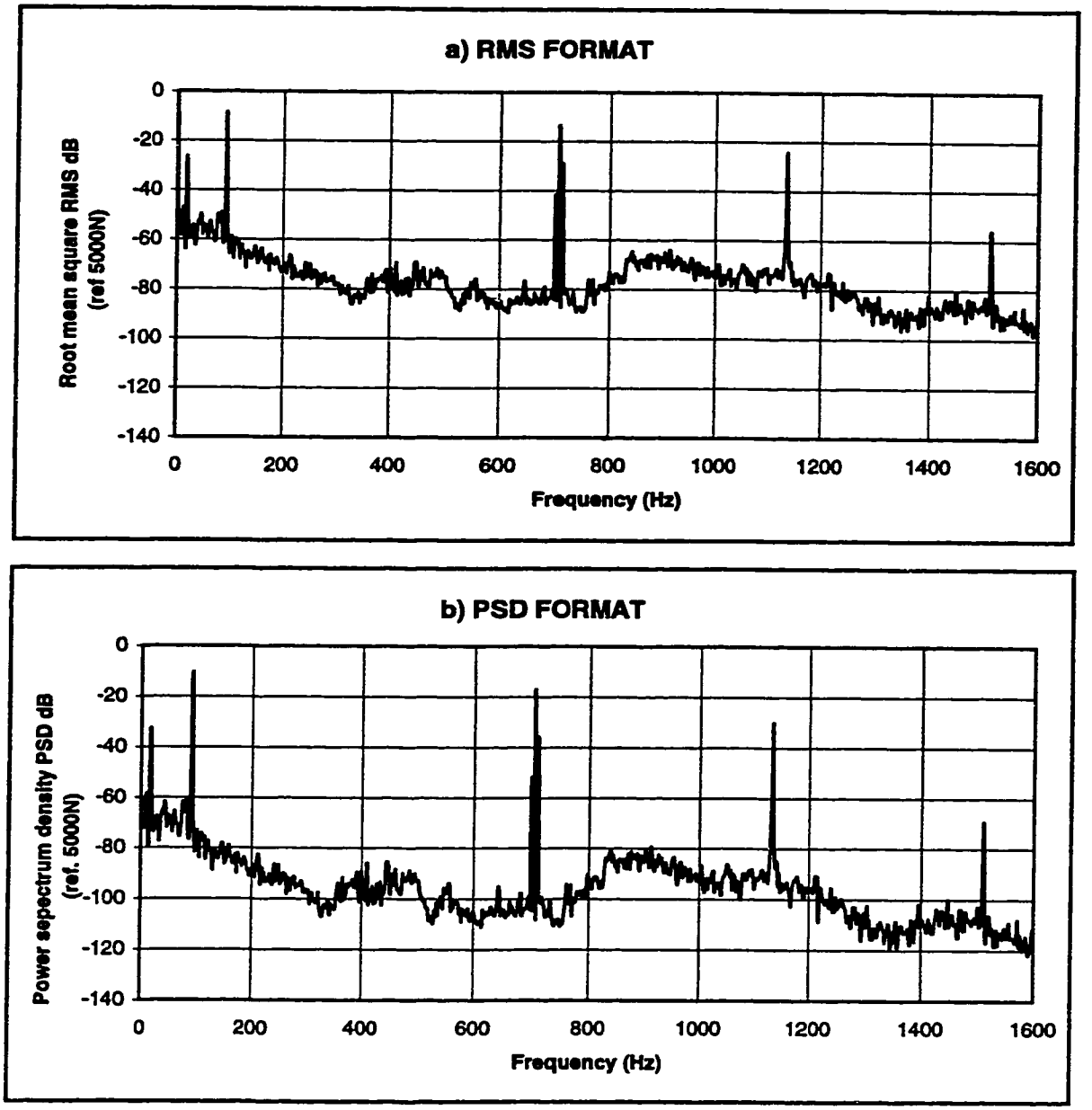

Figure 7.20: Autospectra (RMS vs. PSD Format).

results is in contradiction with the ones reported by some previous works (Osman et al, 1974; Chandrashekhar et al, 1984) where it the conclusion about stochastic nature of the cutting force has been made so that the use of the PSD measure as applicable to the continuous spectra of random signals was recommended.

Then it was necessary to set many parameters which define the measurement setup:

(A) Measurements Mode

The measurement mode is the most important element in determining how the measurements are carried out. There are four measurements modes available with the used analyzers: a) Spectrum averaging mode, b) Spectrum averaging, zero pad mode, c) 1/n Octave spectrum averaging mode and d) Signal enhancement mode. The first mode i.e. spectrum averaging mode was used in the experiments because this mode is suitable for signal and system analysis where the others mode have their implementation for other types of measurements (Randall, 1987).

(B) Spectral Lines

A 800 spectral lines option has been selected to get the best frequency resolution since there is no large change in signal amplitude or frequency within the signal record (Bruel & Kajaer, 1992).

(C) Sampling Frequency

The FFT analyzer can not execute the Fourier transformation continuously. It has a dedicated internal computer that is very fast to perform these calculations, but it must look at a time block of data. This is the purpose of the sampling zone in the FFT analyzer. The typical spectrum analyzer takes about 50,000 readings per second, on the input waveform.

The analyzers measures this fast to overcome a problem of being able to track high frequency signals. An analyzer that has a frequency range of 0 to 20,000 Hz must measure the voltage of the input signal as fast as twice of this frequency (or 40,000 Hz) to be able to see changes at 20,000 Hz. This is called the *Nyquist criterion* (Victor Work, 1991). For the used setup, the sampling frequency was set to 1600 Hz to see the change in at 800 Hz which is the range of interest.

(D) Averaging Number

This is a number, ranging from 1 to 32767, which determines the number of spectra that contribute to the average. Choosing this number depends on: a) the desired accuracy; the greater the accuracy, the higher the required averaging number, b) the amount of the noise in the measurements and c) the type of signal being analyzed. For stationary signals, only a few averages are needed to obtain a good estimate. However, averaging of 15 has been chosen in the experiments setup to increase the accuracy and to get ride of the noise as much as possible.

(E) Anti-aliasing the Signal Record

Aliasing is a mirror of the high frequency signals into the lower frequency range where the high frequency signals can form false peaks in the frequency domain. This is a consequence of the digitizing process. They appear as vertical lines in the frequency domain of the FFT spectrum analyzer. They are the ghost images of high frequency data that is input to the analyzer. Aliasing has been overcome by two methods. The first method is measuring the input data at more than the twice the highest frequency of interest. The second methods ,used in conjunction with the first method, is applying the analyzer built-in low pass filters

appropriate to each frequency range with cutoff frequency at about 80% of the *Nyquist* frequency and displaying the results unaffected by filter. Typically for 2048 points, 800 frequency lines are displayed (or 801where the DC components is included).

(G) Windowing the Data

Windowing the data is the most important parameter that the experimentalist needs to be aware of.. In the FFT analyzer, the digital sampling takes place during discrete blocks of time. The FFT analyzer assumes that the signal which exists in that blick of time also exists for all the time before and after the sampling. This block processing is necessary in real-time data acquisition. Therefore, it is not possible for the analyzer to wait for an extended time period to check if the signal is periodic. The Fourier transformation, however, should make assumption of periodicity to start the acquisition process. In doing so, it can produce an error called leakage if the signal does not match up at the beginning and end of the current time block. This leakage is undesirable since it may hide low level signals causing distortions in the resultant spectrum. To avoid this leakage, the input data is weighted with a mathematical function that favors the data in the center of the time block and reduces the data at both ends to zero. There are many useful window function which can be used such as rectangular, Hanning, hamming,, Kaiser-Bessel, and flat top.

A better choice of window function for stationary signals, as it is the case with the signal of the cutting force, is one which is equal to zero at each end, and whose amplitude varies smoothly. An excellent window function which meets these requirements is Hanning which has been used to process the experiment data (Bendat and Piersol, 1980) .

8

METHODOLOGY OF STUDYING THE CHIP MORPHOLOGY

To put the analysis of any chip formation model on a qualitative and quantitative basis, certain observations must be made during, and after the cutting (Shaw, 1984). While the modern experimentalist has many investigation techniques at his disposal, the optical reflection microscope remains the most effective mean for examining the structures of workpiece material, deformation zone and chip. In particular, the chips is the only testimony which reflect the history of the loading, strain and strain rate of the cutting process and since

any proposed cutting model considers the structure of deformed and partially deformed chip, a special attention has been paid to the chip morphology to verify the proposed model. With skill and experience there is always much more to be gained. The recognition of significant features combined with an appreciation of physical metallurgy provides a powerful basis for rationalization and diagnosis (Rostoker and Dvorak, 1977).

While metallography remains a versatile tool, modern metallurgy makes use of a wide variety of physical and mechanical properties and radiation interactive measurements in the definition of states of a metal as polycrystalline. In sober appraisal there is little room for controversies on the relative merits of various tools. The fact stands out that no tool is self-sufficient to describe different aspects of the nature of a material. Considered separately, these aspects may not be adequate but in join appraisal may permit unambiguous interpretation. It remains, therefore, to identify properly the limitations as well as the capabilities of the tools of metallurgical study.

Metallography of the chip was first presented by Ernst (Ernst, 1938). Based on the results of his metallographic study, Ernst has identified three basic types of chip found in metal cutting. Although no magnification, sample preparation technique, cutting regime and workpiece material have been reported, Merchant (1945) considered these results as classical examples. Merchant did not provide any explanations why these examples do not mach his own model shown in his classical paper (Merchant, 1945) right after the discussed examples. Since then, these examples are used in many of the work on metal cutting and in textbooks (Boothroyd and Knight, 1989).

Trent in his book (1991) presents a great number of microstructure of the formed and

partially formed chips to support his qualitative description of the metal cutting process. Unfortunately, they are not related to any particular model of chip formation. As a results, there is no justification for the magnifications selected, chemical treatment of different phases used, and deformation mechanisms.

Metallography can be considered as a kind of visual art unless one or more of the following conditions are justified:

1. The initial structure of workpiece material should be reported.
2. The chip structure is considered at the macro- and micro levels to study, depending on particular phenomenon to be investigated, because each phenomenon can be observed at a certain magnification and requires different preparation techniques of the specimen.
3. The structures of the chip and deformation zone are compared with those predicted theoretically to verify the theory used in the analysis.
4. A microhardness survey is performed on the structure to reconstruct the distributions of stress and strain gained by different regions of the chip and deformation zone at the last stage of deformation. The obtained results are compared then with those obtained theoretically.

Unfortunately, the known metallographical studies in metal cutting (Shaw, 1984; Oxley, 1989; Trent, 1991) only partially meet these conditions. The reported structures have never been compared with the initial structures of workpiece materials so that it is next to impossible to distinguish the changes produced by the cutting process. The known studied on macrohardness of the chip do not account on the grain location in the chip that may result

in non-adequate results since the microhardeness of the grain boundaries (pearlite) is higher then that of grains (ferrite). Therefore, these boundaries should be avoided in the measurements which has to be produced with the aid of a special microscope.

The section concerns itself with techniques of preparation of metallic specimens for examination. A detailed description of the equipments, devices and procedure of preparation and testing the specimens are presented. It begins with a description of the quick stop device which is designed to obtain samples of partially formed chip. This is followed by the details of the stages for the preparation of the specimens for the metallographic and microhardness tests. Next, the microhardness procedure is presented.

8.1 QUICK STOP DEVICE

Quick stop devices has became essential tool for any fundamental research of the mechanics of chip formation (Trent, 1991). The quick stop technique is one in which the velocity of the tool relative to the workpiece is rapidly brought to zero. This can be performed by arresting the machining operation by disengaging the tool and workpiece quickly so that the resulting static situation accurately represents the actual dynamic situation. Detachment of the tool and the workpiece can be achieved by either accelerating the workpiece from the tool or by accelerating the tool from the workpiece.

Since the cutting experiments in the present study have been performed using a deep-hole machine, a special quick-stop device has been designed. Figures 8.1 shows a systematic drawing of the designed quick stop device which is pictured in Figures 8.2 and 8.3. As can be seen from these figures, the quick stop body has the following components:

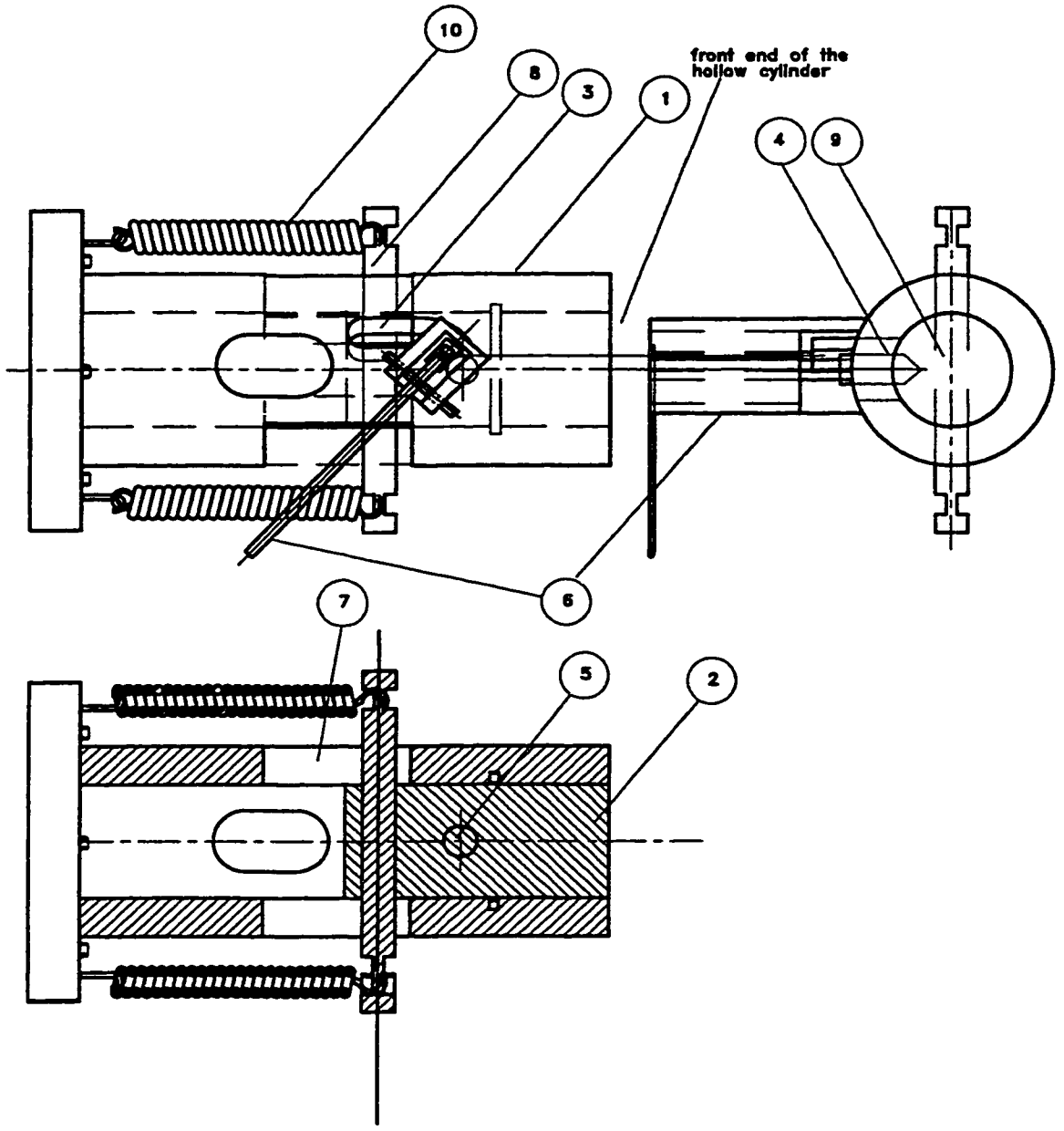

Figure 8.1: An assembly drawing of the designed quick stop device.

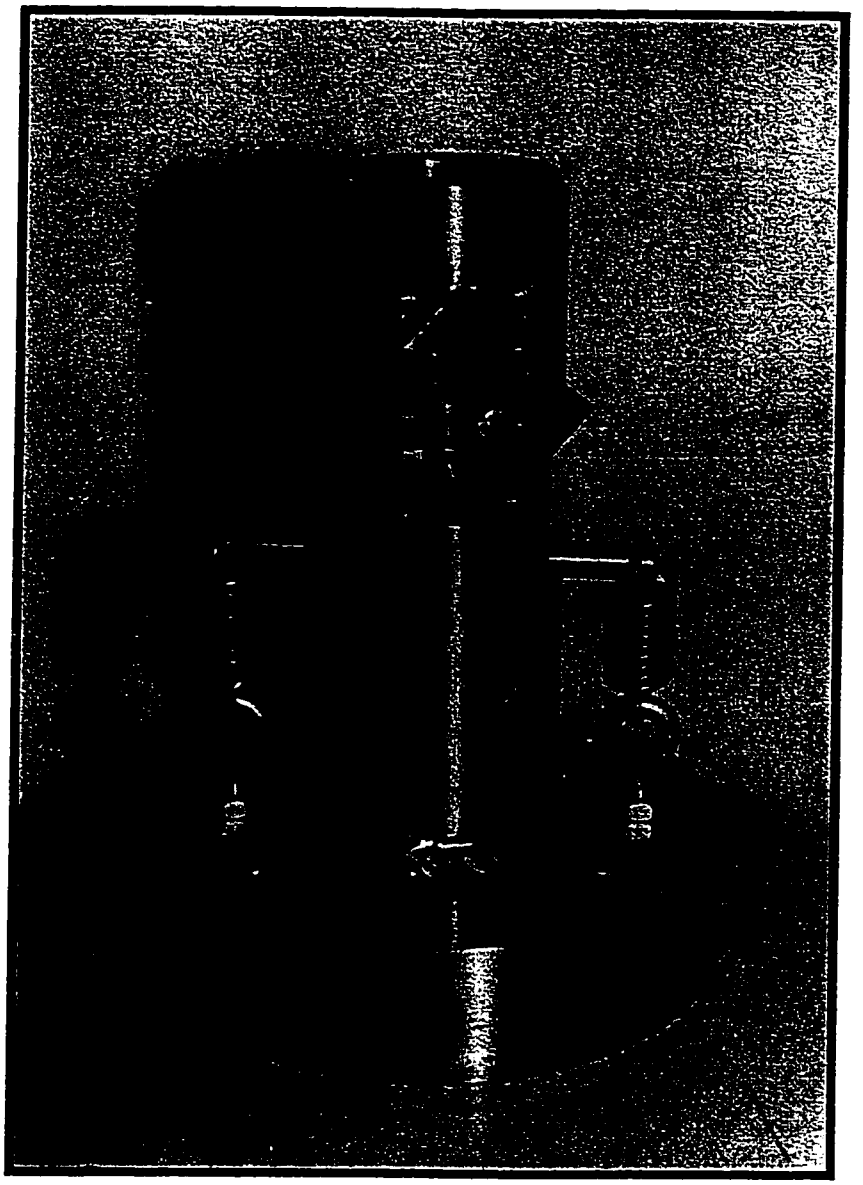

Figure 8.2: A photograph of the quick stop device.

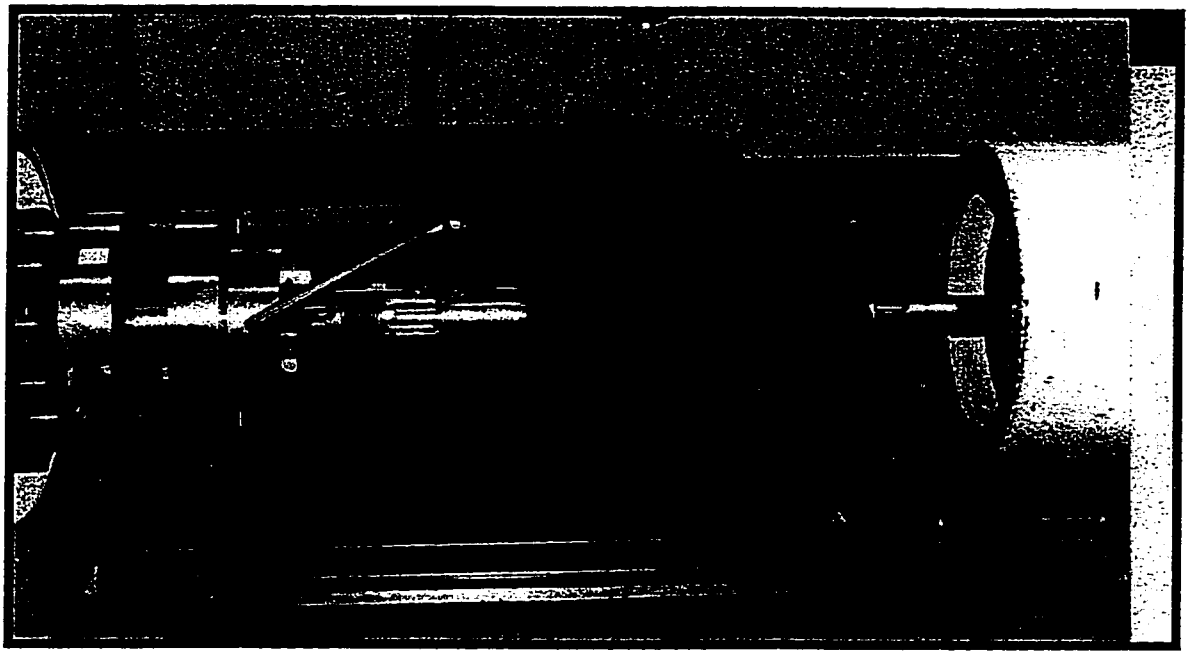

Figure 8.3:A photograph of the quick stop device in the loading position.

- A longitudinal hollow cylinder (**1**) through it the workpiece (**2**) can slide freely.
- A helical piloting slot (**3**) in the direction of the rotating of the tool head located at the front end of longitudinal hollow cylinder.
- An arm (**4**) protruding radially from a hole (**5**) located nearly at the middle of the workpiece (**6**) (Figure 8.4). The workpiece and the arm assembly is constrained to move in a helical direction (axial and radial directions) along the piloting helical slot with speed exceeding the cutting speed..
- A mechanism (**6**) has a lever arm where the short part of the lever arm is used to prevent the workpiece and arm assembly moving during the drilling operation by holding a pin in front of the arm protruding from the workpiece. The long part of the lever arm is used to activate the separation of the workpiece and arm assembly along the helical slot from the tool head. Striking the far end of the long part of lever arm causes large force sufficient to disengage the workpiece and arm assembly.
- Two rectangular slots (**7**) 90 degree apart from the helical slot.
- A rod (**8**) passing a hole (**9**) at the rear end of the workpiece and the above mentioned two slots (**7**) is held by two high stiffness springs (**10**) fixed to the base of the device.

To load the quick stop device, the following steps are taken:

- Inserting the rod (**8**) through the two slots (**7**) and the hole at the rear end of the workpiece.
- Attaching the springs with ends of the rod (**8**).
- Assembling the arm (**4**) and the workpiece (**2**).

- Pushing the workpiece and the arm assembly using pressing machine to overcome the springs forces.
- Locking the arm(4) by raising the long part of the lever arm up.

To capture a quick stop device sample at the desirable instant, the device is activated by hitting down the long part of the lever arm quickly during the drilling operation after the pads had fully entered the hole such that the workpiece and the arm assembly is rotating in a helical direction with angular speed more than the angular speed of the boring bar by the action of the springs force.

An illustrative quick stop samples is shown in Figures 8.4., and 8.5 in which a partially formed chip can be seen at the bottom of the hole.

8.2 SPECIMEN PREPARATION FOR MICROSCOPY AND MICROHARDNESS MEASUREMENTS

The preparation steps for microscopy are of great importance, since the true microstructure may be fully obscured by poor technique or execution. Improperly prepared samples can lead to misled interpretations. Therefore, a special care have been paid in the preparation the samples. A standard methods of preparation of metallographic specimens according to the *ASTM E 3-86, ASTM E 340-89* and *ASTM E 407-87* have been used.

8.2.1 Samples Selection

The first step in metallographic analysis is to select a sample that represents the material to be studied. In this study three types of specimens has been investigated:

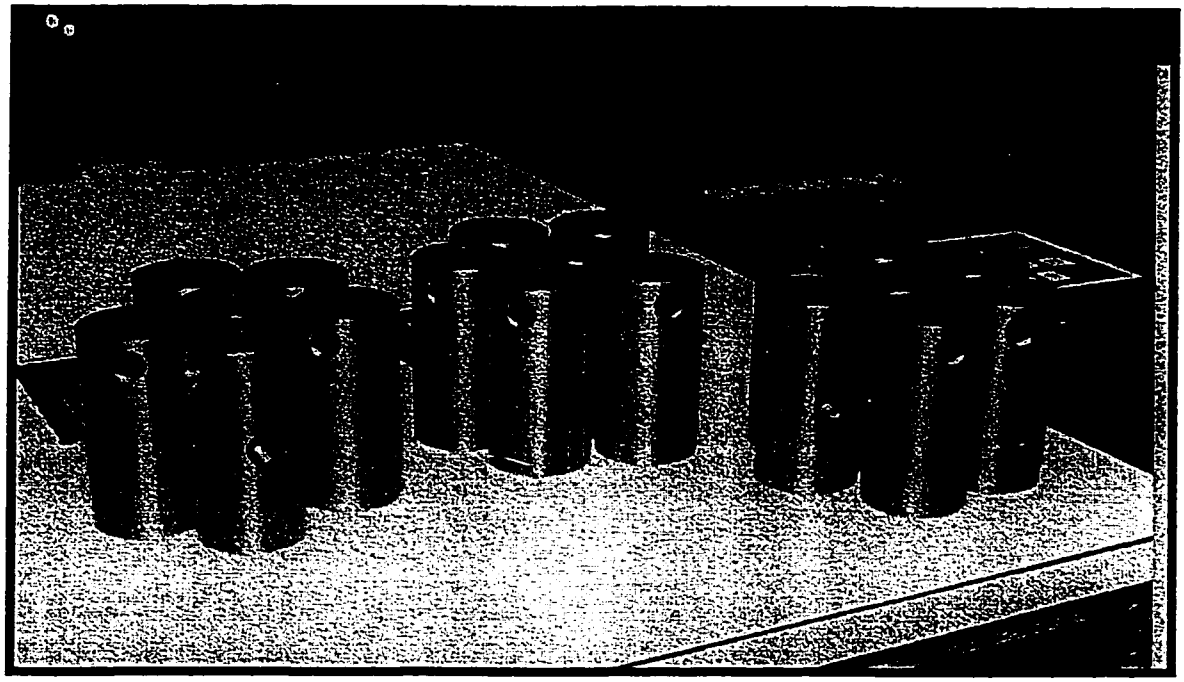

Figure 8.4: A phonograph of the workpieces used in the quick stop device.

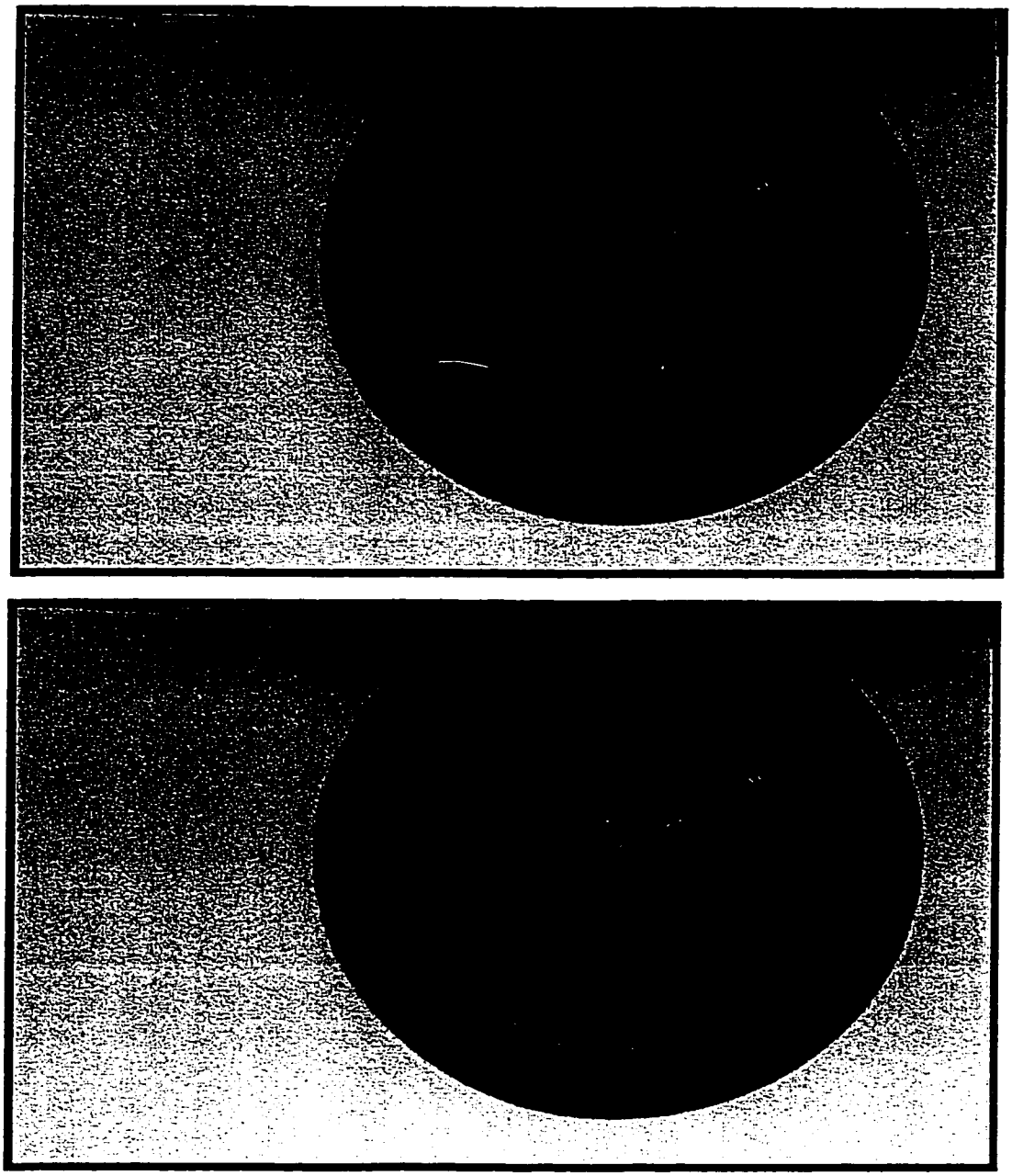

Figure 8.5: Illustrative quick stop samples in which a partially chip can be seen at the bottom of the hole.

1. Samples to study the initial structure of workpiece material. Three samples from each material have been selected from the bulk material at certain distance from the surface of the workpieces to avoid the influence of primary process (hot rolling) on the samples' microstrcture.
2. Samples of the chip. Three samples have been selected randomly from the chips for each material after the cutting.
3. Samples of partially formed chips as obtained using the quick-stop device.

8.2.2 Sectioning

Sectioning of a metallographic sample must be performed carefully to avoid altering or destroying the structure of interest. A abrasive cutoff saw has been used to section the sample that is of interest. To minimize burning and deformation, a lubricant of high flow rate has been used in the cutoff operations.

8.2.3 Mounting

Mounting facilitates the handling of the specimens especially when it is very small. Mounting involves placing the specimen in a mold and surrounding it with the appropriate powders.

Two types of mounting have been used in this study, hot mounting for the initial structure material and cold mounting for the chip specimens. The hot mounting is easier in terms of grinding and polishing but it is not good for very small specimen such as the chip because the pressure and temperature may alter the structure of the tested specimens. In hot

mounting, the mold and its content (specimen and bakelite powder) are heated under pressure to the thermosetting temperature of the content. Once the powder is cured, thermosetting mounts is removed and cooled to the ambient temperature. In cold mounting plastic set at room temperature. Epoxy resins material has been used in this study.

8.2.4 Grinding

Grinding is an important phase of the sample preparation sequence because the damage introduced by sectioning must be removed at this phase. If sectioning produces an extensive damage then it cannot re remover by grinding. It is usually better to resection the material in unaffected area with more gentle cutting method. Special care was taken to minimize mechanical surface damage especially in this study where it is important to preserve the surface without any alteration.

Grinding is generally performed by the abrasion of the specimens surface against water-lubricated abrasive wheels. The specimens have been subjecting to mechanical grinding beginning with 120-grits papers and proceeding to 240, 320, 400, 600, 800 grit SiC papers. Scratches and damage to the specimen surface from each grit must be removed by the next finer grinding step. A distilled water has been used to clean the specimens before it is subjected to the next grit.

8.2.5 Polishing

The surface damage remaining on the specimen after grinding must be removed by polishing. Polishing of the metallographic specimen generally involves rough polishing and

fine polishing. The rough polishing has been performed using a kitten ear cloth with 6 μm and 1 μm diamond paste with lubricating oil while the fine polishing has been performed with 0.3 μm and then 0.05 μm alumina (α-Al_2O_3) with distilled water. Between any two stages, the specimens has been tested on the optical microscope to check if the scratches were removed.

8.2.6 Etching

Etching includes the process used to reveal the micostructure of a metal. Because many microstrucural details are not observable on an as-polished specimen, the specimens surface must be treated to reveal such structural features as grains, grain boundaries, slip lines and phase boundaries. To obtain a sharply delineated contrasty conditions, a special attention has been paid during the polishing stage such that these surfaces were free from any artifact. Following, the samples have been cleaned throughly, and subjected to a carefully controlled etching process using the appropriate etchants (Table 8.1). After this stage the samples were ready for metallographic and microhardness tests.

Table 8.1. The Etchants for the used materials.

Material	Etchant
AISI 1045	10 mL Nital, 90 ml alcohol
AISI 303	40 mL hydrofluoric (HF), 20 mL Nitric acid (HNO_3), 40 mL glecren
AISI 4340	10 mL Nital, 90 mL alcohol

8.3 MICROHARDNESS MEASUREMENTS

It is known that the microhardness of the deformed material is related with the preceding deformation and with the shear stress gained by the specimen under consideration at the final stage of its deformation. This makes it possible to know the distribution of deformation on the basis of microhardness measurements. The flow shear stress is related with microhardness as (Astakhov, 1998; Nakayama and Tamra, 1964)

$$HV=5.2\tau_s \tag{8.1}$$

where HV is the hardness (Vickeres) and ε is the strain.

A microhardness survey of the formed chips was undertaken to map out different zones through the chip section. The microharness tests have been carried out according to the *ASTM E384-84* standard. In this study, a Leco M-400-G2 microhardness tester has been used. This tester supports the mounting specimens and permits the indenter and the specimen to be brought into contact gradually and smoothly under a predetermined load. This tester has a feature such that no rocking or lateral movement of the indenter or specimen is permitted while the load is being applied or removed. A measuring microscope is mounted on the tester in such a manner that the indentation may be readily located in the field of view. The following steps have been made to do the microhardness tests:

1. Verification of the microhardness tester by making a series of indentations on standardized hardness test blocks.
2. Preparation of the specimens as mentioned above.
3. Supporting the specimens so that the test surface is normal to the axis of the indenter.
4. Selecting the correct objective by adjusting the optical equipment.

5. Deciding on the test parameters where the test load is fixed by means of two dials towards the top right of the machine and the loading speed is set in conjunction with the test load to give the largest measurable indentation. A 25 g load was selected so that tests could be taken very close to the edges.

6. Using a highly polished , pointed and square-based pyramidal diamond with face angles of 136° to indent the specimen.

7. Measuring the diagonals of the indentation by a micrometer screw.

8. Reading the microhardness value from the hardness display.

9

RESULTS AND DISCUSSION

This chapter presents the major results obtained in the experimental part of the study. The experiments have been curried out to conform the developed theory of metal cutting and to understand the relationship between modeled and real cutting conditions. The experimental methodologies are discussed in details in Chapters 6, 7 and 8.

In the view of the discussion presented in the previous chapter, the output has been chosen to cover:

1. The influence of misalignment on the cutting process (the steady-state and dynamic

cutting forces).

2. Comparison between the measured and the predicted steady state cutting forces under nearly perfect alignment conditions.
3. Comparison of the results of the simulation study of proposed dynamic model for wave removing process with those predicted by the proposed model.
4. Frequency autospectra for the axial cutting forces and the cutting torque for different cutting conditions.
5. Dynamic system signatures for different cutting conditions.
6. Results of the study of chip morphology for the fully and partially formed chips.

9.1 MISALIGNMENT EFFECT

Tables 9.1 and 9.2 together with Figures 9.1 through 9.3 quantify the effect of misalignment on the steady-state axial cutting force and cutting torque for different cutting regimes. As seen from these tables and figures, the misalignment affects the results dramatically where an increase in the steady-state axial cutting force and cutting torque can be noted as the misalignment increases. In particular, the cutting axial cutting force and cutting torque increase with increasing the cutting feed much more significant than that with the cutting speed.

Using the obtained experimental results, we have arrived to the following conclusions:

Table 9.1. Effect of misalignment on the measured axial cutting forces.

Cutting tool: Single cutting edge BTAS drill 1" (25.4 mm) diameter. Material: AISI 303						
Rotational spindle Speed (rpm)	Cutting speed (m/min)	Feed (mm/rev)	Measured axial cutting force (N) for misalignment of			
			15μm	205μm	422μm	856μm
626	50	0.08	2020.5	2306.5	2702.7	3100.4
		0.12	3056.4	3200.6	3456.8	3890.2
		0.16	3907.5	4106.9	4389.3	4620.9
939	75	0.08	1950.6	2356.9	2760.9	3178.9
		0.12	3002.5	3245.1	3506.9	3910.9
		0.16	3811.4	4165.2	4487.4	4710.6
1253	100	0.08	1900.4	2400.6	2810.3	3206.9
		0.12	2983.4	3290.2	3610.7	3967.9
		0.16	3778.4	4208.7	4520.8	4804.8

Table 9.2. Effect of misalignment on the measured cutting torque.

Cutting tool: Single cutting edge BTAS drill 1" (25.4 mm) diameter. Material: AISI 303						
Rotational spindle Speed (rpm)	Cutting speed (m/min)	Feed (mm/rev)	Measured cutting torque (N.m) for misalignment of			
			15μm	205μm	422μm	856μm
626	50	0.08	19.49	21.23	24.47	28.83
		0.12	30.43	32.84	34.23	38.72
		0.16	38.69	41.57	43.44	45.91
939	75	0.08	20.01	21.82	24.54	28.95
		0.12	30.42	33.13	35.19	38.94
		0.16	37.45	41.83	44.28	46.92
1253	100	0.08	19.52	22.12	24.83	29.34
		0.12	29.78	33.45	35.98	39.56
		0.16	38.32	42.95	45.43	47.67

1. A significant scatter in the reported experimental results on the steady-state cutting force measurements in deep-hole machining. (Griffith,1982; Griffith,1978, Chandarcheckar,1984; Sakuma et al ,1980a; Sakuma et al, 1980b; Sakuma et al, 1981) is readily explained with the obtained results as follows. Since in the known studies, the misalignment has never been reported thus controlled, these are obtained under different misalignment of the deep-hole machines. For this reason, therefore, the results reported by different researches cannot be compared with each other or/and be used to verify any proposed theory.

2. The reported experimental results cannot be used to design the deep-hole process as the whole. Deep-hole machining combines two machining processes namely drilling and burnishing and forces generated in drilling are used to complete burnishing. As shown by Astakhov (1994), burnishing process defines the quality of the machined surface in terms of its roughness, roundness, residual stresses, etc. It is also known that this process is relatively sensitive to the burnishing force applied. For a given drill design, the ration 'cutting force-burnishing force' is constant and, therefore, a change in the cutting force directly affects the corresponding change in the burnishing force. This simple consideration explains a significant scatter in the reported results on quality in the machining surface in deep hole machining. This also explains a relatively poor reproductivity of the deep-hole machining results since the same tools are used in the machines having different misalignments that causes the scatter.

Figures 9.4 through 9.27 show the frequency autospectra of the axial dynamic cutting force and dynamic cutting torque for different cutting regimes under different misalignments. The misalignment shows up as a series of harmonics associated with the running speed.

Comparing the autospectra of the axial cutting force under different misalignments for the same cutting feed and spindle rotational speed show that the misalignment introduce a series of different amplitude harmonics at frequencies associated with the multiple of the running speed (2X, 4X, 6X etc, X is the frequency corresponding of the running speed). For example at running speed of 654 rpm, the misalignment show up at 22Hz, 44Hz, 66Hz, 66Hz, 88Hz etc.

In the case of the cutting torque, the misalignments also show up as a series of different amplitude harmonics but at frequencies associated with an odd number of the running speed (3X,5X, 7X, 9X etc, X is the frequency corresponding of the running speed). For example at running speed of 654 rpm, the misalignment show up at 33Hz, 55Hz, 66Hz, 99Hz, etc.

Comparing the autospectra of the axial cutting force and cutting torque under different misalignment for the same cutting feed and spindle rotational speed show that the amplitudes of the different harmonics increase as the misalignment increases.

Also, it can be noted that in the case of the axial cutting forces, the dominant amplitude is associated with the second harmonic (2X) of the operating speed where the amplitudes of the spikes which are observed at the forth, sixth, etc harmonic are seen to progressively lowered. In the case of torque, the dominant amplitude is associated with the third harmonic of the operating speed. This spike which was observed at the third harmonic

was also seen at fifth, seventh, etc. though the amplitude was seen to progressively reduced.

The following important conclusions follow from the obtained results:

1. The deep-hole machining system has very distinctive dynamic signatures under different misalignments. As seen from the results, if the deep-hole machining system is aligned, it much more stable dynamically. In practical terms it means the following. First of all, there is no chance for lobbing as hole defects (considered as an inherent feature of deep-hole machining (Sakuma et al ,1980a; Sakuma et al, 1980b; Sakuma et al, 1981) to occur. Moreover, there would be no spiraling (Gessesse, 1990) to be observed since spiraling is caused by dynamic system instability. Unfortunately, in the known studies of these common defects, the misalignment has never been considered.

2. The misalignment change the autospectra in a such manner that it becomes difficult to distinguish between the spectra that reflects the cutting process contribution and the spectra that come from other sources. This produces the signal from the force transducers with high noise. This explains why the known studies (Chandrachaker, 1984) concluded that the cutting force in deep-hole machining has random nature. High-noisy signal used in these studies to judge the nature of the cutting force resulted in such a conclusion.

9.2 STEADY- STATE AXIAL CUTTING FORCE AND CUTTING TORQUE

Tables 9.3 through 9.8. show a comparison between the measured and the predicted steady-state axial cutting force and cutting torque for two cutting tools (American Heller design (BTAH) and Sandvic design (BTAS)) and three different materials (AISI 1045, AISI 303 and AISI 4340) under different cutting regimes. These tables reveal fairly good agreement between the experimental and predicted values. Also, these tables shows that always the experimental values are little more than the predicted ones. The explanation may be that the oil whirling augment the steady state axial cutting force and torque.

Figures 9.28 through 9.36 show the variations of the cutting forces (axial, radial and tangential) and cutting torque with feed for each cutting tool and material under different cutting speed. Also, these figures reveal the experimental results for the axial cutting force and cutting torque.

Table 9.3. Steady-state cutting forces (BTAH drill 1" diameter, AISI 1045).

Rotational spindle Speed (rpm)	Cutting speed (m/min)	Feed (mm/rev)	Axial cutting force (N)			Cutting torque (N.m)		
			Measured	Calculated	error %	Measured	Calculated	error %
626	50	0.08	3003.2	2588.9	13.8	21.32	18.52	10.5
		0.12	4397.5	3837.9	12.7	30.36	27.65	8.7
		0.16	5523.9	5067.8	8.2	42.04	36.74	12.5
939	75	0.08	2776.0	2558.6	7.8	20.53	18.10	11.7
		0.12	4503.4	3784.4	15.9	30.59	27.98	8.5
		0.16	5486.5	4987.7	9.0	42.65	36.52	14.3
1253	100	0.08	2837.9	2533.9	10.7	20.02	18.37	8.3
		0.12	4114.7	3740.7	9.1	30.14	27.40	9.0
		0.16	5680.7	5064.5	10.8	41.74	36.80	11.7

Table 9.4. Steady-state cutting forces (BTAS drill 1"diameter, AISI 1045).

Rotational spindle Speed (rpm)	Cutting speed (m/min)	Feed (mm/rev)	Axial cutting force (N)			Cutting torque (N.m)		
			Measured	Calculated	error %	Measured	Calculated	error %
626	50	0.08	2661.3	2294.2	13.8	24.62	20.92	15.0
		0.12	3800.2	3393.9	10.7	35.81	31.20	12.8
		0.16	4790.7	4472.8	6.6	44.74	41.42	7.3
939	75	0.08	2545.5	2266.2	11.0	23.93	20.64	13.6
		0.12	3608.8	3343.8	7.3	35.87	30.61	14.5
		0.16	4732.7	4398.2	7.1	45.78	41.02	10.2
1253	100	0.08	2537.6	2240.7	11.7	24.31	20.36	16.2
		0.12	3700.8	3298.8	10.9	33.86	30.38	10.1
		0.16	4905.8	4488.7	8.5	44.28	40.23	9.0

Table 9.5. Steady-state cutting forces (BTAH drill 1" diameter, AISI 303).

Rotational spindle Speed (rpm)	Cutting speed (m/min)	Feed (mm/rev)	Axial cutting force (N)			Cutting torque (N.m)		
			Measured	Calculated	error%	Measured	Calculated	error%
626	50	0.08	2334.3	2094.8	10.3	17.82	15.71	11.7
		0.12	3502.4	3089.2	11.8	27.03	23.43	13.2
		0.16	4367.4	4061.2	7.0	35.64	31.09	12.7
939	75	0.08	2406.4	2063.8	14.2	17.95	15.62	12.8
		0.12	3290.5	3034.4	7.8	27.36	23.20	16.5
		0.16	4367.3	3979.4	8.9	33.77	30.87	8.4
1253	100	0.08	2408.1	2035.4	15.5	18.92	15.55	17.7
		0.12	3311.3	2984.5	9.9	27.57	23.15	15.8
		0.16	4402.8	4013.7	8.8	36.19	31.17	13.7

Table 9.6. Steady-state cutting forces (BTAS drill 1" diameter, AISI 303).

Rotational spindle Speed (rpm)	Cutting speed (m/min)	Feed (mm/rev)	Axial cutting force (N)			Cutting torque (N.m)		
			Measured	Calculated	error %	Measured	Calculated	error %
626	50	0.08	2020.5	1841.1	8.9	19.49	17.72	9.1
		0.12	3056.4	2707.1	11.4	30.43	26.40	13.2
		0.16	3907.5	3549.9	9.2	38.69	35.04	9.4
939	75	0.08	1950.6	1809.2	7.2	20.01	17.60	12.0
		0.12	3002.5	2650.6	11.7	30.42	26.25	13.7
		0.16	3811.4	3465.3	9.1	37.45	34.80	7.1
1253	100	0.08	1900.4	1779.3	6.4	19.52	17.53	10.2
		0.12	2983.4	2598.4	12.9	29.78	26.09	12.4
		0.16	3778.4	3509.2	7.1	38.32	35.10	8.4

Table 9.7. Steady-state cutting forces drill 1" diameter, AISI 4340).

Rotational spindle Speed (rpm)	Cutting speed (m/min)	Feed (mm/rev)	Axial cutting force (N)			Cutting torque (N.m)		
			Measured	Calculated	error%	Measured	Calculated	error%
626	50	0.08	2520.5	2315.7	8.1	18.34	16.35	10.9
		0.12	3910.4	3419.4	12.6	26.78	24.39	8.9
		0.16	4803.3	4500.3	6.3	35.1	32.36	7.8
939	75	0.08	2603.2	2284.3	12.3	18.21	16.27	10.7
		0.12	3678.2	3363.3	8.6	26.5	24.20	8.7
		0.16	4809.1	4416.7	8.2	34.78	32.10	7.7
1253	100	0.08	2578.3	2255.1	12.5	18.45	16.18	12.3
		0.12	3678.2	3312.4	9.9	26.78	24.10	10.0
		0.16	4890.2	4466.4	8.7	34.67	32.36	6.7

Table 9.8. Steady-state cutting forces (BTAS drill 1"diameter, AISI 4340).

Rotational spindle Speed (rpm)	Cutting speed (m/min)	Feed (mm/rev)	Axial cutting force (N)			Cutting torque (N.m)		
			Measured	Calculated	error%	Measured	Calculated	error%
626	50	0.08	2245.6	2056.5	8.4	20.34	18.52	8.9
		0.12	3456.7	3027.9	12.4	30.56	27.62	9.6
		0.16	4487.1	3975.4	11.4	39.12	36.65	6.3
939	75	0.08	2238.9	2023.6	9.6	21.34	18.40	13.8
		0.12	3241.8	2969.8	8.4	30.87	27.45	11.1
		0.16	4278.2	3889.1	9.1	39.1	36.30	7.2
1253	100	0.08	2100.4	1993.5	5.1	21.38	18.41	13.9
		0.12	3300.1	2916.5	11.6	30.26	27.30	9.8
		0.16	4256.1	3949.4	7.2	39.12	36.63	6.4

9.3 WAVE REMOVING CUTTING PROCESS

Figures 9.37 through 9.40 show the simulation results for the wave removing process for different cutting conditions. The simulation has been carried out based on the dynamic model of shear zone with parallel boundaries where four series of testing programs were curried out to assess the effects of the cutting feed, cutting speed, rake angle and frequency of the waves on the work surface on the dynamic force components F_x and F_y. These figures reveal the variations of the force components which follow approximately sinusoidal waves. A certain phase lag relative the variation of the uncut chip thickness is clearly seen.

Figures 9.41 through 9.44 show the comparison between the predicted and the measured dynamic forces. Here, the experimental results obtained in by Nagim and Sadek (1977) are also shown. The comparison shows that the proposed model gives a good agreements with the experimental results.

9.4 CUTTING SIGNATURES

Figures 9.45 through 9.62 show the frequency autospectra of axial cutting force and cutting torque for BTAH tool for different cutting conditions under near perfect misalignment where the Figures 9.63 through 9.80 show the frequency autospectra of axial cutting forces and cutting torque but for BTAS tool.

The following can be drawn from these figures:

1. At frequency equals to 90 Hz, there is a peak associated to the oil whirling. The amplitude of this peak is about 5% of corresponding steady state axial cutting force and about 12% of the corresponding steady state cutting torque.
2. Comparing the autospectra at the same feed and spindle rotational speed show different cutting signatures for different materials. For example, the axial cutting forces autospectra at feed of 0.08 mm/rev and spindle rotational speed of 656 rpm show a peak at frequency of 657 Hz for AISI 1045 steel, 528 for AISI 303 and 345 Hz for AISI 4340. This may be explained by the fact that each material has its own layer thickness. This can be proven by comparing the different fully deformed chips shown in Figure 9.93. Also, this comparison show that these peaks have different amplitudes. For example, the amplitude of peak in the case of AISI 1045 steel is about 10% of the associated steady state axial cutting force where this amplitude is about 13% in the case of AISI 303 and 19% in the case of AISI 4340 steel. This also can be proven by comparing the saw-toothed chip thickness shown in Figure 9.93.
3. Comparing the autospectra at the same spindle rotational speed and the same material show slightly different cutting signatures for different feeds. For example, the axial

cutting force autospectra of AISI 303 at spindle rotational speed of 656 rpm show a peak at frequency of 528 Hz for 0.08mm/rev feed, 520 Hz for 0.12 mm/rev and 515 Hz for 0.16 mm/rev. This may be explained by the fact that the bending moment which cause the chip formation (Astakhov et al, 1997b) depend on the feed. In particular., the bending moment increase with feed that lowers the frequency of chip formation. Also, this comparison show that these peaks have different amplitudes and this amplitude increases as the feed increases. For example, the amplitude of peak in the case of 0.08 mm/rev is about 13% of the associated steady state axial cutting force where this amplitude is about 16% when the feed is 0.12 mm/rev and 19% when the feed is 0.16 mm/rev.

4. Comparing the autospectra at the same feed and the same material show slightly different cutting signatures for different spindle rotational speed. For example, the axial cutting force autospectra of AISI 303 at feed 0.08 mm/rev show a peak at frequency of 528 Hz for n=656 rpm, 589 Hz for n=939 rpm and 665 Hz for n=1253 rpm. This may be explained by the fact that with increasing the cutting speed, the length of the machined surface per unit time is increased, then more sliding surfaces form. Also, this comparison show that these peaks have almost the same amplitude for different cutting speed.

5. Comparing the autospectra at the same feed, spindle rotational speed and the same material show almost the same cutting signatures for the two types of the tool used in the experiments.

Table 9.9 and the figures 9.81 through 9.83 summerize the effect of the feeds,

workpieces material and the cutting speeds on the cutting signatures.

This study shows the fluctuation of the cutting forces is a result of chip segmentation and not the cause of it. Also this study show the effect of materials and cutting conditions on the cutting signatures.

Table 9.9. Effect of material, feed and cutting speed on the cutting fluctuation frequency.

Cutting tool: BTAH and BTAS drill 1" (25.4 mm).					
Rotational spindle Speed (rpm)	Cutting speed (m/min)	Feed mm/rev	Fluctuation Frequence (Hz)		
			AISI 1045	AISI 303	AISI 4340
626	50	0.08	657	528	345
		0.12	645	520	335
		0.16	640	515	330
939	75	0.08	740	589	400
		0.12	700	560	380
		0.16	690	550	365
1253	100	0.08	830	665	470
		0.12	782	620	428
		0.16	750	592	398

9.5 CHIP MORPHOLOGY

The morphology of the formed and partially formed chip is presented in this section. Figures 9.84 through 9.93present the results of the chip morphology for the fully formed chip where the Figures 9.94 through 9.98 show results of chip morphology for the partially formed chip.

Figure 9.84 show the initial structure for the AISI 1045. This structure is mainly pearlite grain (gray) with a network of grain boundary ferrite (white). Figure 9.85 reveal the configuration for the fully formed chip of the AISI 1045 at different magnifications. As can be seen by comparing the initial structure and the formed one, it can easily note the elongation of the grains in the direction of deformation. Figure 9.86 present a typical saw-toothed chip showing the distribution of the microhardness across the chip section. The figure reveal that the microhardness values starts with values equal to the initial material hardness and increase to a certain limit and then start from the beginning again. This proves that the deformation is non-uniform.

Figure 9.87 show the initial structure for the AISI 303. This structure is a matrix of austenite grains bound an intermetallic stringer type inclusions.. Figure 9.88 reveal the configuration for the fully formed chip of the AISI 303 at different magnifications. As can be seen by comparing the initial structure and the formed one, it can easily note the elongation of the grains in the direction of deformation. This figure reveals that the shear zone is composed of two regions. The first region (**A**) is the "wide region" where the deformation changes at a small rate The second region (**B**) is the "narrow region " where the deformation changes at a high rate. Figure 9.89 support the previous finding where the rate

of microhardness change in the narrow region is bigger than that in the wide region.

Figure 9.90 show the initial structure for the AISI 4340. This structure is tempered martensite. Figure 9.91 reveal the configuration for the fully formed chip of the AISI 4340 at different magnifications. As can be seen by comparing the initial structure and the formed one, it can easily note the elongation of the grains in the direction of deformation. Figure 9.92 present a typical saw-toothed chip showing the distribution of the microhardness across the chip section. The figure reveal that the microhardness values starts with values equal to the initial material hardness and increase to a certain limit and then start from the beginning again. This proves that the deformation is non-uniform.

In studying the deformation in metal cutting the main attention is usually paid to the deformation rate which takes place in the shear zone. The rate of deformation is closely related to the displacement and the velocities. To calculate the deformation rate a number of different approaches and formulas were proposed (Boothroyd and Knight, 1989). The known approaches are based on the known velocity diagram (Merchant, 1945) which has to be corrected as shown previously in chapter three. Therefore, the deformation rate for the model of deformation zone with parallel boundaries requires additional study.

Figures 9.94 through 9.97 show the microphotographs of the partially formed chip. Figure 9.97 shows that the deformation is non uniform across the shear zone.

The morphology study support the theoretical considerations of the parallel shear zone model with parallel boundaries where the study reveal that the shear zone is composed of two regions (Manyindo and Oxley, 1986). The first region is termed as the "wide region" where the tangential velocity v_x changes at a small rate. The second region is termed as the

"narrow region " where the tangential velocity v_x changes at a high rate. Also, it can be seen that as n increases, the "wide region" becomes larger and the " narrow region" becomes smaller. The narrow region where a significant change of the tangential velocity takes place may be thought as the region of the discontinuity of this velocity. This model plays a principal role for the foregoing analysis because both the state of stress and strain and the resistance of the work material to cutting in this " narrow region" are very specific.

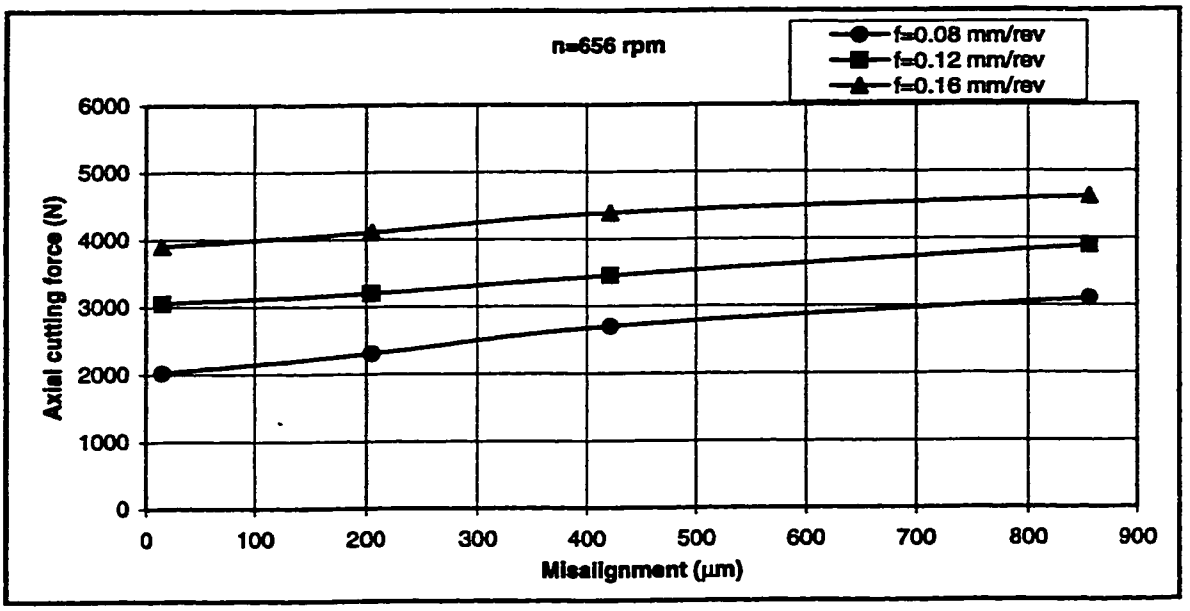

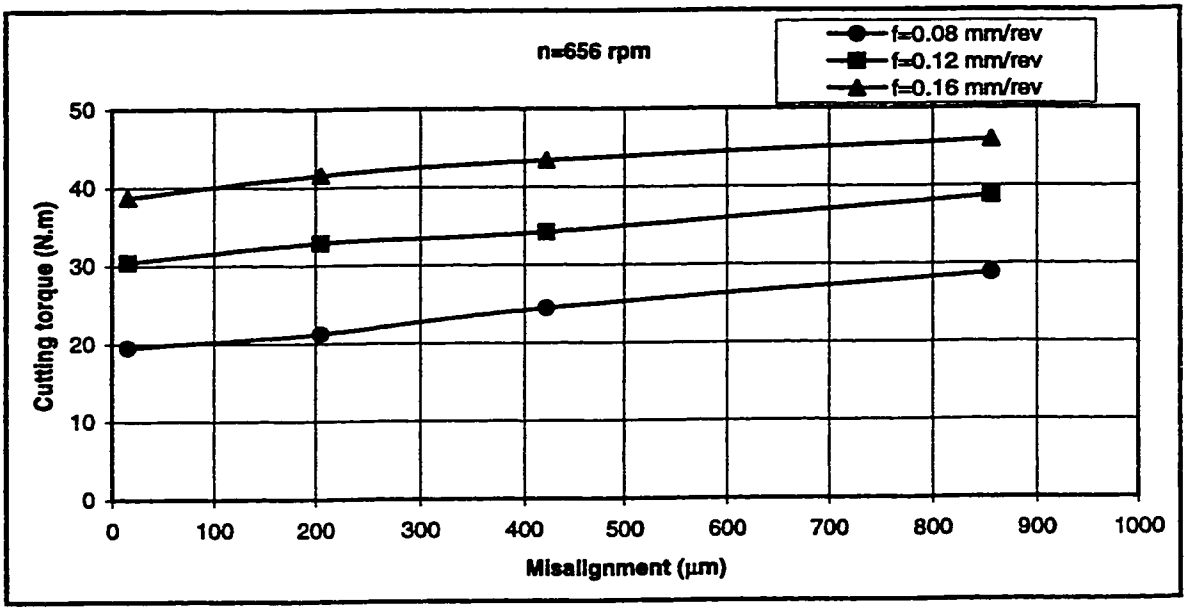

Figure 9.1: Effect of misalignment on the steady-state axial cutting force and torque components. Cutting conditions: workpiece, AISI 303; tool, BTAS 1" inch diameter ; spindle rotational speed n, 656 rpm; boring bar length, 2.0 m; cutting fluid flow rate, 80 l/min.

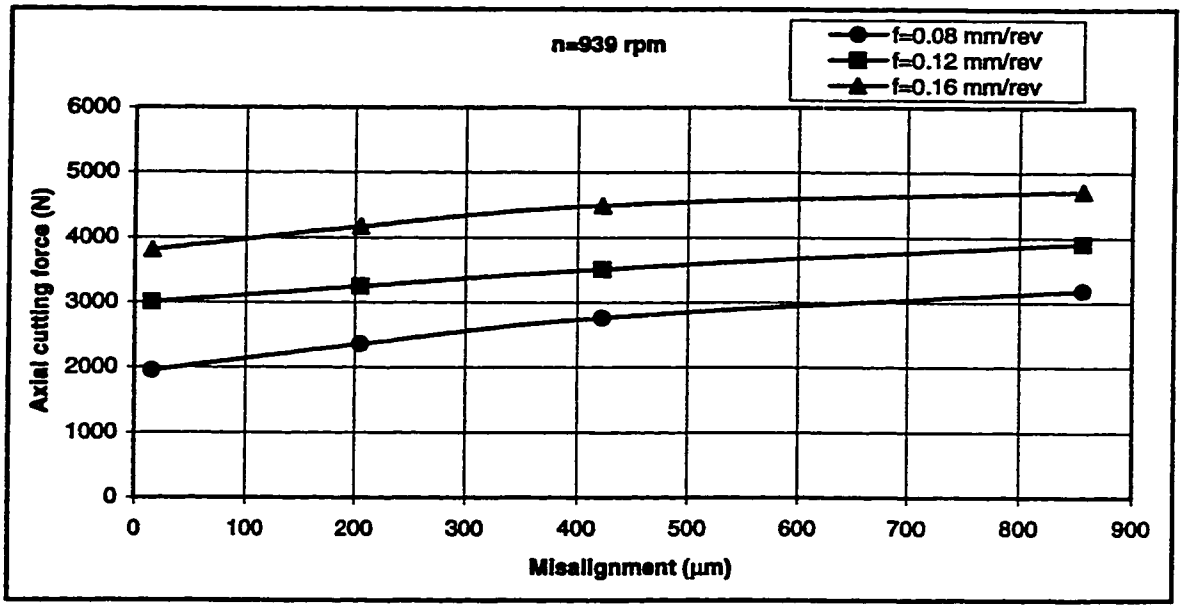

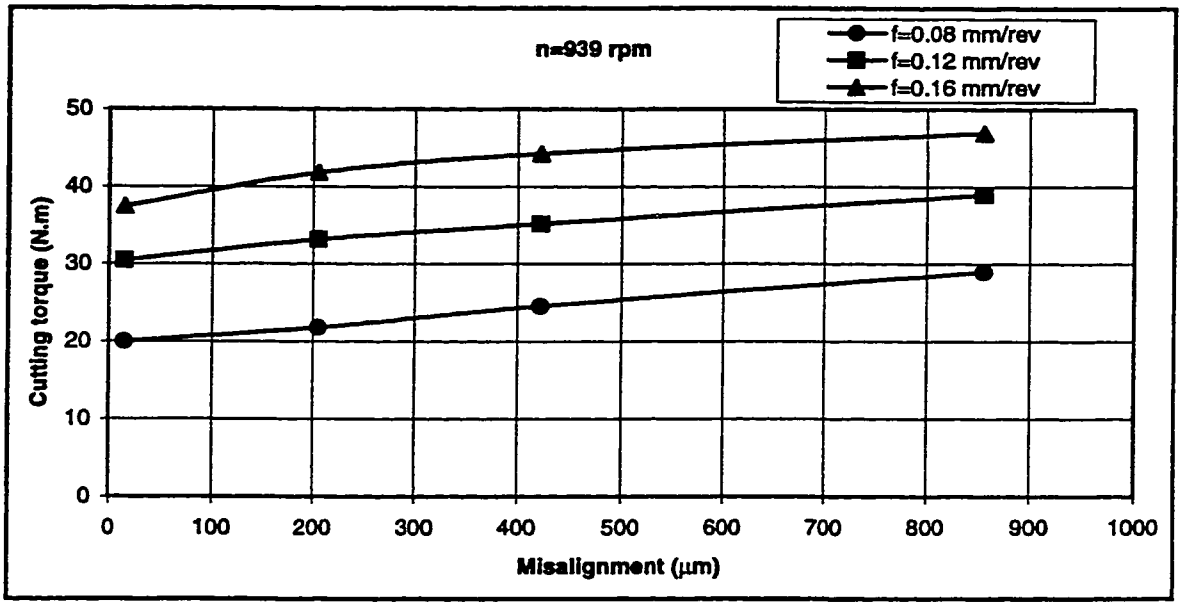

Figure 9.2: Effect of misalignment on the steady-state axial cutting force and torque components. Cutting conditions: workpiece, AISI 303; tool, BTAS 1" inch diameter ;spindle rotational speed n, 939 rpm; boring bar length, 2.0 m; cutting fluid flow rate, 80 l/min.

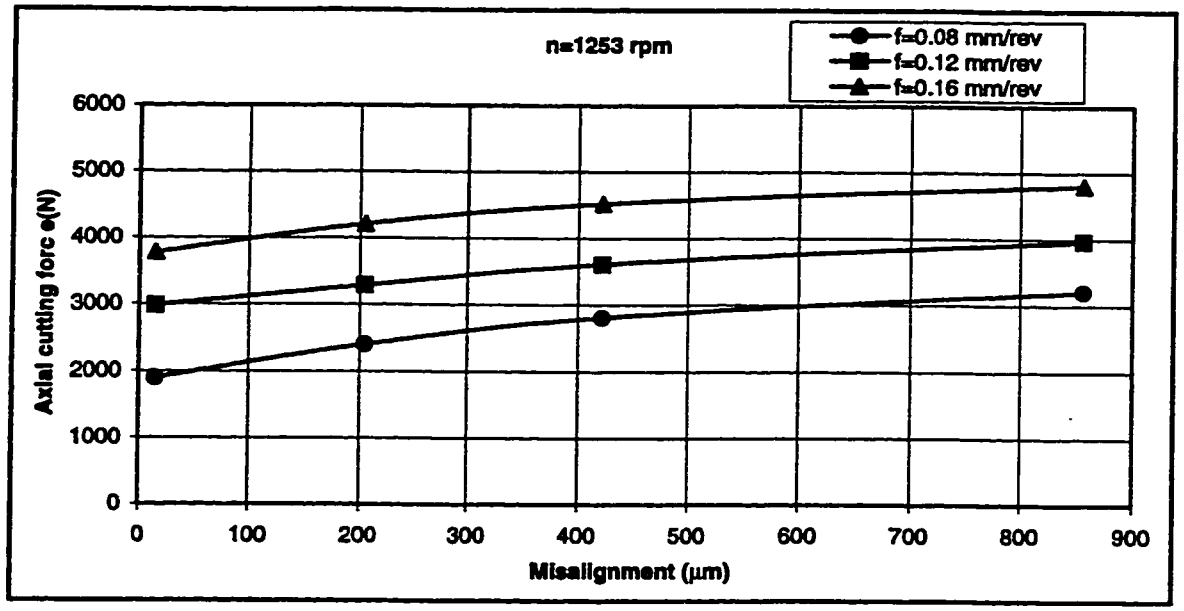

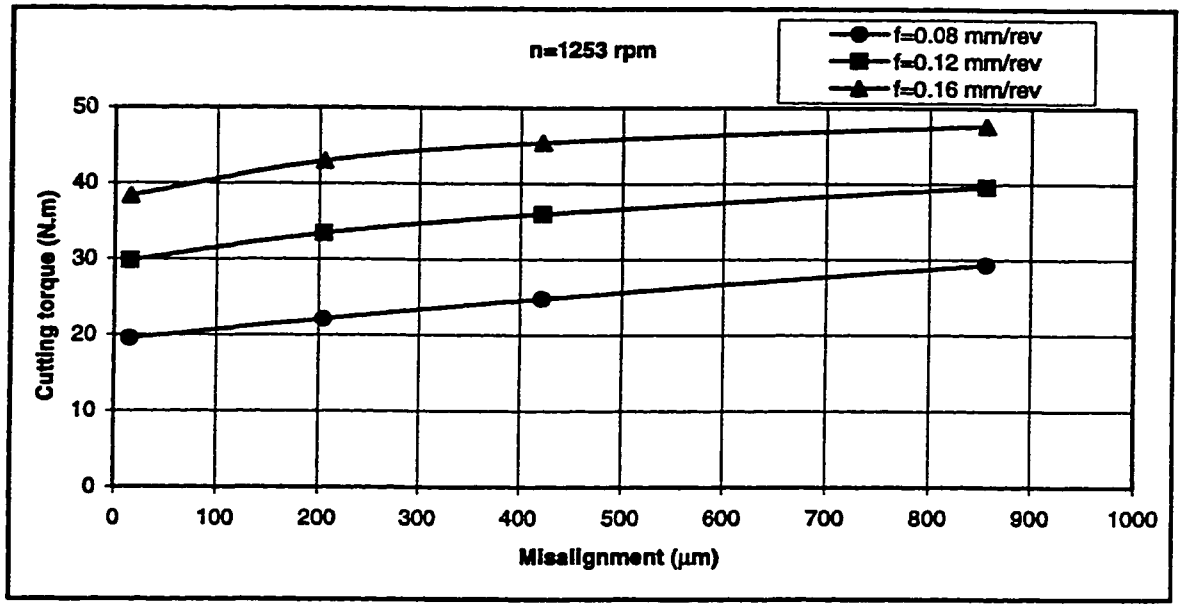

Figure 9.3: Effect of misalignment on the steady-state axial cutting force and torque components. Cutting conditions: workpiece, AISI 303; tool, BTAS 1" inch diameter ; spindle rotational speed n, 1253 rpm; boring bar length, 2.0 m; cutting fluid flow rate, 80 l/min.

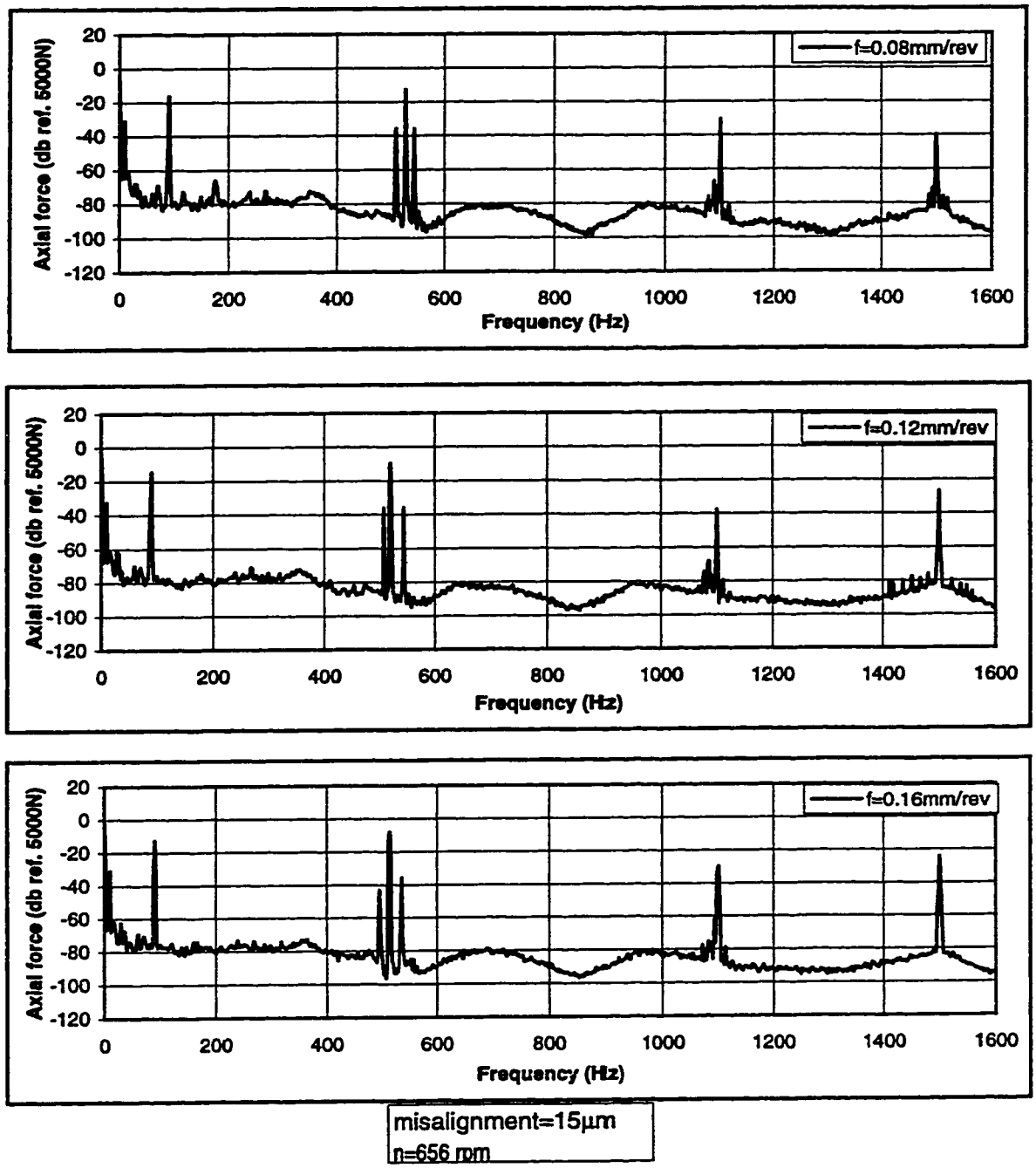

Figure 9.4: Autospectra of the axial cutting force. Cutting conditions: workpiece, AISI 303; tool, BTAS 1" inch diameter ; boring bar length, 2.0 m; spindle rotational speed n, 656 rpm; misalignment, 15µm; cutting fluid flow rate, 80 l/min.

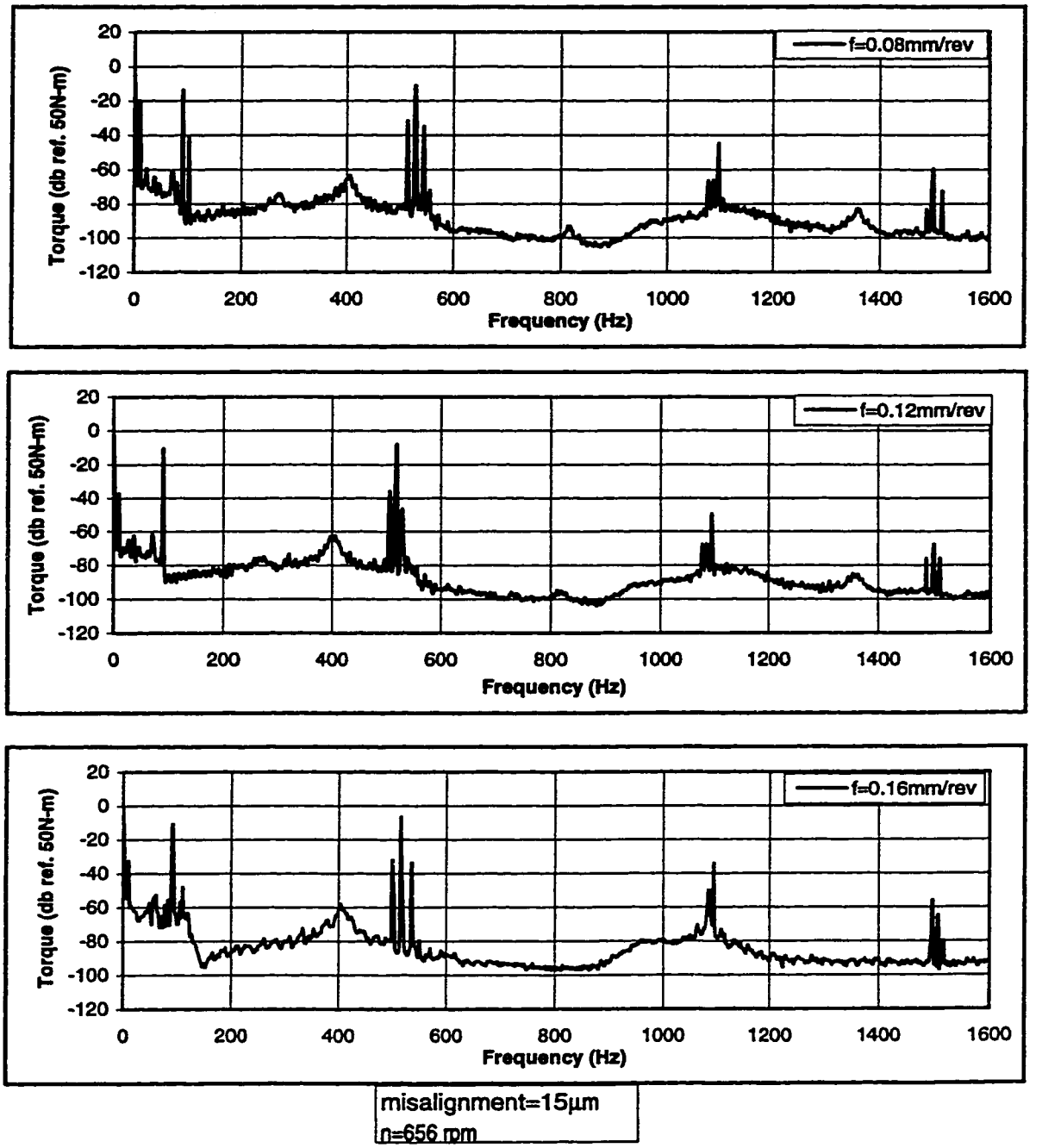

Figure 9.5: Autospectra of the cutting torque. Cutting conditions: workpiece, AISI 303; tool, BTAS " inch diameter ; boring bar length, 2.0 m; spindle rotational speed n, 656 rpm; misalignment, 15µm; cutting fluid flow rate, 80 l/min.

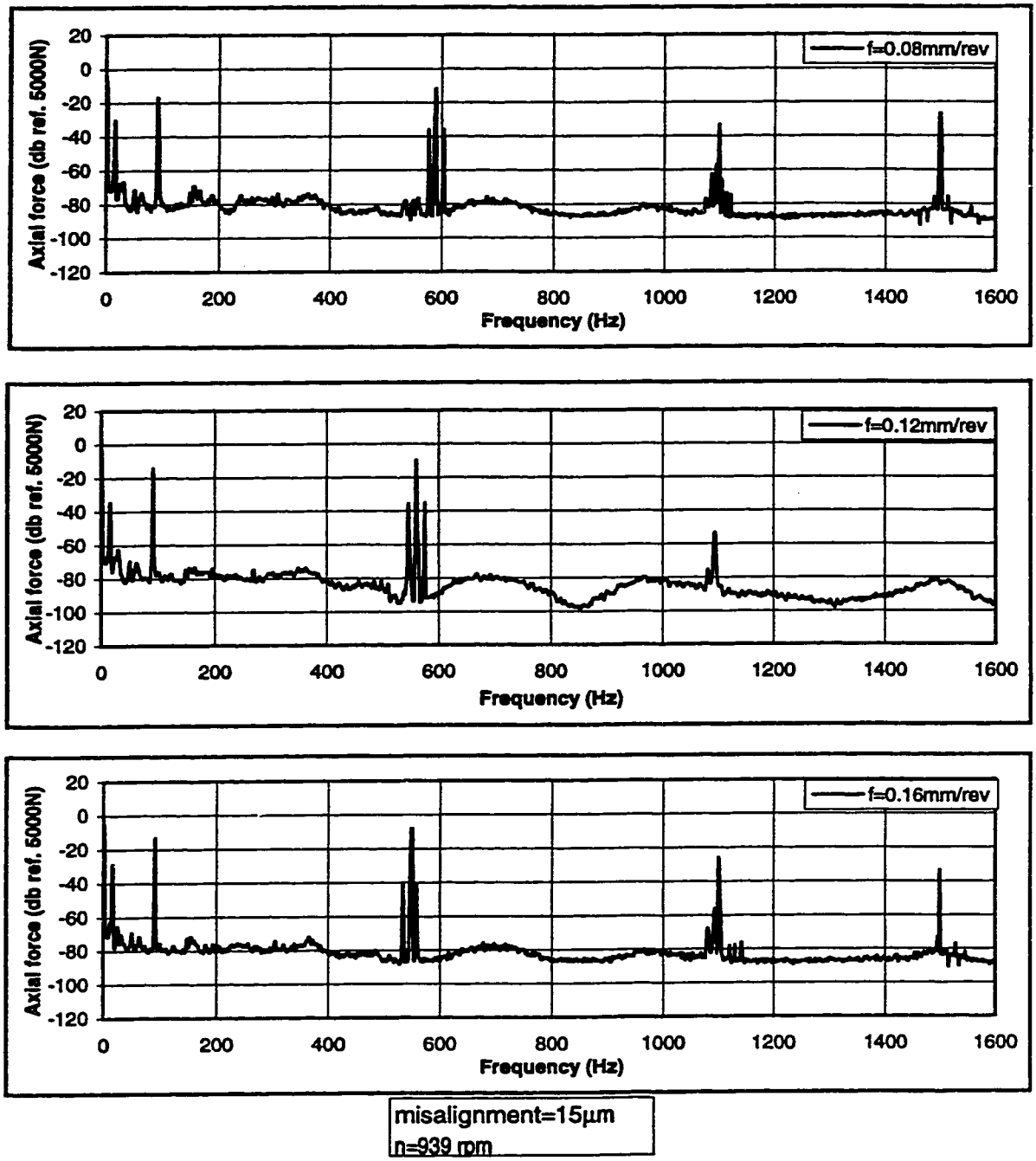

Figure 9.6: Autospectra of the axial cutting force. Cutting conditions: workpiece, AISI 303; tool, BTAS 1" inch diameter ; boring bar length, 2.0 m; spindle rotational speed n, 939 rpm; misalignment, 15µm; cutting fluid flow rate, 80 l/min.

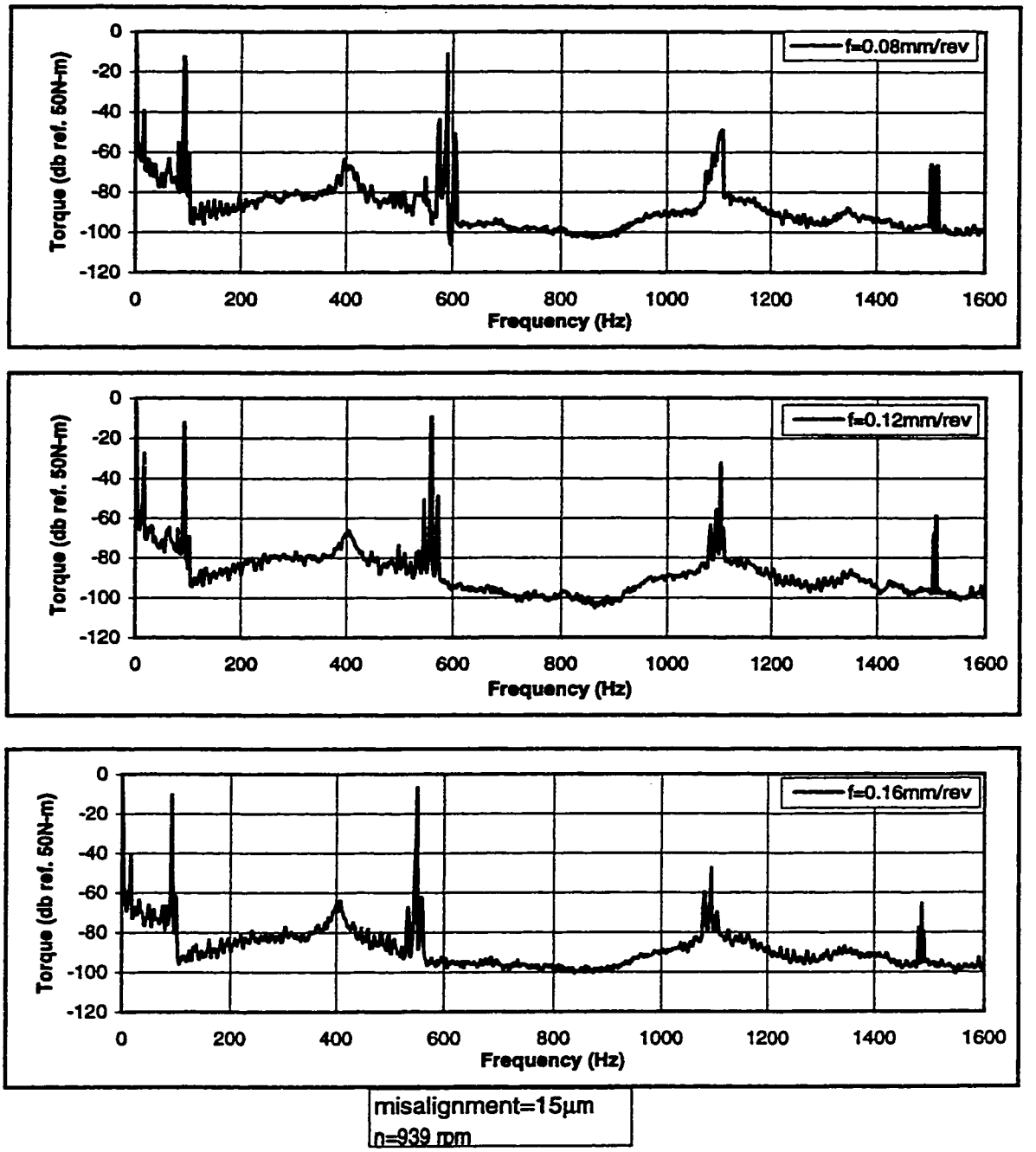

Figure 9.7: Autospectra of the cutting torque. Cutting conditions: workpiece, AISI 303; tool, BTAS 1" inch diameter ; boring bar length, 2.0 m; spindle rotational speed n, 939 rpm; misalignment, 15µm; cutting fluid flow rate, 80 l/min.

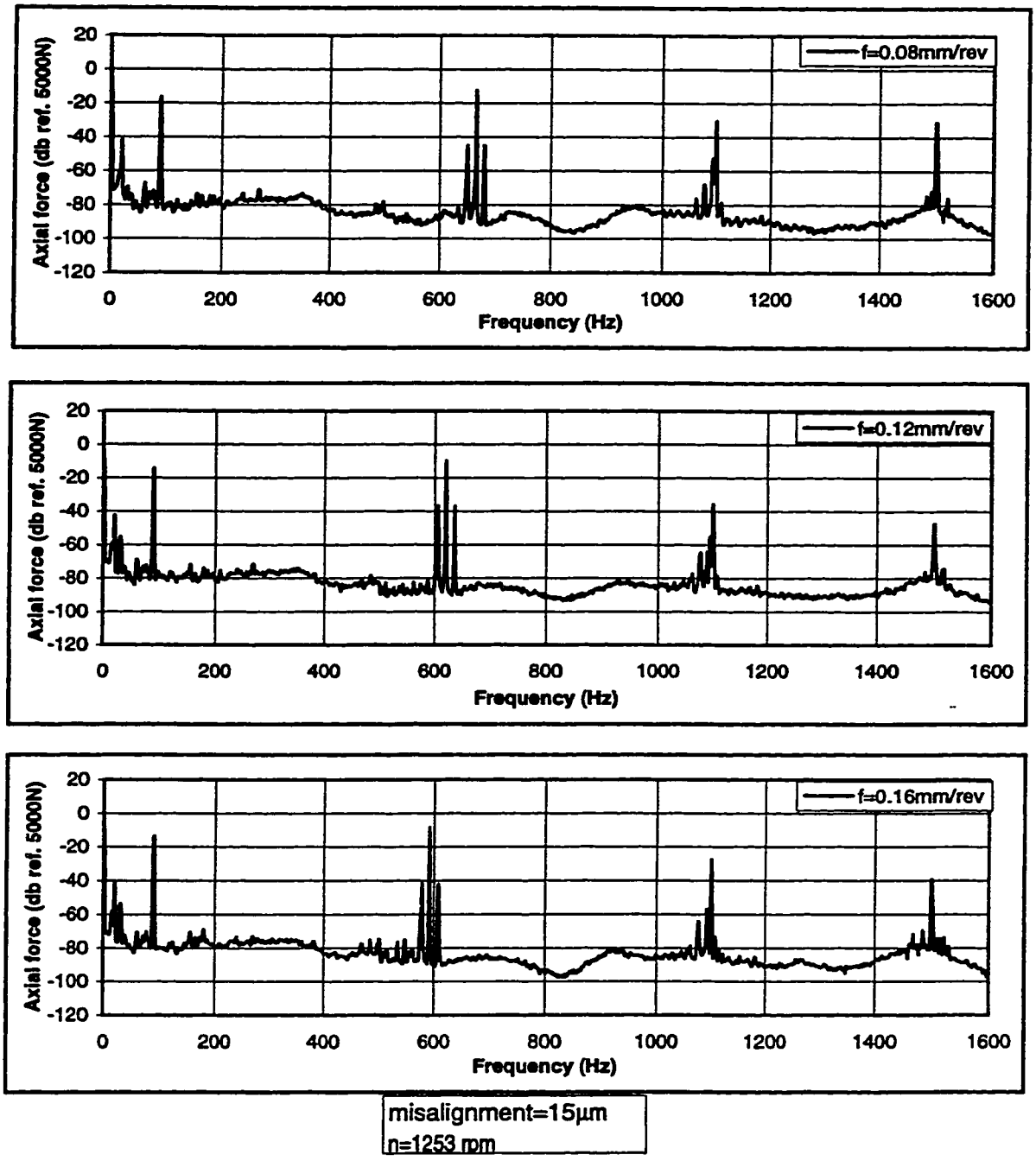

Figure 9.8: Autospectra of the axial cutting force. Cutting conditions: workpiece, AISI 303; tool, BTAS 1" inch diameter ; boring bar length, 2.0 m; spindle rotational speed n, 1253 rpm; misalignment, 15µm; cutting fluid flow rate, 80 l/min.

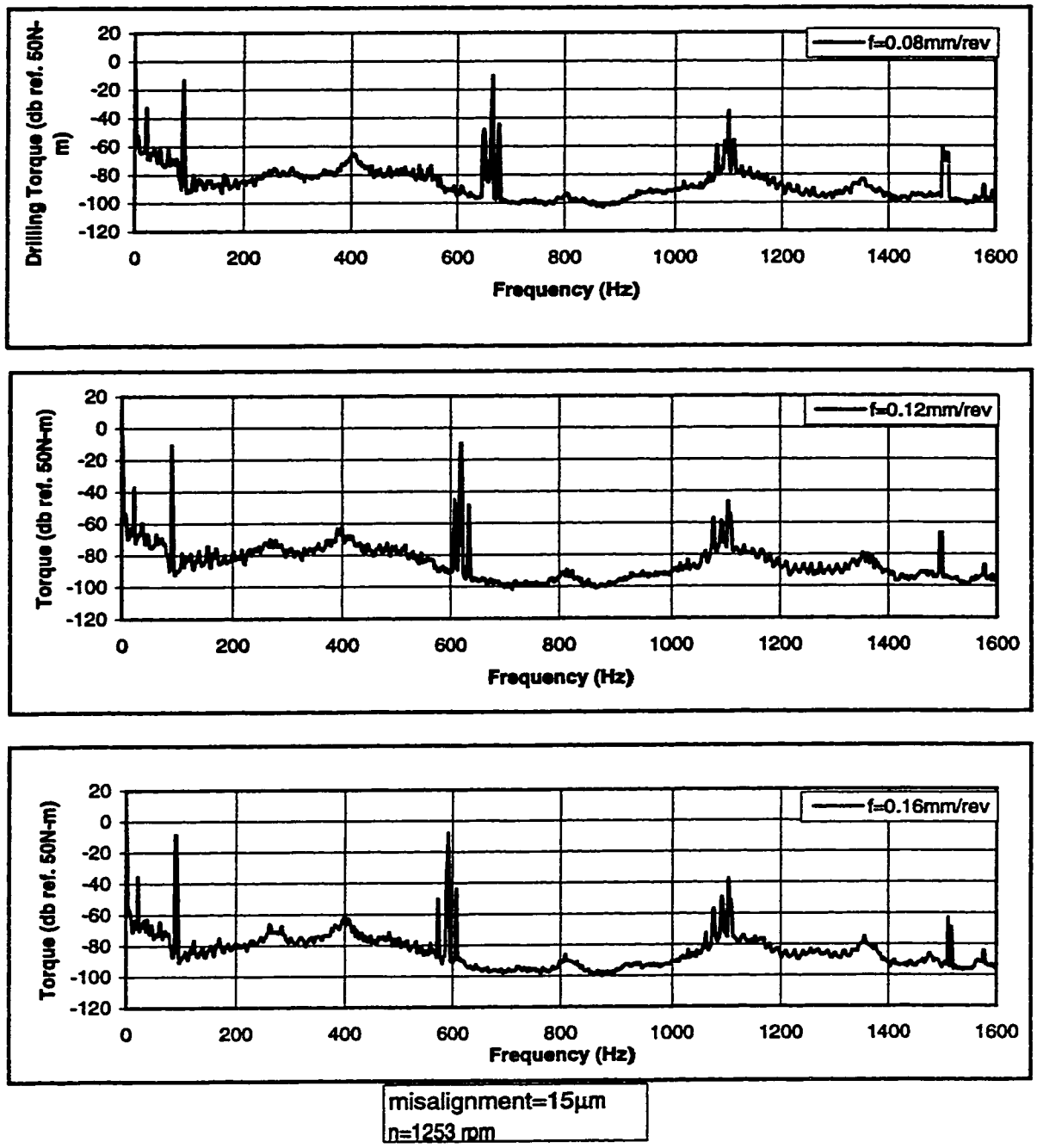

Figure 9.9: Autospectra of the cutting torque. Cutting conditions: workpiece, AISI 303; tool, BTAS 1" inch diameter ; boring bar length, 2.0 m; spindle rotational speed n, 1253 rpm; misalignment, 15µm; cutting fluid flow rate, 80 l/min.

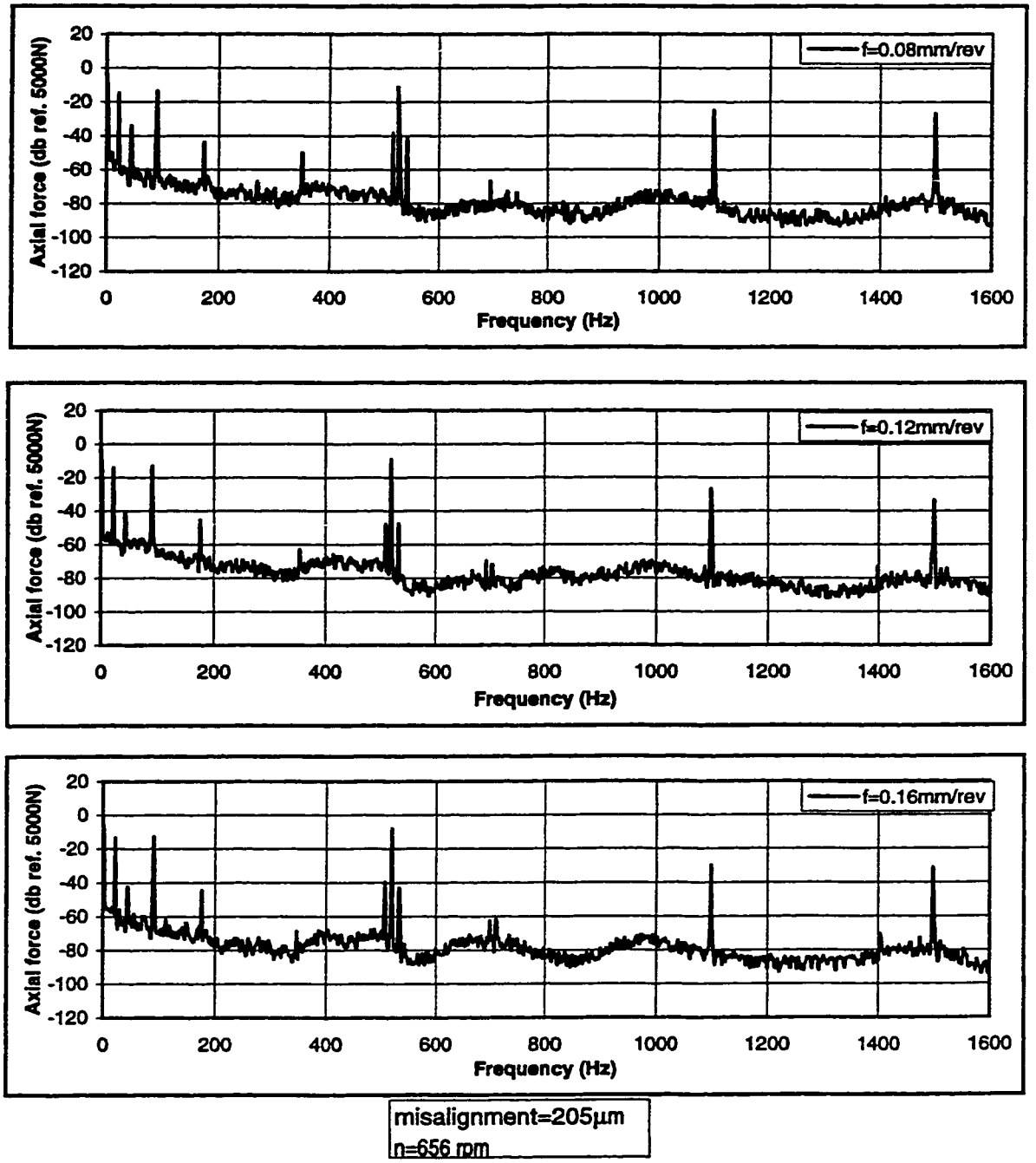

Figure 9.10: Autospectra of the axial cutting force. Cutting conditions: workpiece, AISI 303; tool, BTAS 1" inch diameter ; boring bar length, 2.0 m; spindle rotational speed n, 656 rpm; misalignment, 205µm; cutting fluid flow rate, 80 l/min.

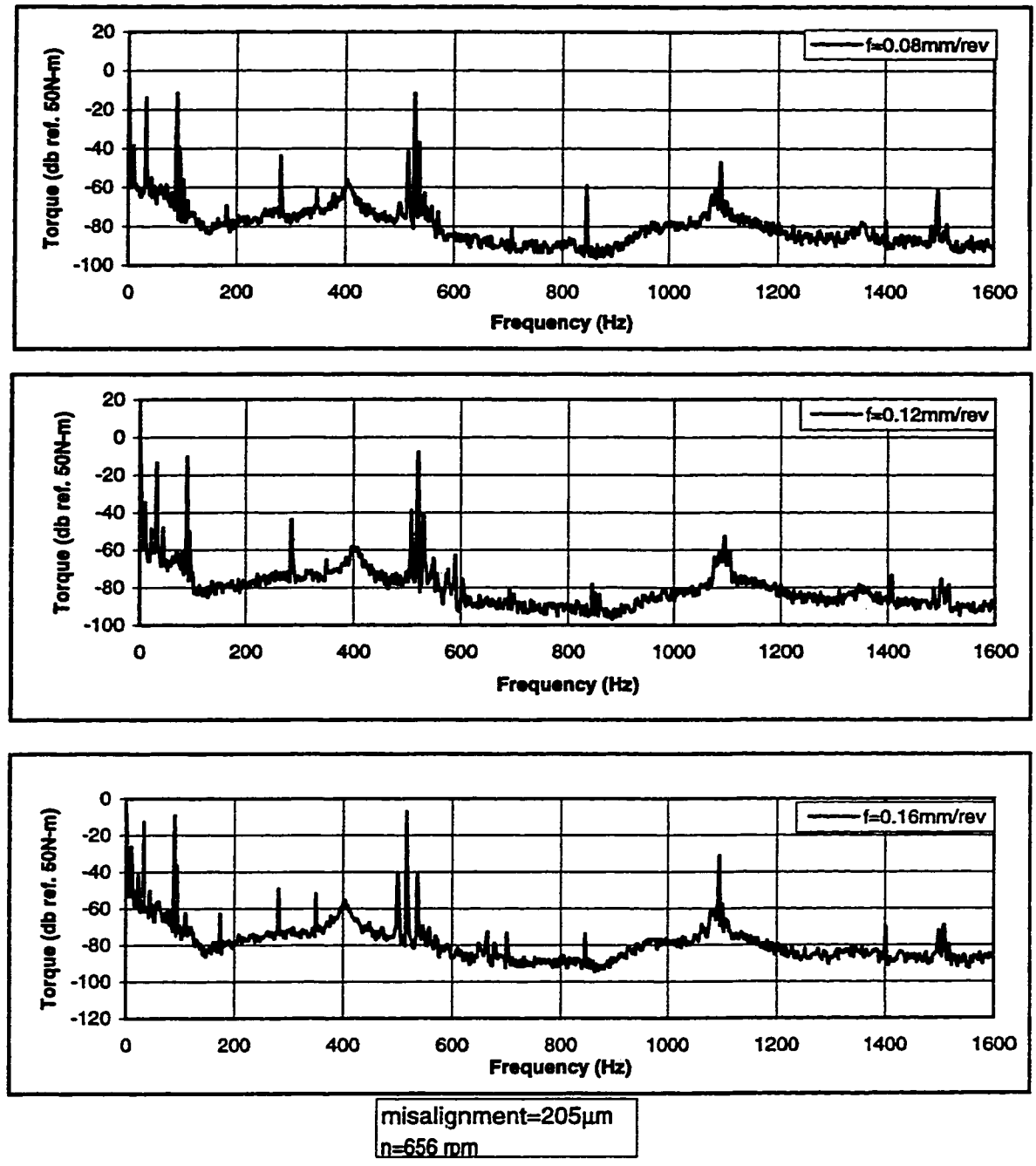

Figure 9.11: Autospectra of the cutting torque. Cutting conditions: workpiece, AISI 303; tool, BTAS 1" inch diameter ; boring bar length, 2.0 m; spindle rotational speed n, 656 rpm; misalignment, 205µm; cutting fluid flow rate, 80 l/min.

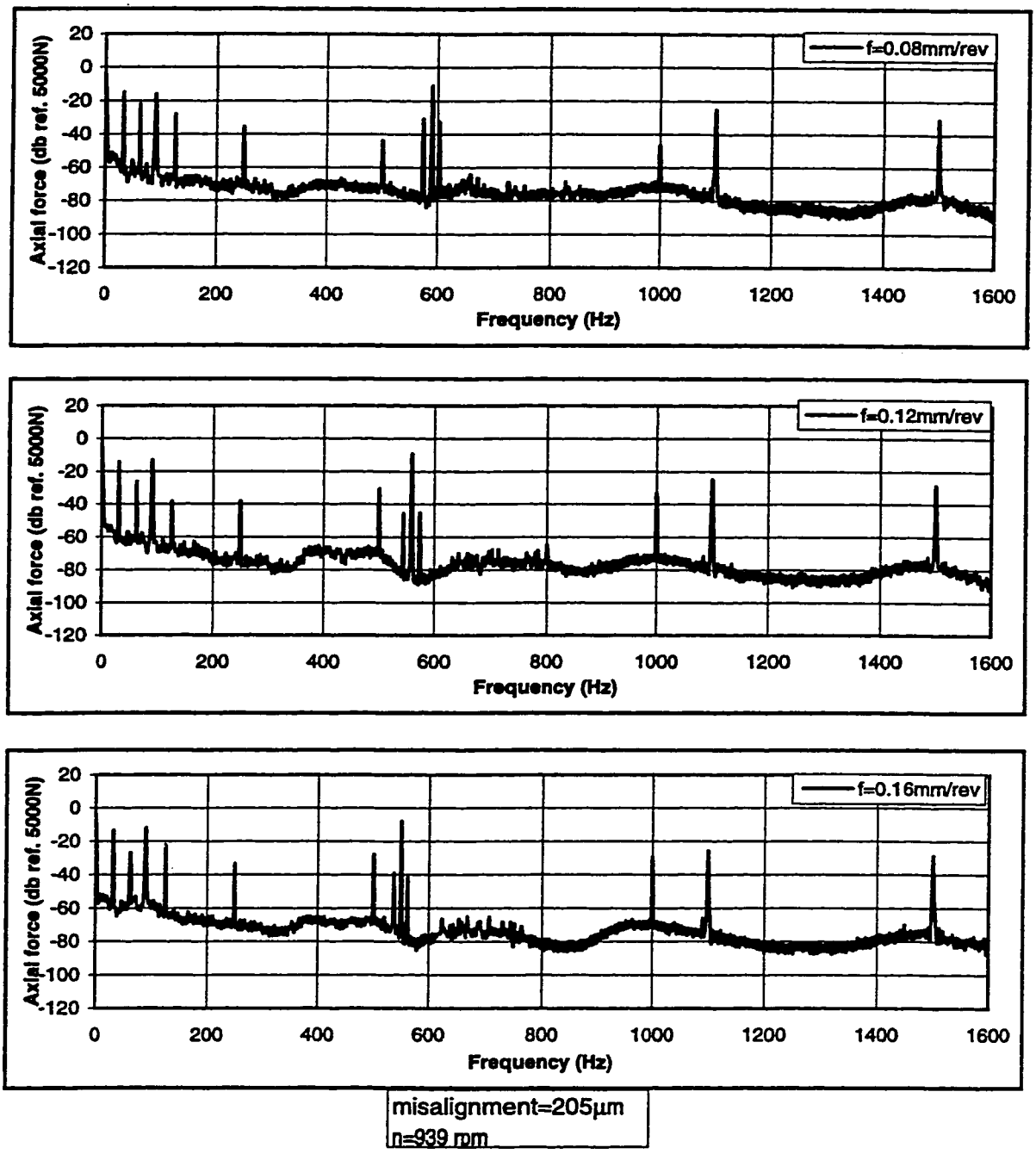

Figure 9.12: Autospectra of the axial cutting force. Cutting conditions: workpiece, AISI 303; tool, BTAS 1" inch diameter ; boring bar length, 2.0 m; spindle rotational speed n, 939 rpm; misalignment, 205µm; cutting fluid flow rate, 80 l/min.

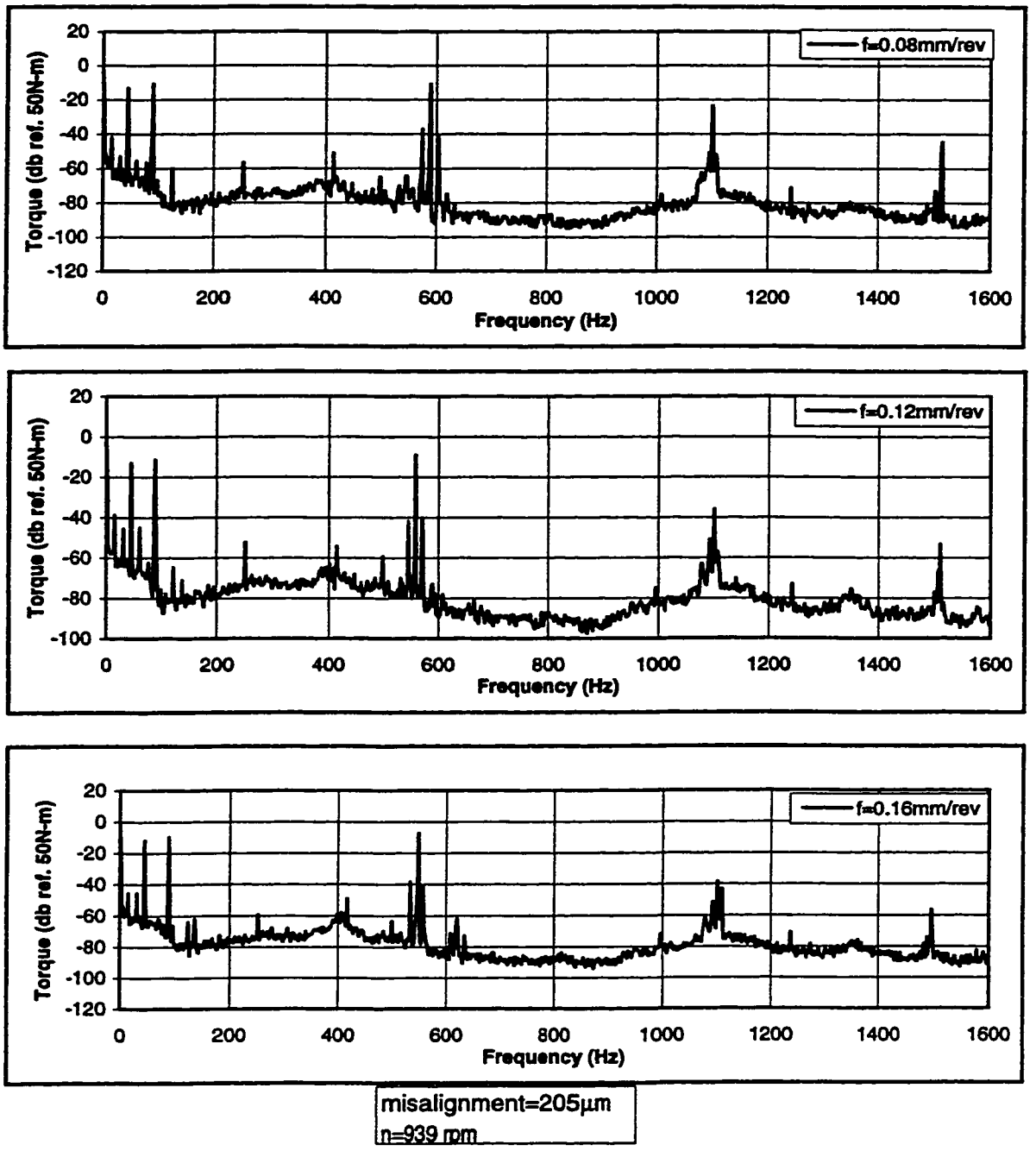

Figure 9.13: Autospectra of the cutting torque. Cutting conditions: workpiece, AISI 303; tool, BTAS 1" inch diameter ; boring bar length, 2.0 m; spindle rotational speed n, 939 rpm; misalignment, 205µm; cutting fluid flow rate, 80 l/min.

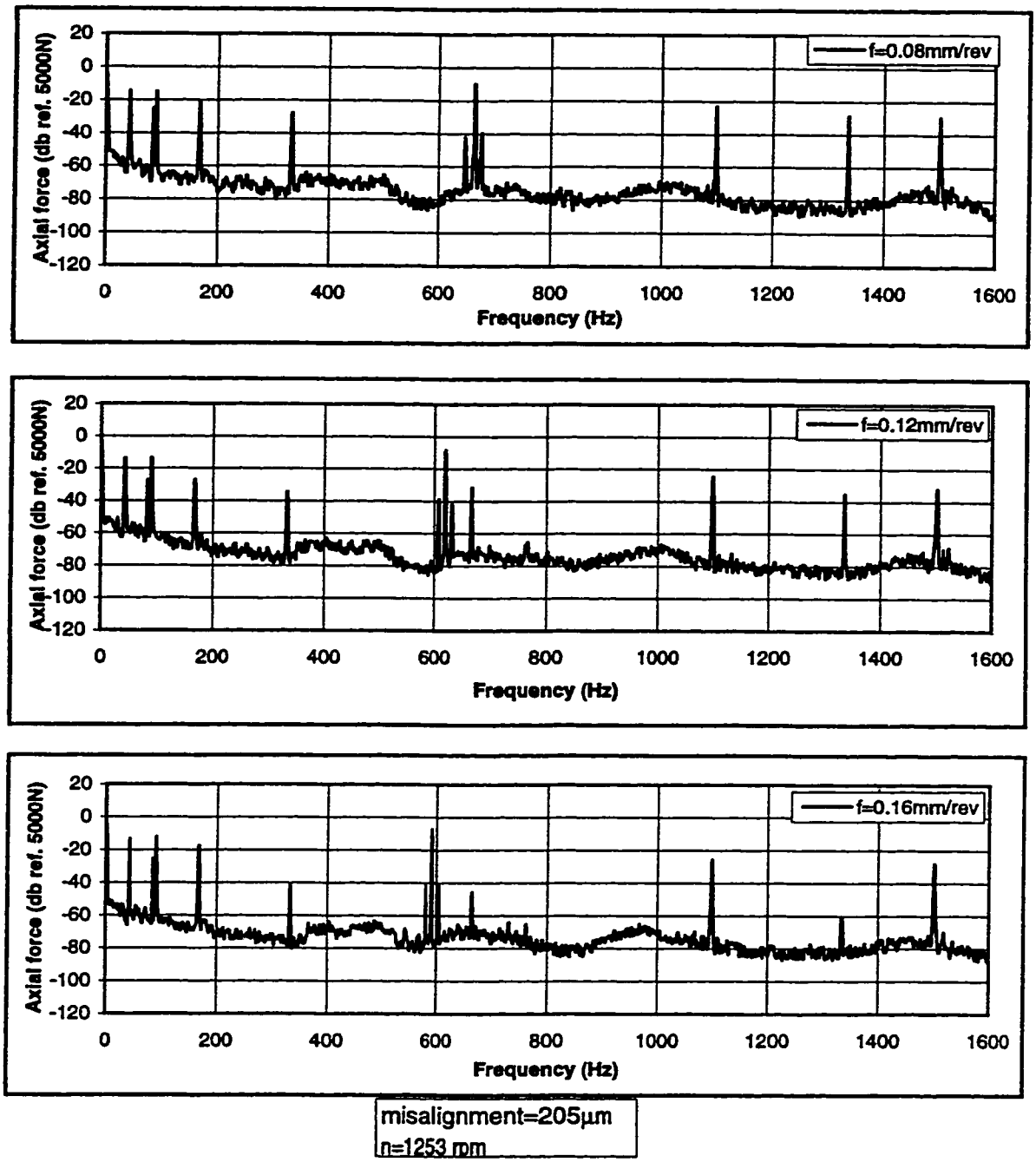

Figure 9.14: Autospectra of the axial cutting force. Cutting conditions: workpiece, AISI 303; tool, BTAS 1" inch diameter ; boring bar length, 2.0 m; spindle rotational speed n, 1253 rpm; misalignment, 205µm; cutting fluid flow rate, 80 l/min.

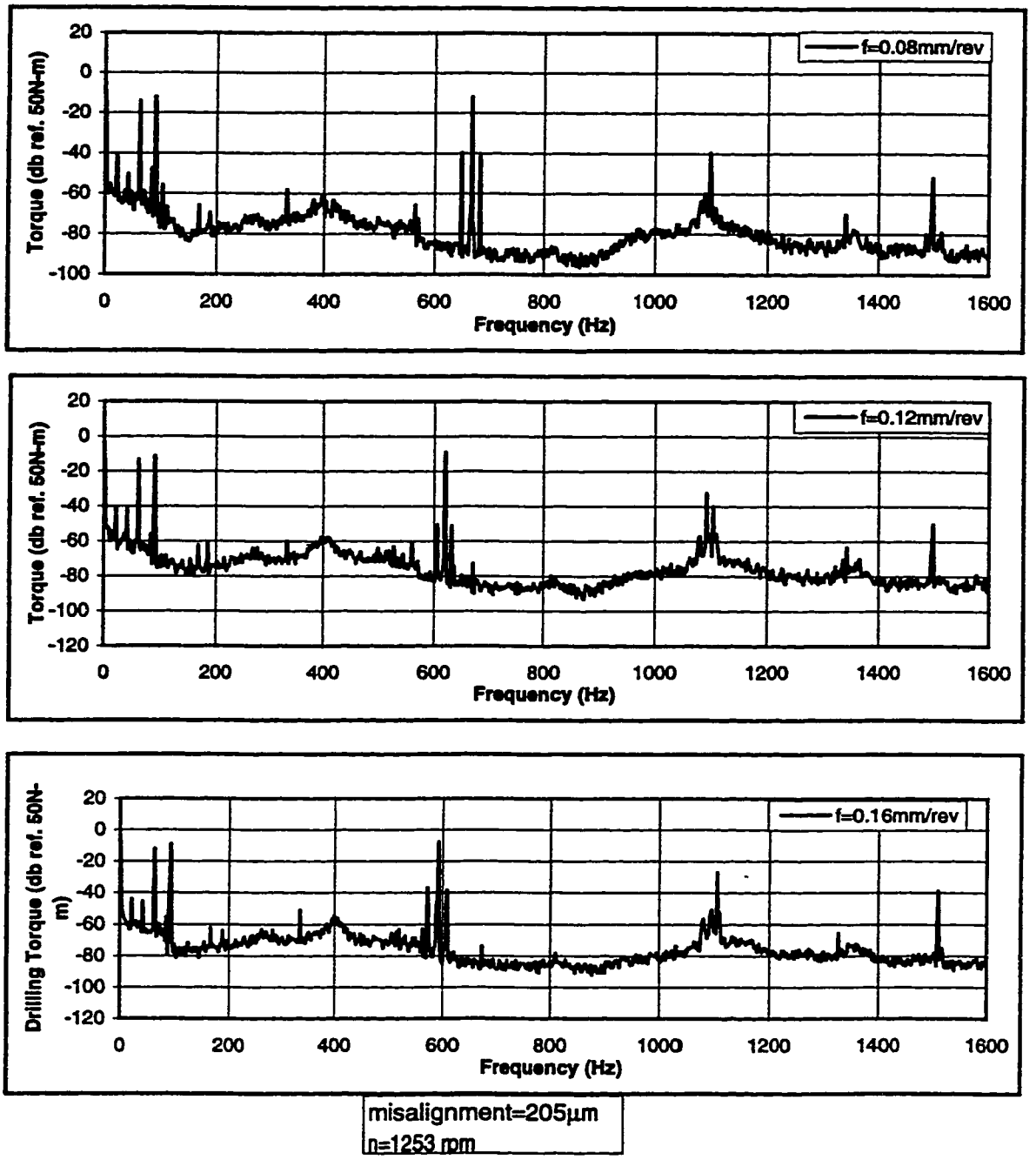

Figure 9.15: Autospectra of the cutting torque. Cutting conditions: workpiece, AISI 303; tool, BTAS 1" inch diameter ; boring bar length, 2.0 m; spindle rotational speed n, 1253 rpm; misalignment, 205µm; cutting fluid flow rate, 80 l/min.

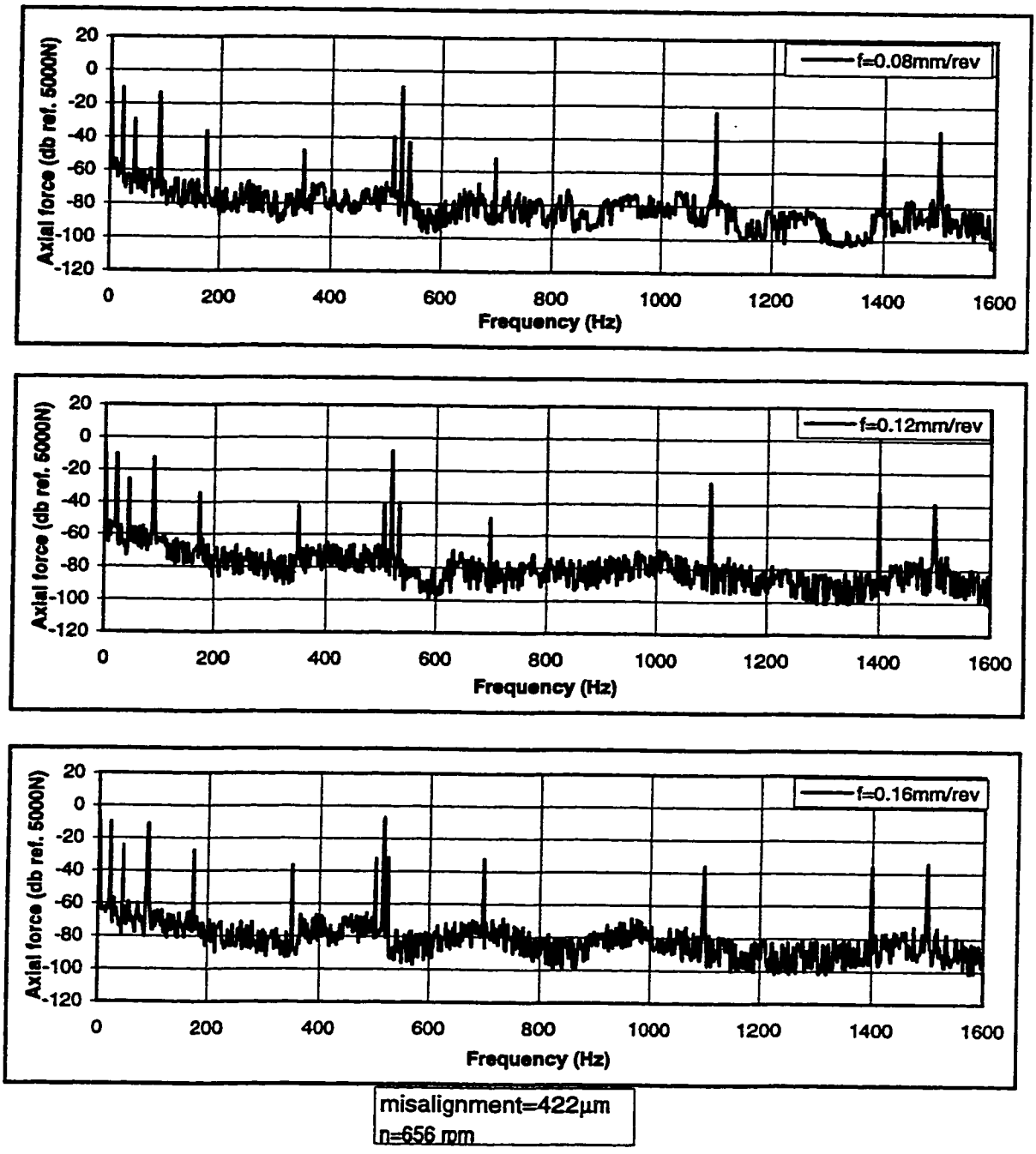

Figure 9.16: Autospectra of the axial cutting force. Cutting conditions: workpiece, AISI 303; tool, BTAS 1" inch diameter ; boring bar length, 2.0 m; spindle rotational speed n, 656 rpm; misalignment, 422µm; cutting fluid flow rate, 80 l/min.

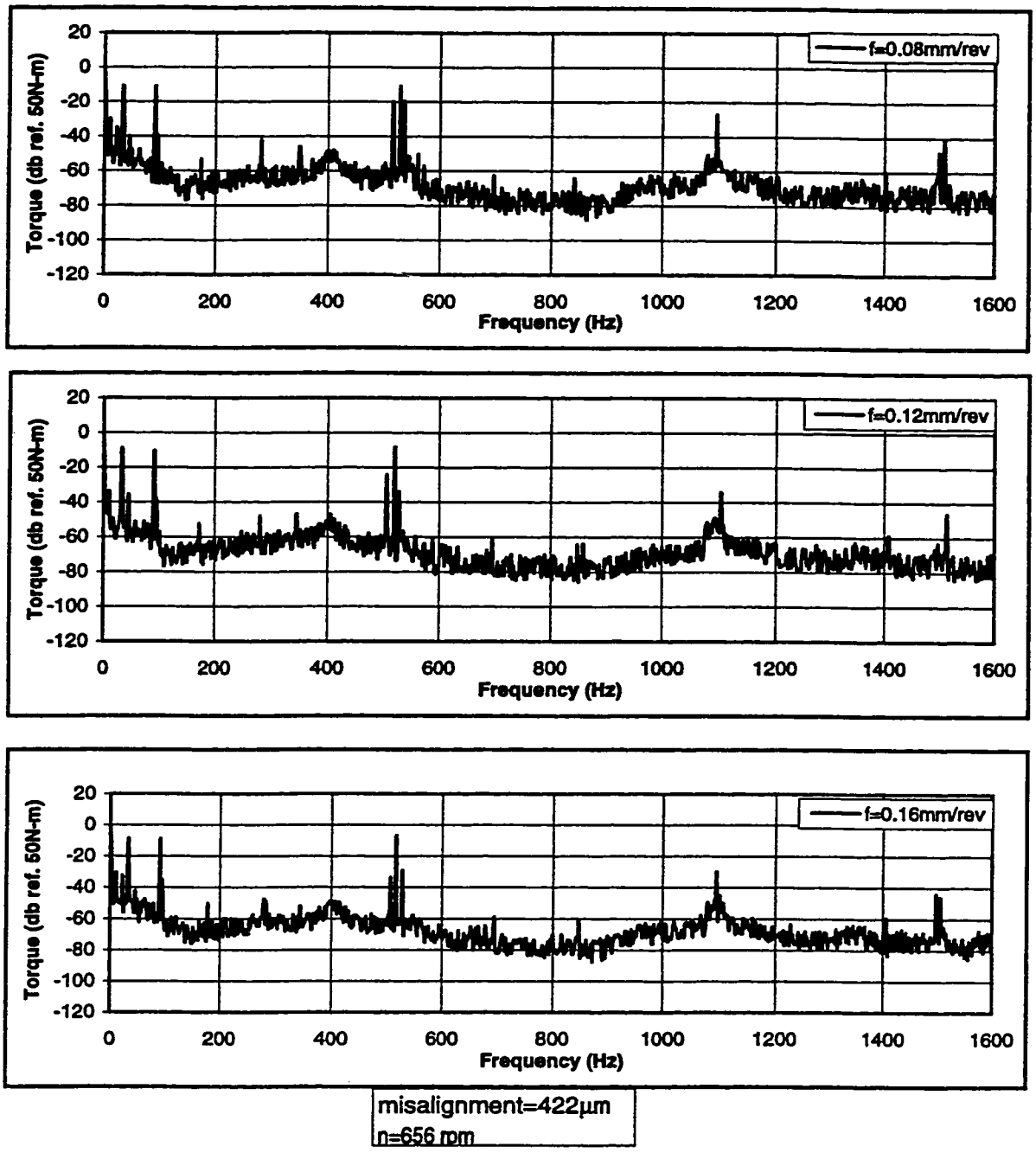

Figure 9.17: Autospectra of the cutting torque. Cutting conditions: workpiece, AISI 303; tool, BTAS 1" inch diameter ; boring bar length, 2.0 m; spindle rotational speed n, 656 rpm; misalignment, 422µm; cutting fluid flow rate, 80 l/min.

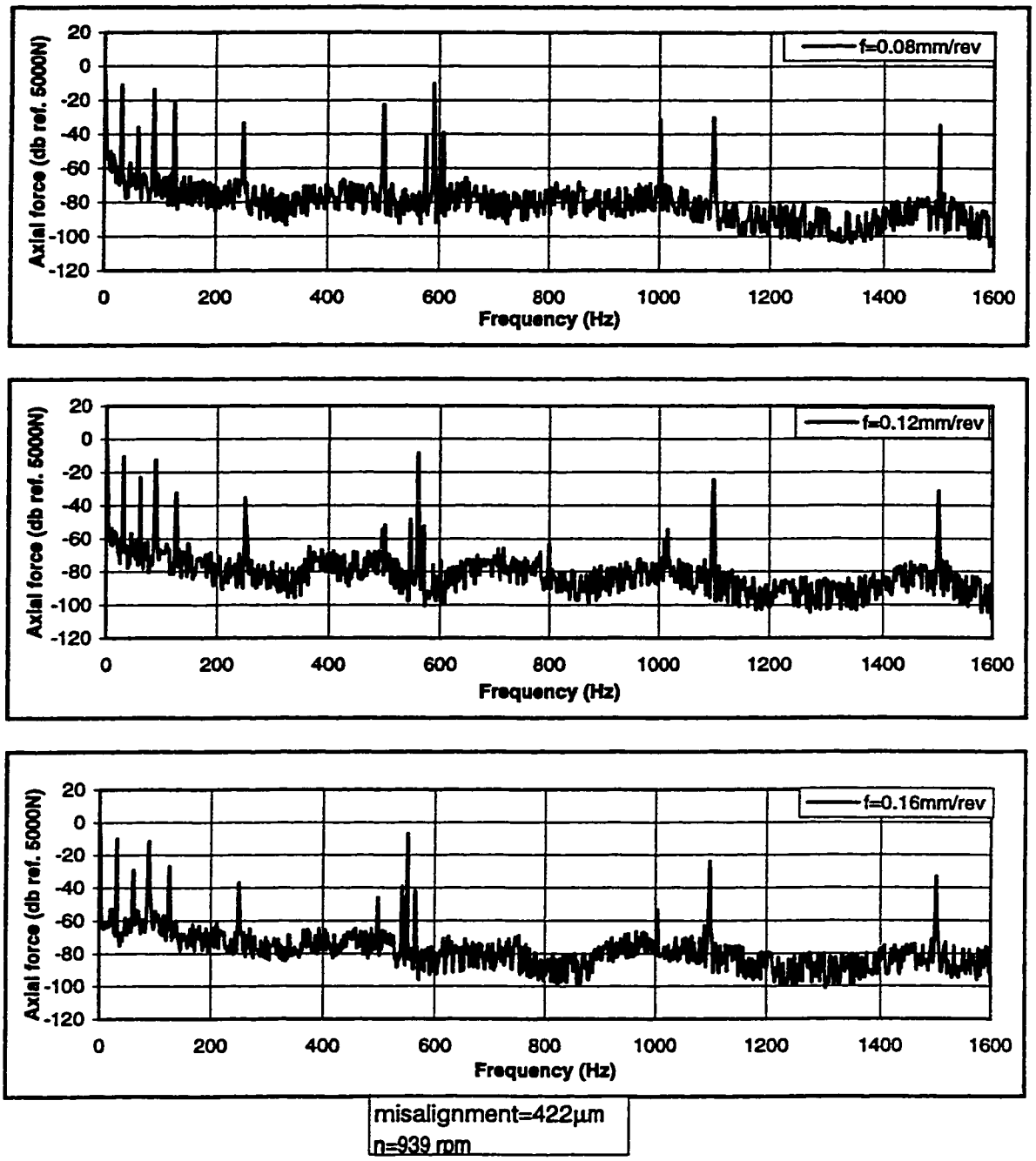

Figure 9.18: Autospectra of the axial cutting force. Cutting conditions: workpiece, AISI 303; tool, BTAS 1" inch diameter ; boring bar length, 2.0 m; spindle rotational speed n, 939 rpm; misalignment, 422µm; cutting fluid flow rate, 80 l/min.

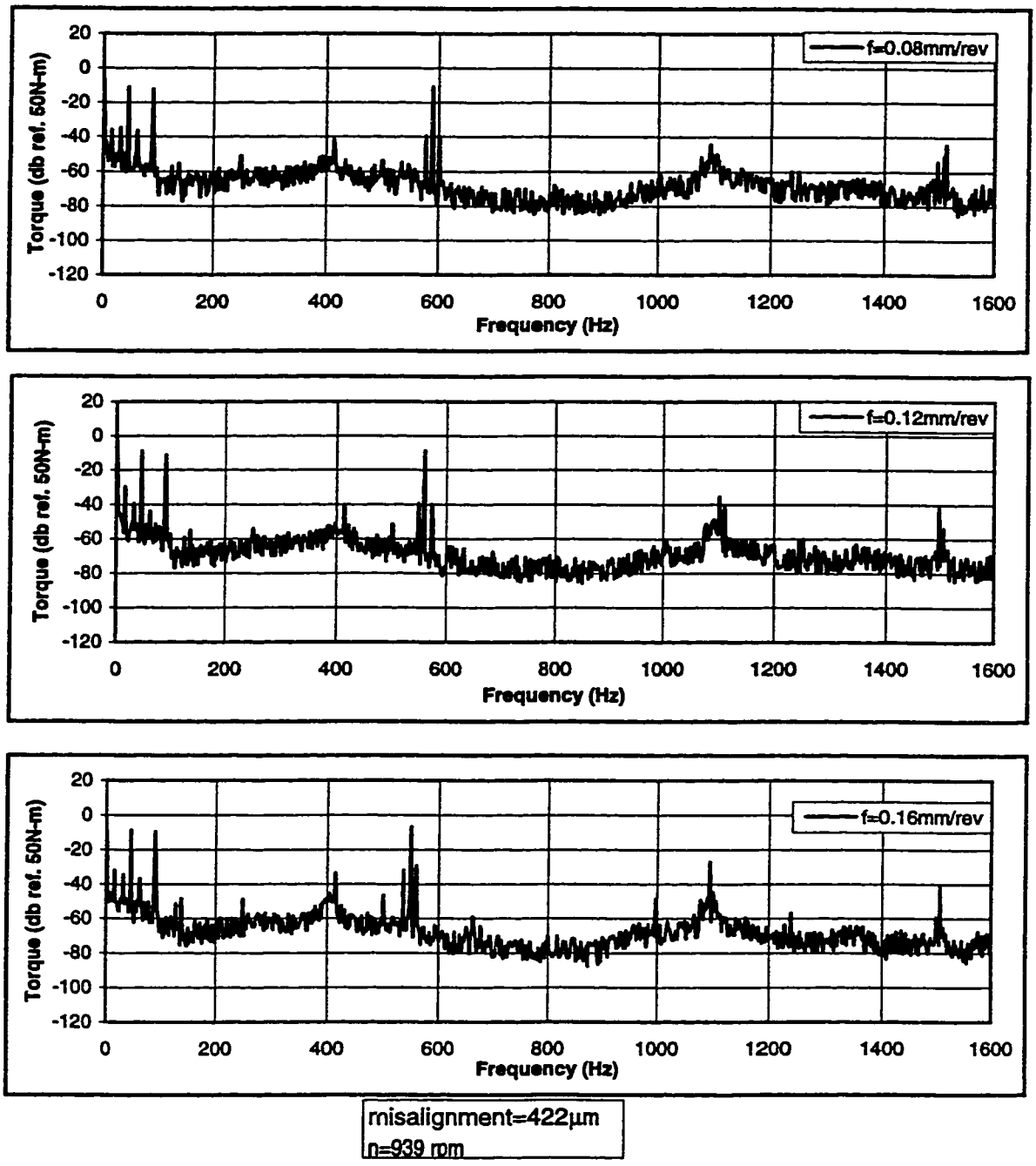

Figure 9.19: Autospectra of the cutting torque. Cutting conditions: workpiece, AISI 303; tool, BTAS 1" inch diameter ; boring bar length, 2.0 m; spindle rotational speed n, 939 rpm; misalignment, 422µm; cutting fluid flow rate, 80 l/min.

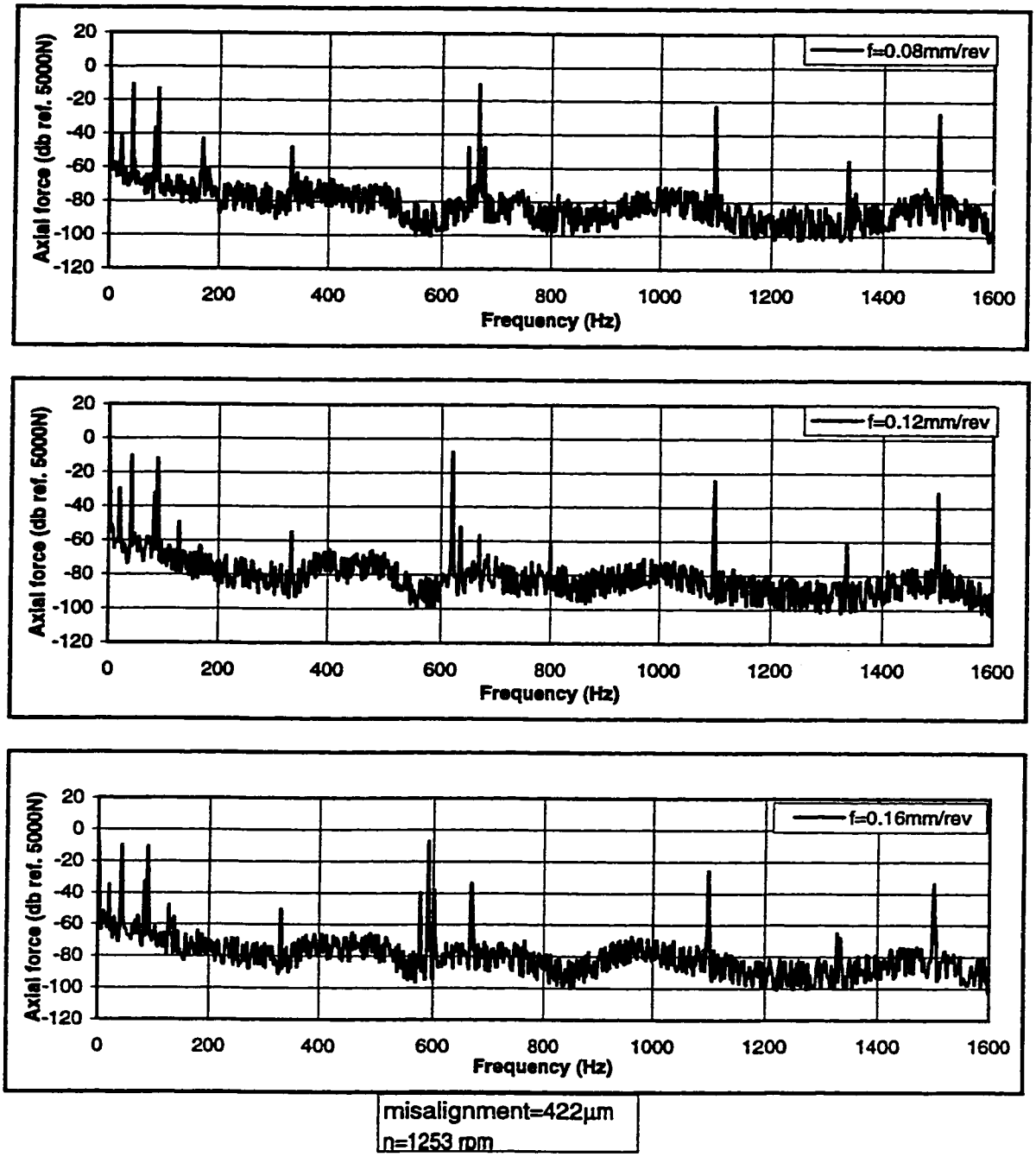

Figure 9.20: Autospectra of the axial cutting force. Cutting conditions: workpiece, AISI 303; tool, BTAS 1" inch diameter ; boring bar length, 2.0 m; spindle rotational speed n, 1253 rpm; misalignment, 422µm; cutting fluid flow rate, 80 l/min.

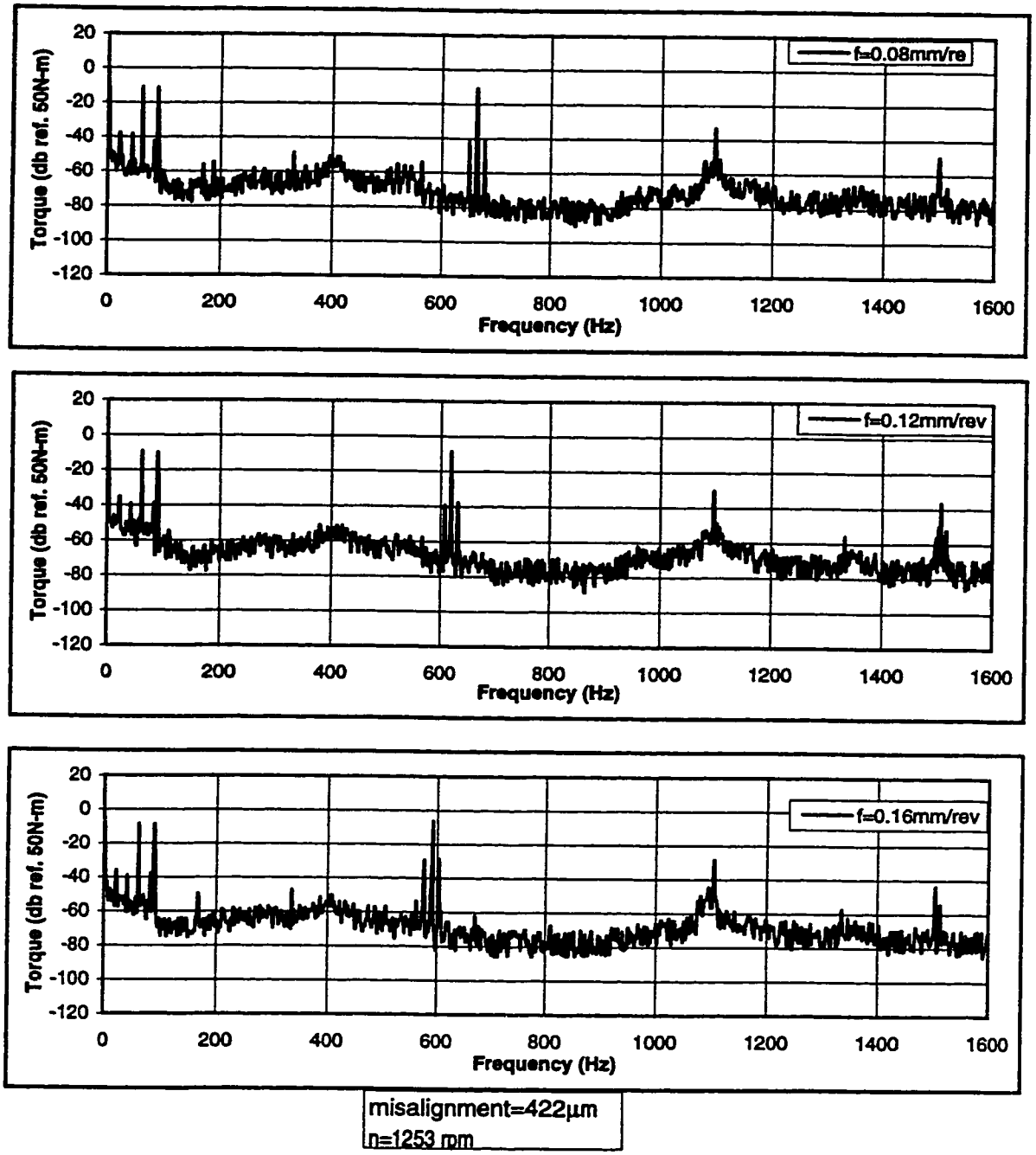

Figure 9.21: Autospectra of the cutting torque. Cutting conditions: workpiece, AISI 303; tool, BTAS 1" inch diameter ; boring bar length, 2.0 m; spindle rotational speed n, 1253 rpm; misalignment, 422µm; cutting fluid flow rate, 80 l/min.

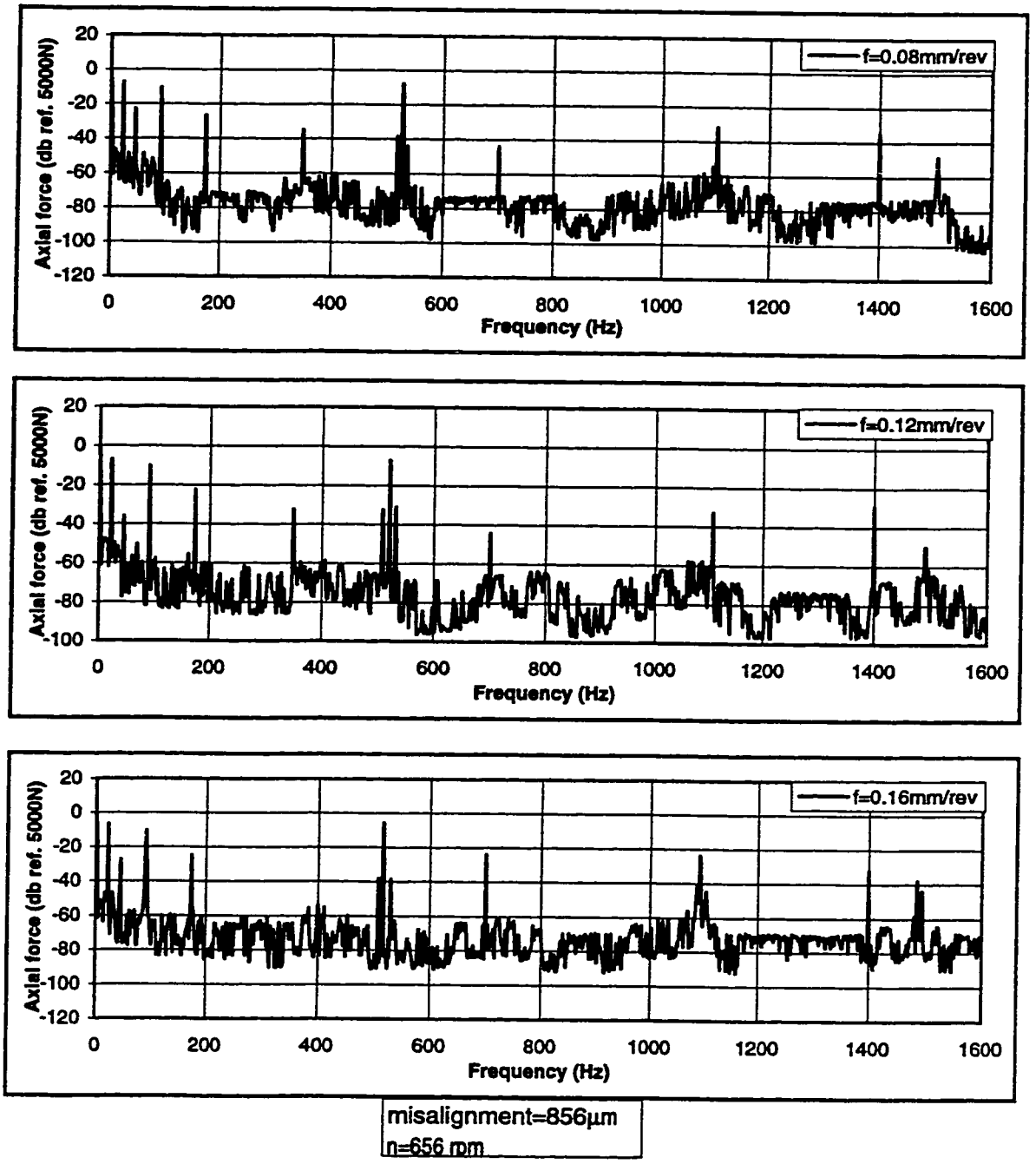

Figure 9.22: Autospectra of the axial cutting force. Cutting conditions: workpiece, AISI 303; tool, BTAS 1" inch diameter ; boring bar length, 2.0 m; spindle rotational speed n, 656 rpm; misalignment, 856µm; cutting fluid flow rate, 80 l/min.

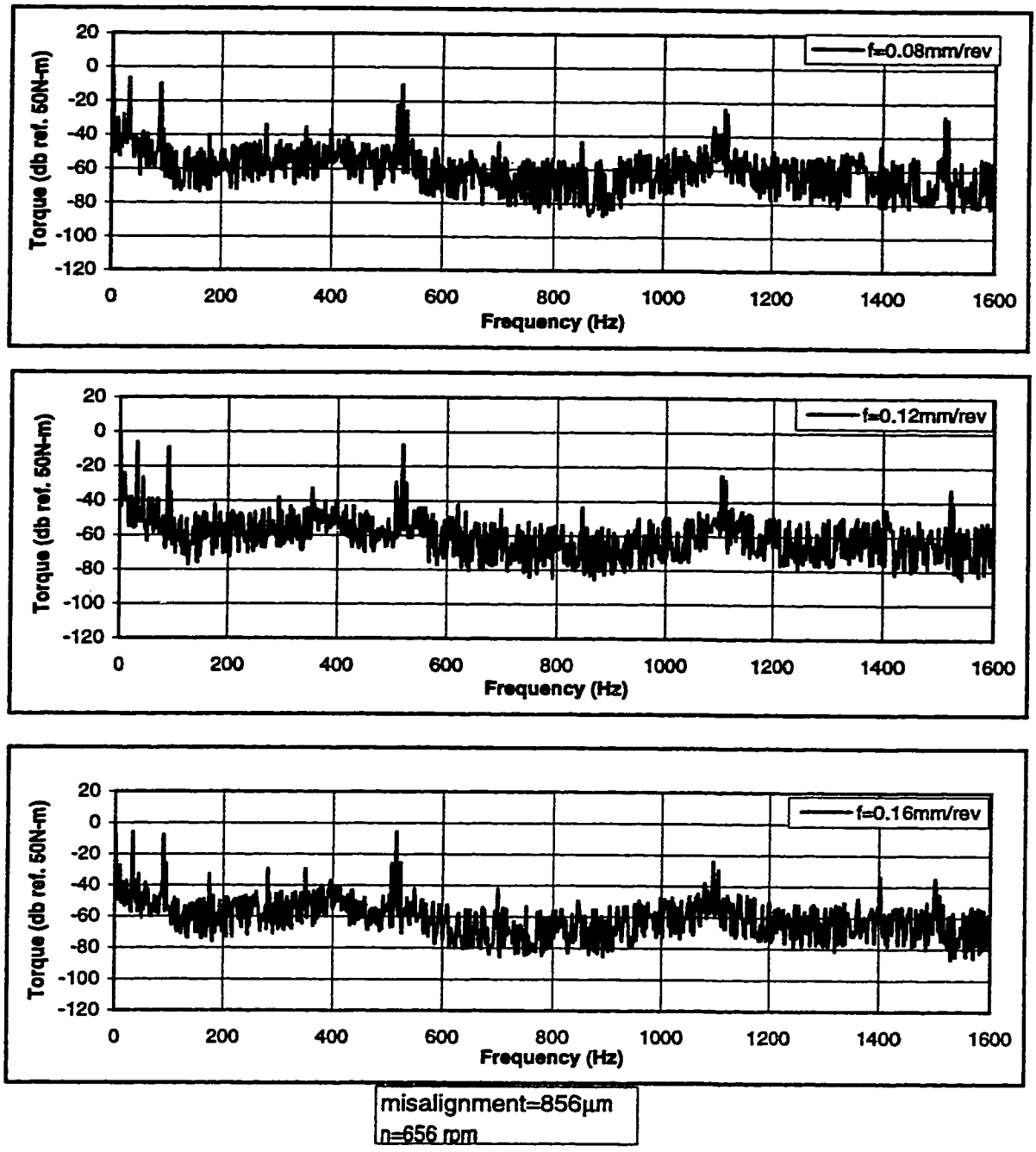

Figure 9.23: Autospectra of the cutting torque. Cutting conditions: workpiece, AISI 303; tool, BTAS 1" inch diameter ; boring bar length, 2.0 m; spindle rotational speed n, 656 rpm; misalignment, 856µm; cutting fluid flow rate, 80 l/min.

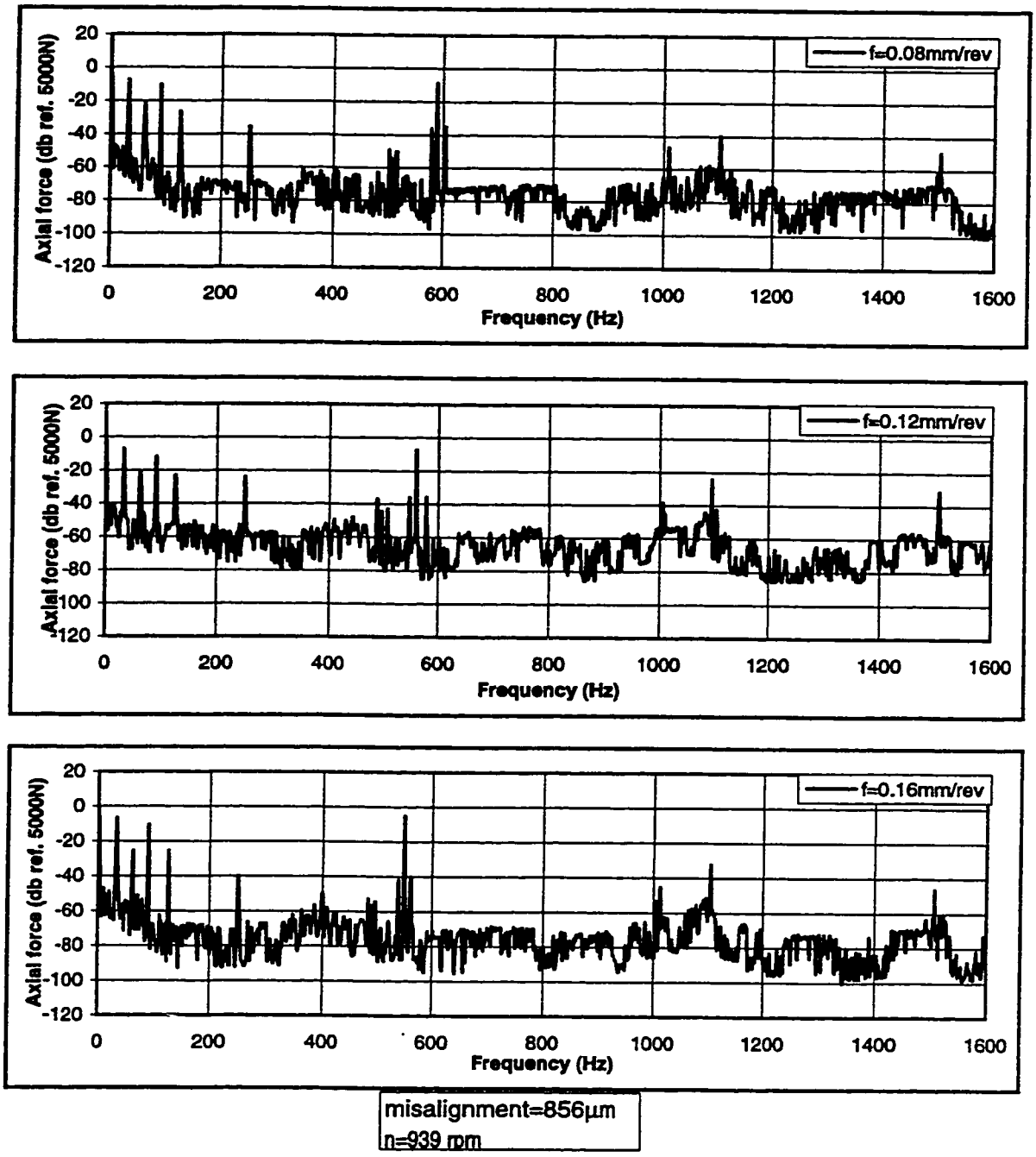

Figure 9.24: Autospectra of the axial cutting force. Cutting conditions: workpiece, AISI 303; tool, BTAS 1" inch diameter ; boring bar length, 2.0 m; spindle rotational speed n, 939 rpm; misalignment, 856µm; cutting fluid flow rate, 80 l/min.

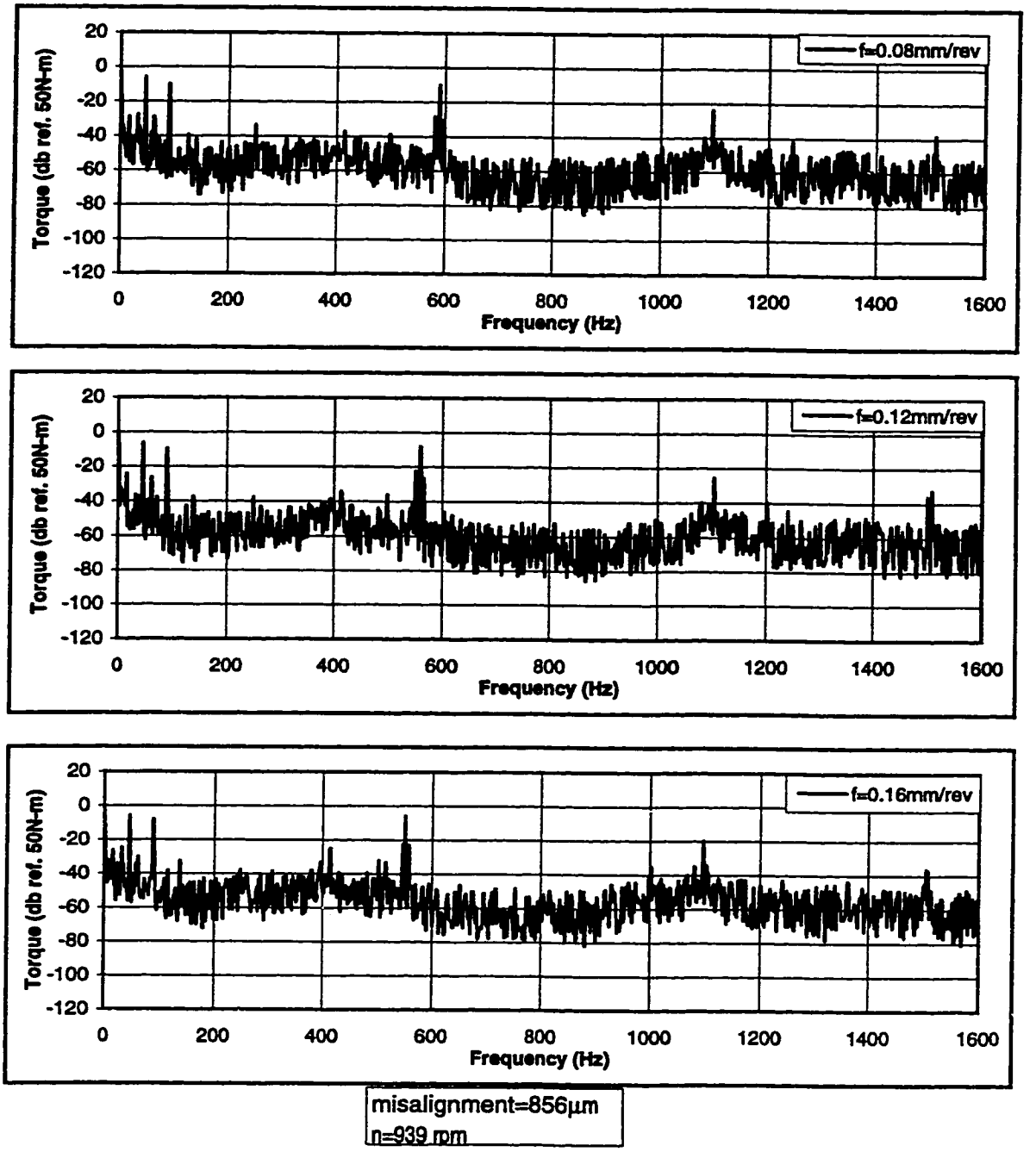

Figure 9.25: Autospectra of the cutting torque. Cutting conditions: workpiece, AISI 303; tool, BTAS 1" inch diameter ; boring bar length, 2.0 m; spindle rotational speed n, 939 rpm; misalignment, 856µm; cutting fluid flow rate, 80 l/min.

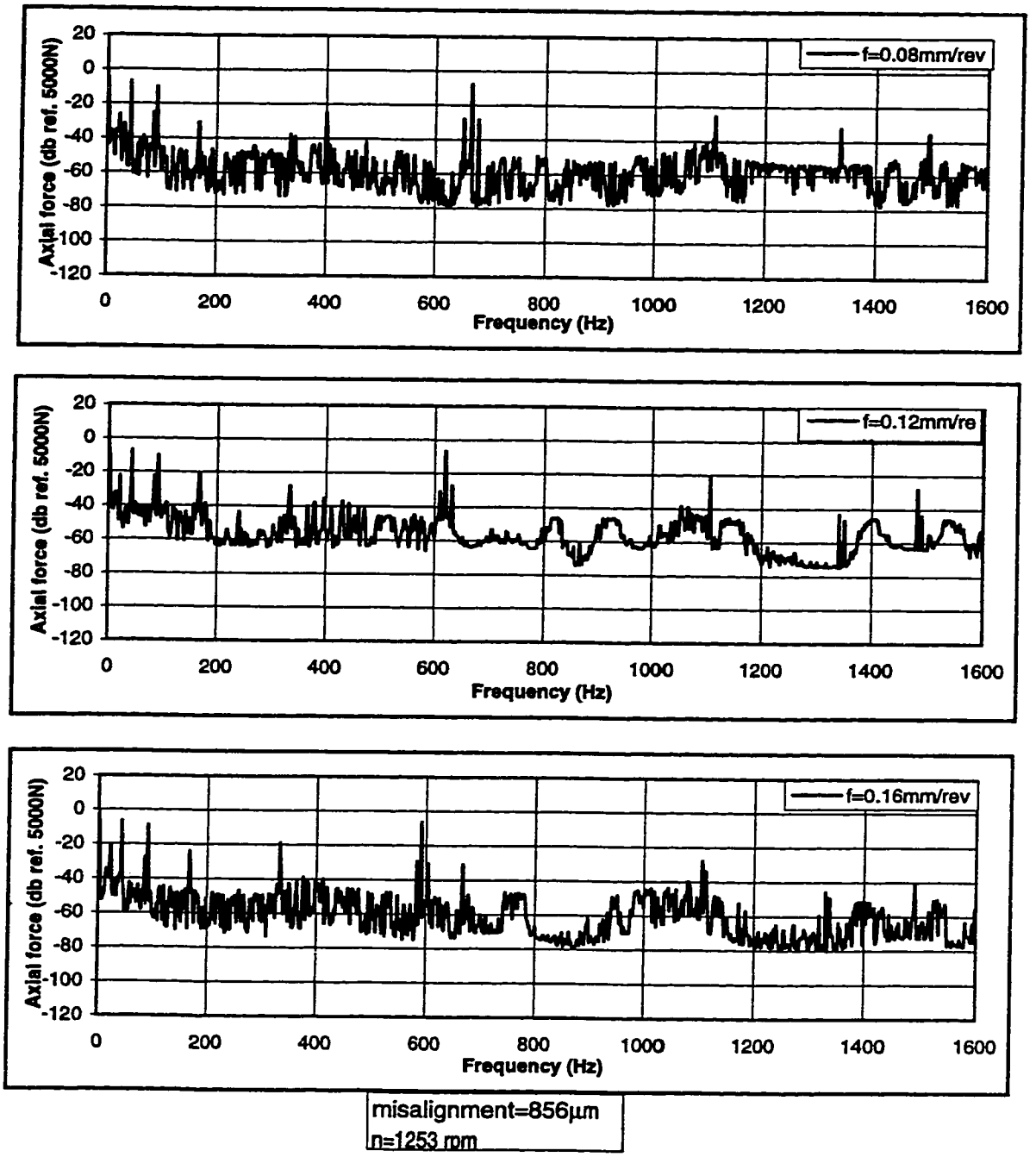

Figure 9.26: Autospectra of the axial cutting force. Cutting conditions: workpiece, AISI 303; tool, BTAS 1" inch diameter ; boring bar length, 2.0 m; spindle rotational speed n, 1253 rpm; misalignment, 856µm; cutting fluid flow rate, 80 l/min.

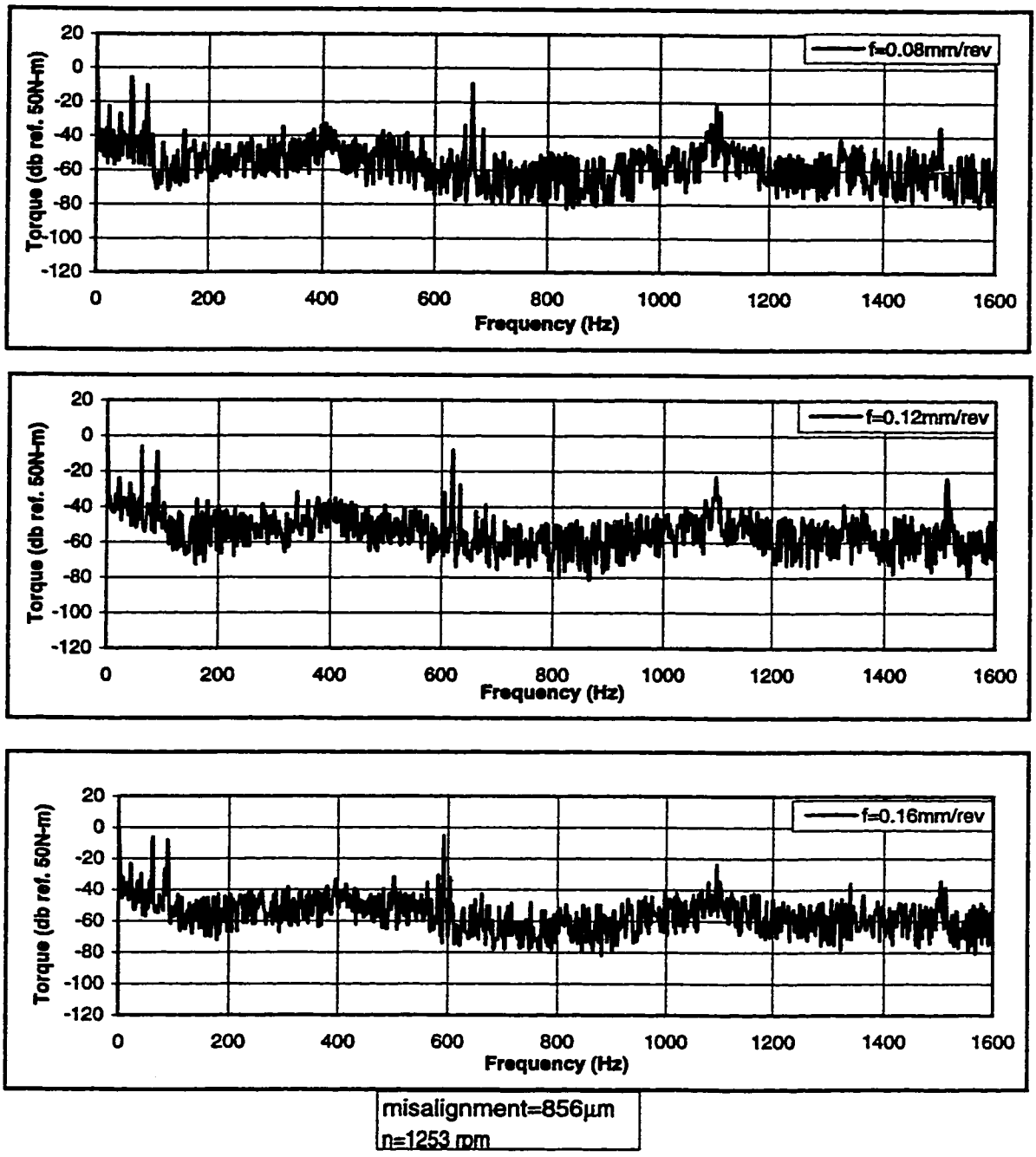

Figure 9.27. Autospectra of the cutting torque. Cutting conditions: workpiece, AISI 303; tool, BTAS 1" inch diameter ; boring bar length, 2.0 m; spindle rotational speed n, 1253 rpm; misalignment, 856µm; cutting fluid flow rate, 80 l/min.

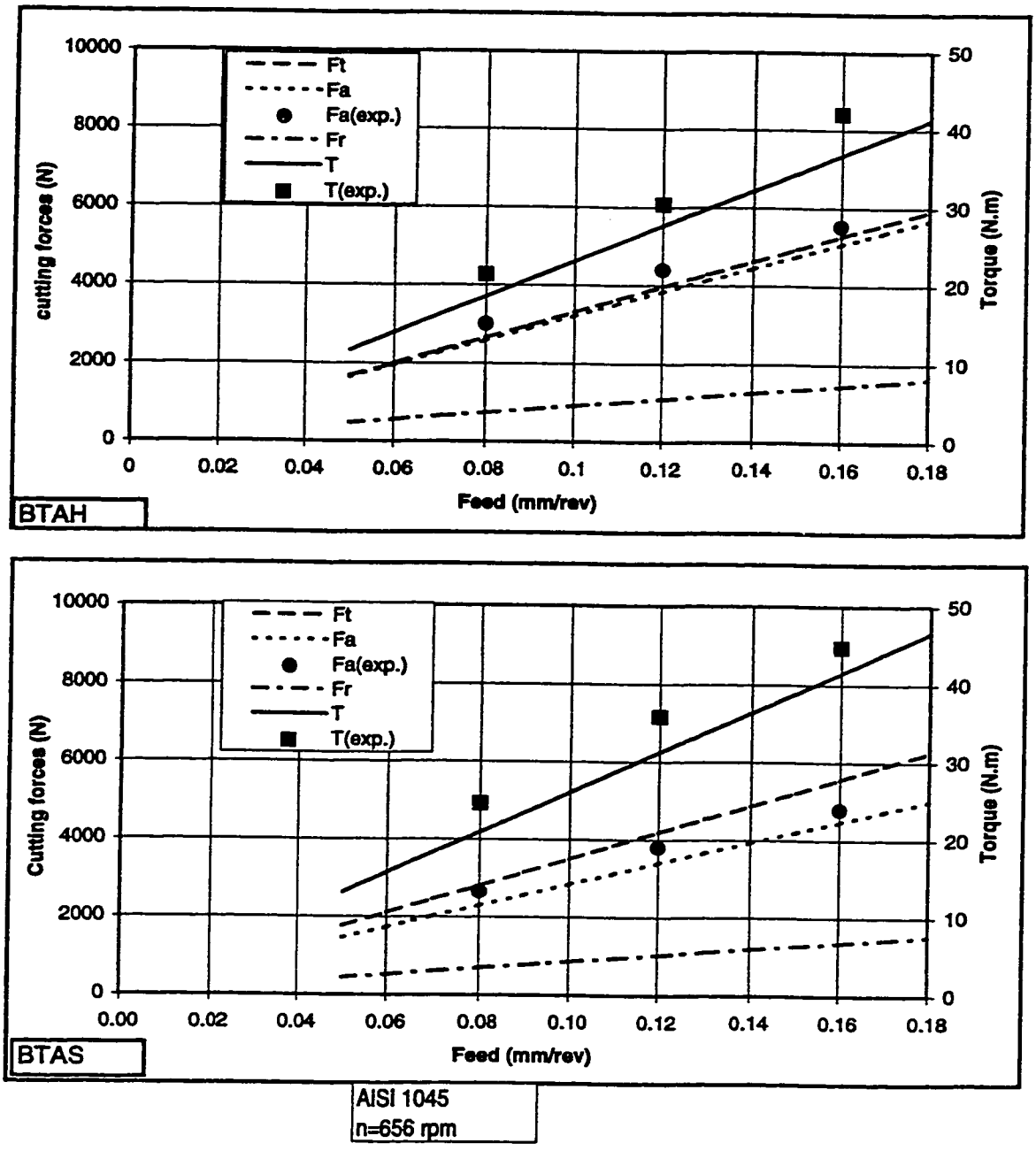

Figure 9.28: Steady-state cutting forces and torque components. Cutting conditions: workpiece, AISI 1045; tools, BTAH and BTAS 1" inch diameter ; boring bar length, 2.0 m; spindle rotational speed n, 656 rpm; misalignment, 15μm; cutting fluid flow rate, 80 l/min.

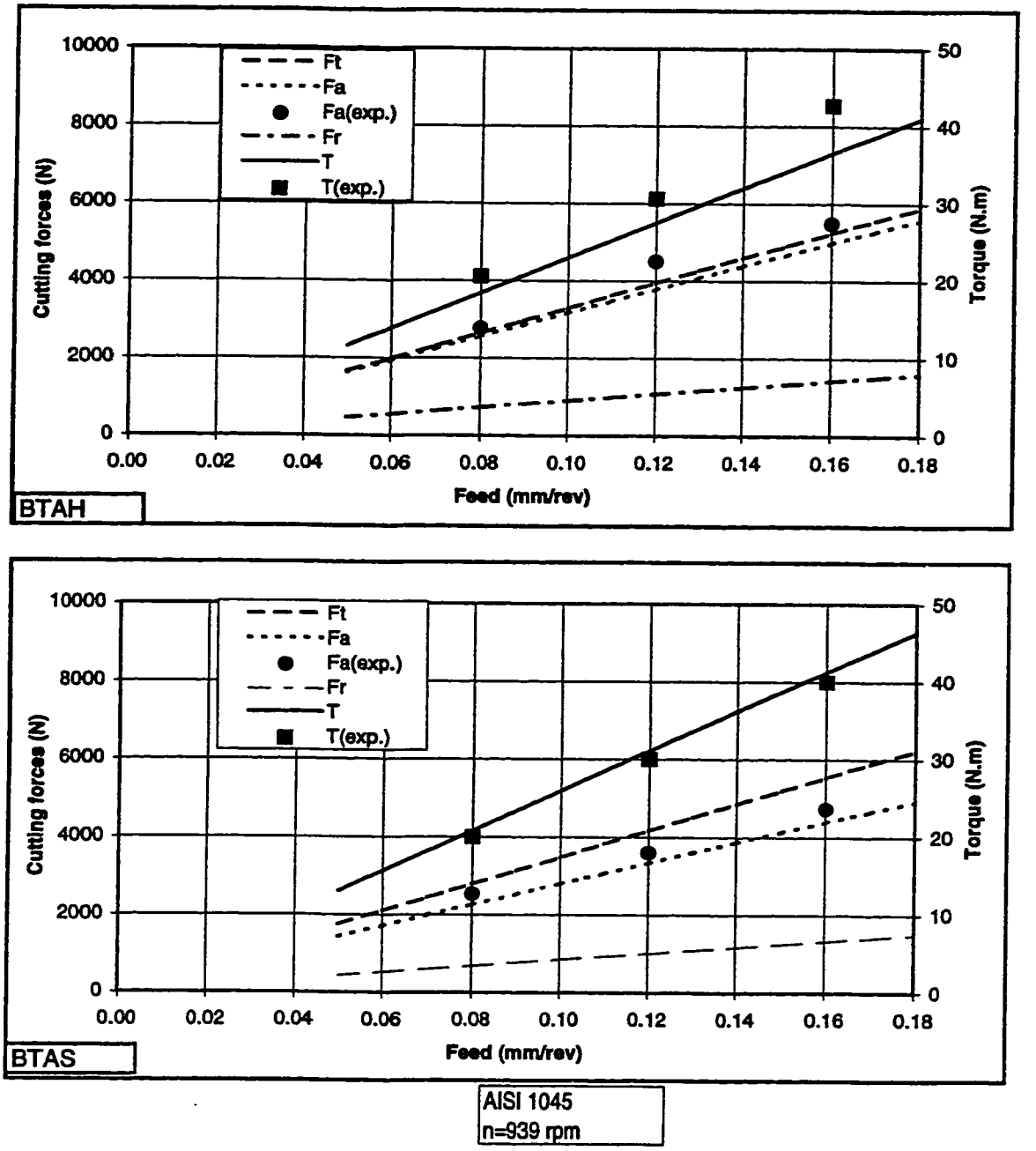

Figure 9.29: Steady-state cutting forces and torque components. Cutting conditions: workpiece, AISI 1045; tools, BTAH and BTAS 1" inch diameter ; boring bar length, 2.0 m; spindle rotational speed n, 939 rpm; misalignment, 15µm; cutting fluid flow rate, 80 l/min.

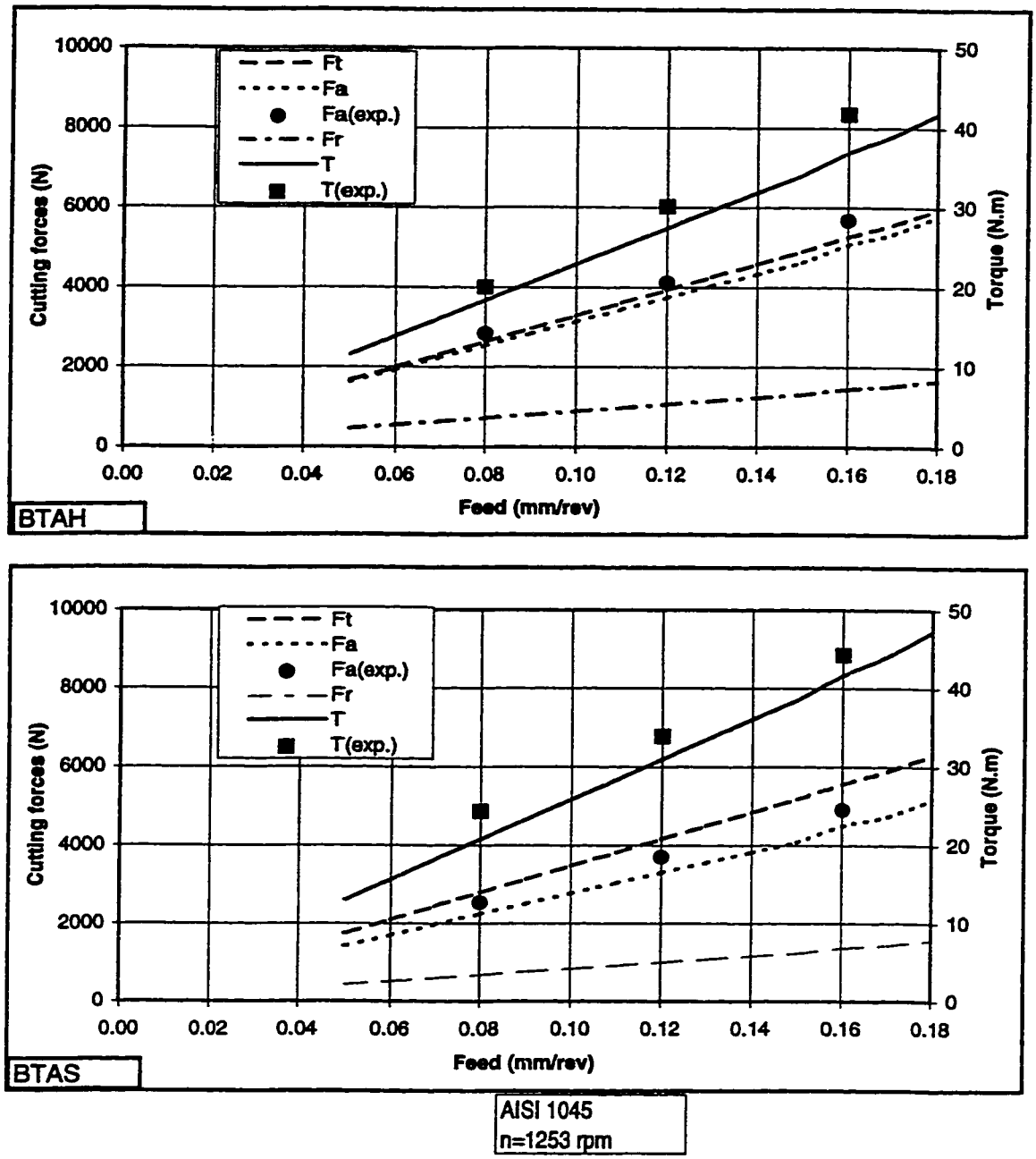

Figure 9.30: Steady-state cutting forces and torque components. Cutting conditions: workpiece, AISI 1045; tools, BTAH and BTAS 1" inch diameter ; boring bar length, 2.0 m; spindle rotational speed n, 1253 rpm; misalignment, 15µm; cutting fluid flow rate, 80 l/min.

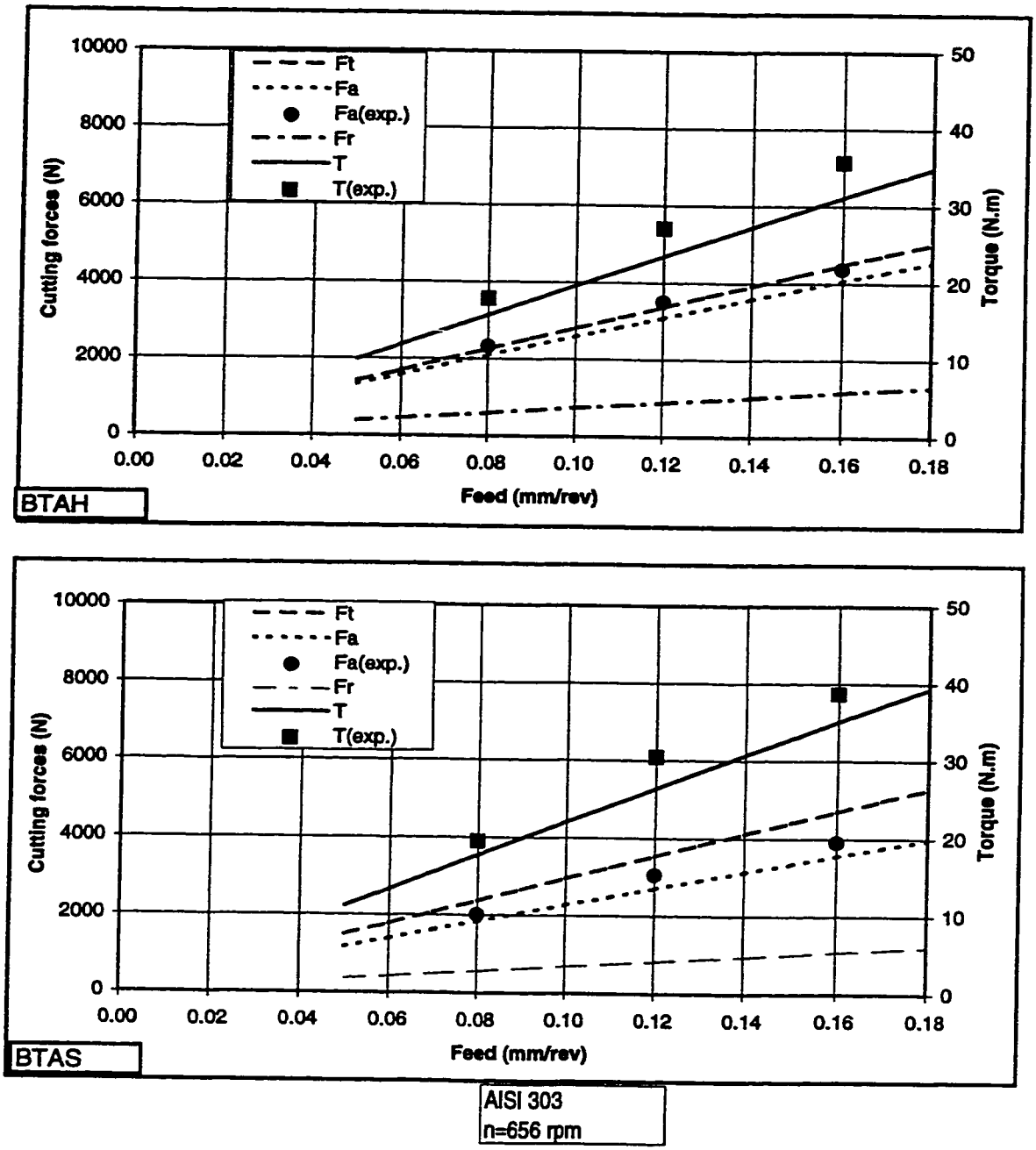

Figure 9.31: Steady-state cutting forces and torque components. Cutting conditions: workpiece, AISI 303; tool, BTAH nd BTAS 1" inch diameter ; boring bar length, 2.0 m; spindle rotational speed n, 656 rpm; misalignment, 15μm; cutting fluid flow rate, 80 l/min.

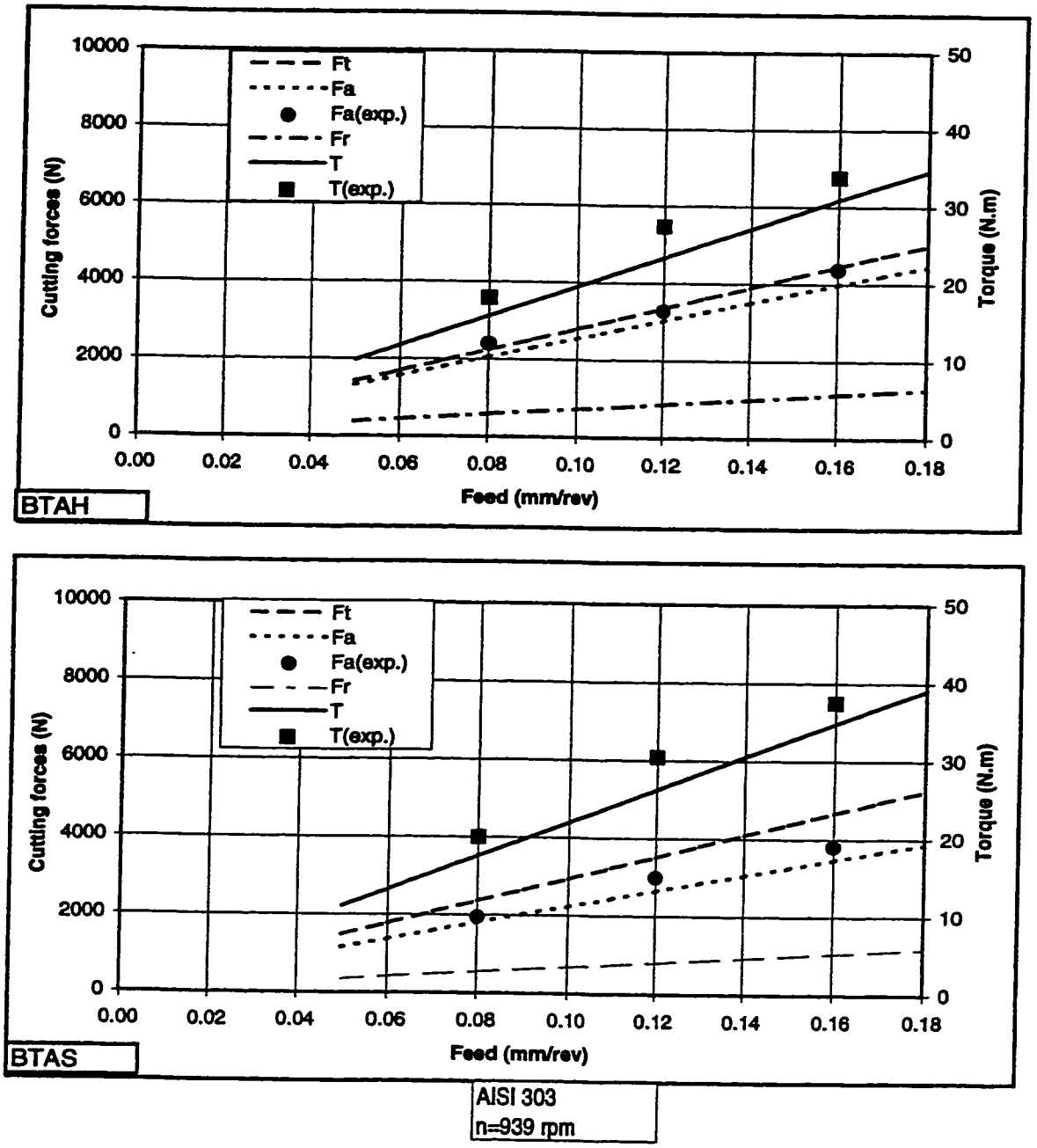

Figure 9.32: Steady-state cutting forces and torque components. Cutting conditions: workpiece, AISI 303; tools, BTAH and BTAS 1" inch diameter ; boring bar length, 2.0 m; spindle rotational speed n, 939 rpm; misalignment, 15μm; cutting fluid flow rate, 80 l/min.

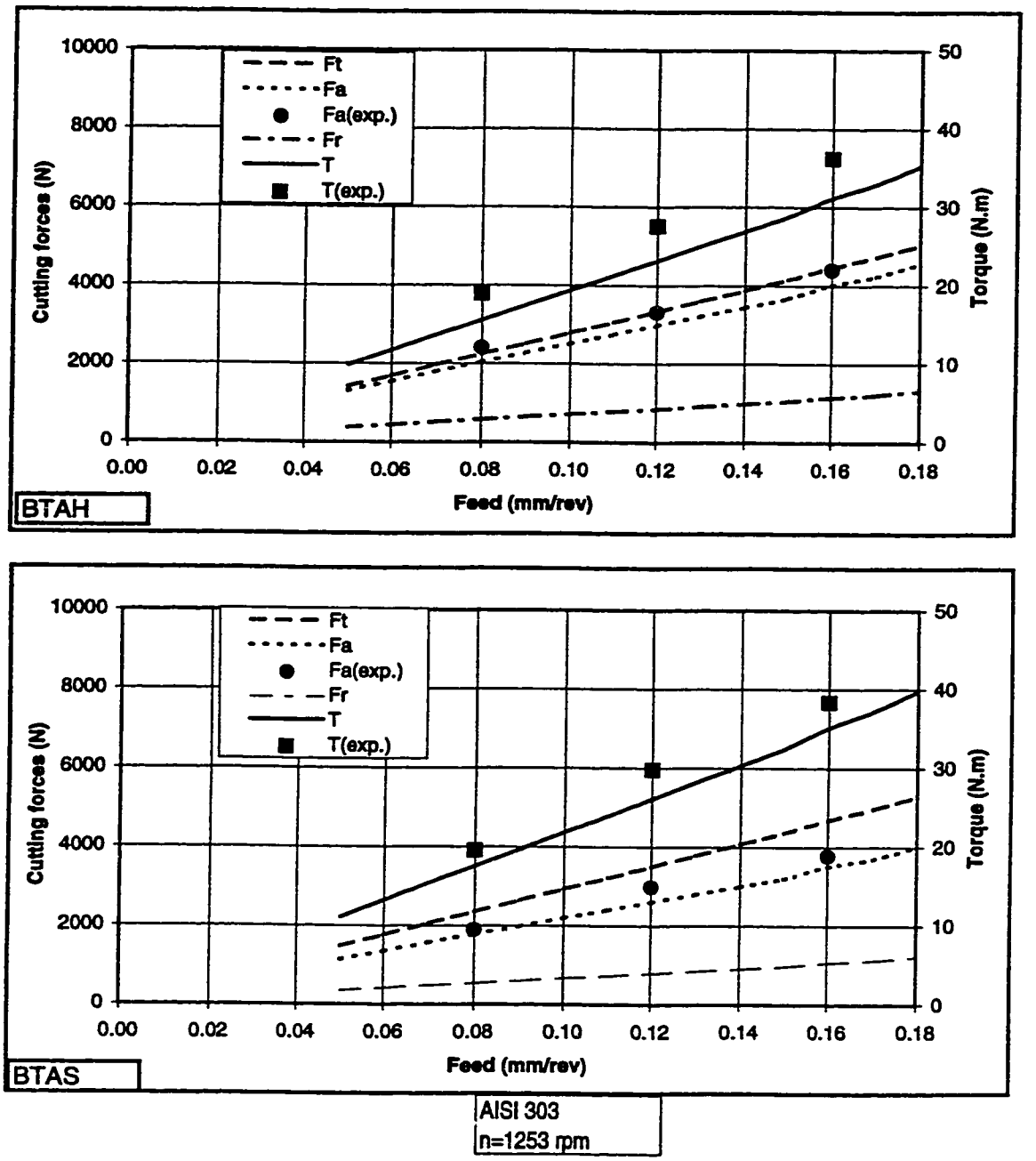

Figure 9.33: Steady-state cutting forces and torque components. Cutting conditions: workpiece, AISI 303; tool, BTAH and BTAS 1" inch diameter ; boring bar length, 2.0 m; spindle rotational speed n, 1253 rpm; misalignment, 15μm; cutting fluid flow rate, 80 l/min.

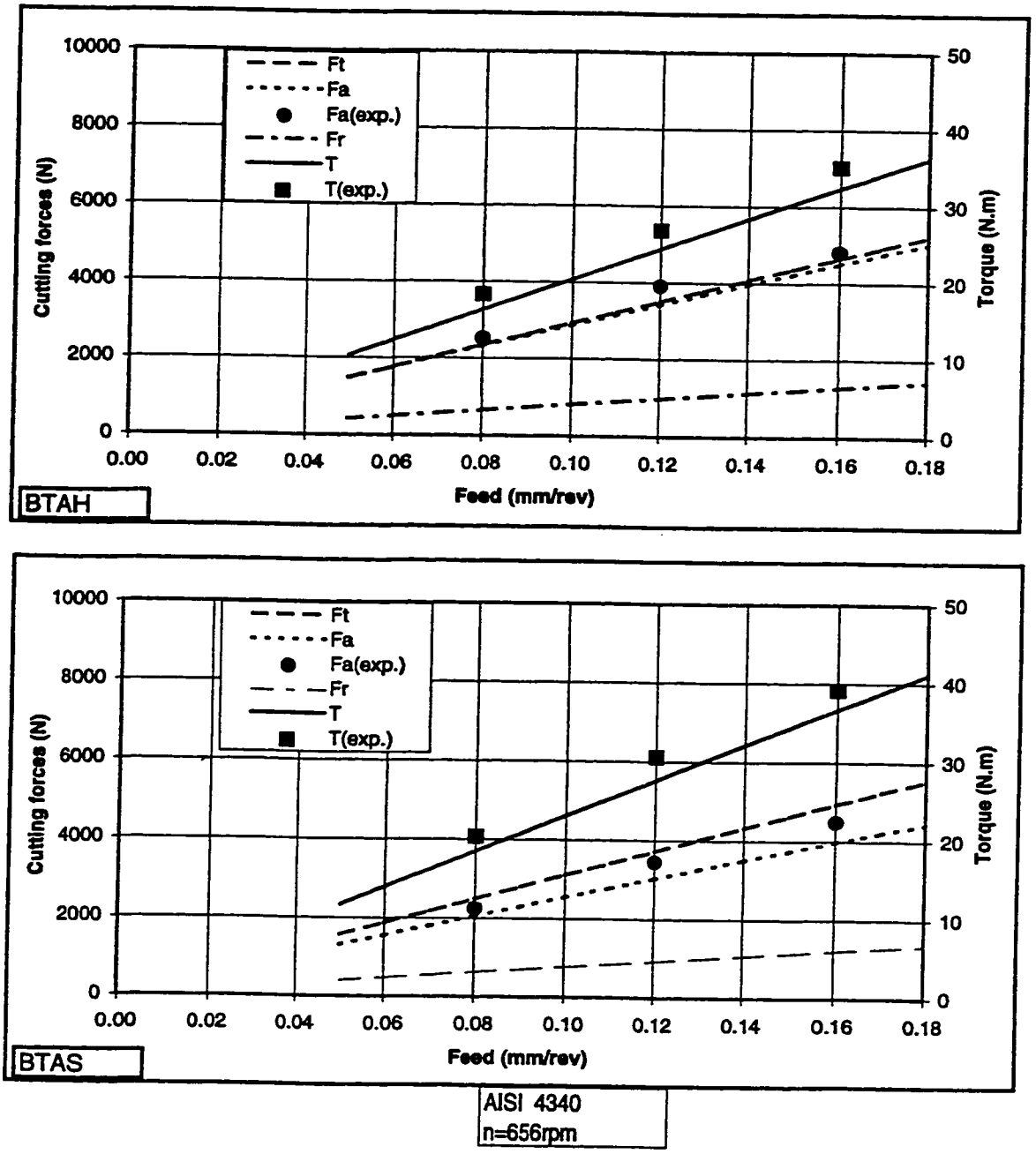

Figure 9.34: Steady-state cutting forces and torque components. Cutting conditions: workpiece, AISI 4340; tools, BTAH and BTAS 1" inch diameter ; boring bar length, 2.0 m; spindle rotational speed n, 656 rpm; misalignment, 15µm; cutting fluid flow rate, 80 l/min.

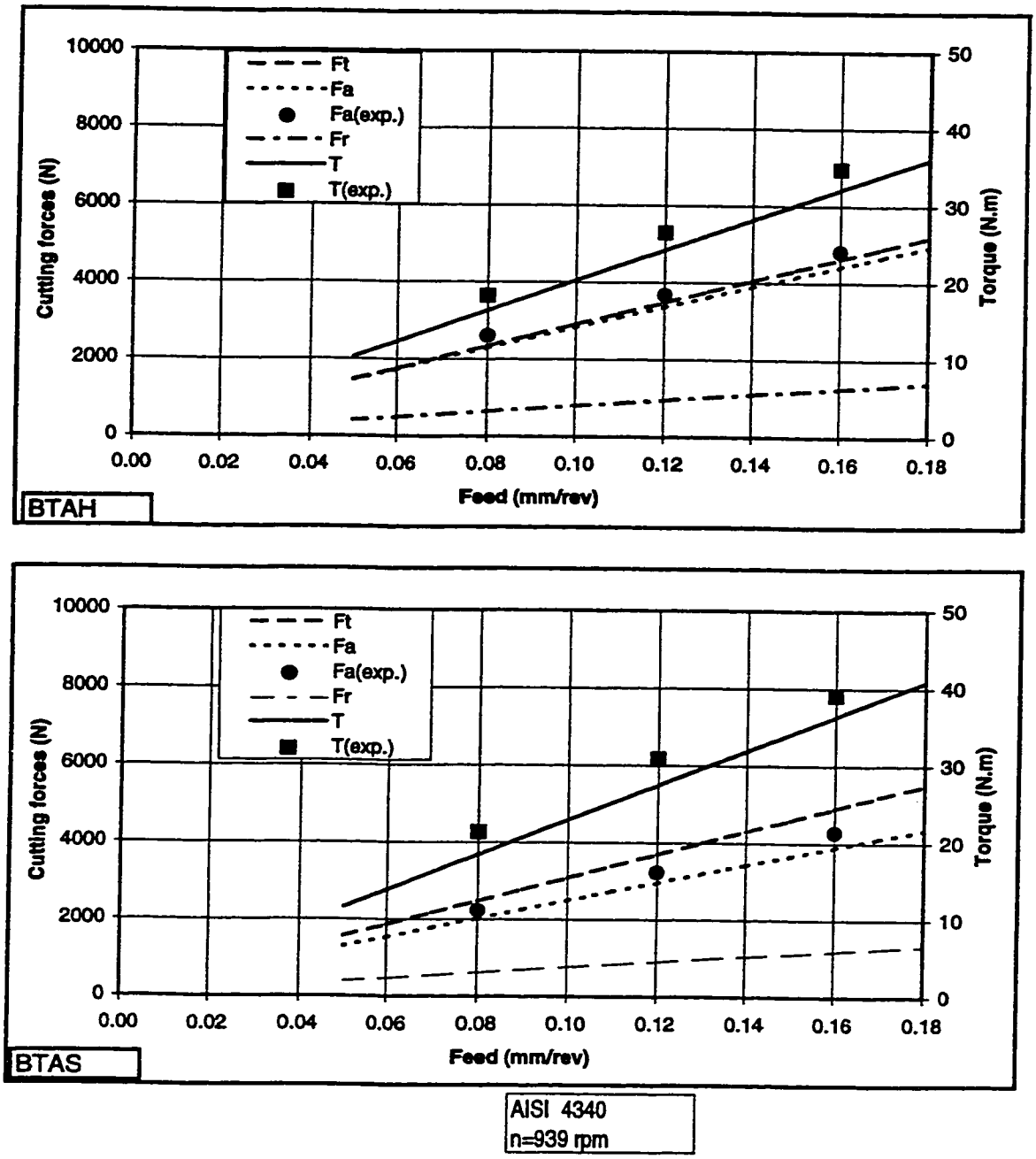

Figure 9.35: Steady-state cutting forces and torque components. Cutting conditions: workpiece, AISI 4340; tools, BTAH BTAS 1" inch diameter ; boring bar length, 2.0 m; spindle rotational speed n, 939 rpm; misalignment, 15µm; cutting fluid flow, 80 l/min.

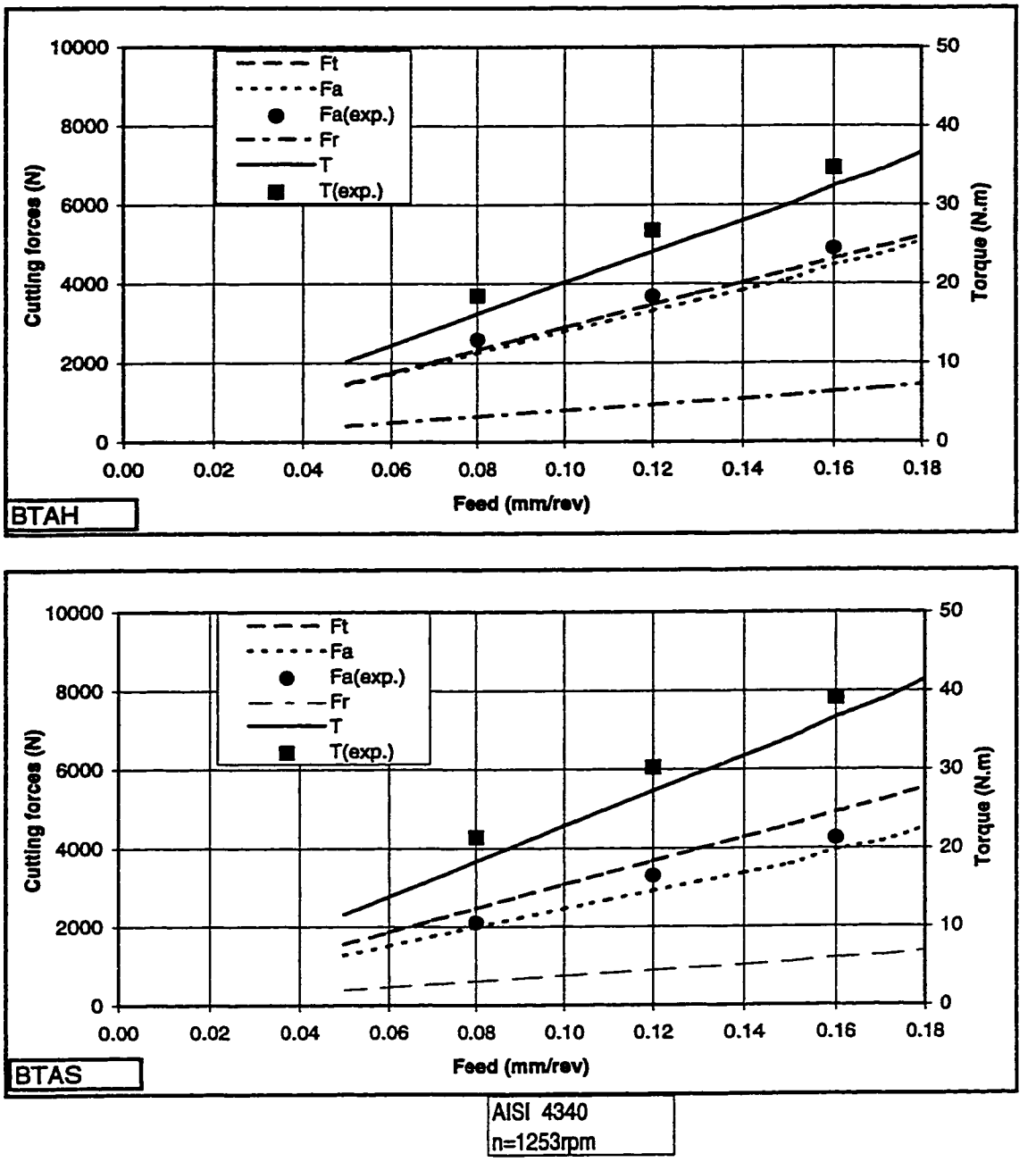

Figure 9.36: Steady-state cutting forces and torque components. Cutting conditions: workpiece, AISI 4340; tool, BTAH and BTAS esign 1" inch diameter ; boring bar length, 2.0 m; spindle rotational speed n, 1253 rpm; misalignment, 15µm; cutting fluid flow rate, 80 l/min.

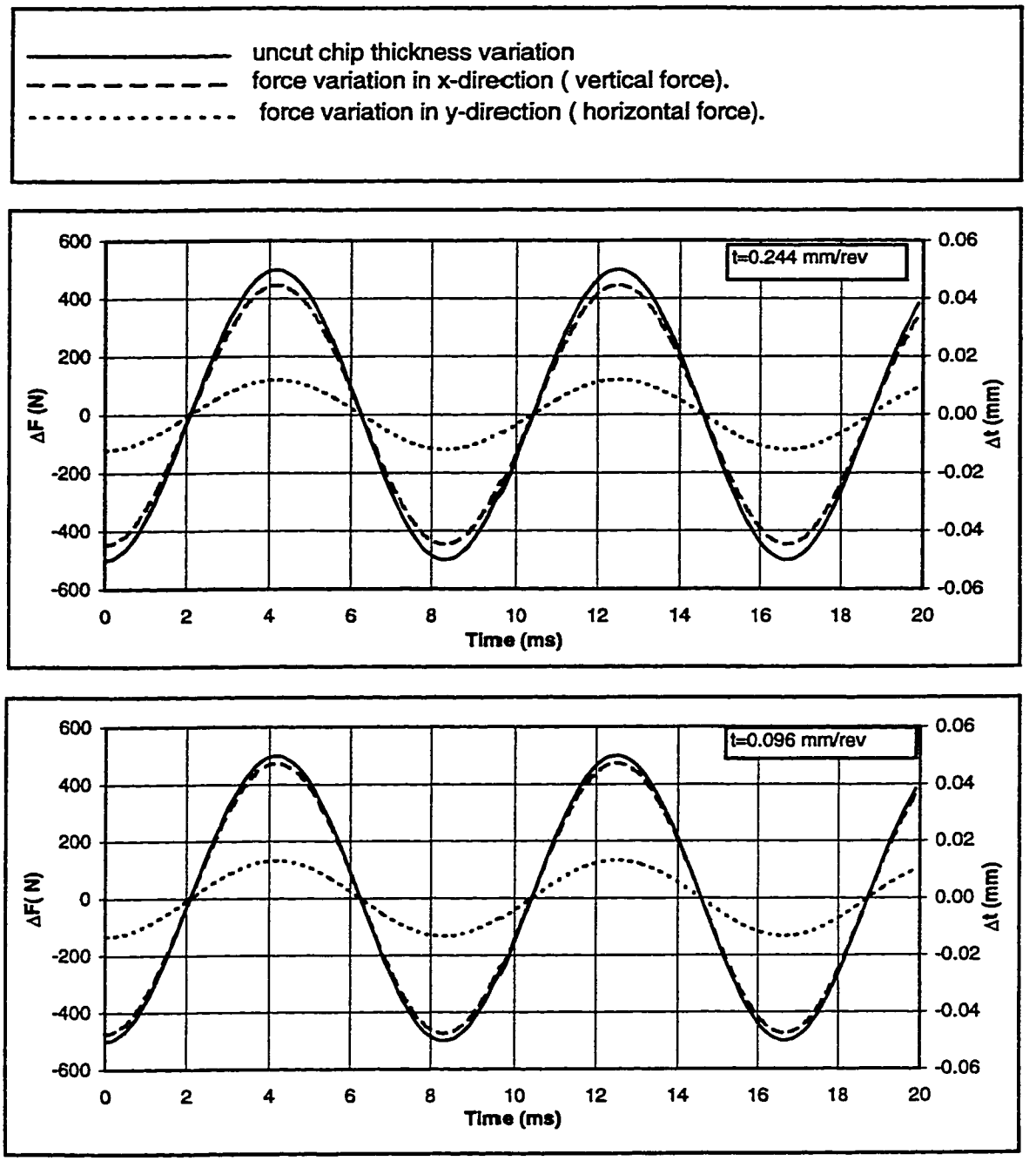

Figure 9.37: Simulation results (series 1) : v=140 m/min, α=5 deg., frequency=120 Hz, b=3.5 mm.

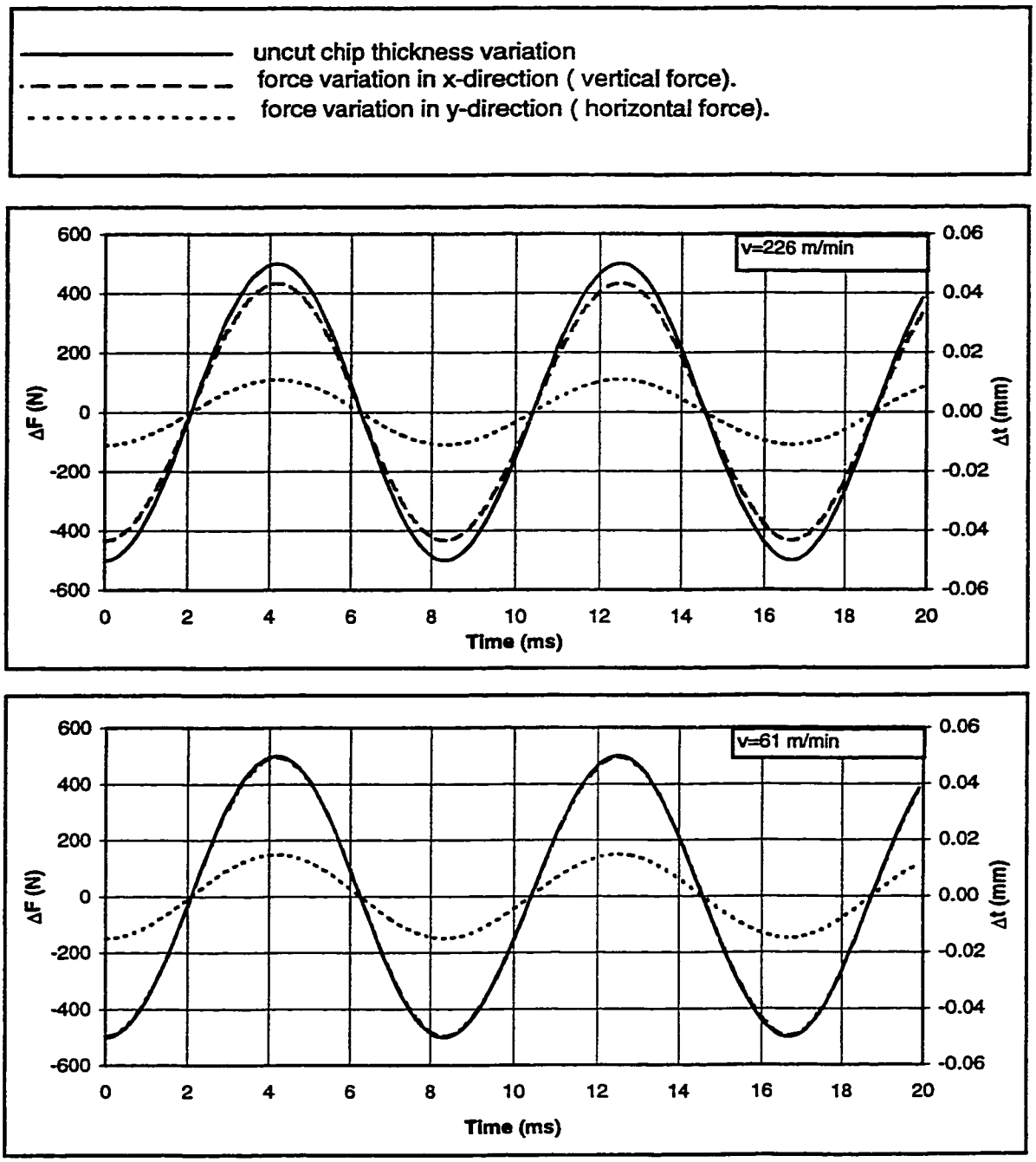

Figure 9.38: Simulation results (series 2): t=0.19 mm/rev, α=5 deg., frequency=120 Hz, b=3.5 mm

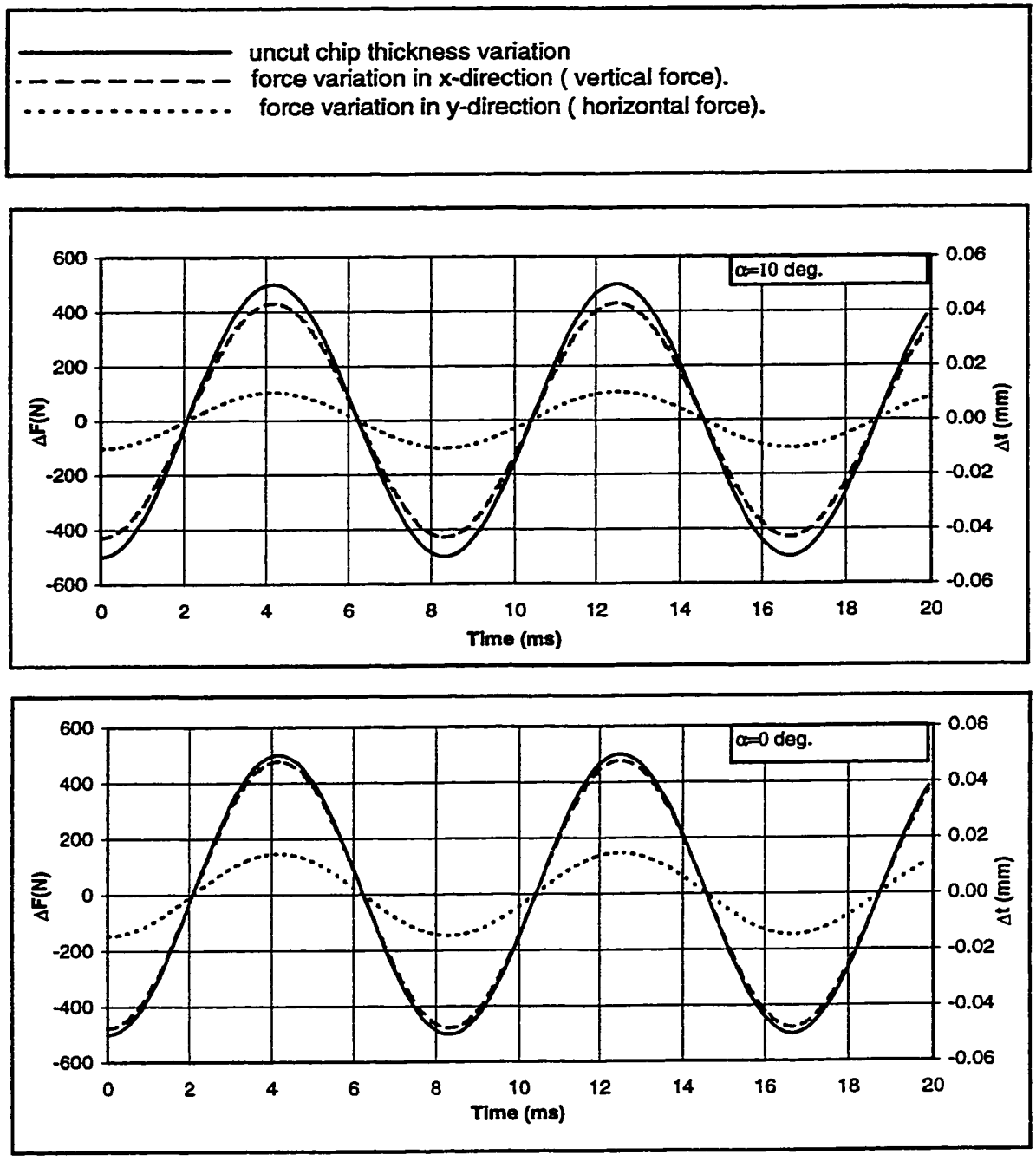

Figure 9.39: Simulation results (series 3): v=140 m/min, t=0.19 mm/rev, frequency=120 Hz, b=3.5 mm.

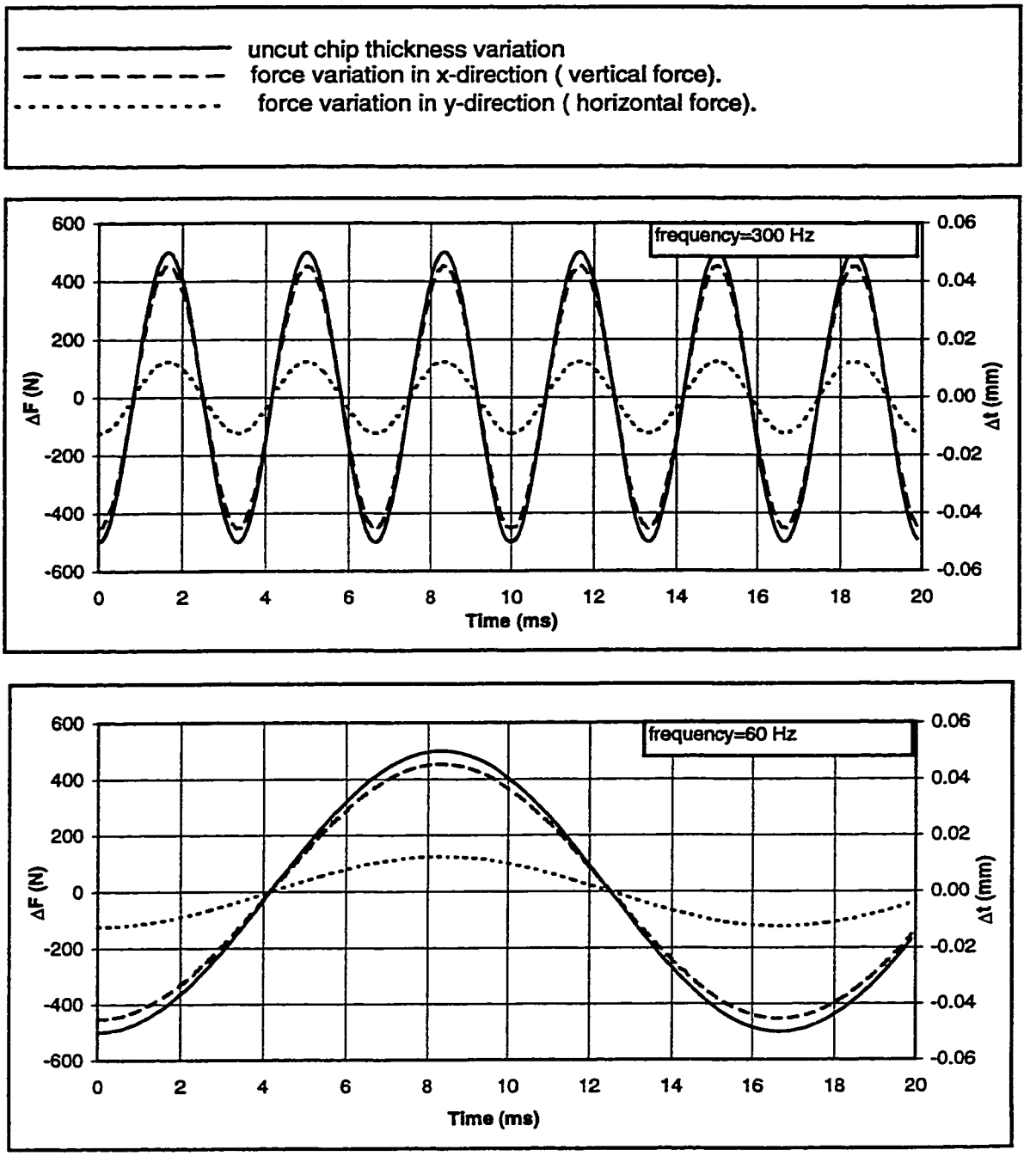

Figure 9.40: Simulation results (series 4): v=140 m/min, t=0.19 mm/rev, α=5 deg., b=3.5 mm.

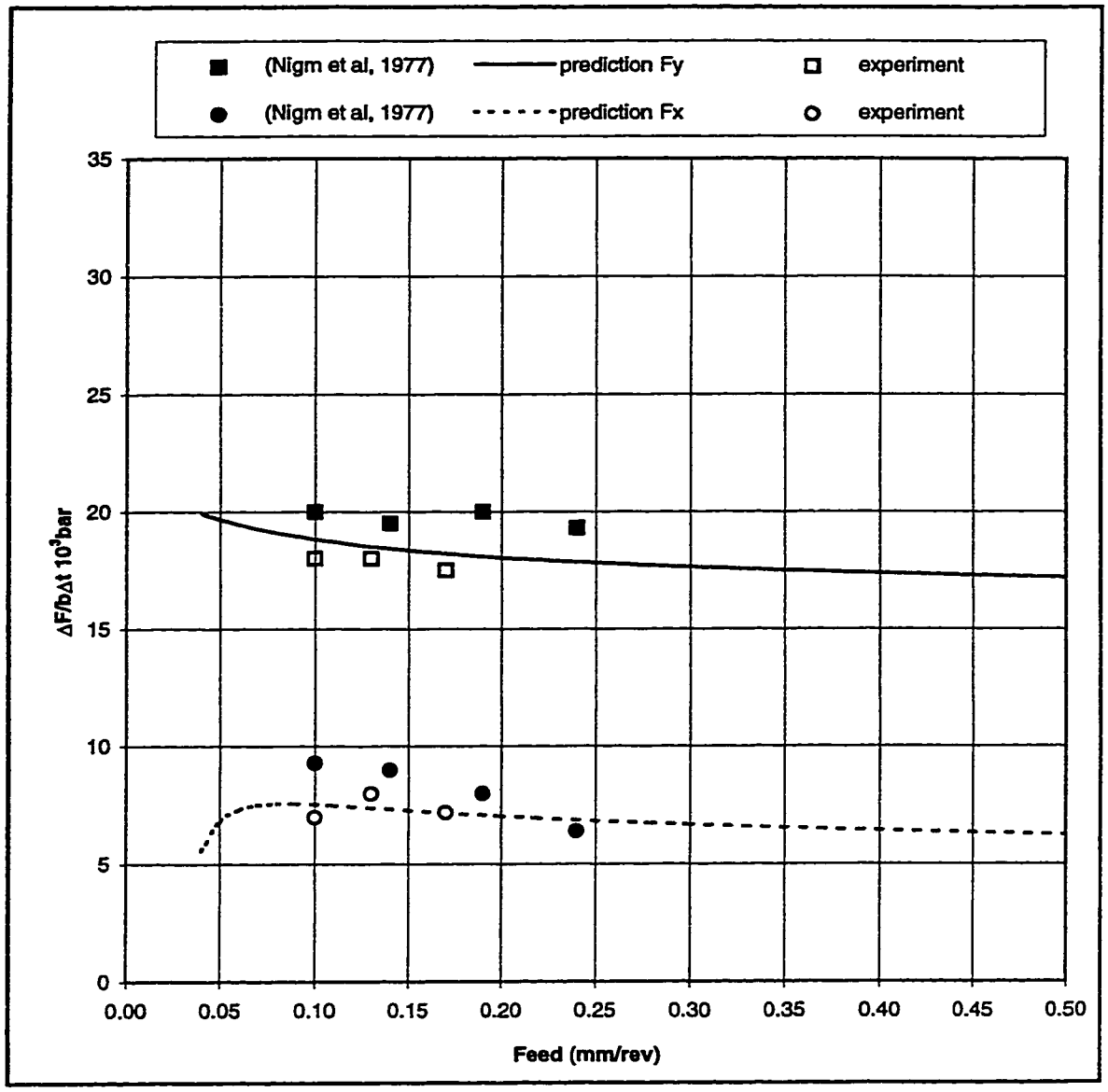

Figure 9.41: Effect of feed on the dynamic forces.

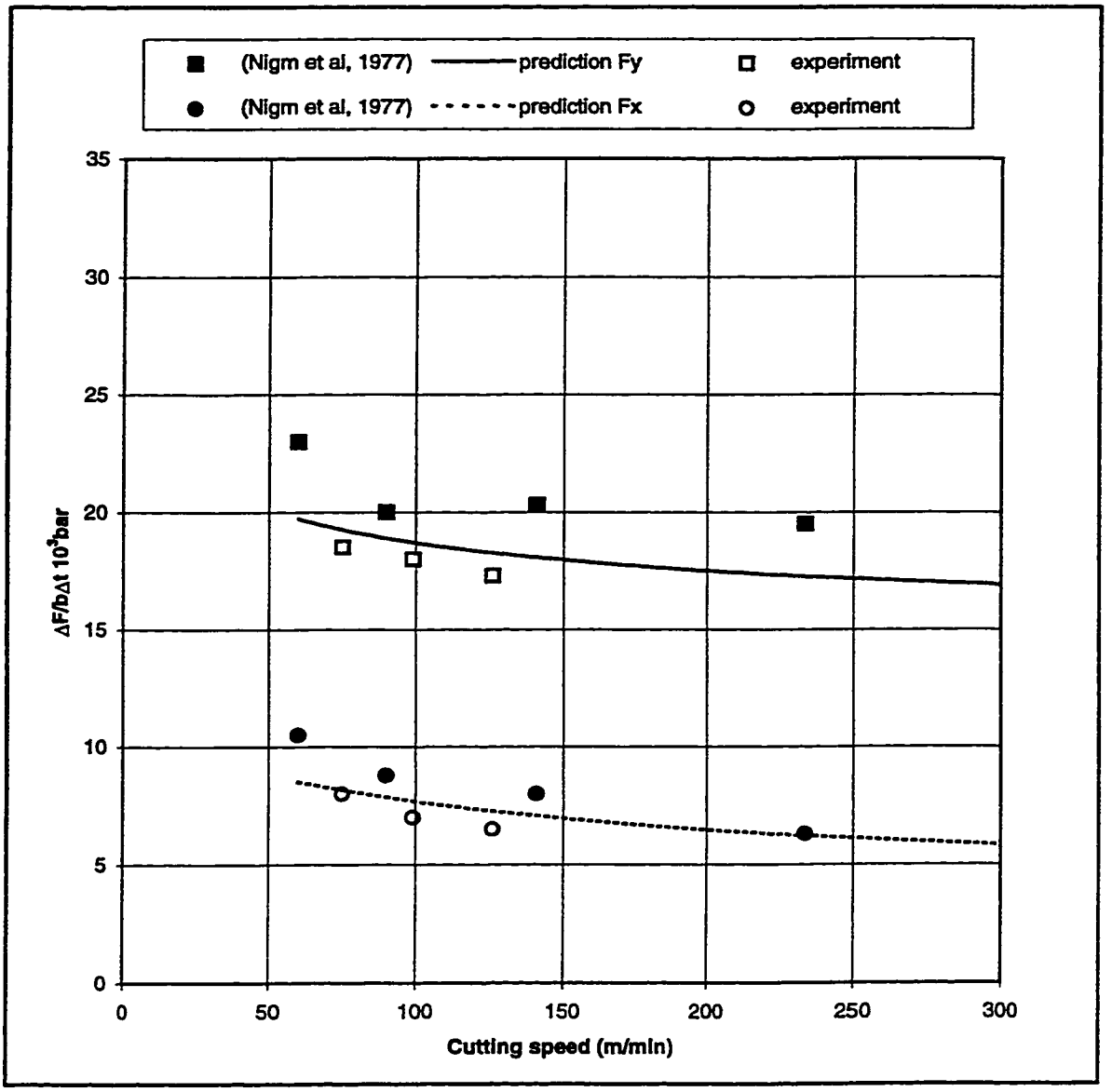

Figure 9.42: Effect of cutting speed on the dynamic forces.

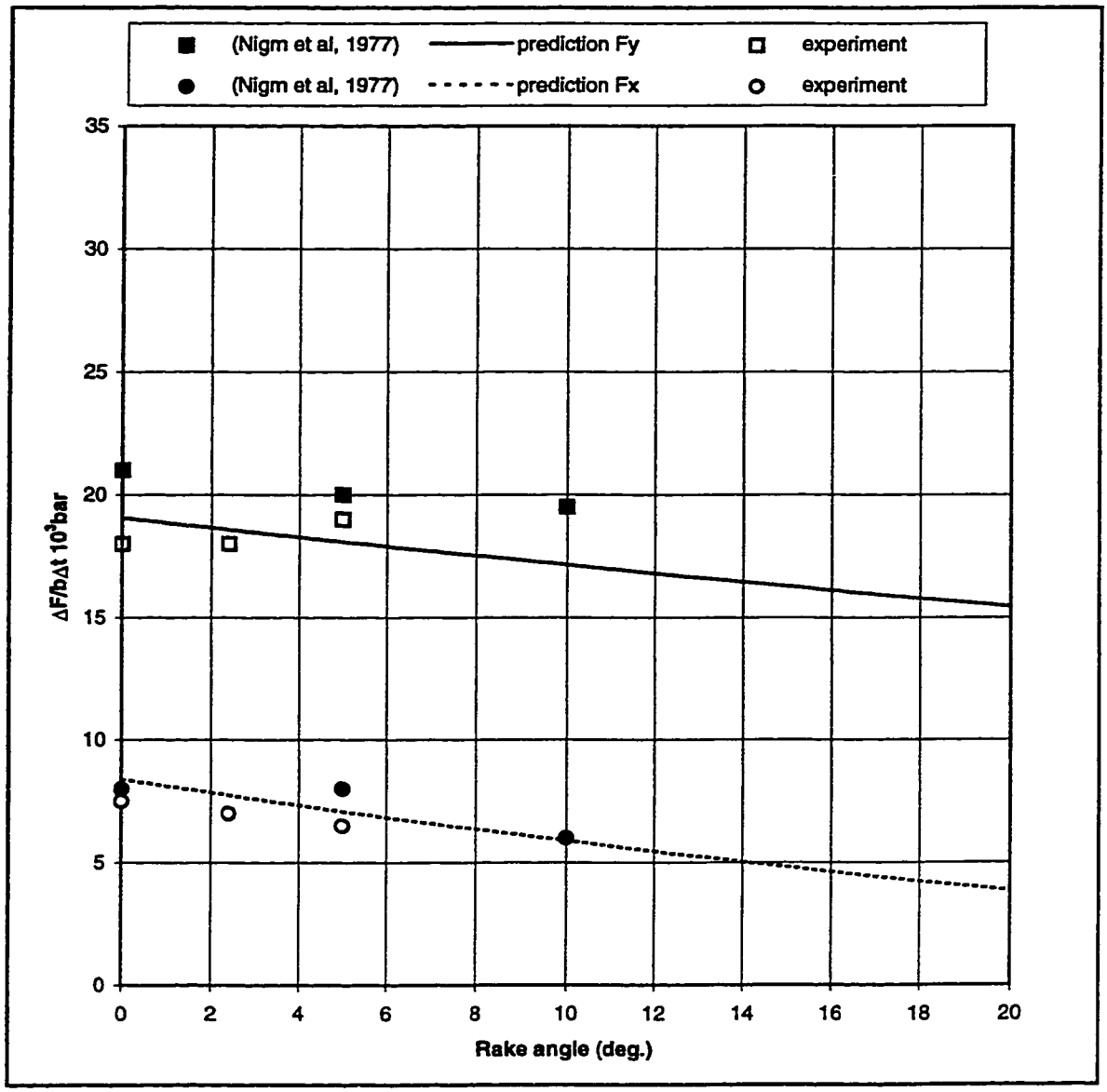

Figure 9.43: Effect of rake angle on the dynamic forces.

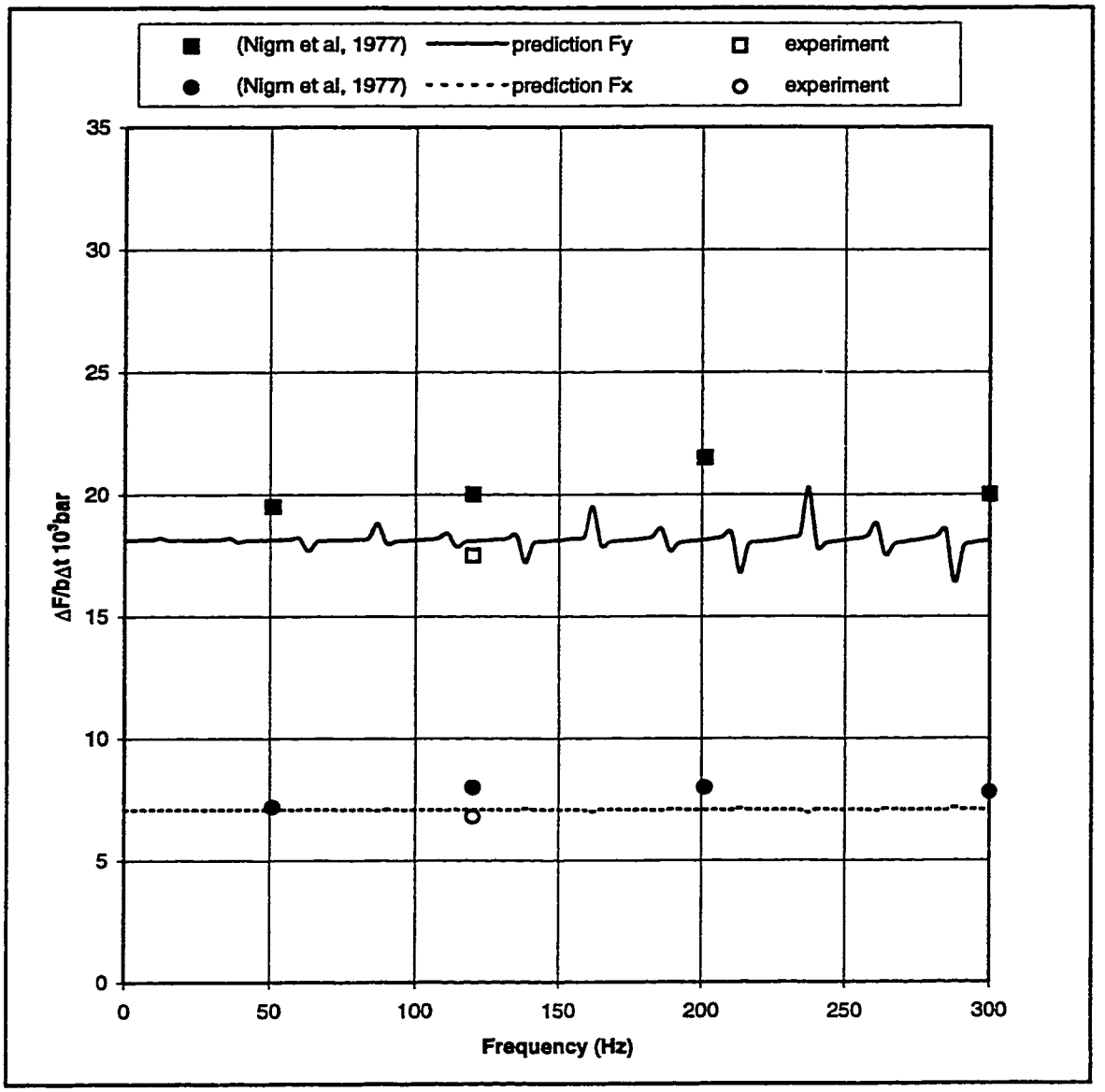

Figure 9.44: Effect of frequency on the dynamic forces.

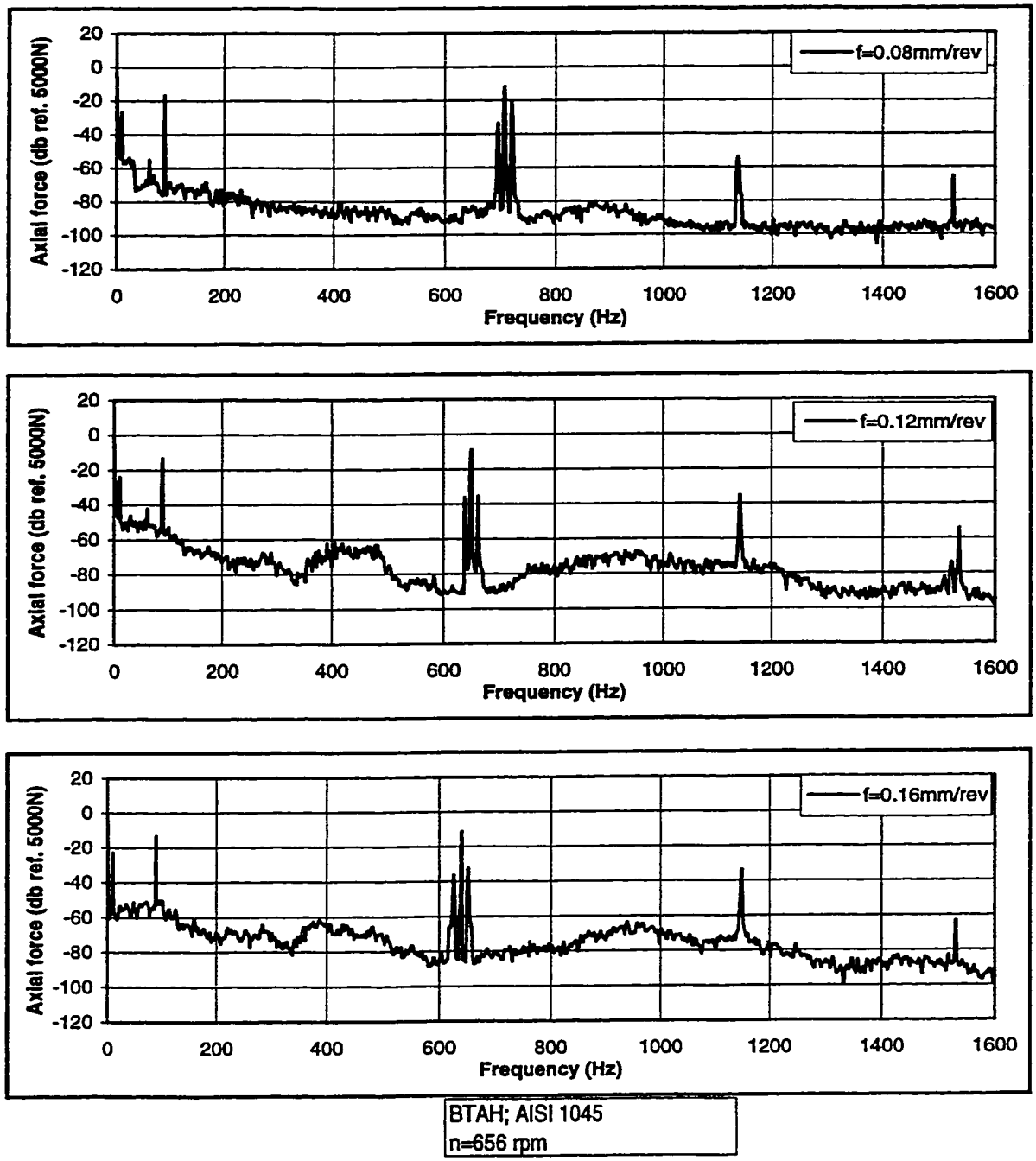

Figure 9.45: Autospectra of the axial cutting force. Cutting conditions: workpiece, AISI 1045; tool, BTAH 1" inch diameter ; boring bar length, 2.0 m; spindle rotational speed n, 656 rpm; misalignment, 15µm; cutting fluid flow rate, 80 l/min.

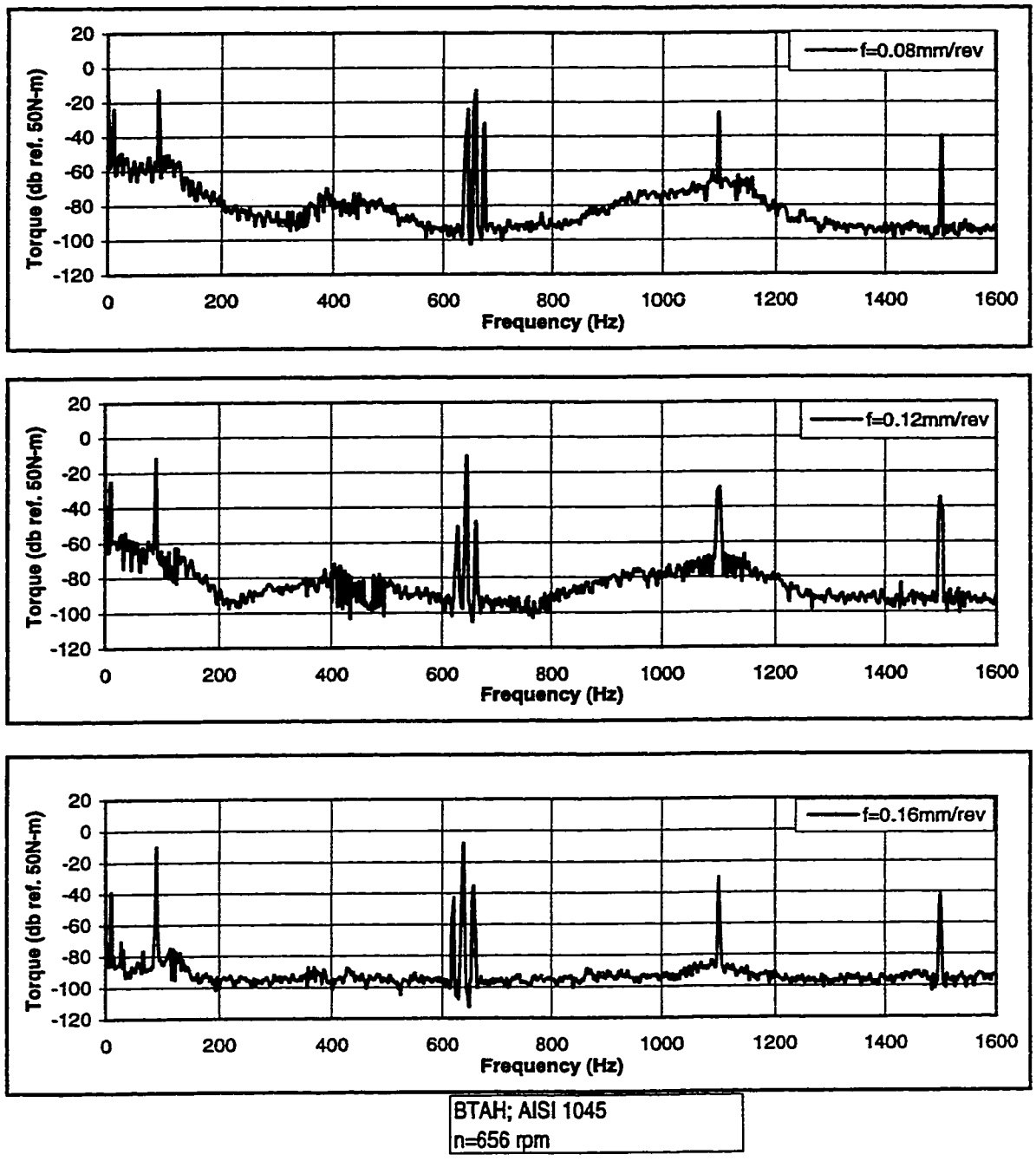

Figure 9.46: Autospectra of the cutting torque. Cutting conditions: workpiece, AISI 1045; tool, BTAH 1" inch diameter ; boring bar length, 2.0 m; spindle rotational speed n, 656 rpm; misalignment, 15μm; cutting fluid flow rate, 80 l/min.

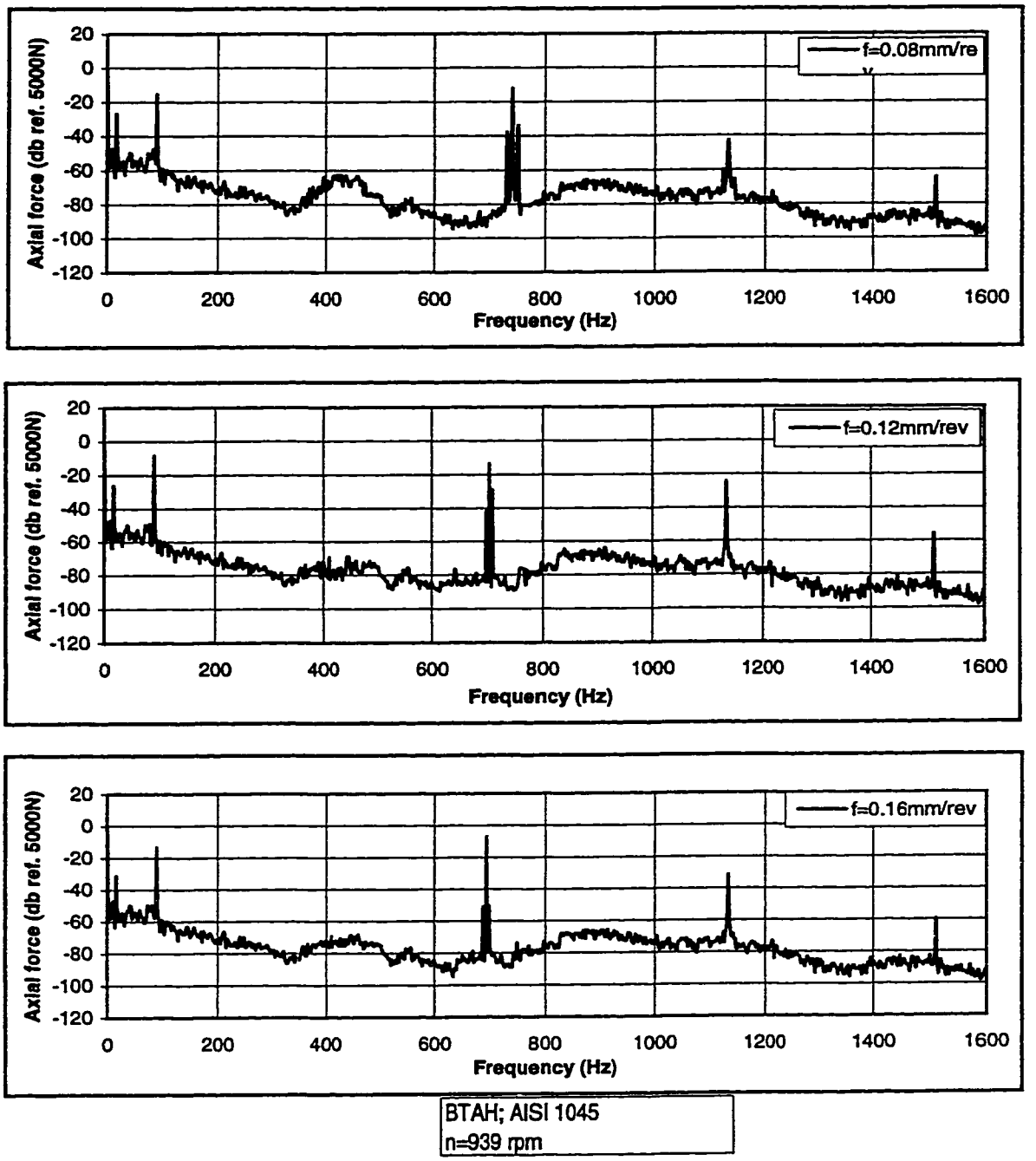

Figure 9.47: Autospectra of the axial cutting force. Cutting conditions: workpiece, AISI 1045; tool, BTAH 1" inch diameter ; boring bar length, 2.0 m; spindle rotational speed n, 939 rpm; misalignment, 15µm; cutting fluid flow rate, 80 l/min.

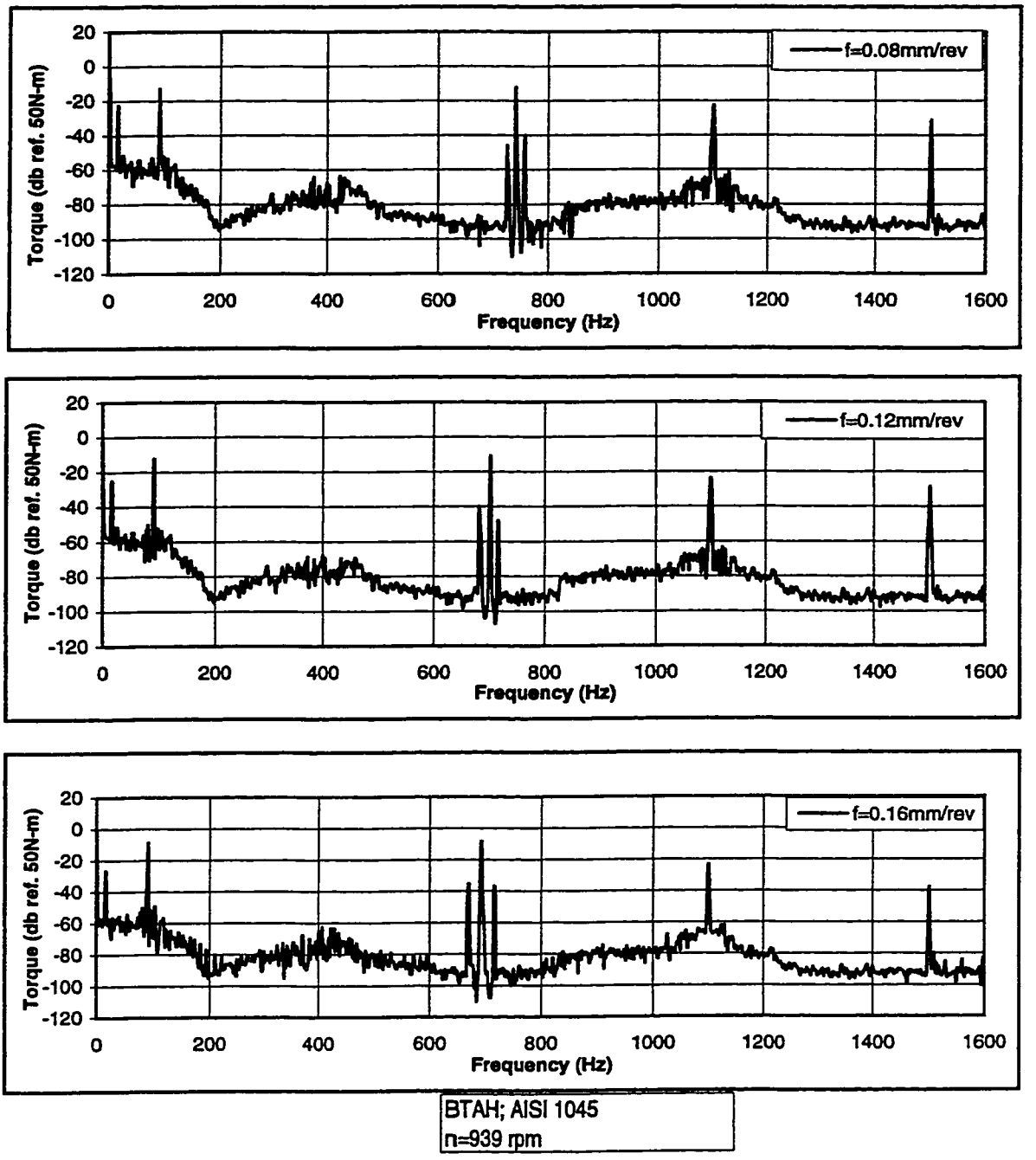

Figure 9.48: Autospectra of the cutting torque. Cutting conditions: workpiece, AISI 1045; tool, BTAH 1" inch diameter ; boring bar length, 2.0 m; spindle rotational speed n, 939 rpm; misalignment, 15μm; cutting fluid flow rate, 80 l/min.

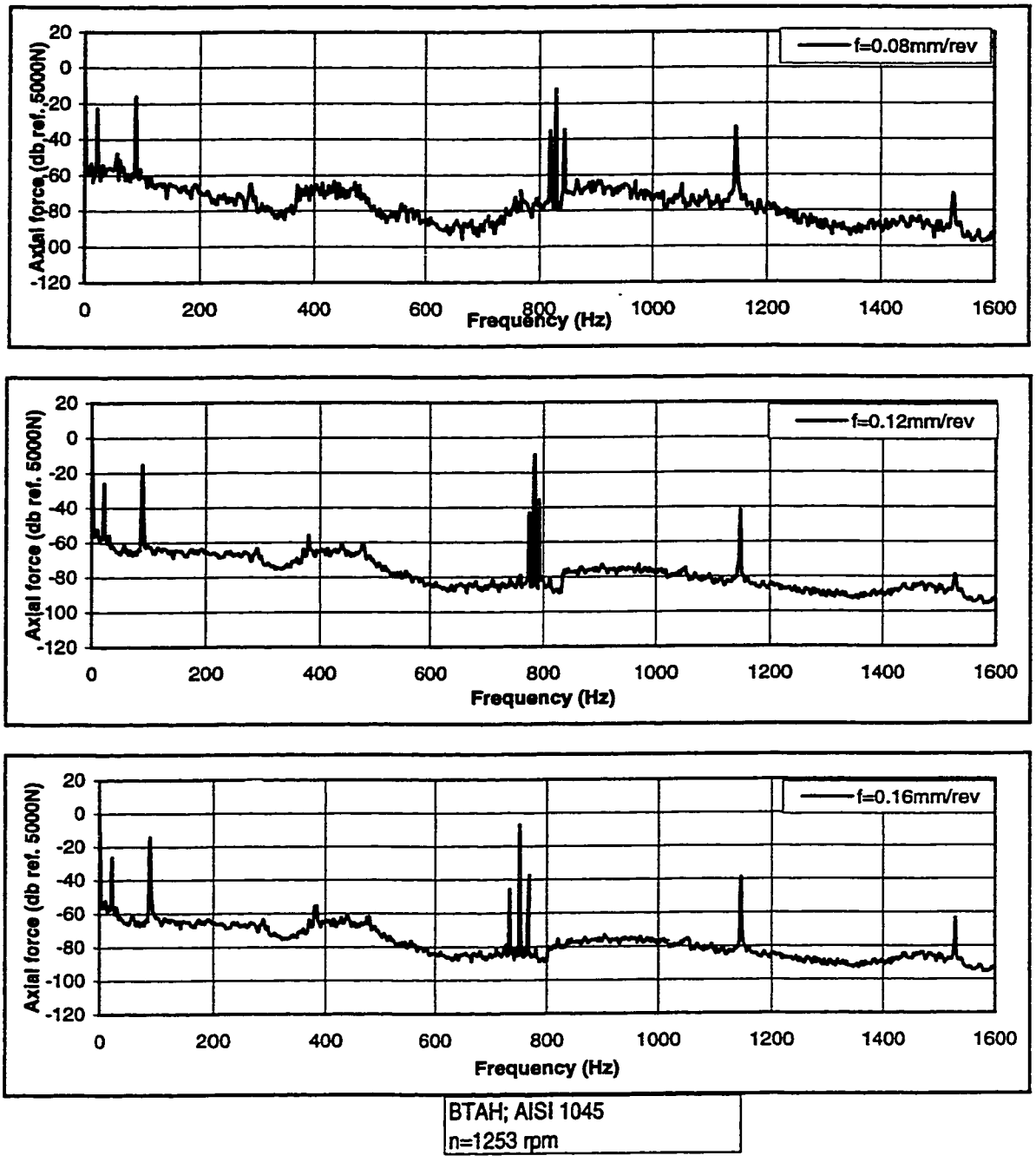

Figure 9.49: Autospectra of the axial cutting force. Cutting conditions: workpiece, AISI 1045; tool, BTAH 1" inch diameter ; boring bar length, 2.0 m; spindle rotational speed n, 1253 rpm; misalignment, 15µm; cutting fluid flow rate, 80 l/min.

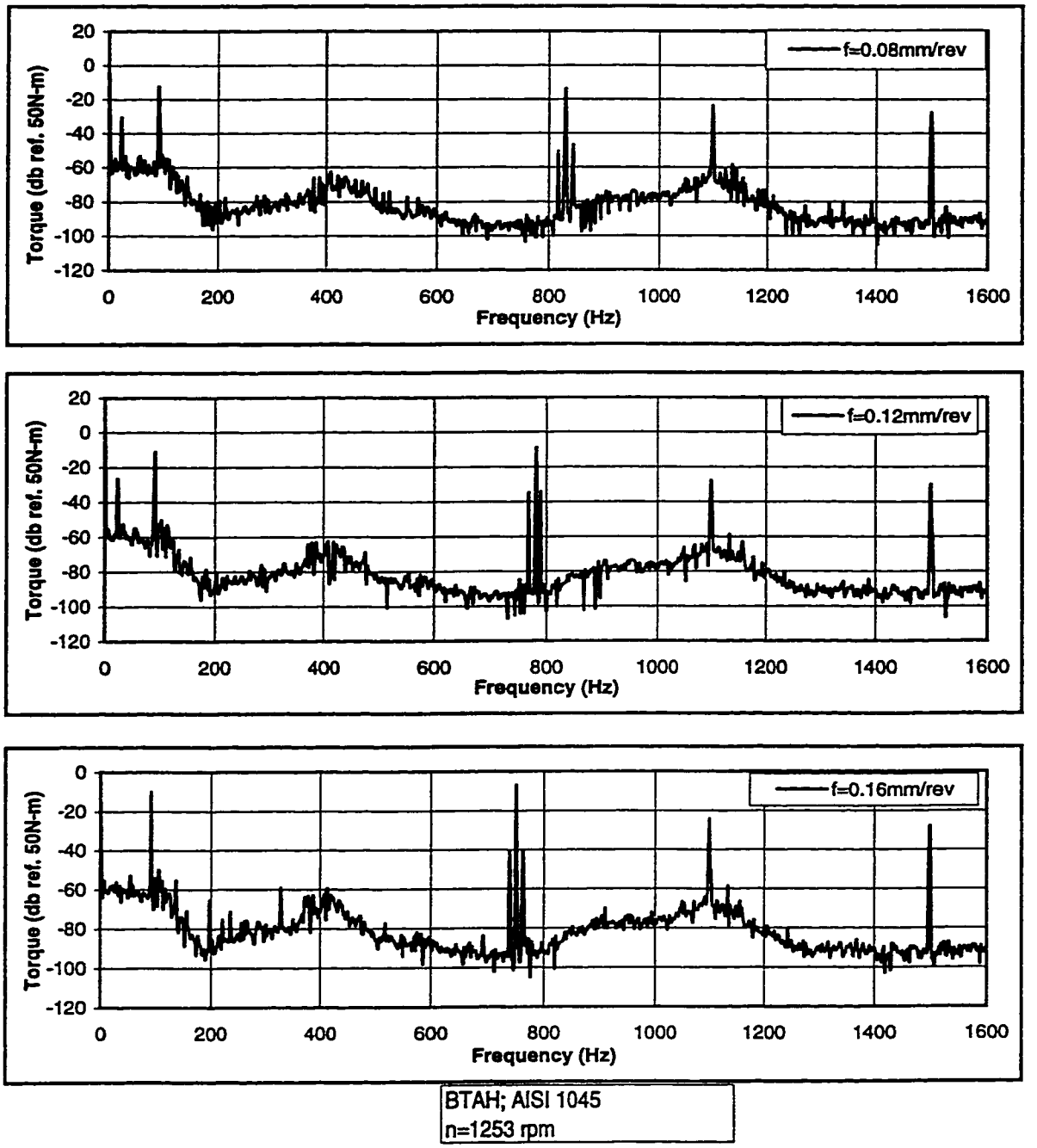

Figure 9.50: Autospectra of the cutting torque. Cutting conditions: workpiece, AISI 1045; tool, BTAH 1" inch diameter ; boring bar length, 2.0 m; spindle rotational speed n, 1253 rpm; misalignment, 15μm; cutting fluid flow rate, 80 l/min.

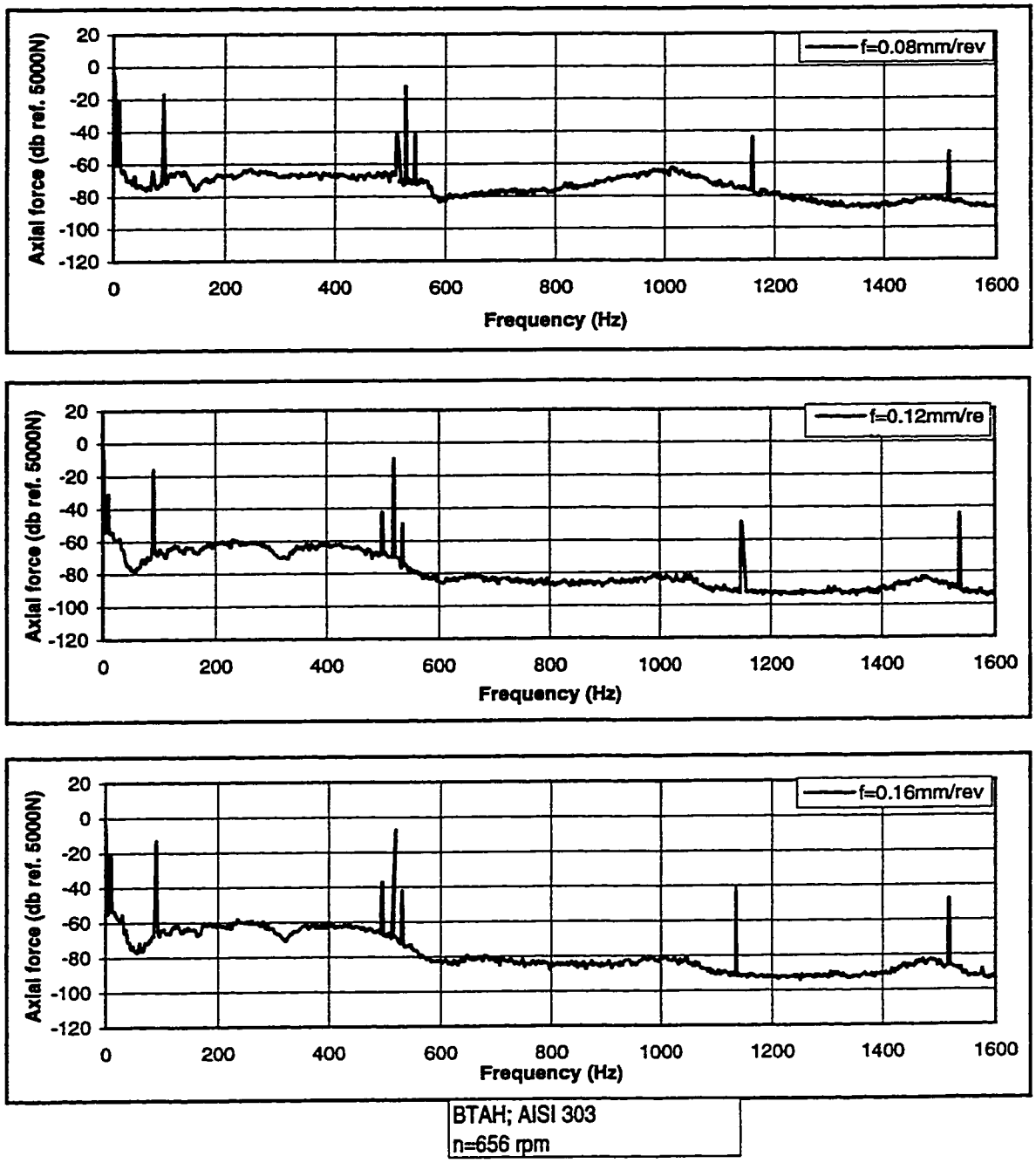

Figure 9.51: Autospectra of the axial cutting force. Cutting conditions: workpiece, AISI 303; tool, BTAH 1" inch diameter ; boring bar length, 2.0 m; spindle rotational speed n, 656 rpm; misalignment, 15μm; cutting fluid flow rate, 80 l/min.

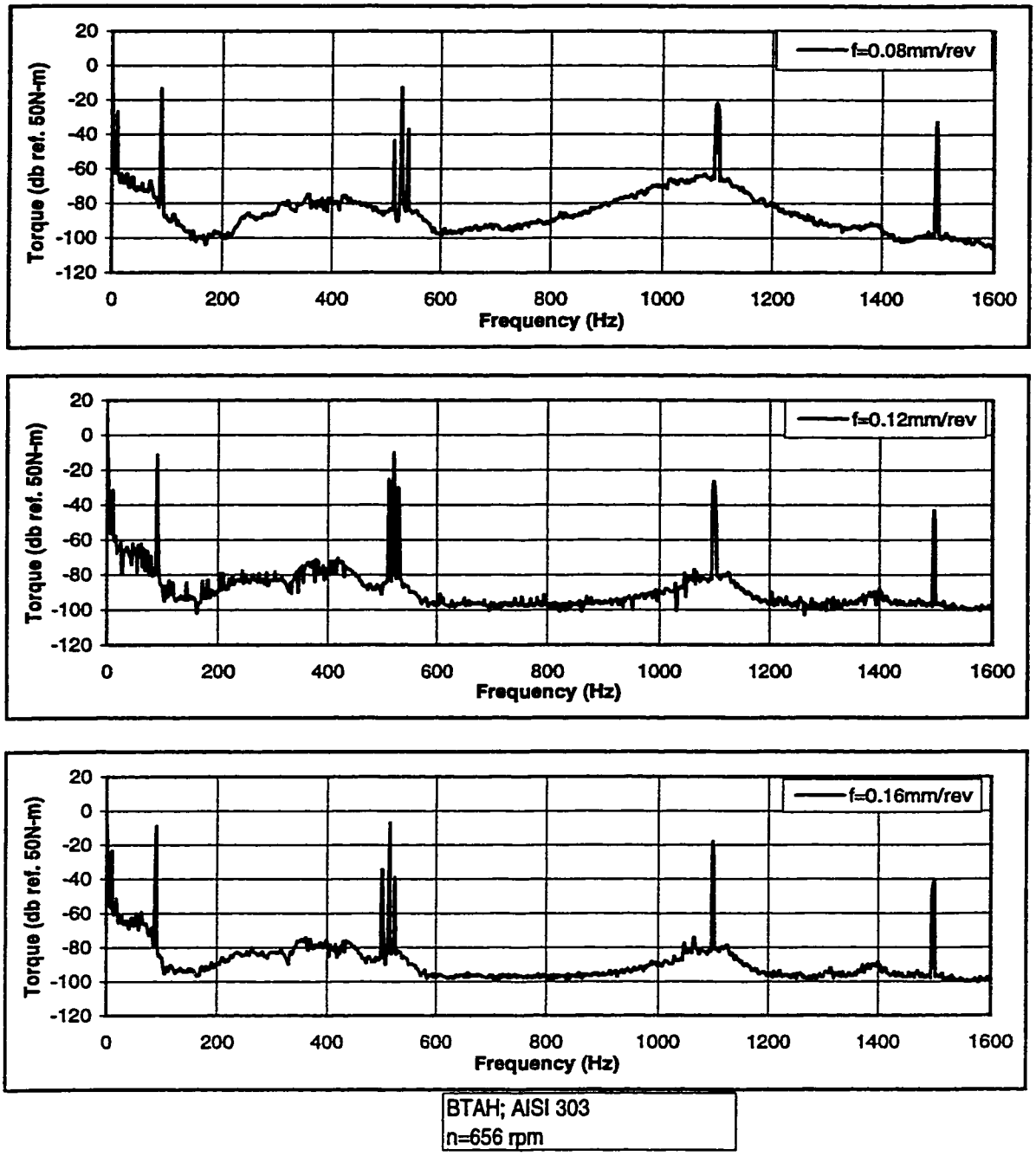

Figure 9.52: Autospectra of the cutting torque. Cutting conditions: workpiece, AISI 303; tool, BTAH 1" inch diameter ; boring bar length, 2.0 m; spindle rotational speed n, 656 rpm; misalignment, 15μm; cutting fluid flow rate, 80 l/min.

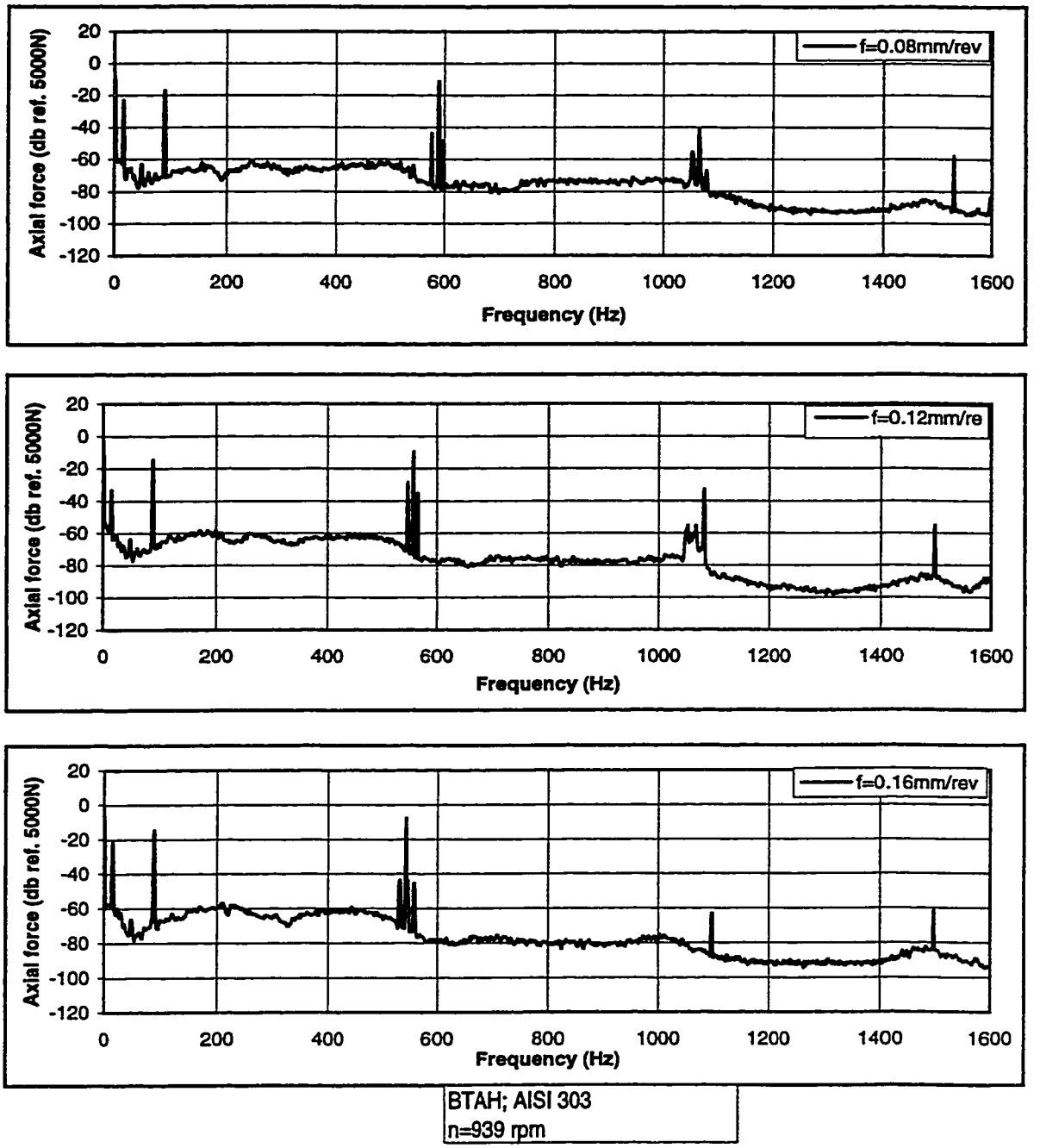

Figure 9.53: Autospectra of the axial cutting force. Cutting conditions: workpiece, AISI 303; tool, BTAH 1" inch diameter ; boring bar length, 2.0 m; spindle rotational speed n, 939 rpm; misalignment, 15µm; cutting fluid flow rate, 80 l/min.

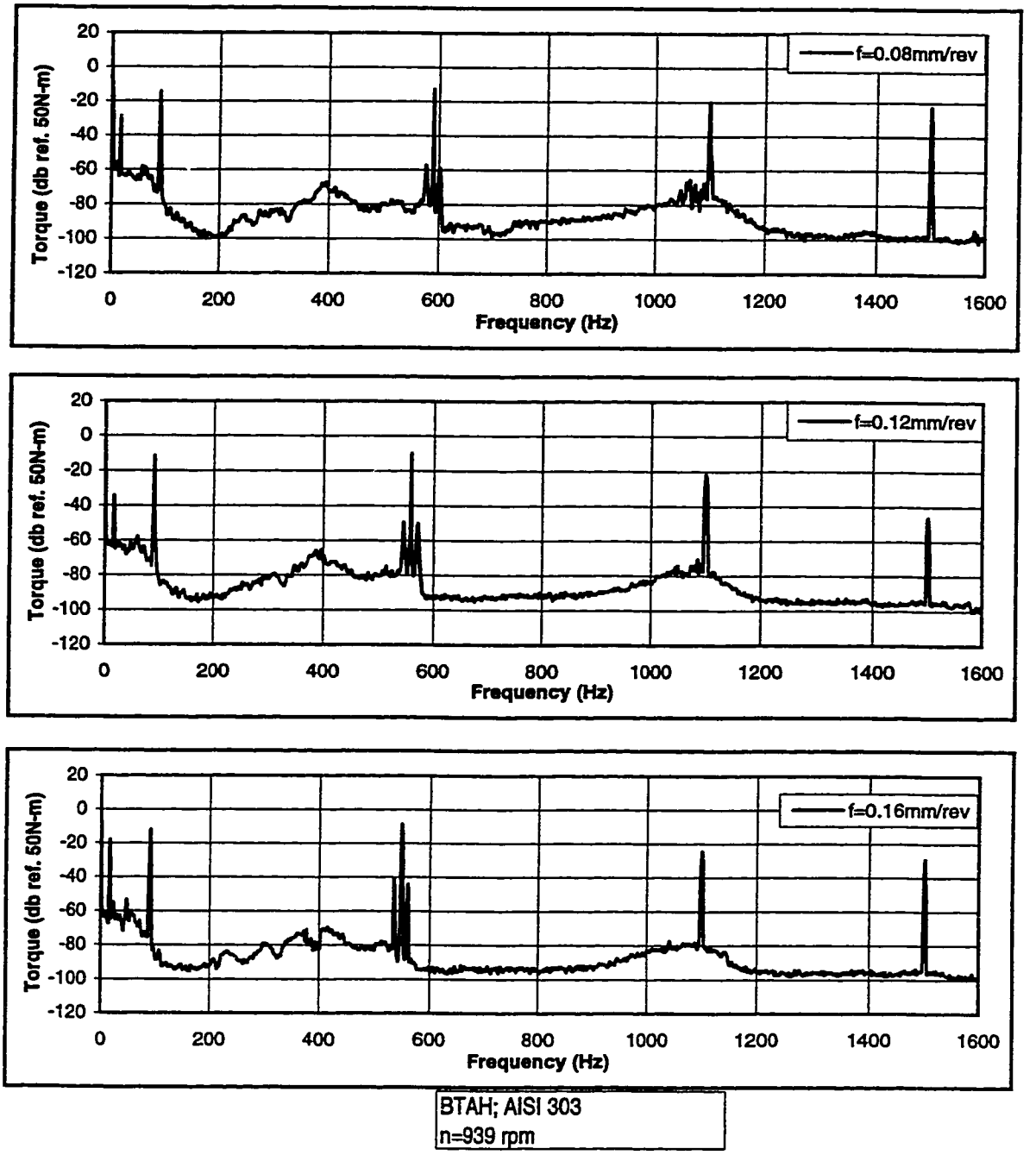

Figure 9.54: Autospectra of the cutting torque. Cutting conditions: workpiece, AISI 303; tool, BTAH 1" inch diameter ; boring bar length, 2.0 m; spindle rotational speed n, 939 rpm; misalignment, 15µm; cutting fluid flow rate, 80 l/min.

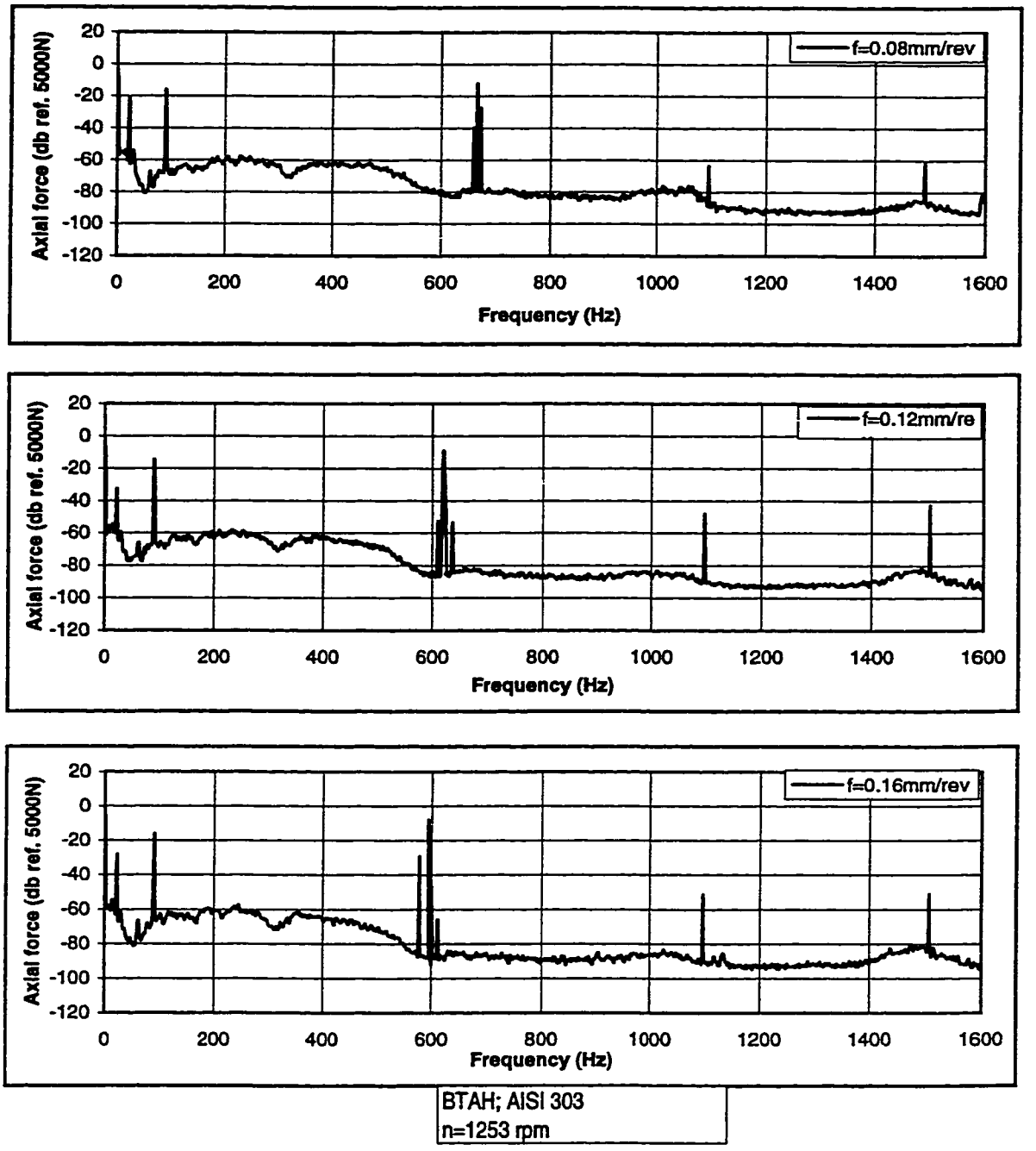

Figure 9.55: Autospectra of the axial cutting force. Cutting conditions: workpiece, AISI 303; tool, BTAH 1" inch diameter ; boring bar length, 2.0 m; spindle rotational speed n, 1253 rpm; misalignment, 15µm; cutting fluid flow rate, 80 l/min.

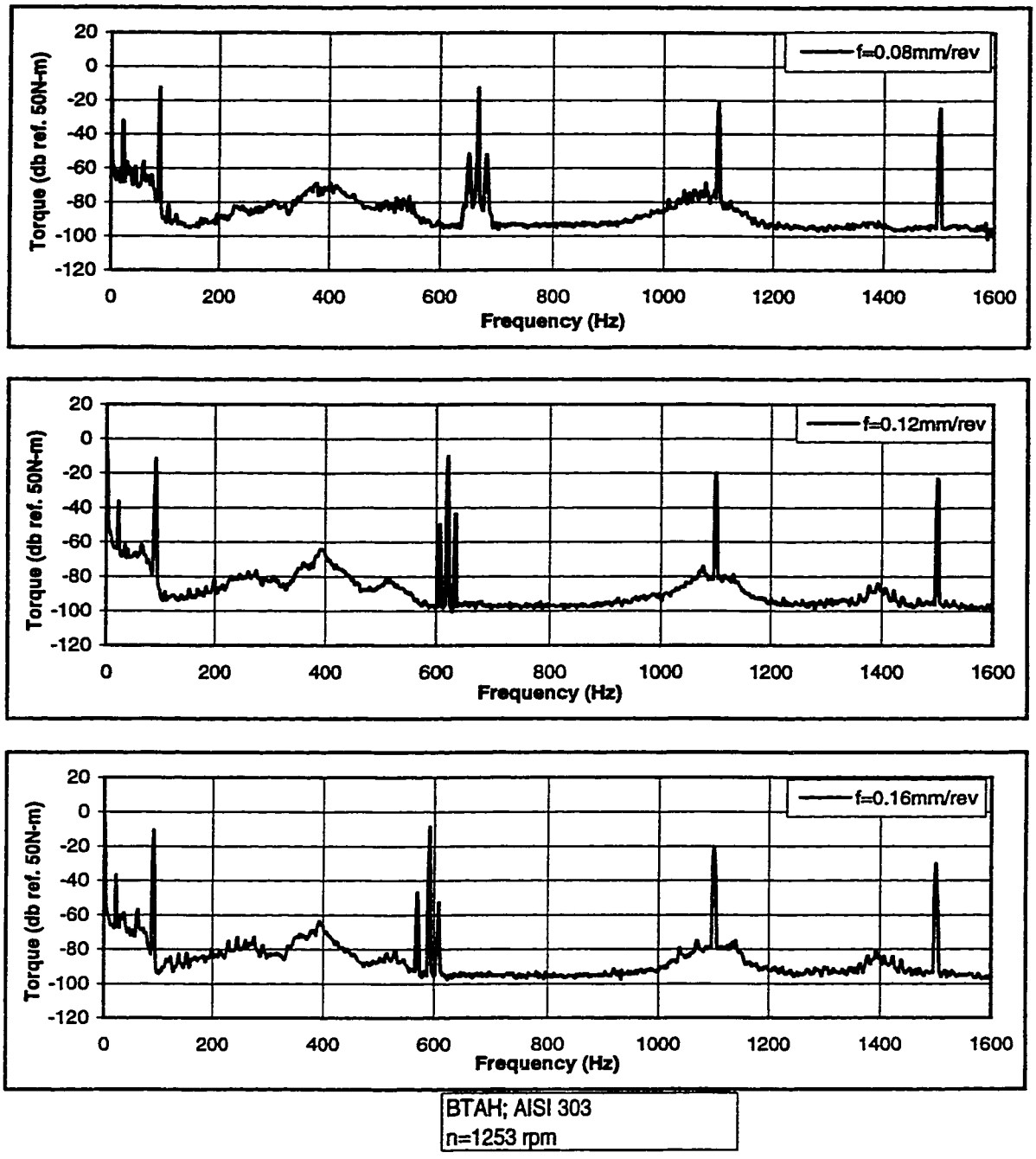

Fig. 9.56: Autospectra of the cutting torque. Cutting conditions: workpiece, AISI 303; tool, BTAH 1" inch diameter ; boring bar length, 2.0 m; spindle rotational speed n, 1253 rpm; misalignment, 15µm; cutting fluid flow rate, 80 l/min.

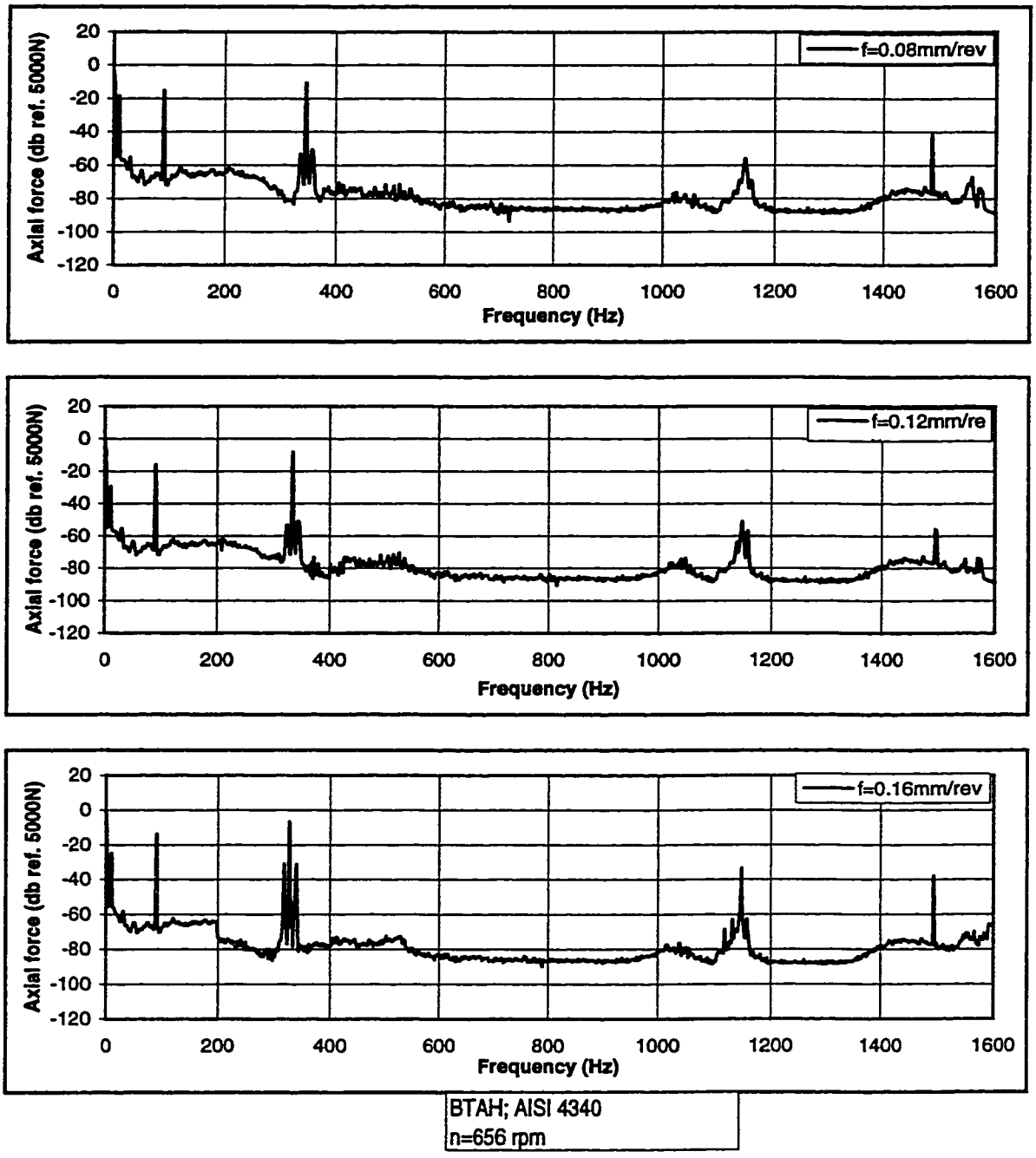

Figure 9.57:. Autospectra of the axial cutting force. Cutting conditions: workpiece, AISI 4340; tool, BTAH 1" inch diameter ; boring bar length, 2.0 m; spindle rotational speed n, 656 rpm; misalignment, 15µm; cutting fluid flow rate, 80 l/min.

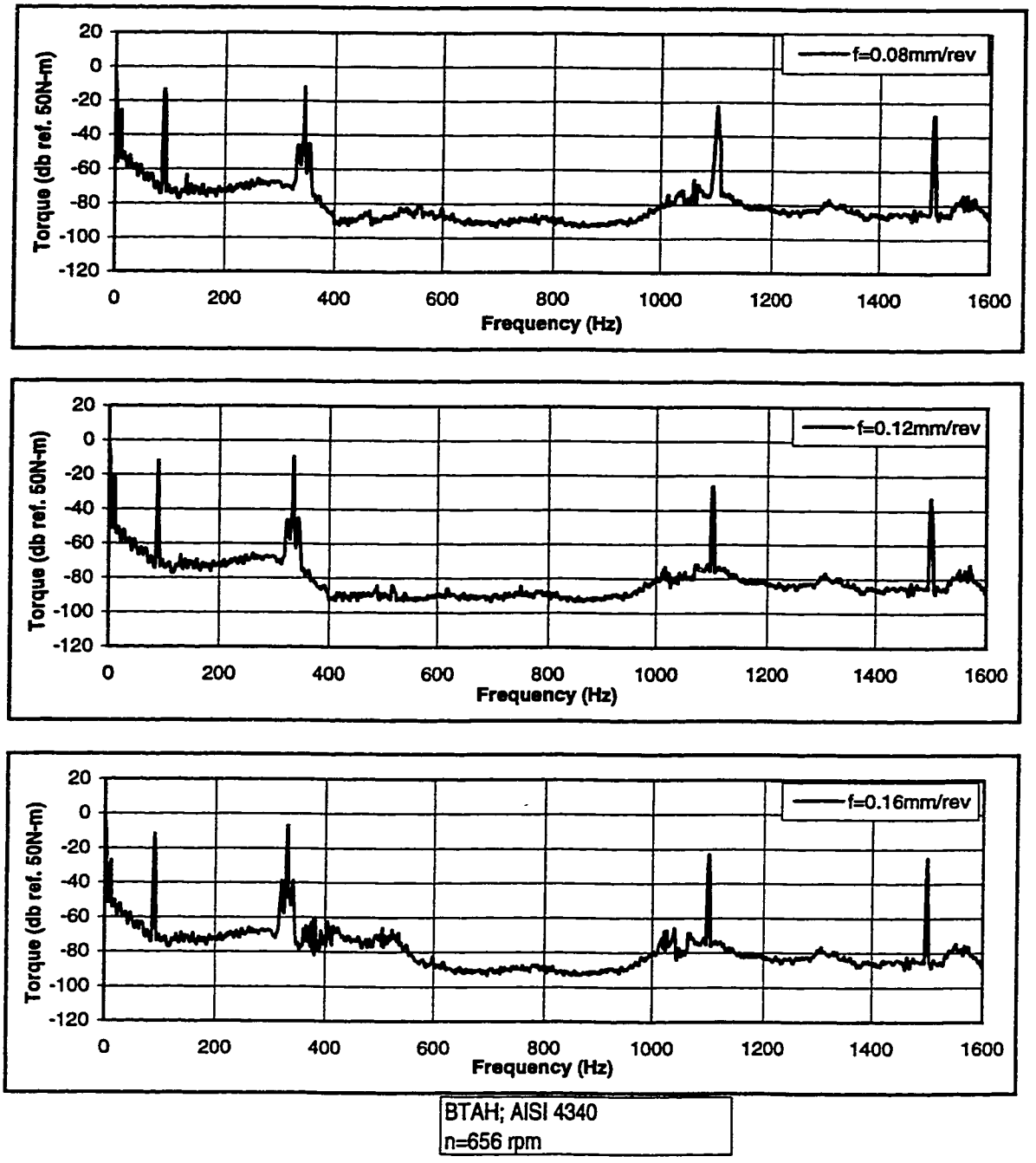

Figure 9.58: Autospectra of the cutting torque. Cutting conditions: workpiece, AISI 4340; tool, BTAH 1" inch diameter ; boring bar length, 2.0 m; spindle rotational speed n, 656 rpm; misalignment, 15μm; cutting fluid flow rate, 80 l/min.

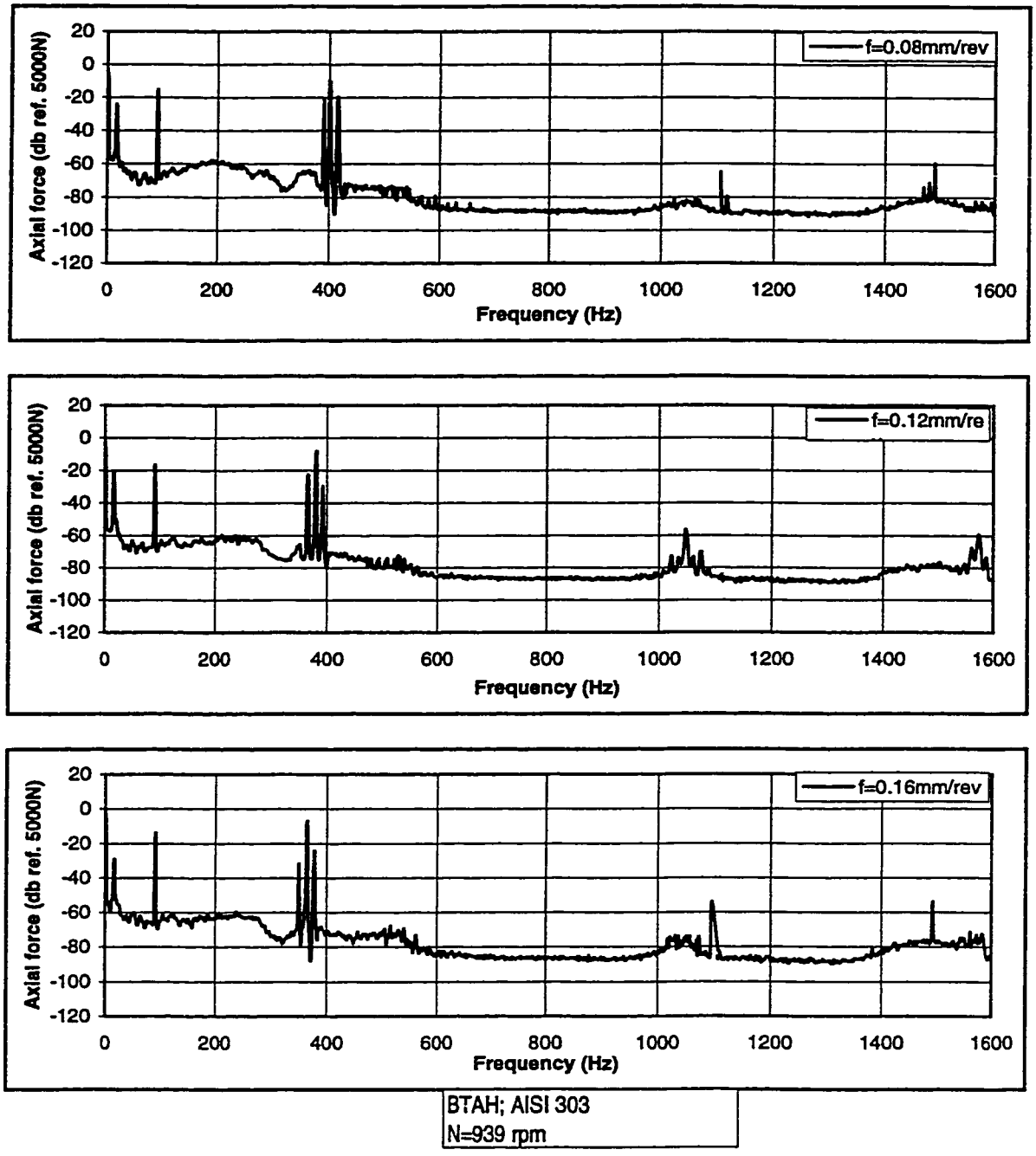

Figure 9.59: Autospectra of the axial cutting force. Cutting conditions: workpiece, AISI 4340; tool, BTAH Heller design 1" inch diameter ; boring bar length, 2.0 m; spindle speed N, 939 rpm; misalignment, 15µm; cutting fluid flow, 80 l/min.

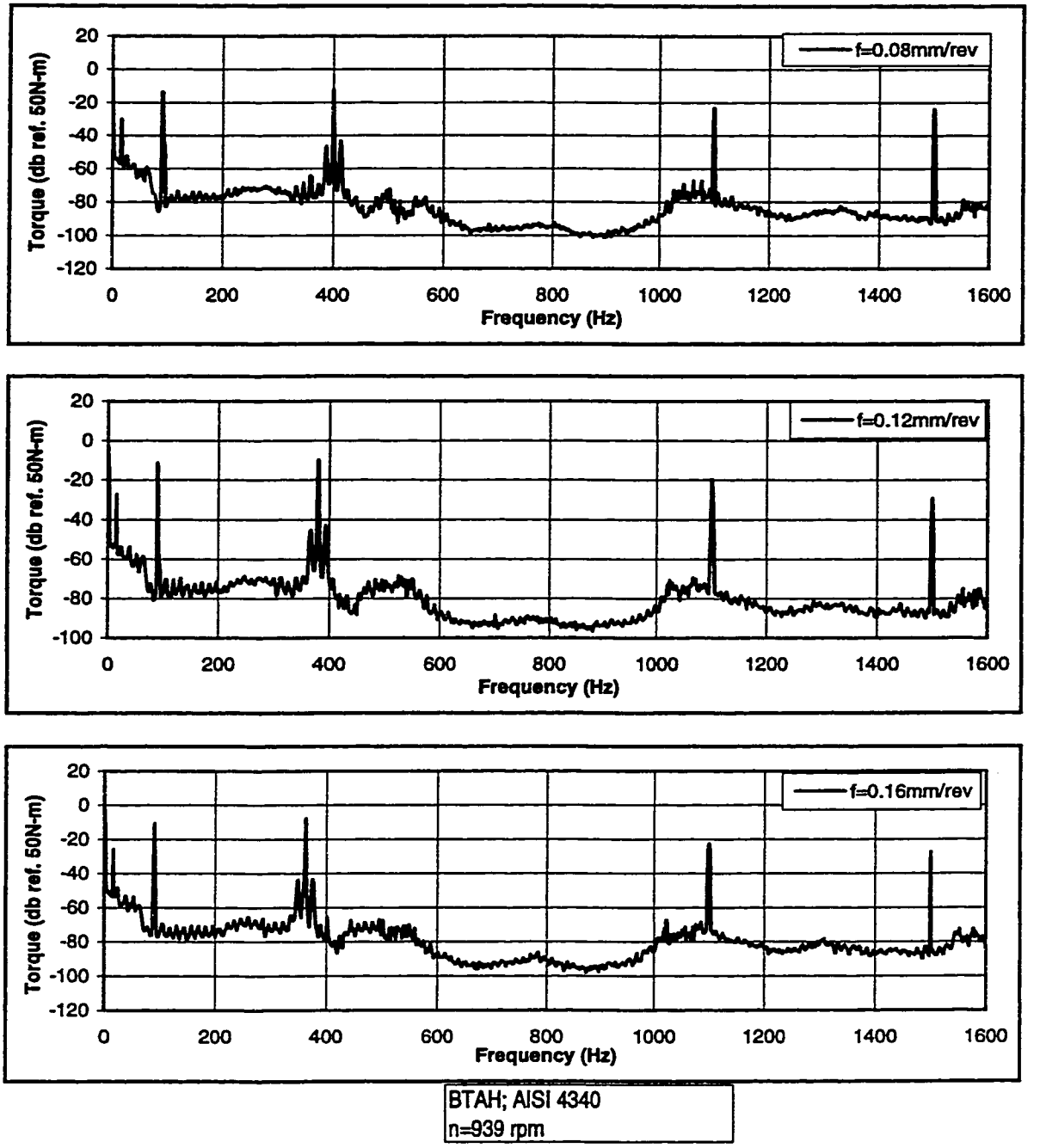

Figure 9.60: Autospectra of the cutting torque. Cutting conditions: workpiece, AISI 4340; tool, BTAH 1" inch diameter ; boring bar length, 2.0 m; spindle rotational speed n, 939 rpm; misalignment, 15µm; cutting fluid flow rate, 80 l/min.

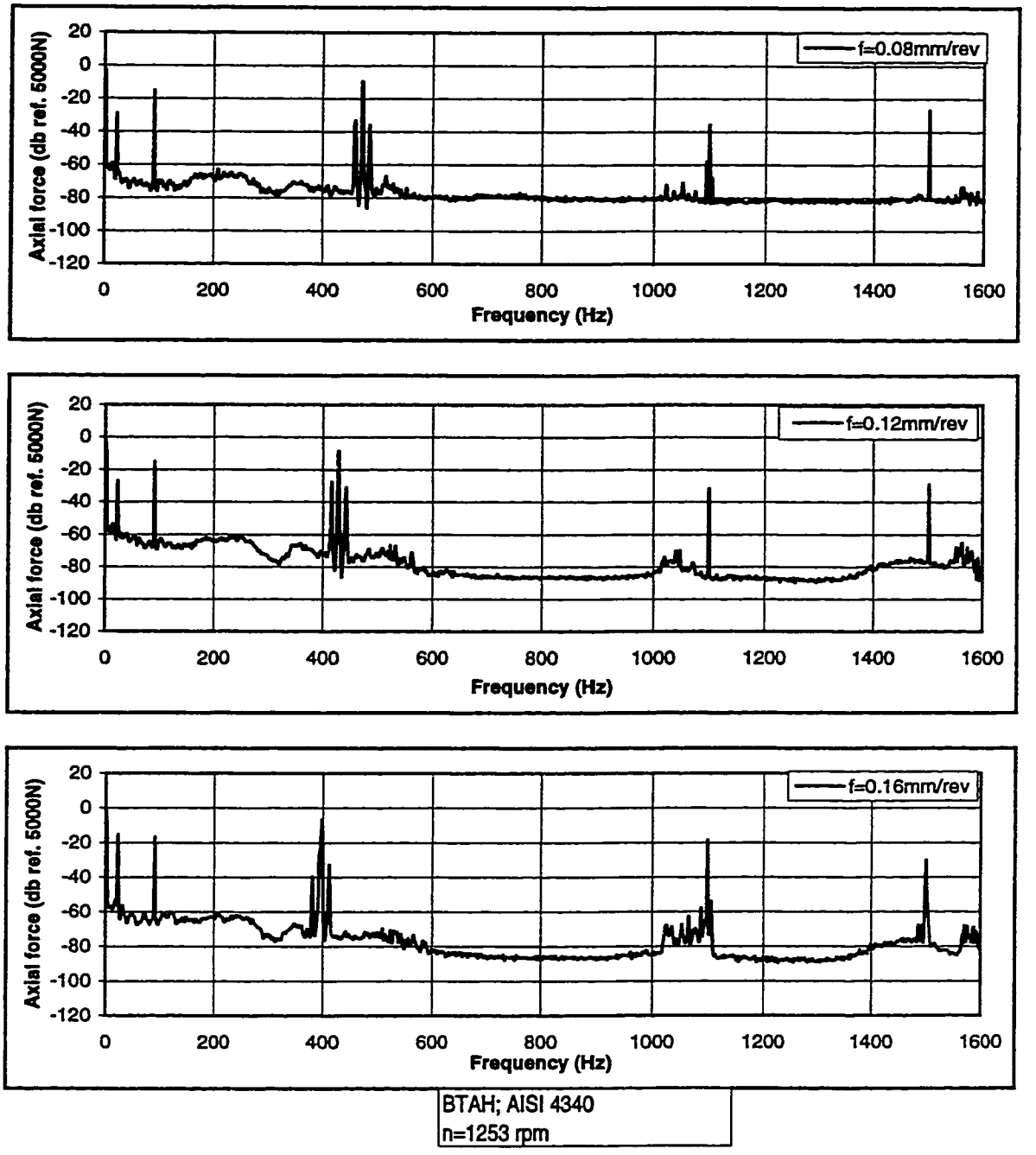

Figure 9.61: Autospectra of the axial cutting force. Cutting conditions: workpiece, AISI 4340; tool, BTAH 1" inch diameter ; boring bar length, 2.0 m; spindle rotational speed n, 1253 rpm; misalignment, 15μm; cutting fluid flow rate, 80 l/min.

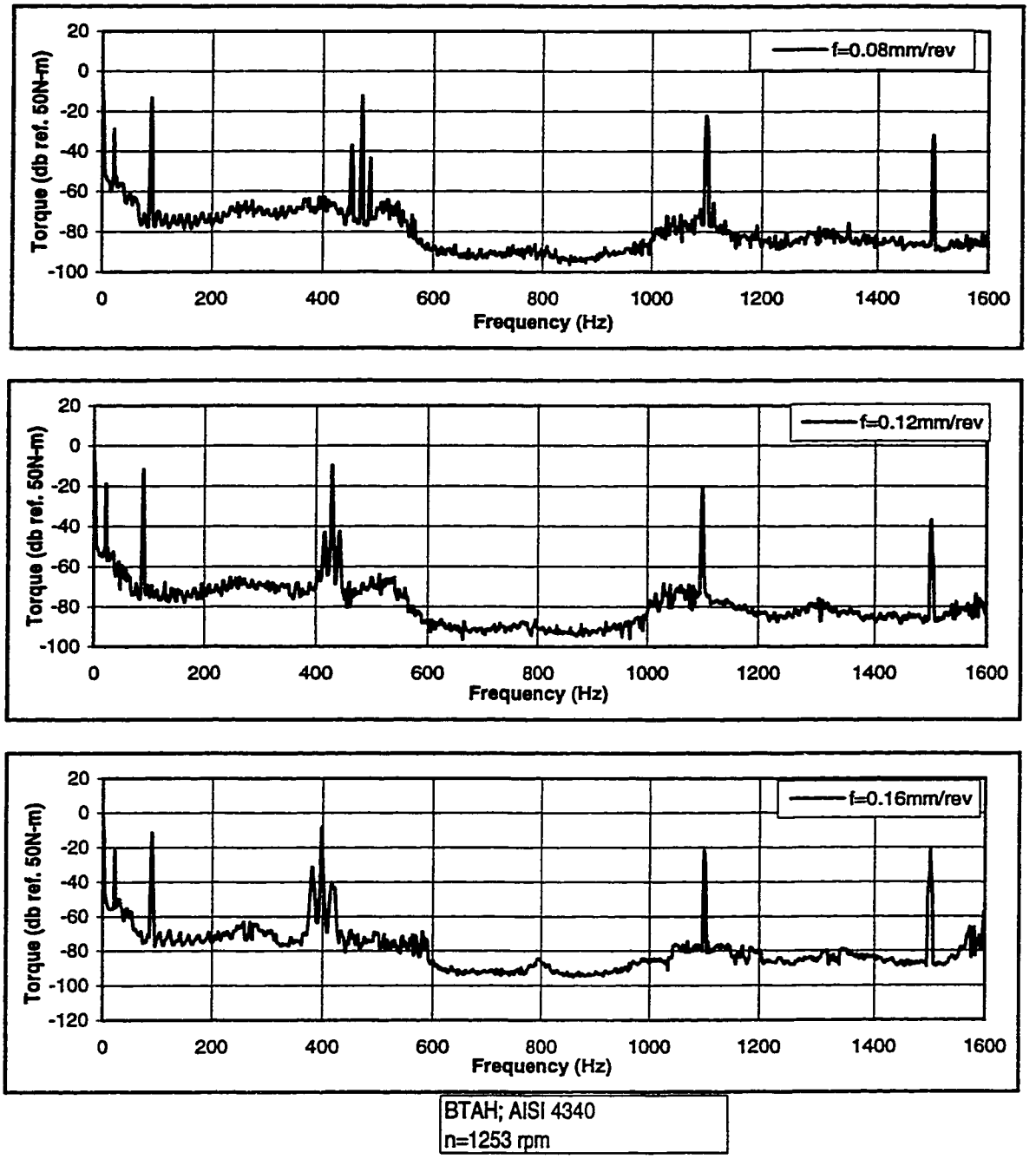

Figure 9.62. Autospectra of the cutting torque. Cutting conditions: workpiece, AISI 4340; tool, BTAH 1" inch diameter ; boring bar length, 2.0 m; spindle rotational speed n, 1253 rpm; misalignment, 15µm; cutting fluid flow rate, 80 l/min.

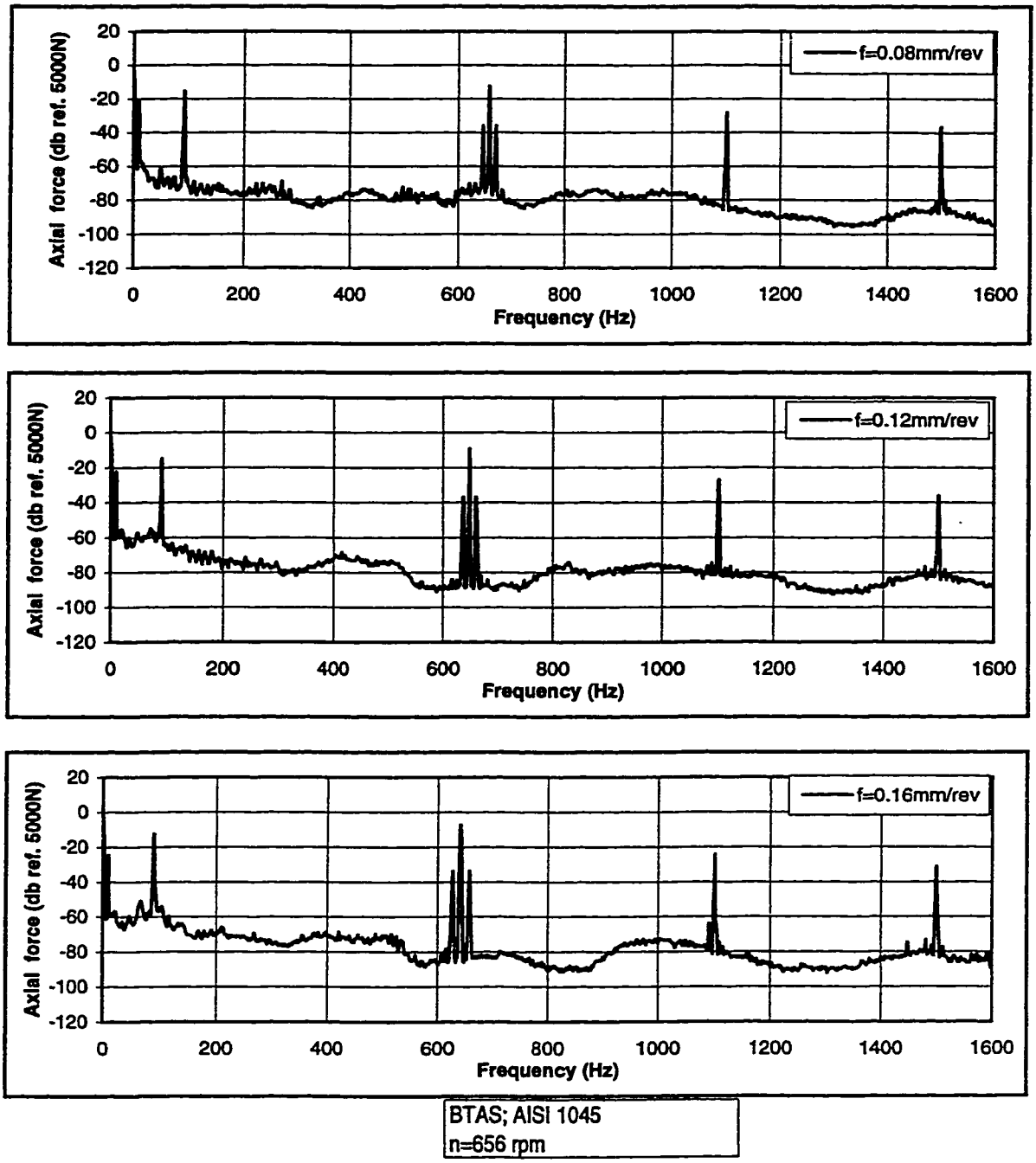

Figure 9.63: Autospectra of the axial cutting force. Cutting conditions: workpiece, AISI 1045; tool, BTAS 1" inch diameter ; boring bar length, 2.0 m; spindle rotational speed n, 656 rpm; misalignment, 15µm; cutting fluid flow rate, 80 l/min.

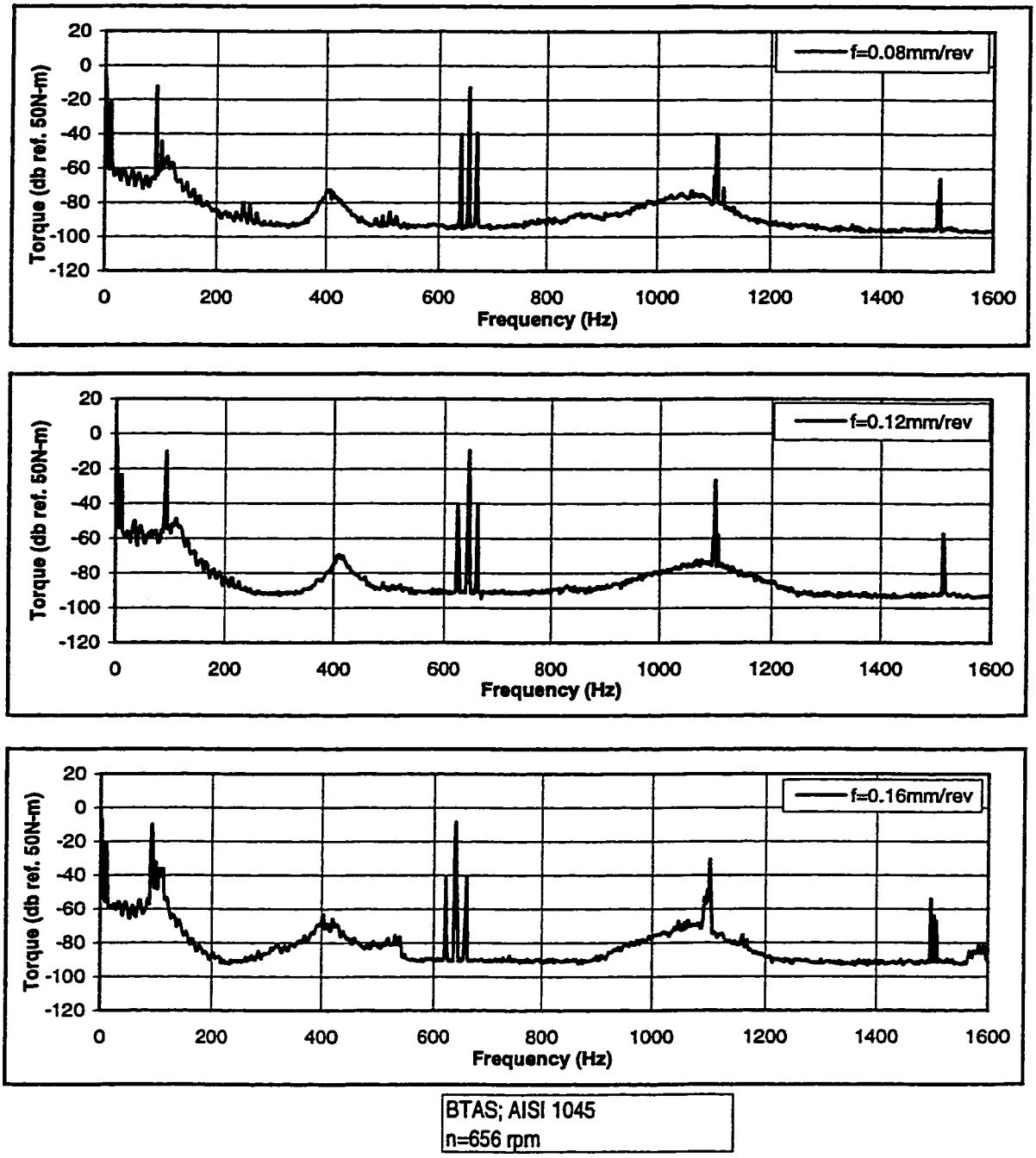

Figure 9.64: Autospectra of the cutting torque. Cutting conditions: workpiece, AISI 1045; tool, BTAS 1" inch diameter ; boring bar length, 2.0 m; spindle rotational speed n, 656 rpm; misalignment, 15µm; cutting fluid flow rate, 80 l/min.

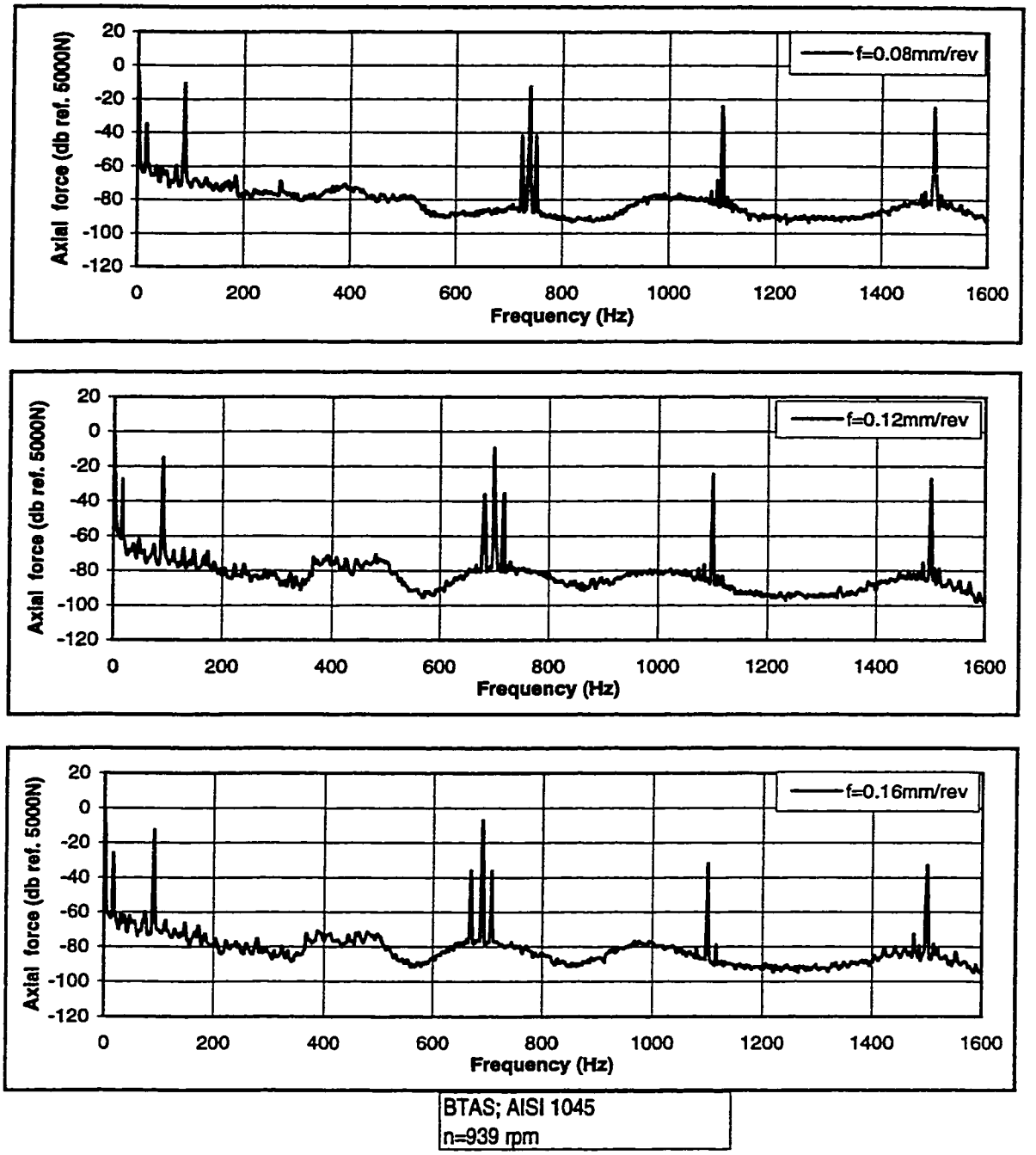

Figure 9.65: Autospectra of the axial cutting force. Cutting conditions: workpiece, AISI 1045; tool, BTAS 1" inch diameter ; boring bar length, 2.0 m; spindle rotational speed n, 939 rpm; misalignment, 15µm; cutting fluid flow rate, 80 l/min.

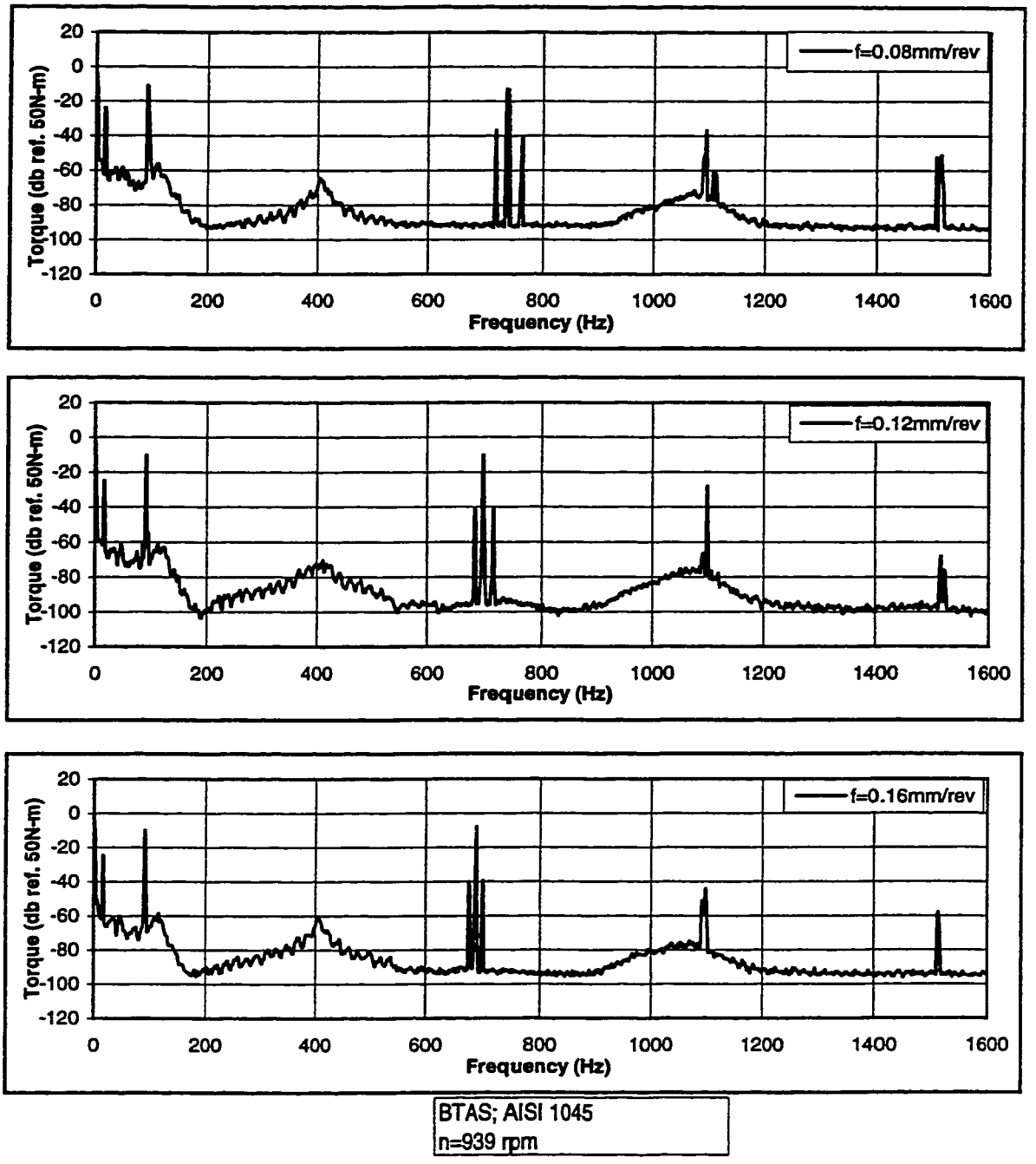

Figure 9.66: Autospectra of the cutting torque. Cutting conditions: workpiece, AISI 1045; tool, BTAS 1" inch diameter ; boring bar length, 2.0 m; spindle rotational speed n, 939 rpm; misalignment, 15μm; cutting fluid flow rate, 80 l/min.

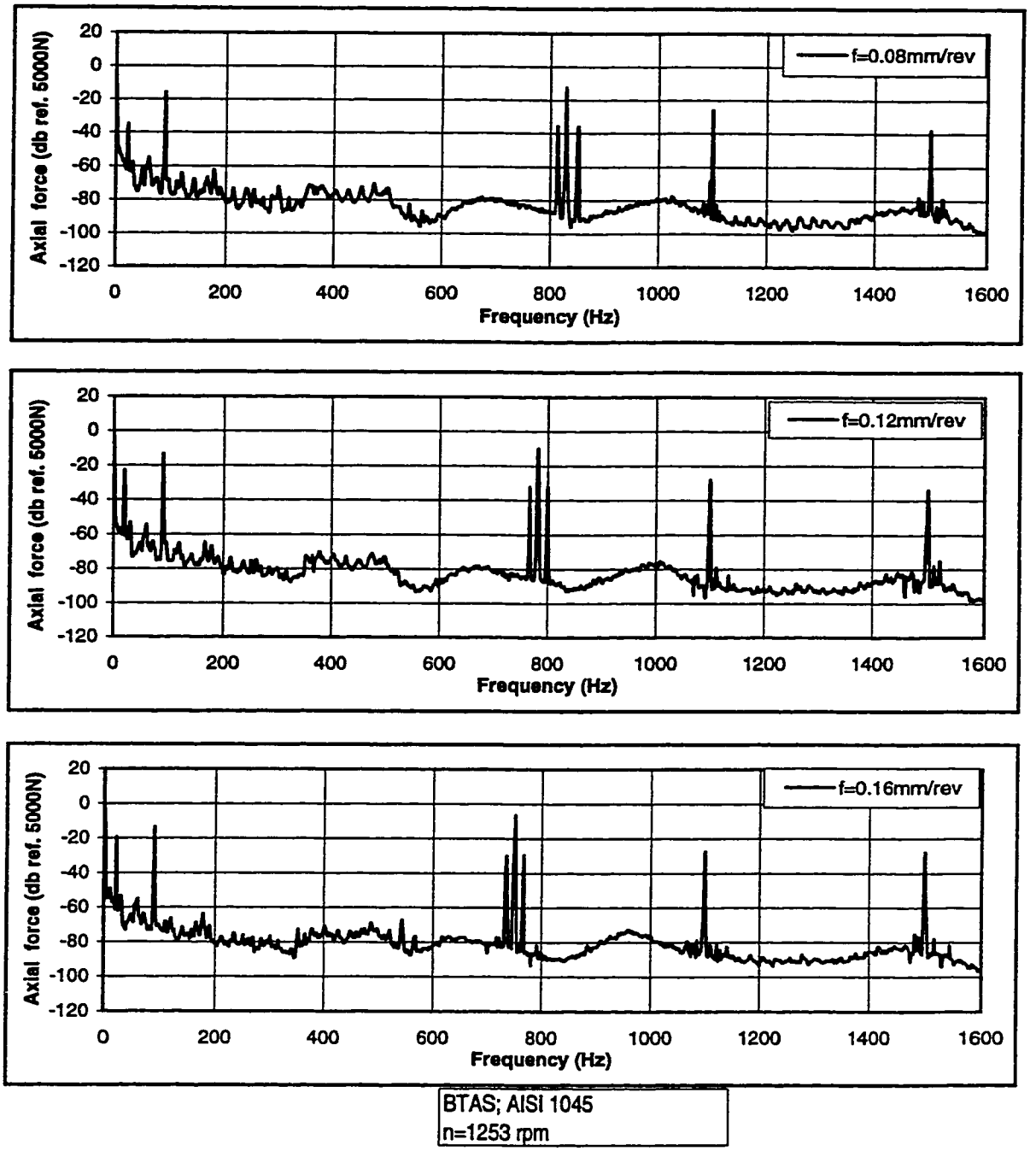

Figure 9.67: Autospectra of the axial cutting force. Cutting conditions: workpiece, AISI 1045; tool, BTAS 1" inch diameter ; boring bar length, 2.0 m; spindle rotational speed n, 1253 rpm; misalignment, 15µm; cutting fluid flow rate, 80 l/min.

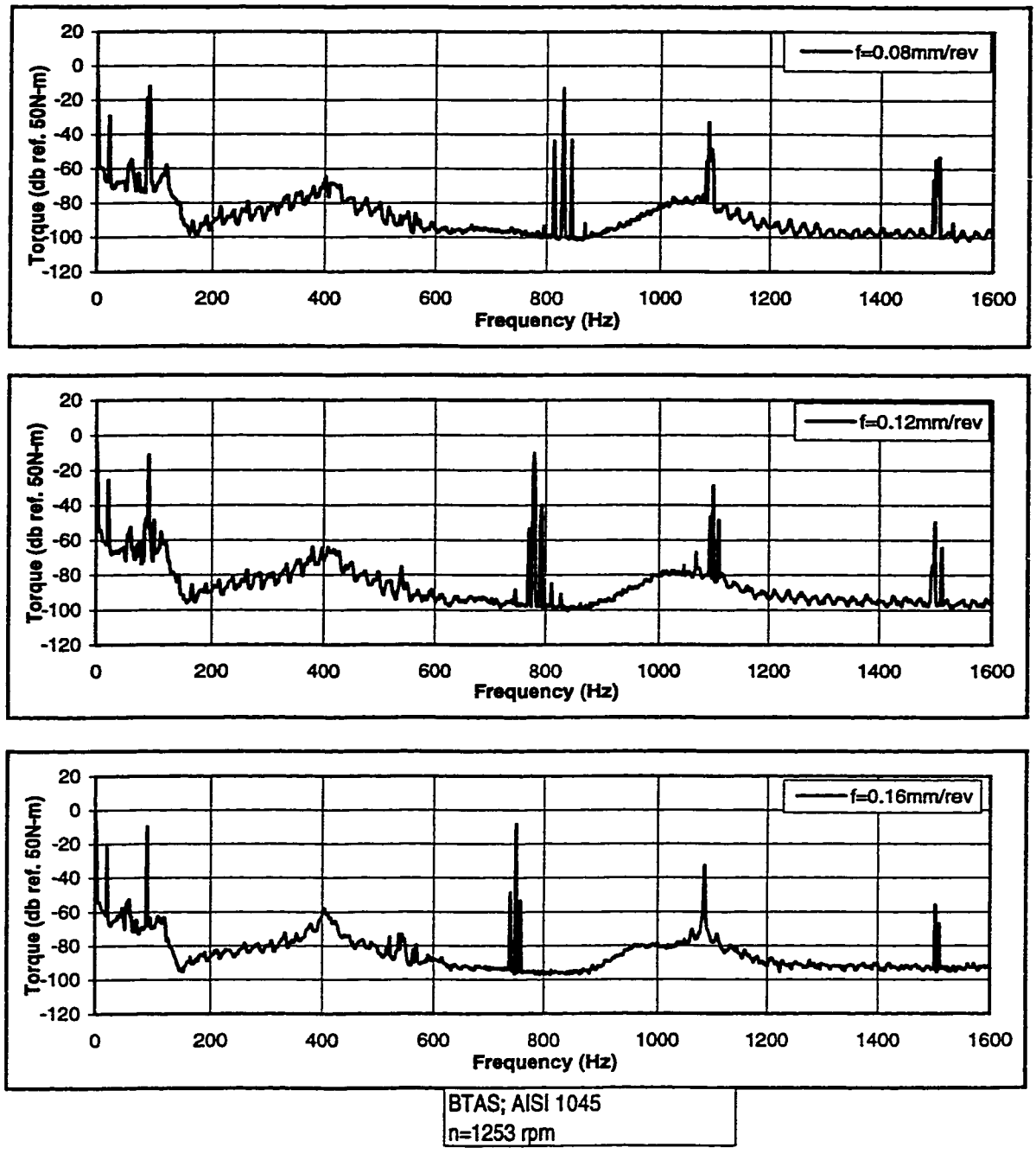

Figure 9.68: Autospectra of the cutting torque. Cutting conditions: workpiece, AISI 1045; tool, BTAS 1" inch diameter ; boring bar length, 2.0 m; spindle rotational speed n, 1253 rpm; misalignment, 15µm; cutting fluid flow rate, 80 l/min.

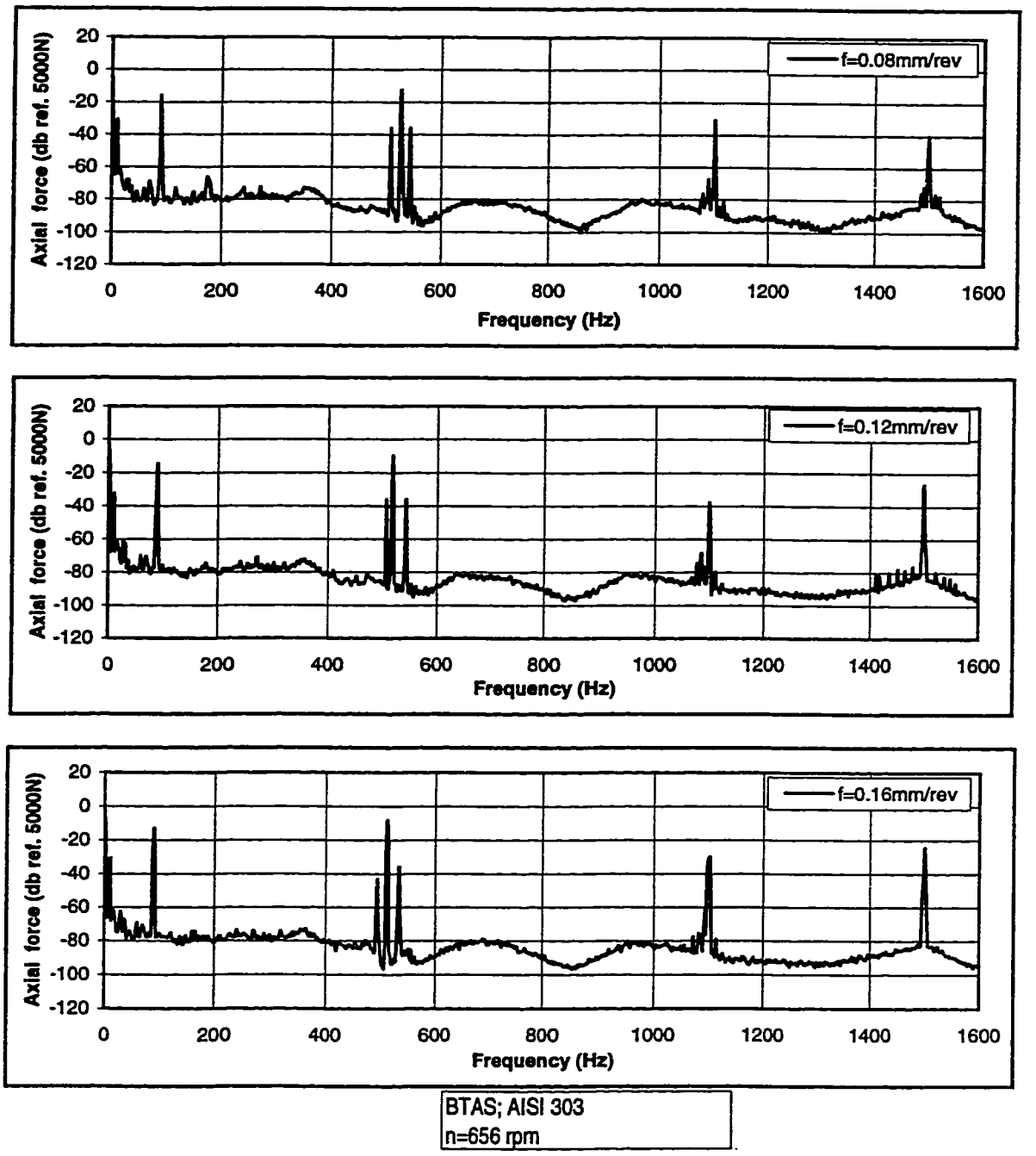

Figure 9.69: Autospectra of the axial cutting force. Cutting conditions: workpiece, AISI 303; tool, BTAS 1" inch diameter ; boring bar length, 2.0 m; spindle rotational speed n, 656 rpm; misalignment, 15µm; cutting fluid flow rate, 80 l/min.

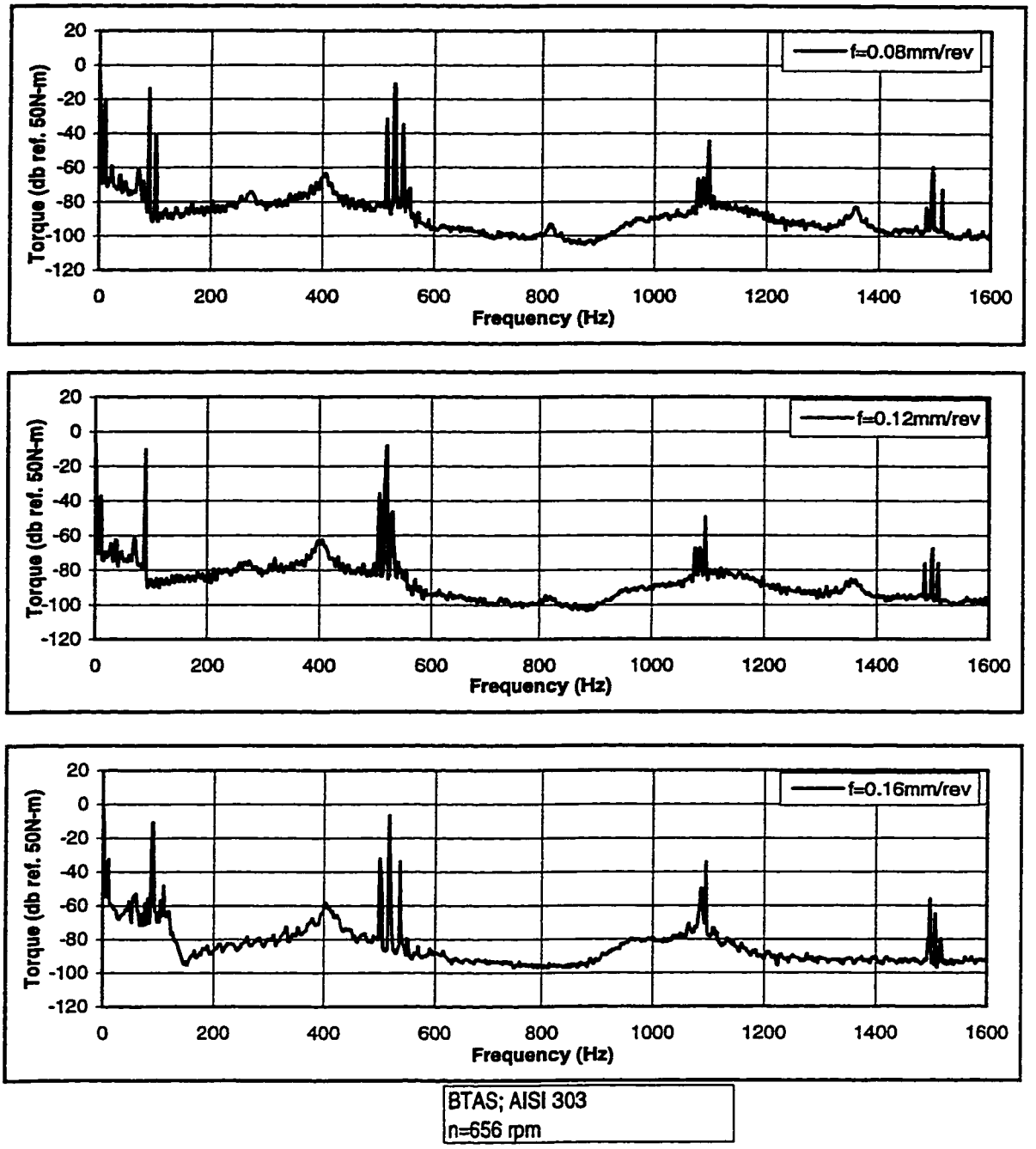

Figure 9.70: Autospectra of the cutting torque. Cutting conditions: workpiece, AISI 303; tool, BTAS 1" inch diameter ; boring bar length, 2.0 m; spindle rotational speed n, 656 rpm; misalignment, 15µm; cutting fluid flow rate, 80 l/min.

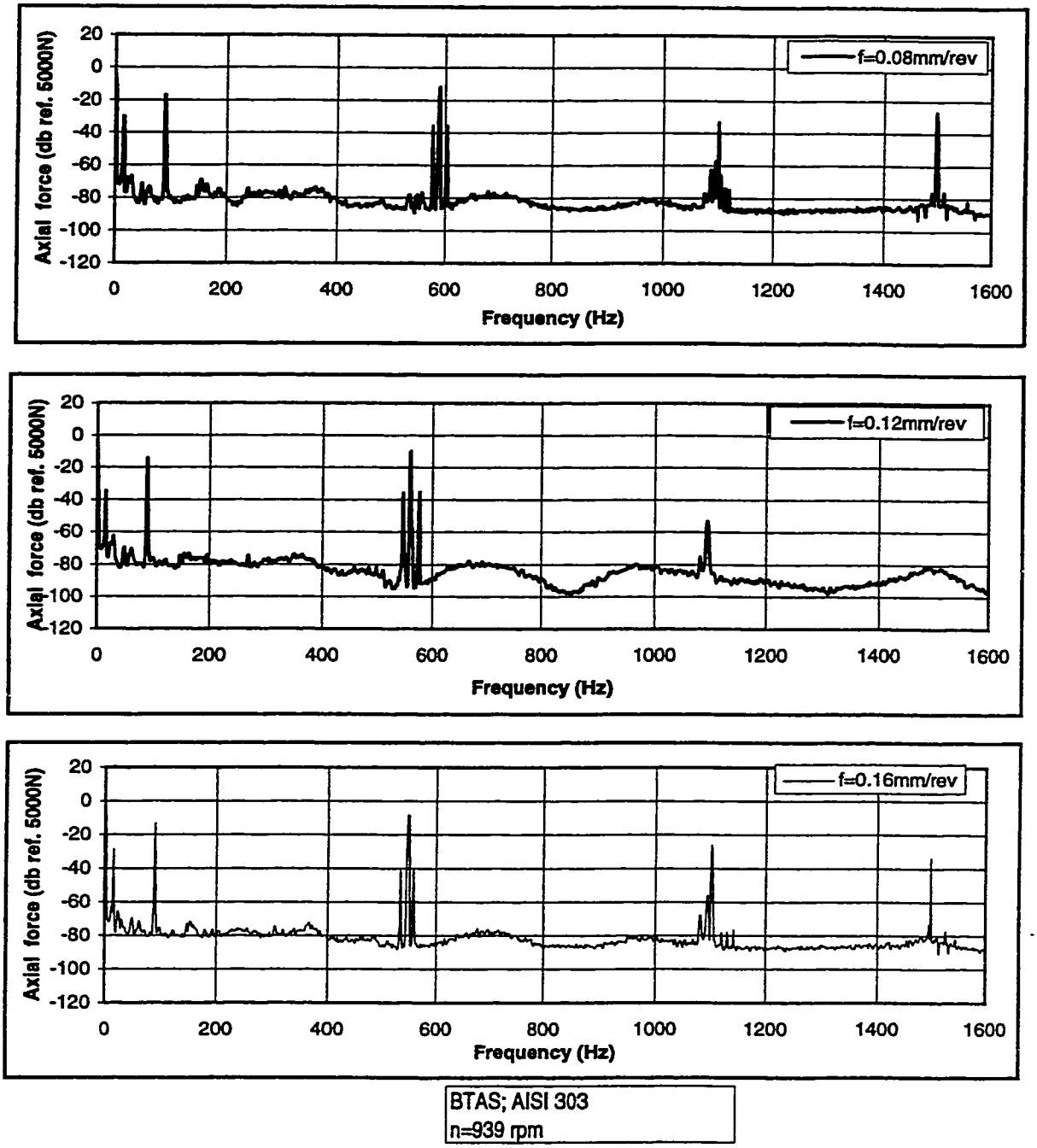

Figure 9.71: Autospectra of the axial cutting force. Cutting conditions: workpiece, AISI 303; tool, BTAS 1" inch diameter ; boring bar length, 2.0 m; spindle rotational speed n, 939 rpm; misalignment, 15µm; cutting fluid flow rate, 80 l/min.

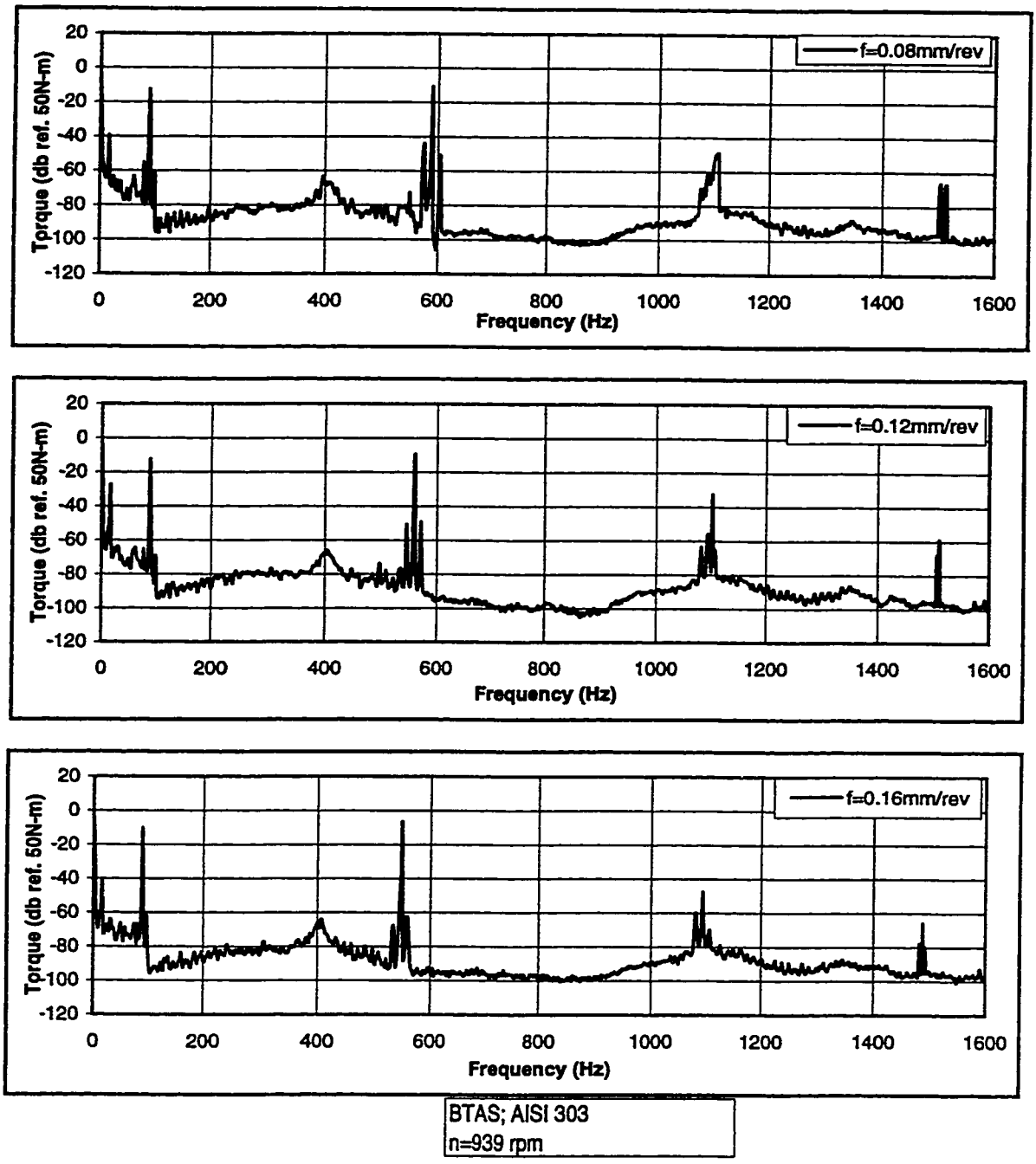

Figure 9.72: Autospectra of the cutting torque. Cutting conditions: workpiece, AISI 303; tool, BTAS 1" inch diameter ; boring bar length, 2.0 m; spindle rotational speed n, 939 rpm; misalignment, 15µm; cutting fluid flow rate, 80 l/min.

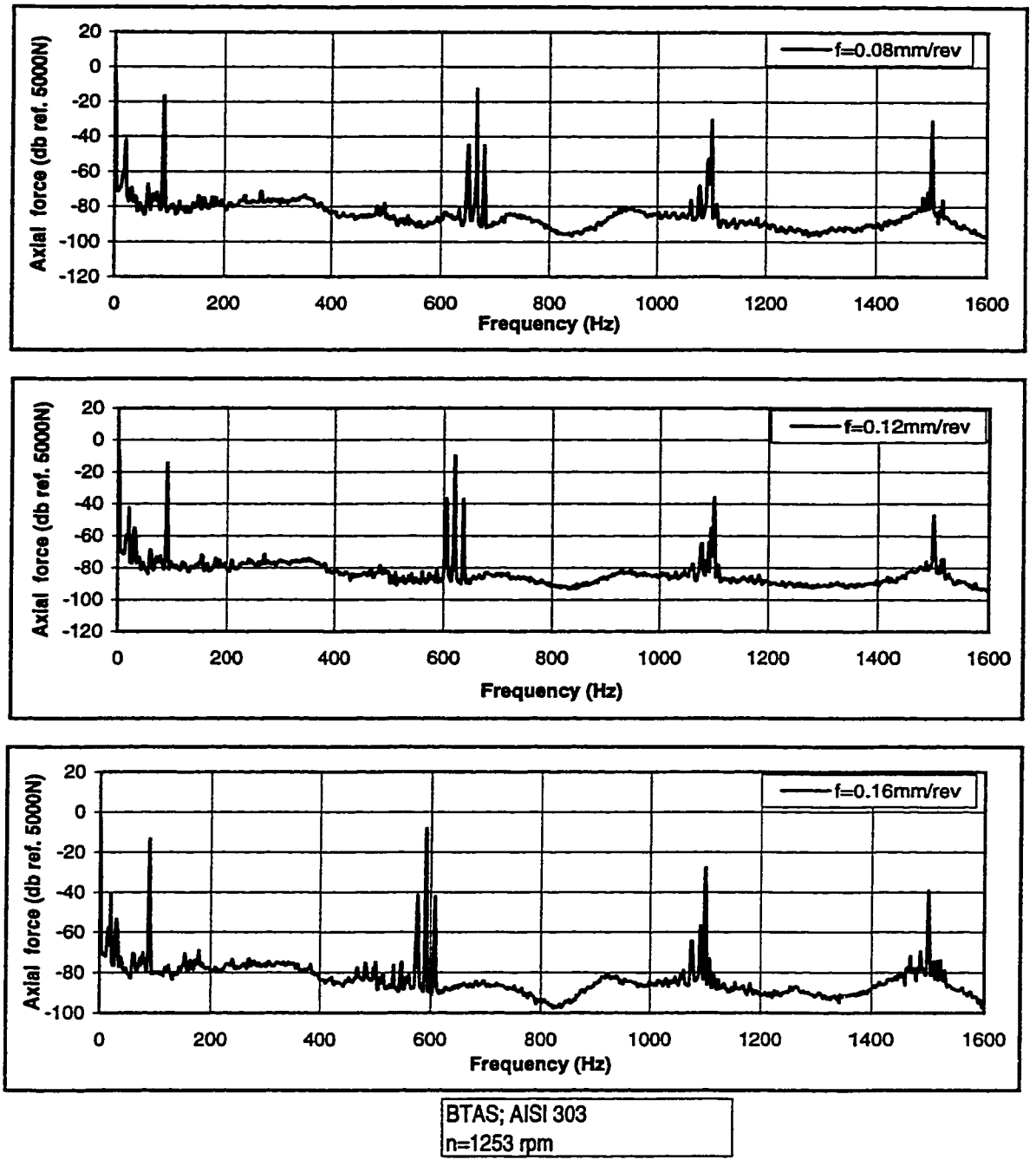

Figure 9.73: Autospectra of the axial cutting force. Cutting conditions: workpiece, AISI 303; tool, BTAS 1" inch diameter ; boring bar length, 2.0 m; spindle rotational speed n, 1253 rpm; misalignment, 15µm; cutting fluid flow rate, 80 l/min.

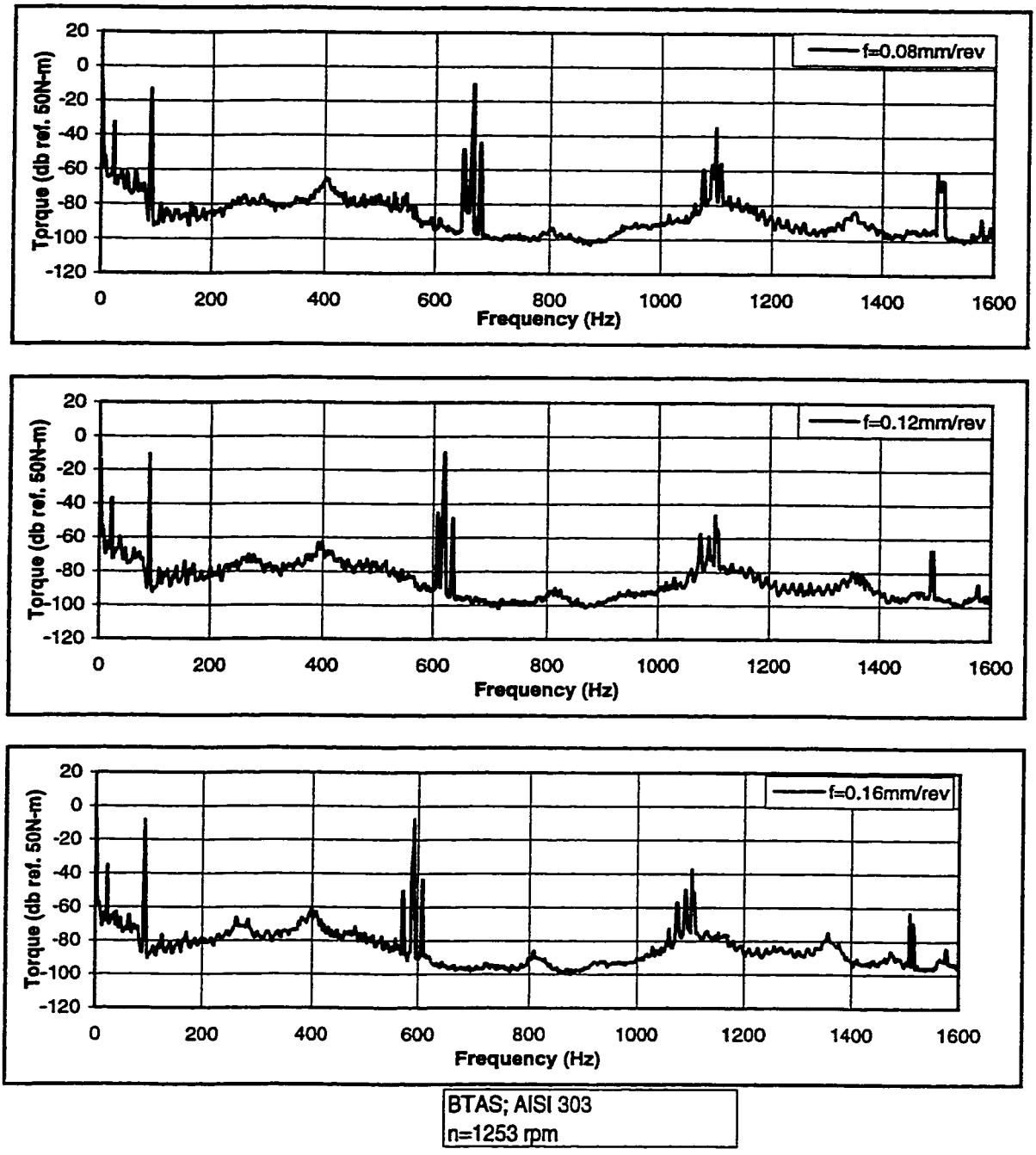

Figure 9.74: Autospectra of the cutting torque. Cutting conditions: workpiece, AISI 303; tool, BTAS 1" inch diameter ; boring bar length, 2.0 m; spindle rotational speed n, 1253 rpm; misalignment, 15µm; cutting fluid flow rate, 80 l/min.

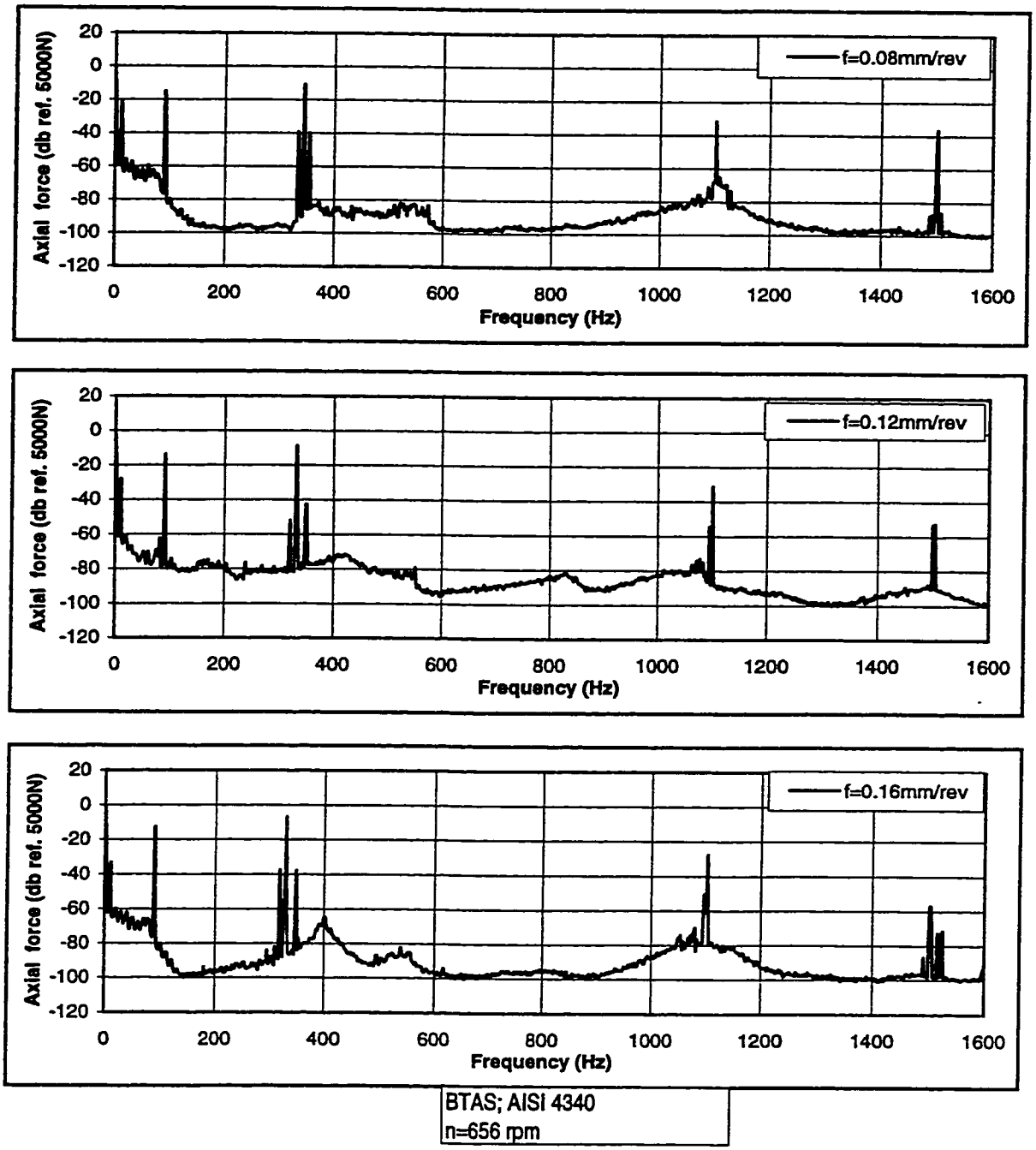

Figure 9.75: Autospectra of the axial cutting force. Cutting conditions: workpiece, AISI 4340; tool, BTAS 1" inch diameter ; boring bar length, 2.0 m; spindle rotational speed n, 656 rpm; misalignment, 15µm; cutting fluid flow rate, 80 l/min.

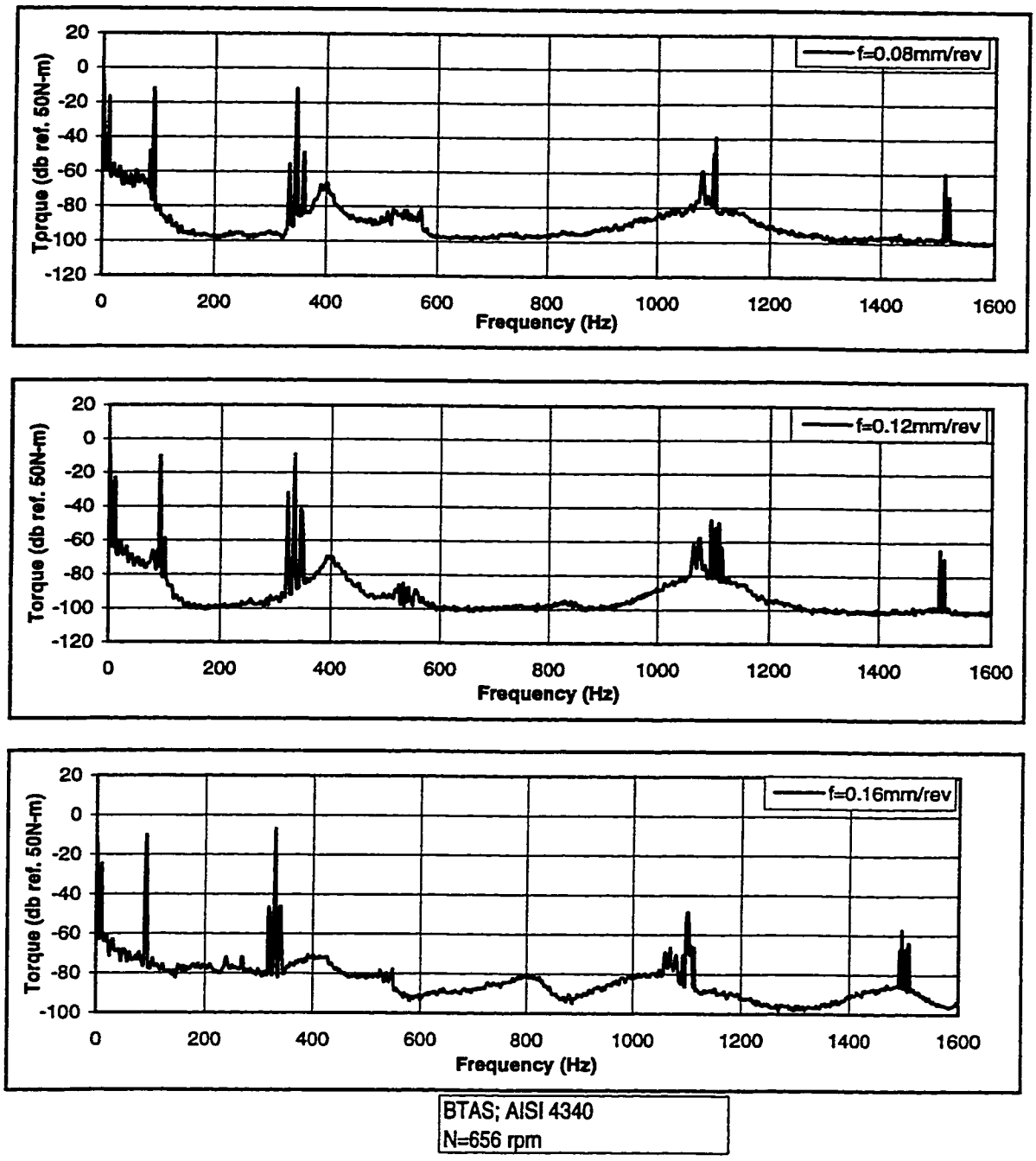

Figure 9.76: Autospectra of the cutting torque. Cutting conditions: workpiece, AISI 4340; tool, BTAS 1" inch diameter ; boring bar length, 2.0 m; spindle rotational speed n, 656 rpm; misalignment, 15µm; cutting fluid flow rate, 80 l/min.

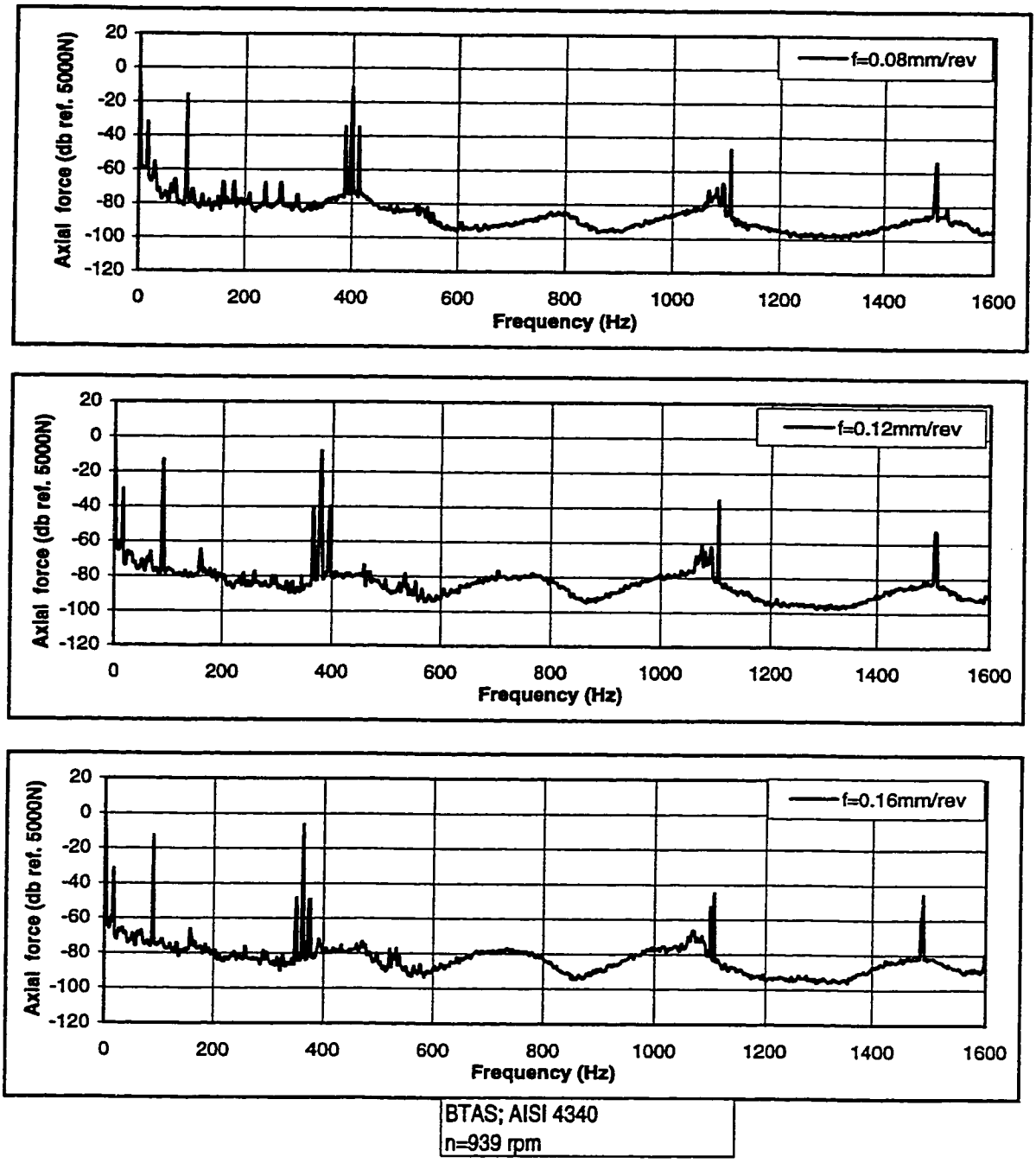

Figure 9.77: Autospectra of the axial cutting force. Cutting conditions: workpiece, AISI 4340; tool, BTAS 1" inch diameter ; boring bar length, 2.0 m; spindle rotational speed n, 939 rpm; misalignment, 15µm; cutting fluid flow rate, 80 l/min.

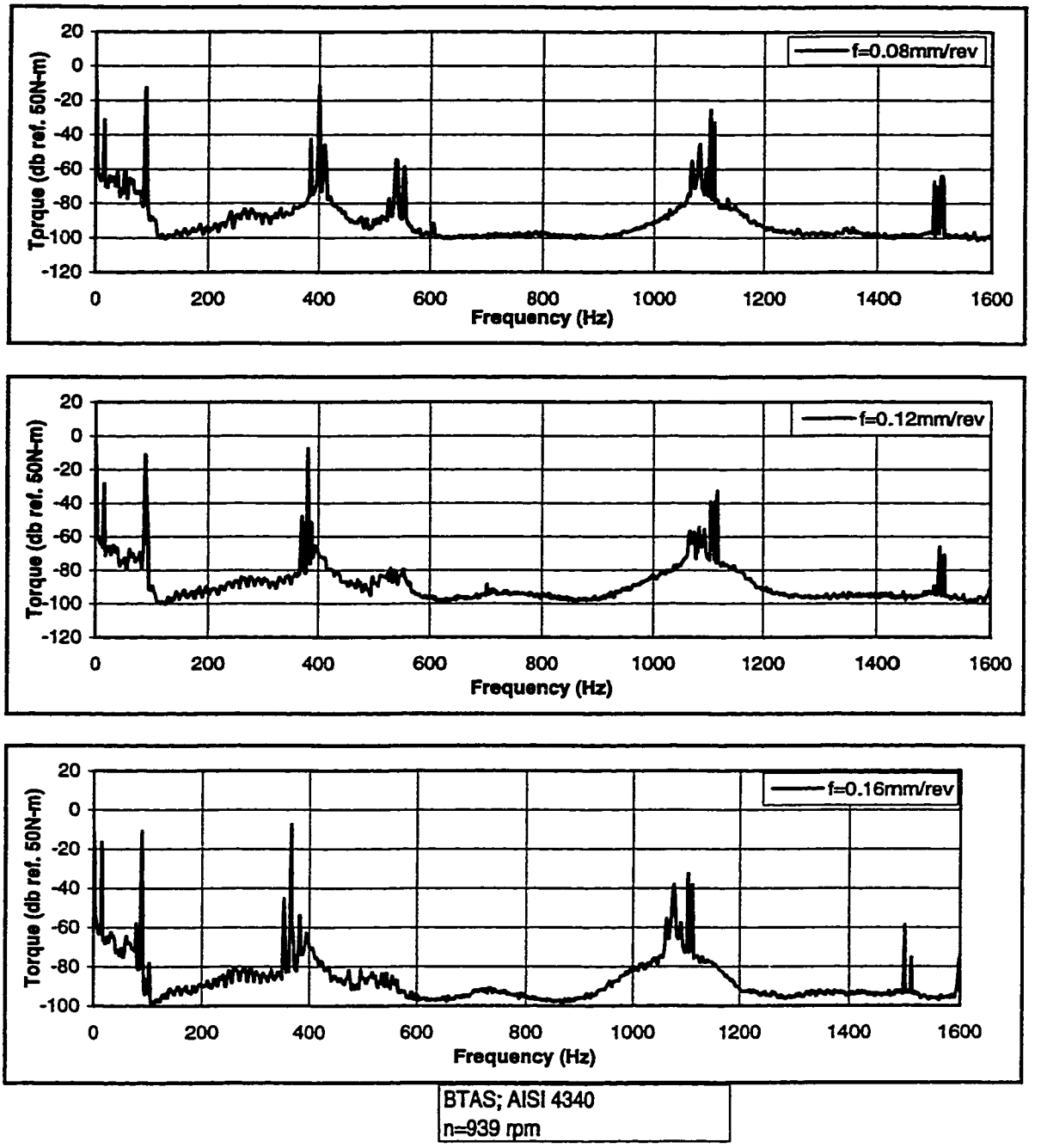

Figure 9.78: Autospectra of the cutting torque. Cutting conditions: workpiece, AISI 4340; tool, BTAS 1" inch diameter ; boring bar length, 2.0 m; spindle rotational speed n, 939 rpm; misalignment, 15μm; cutting fluid flow rate, 80 l/min.

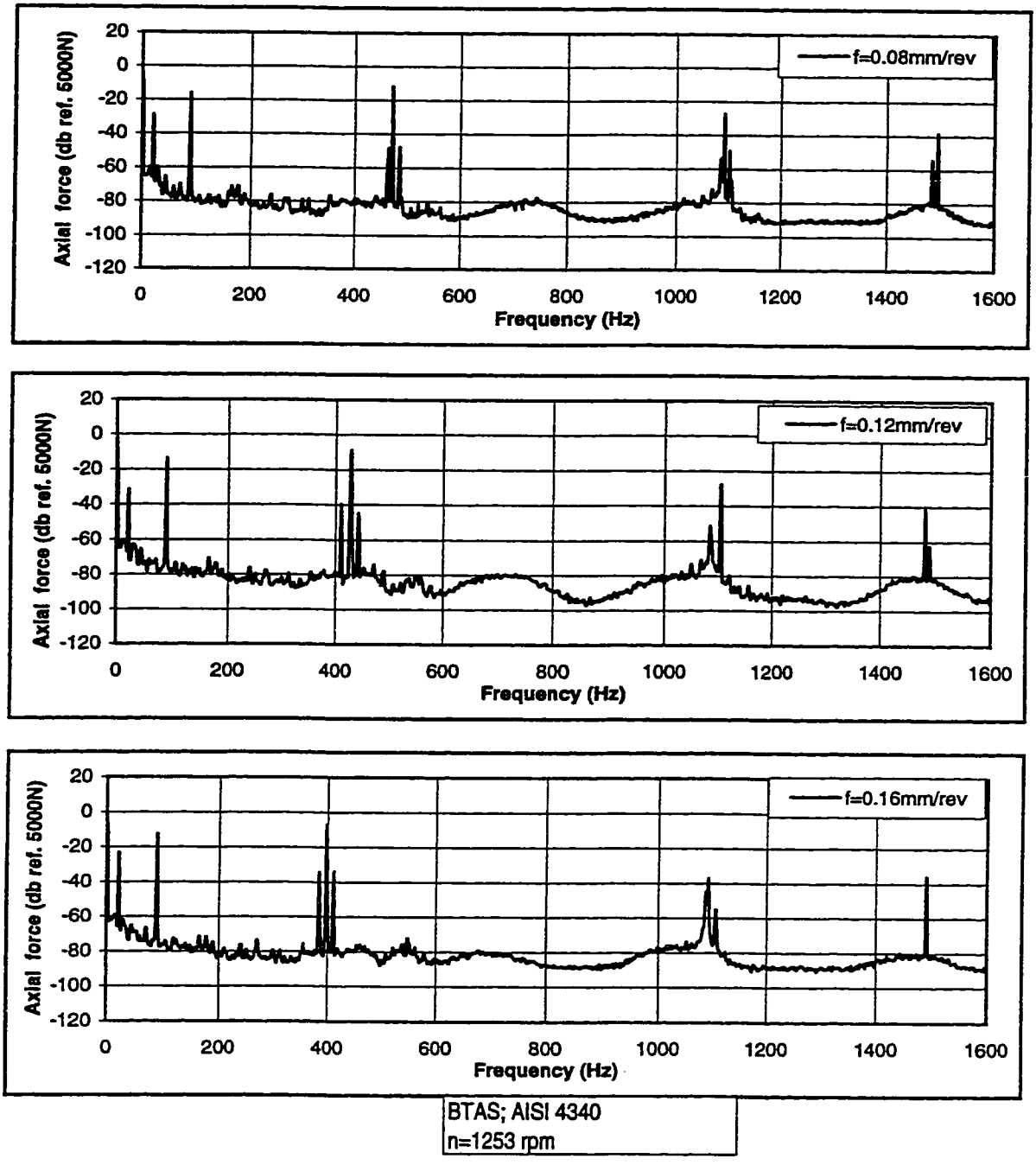

Figure 9.79: Autospectra of the axial cutting force. Cutting conditions: workpiece, AISI 4340; tool, BTAS 1" inch diameter ; boring bar length, 2.0 m; spindle rotational speed n, 1253 rpm; misalignment, 15μm; cutting fluid flow rate, 80 l/min.

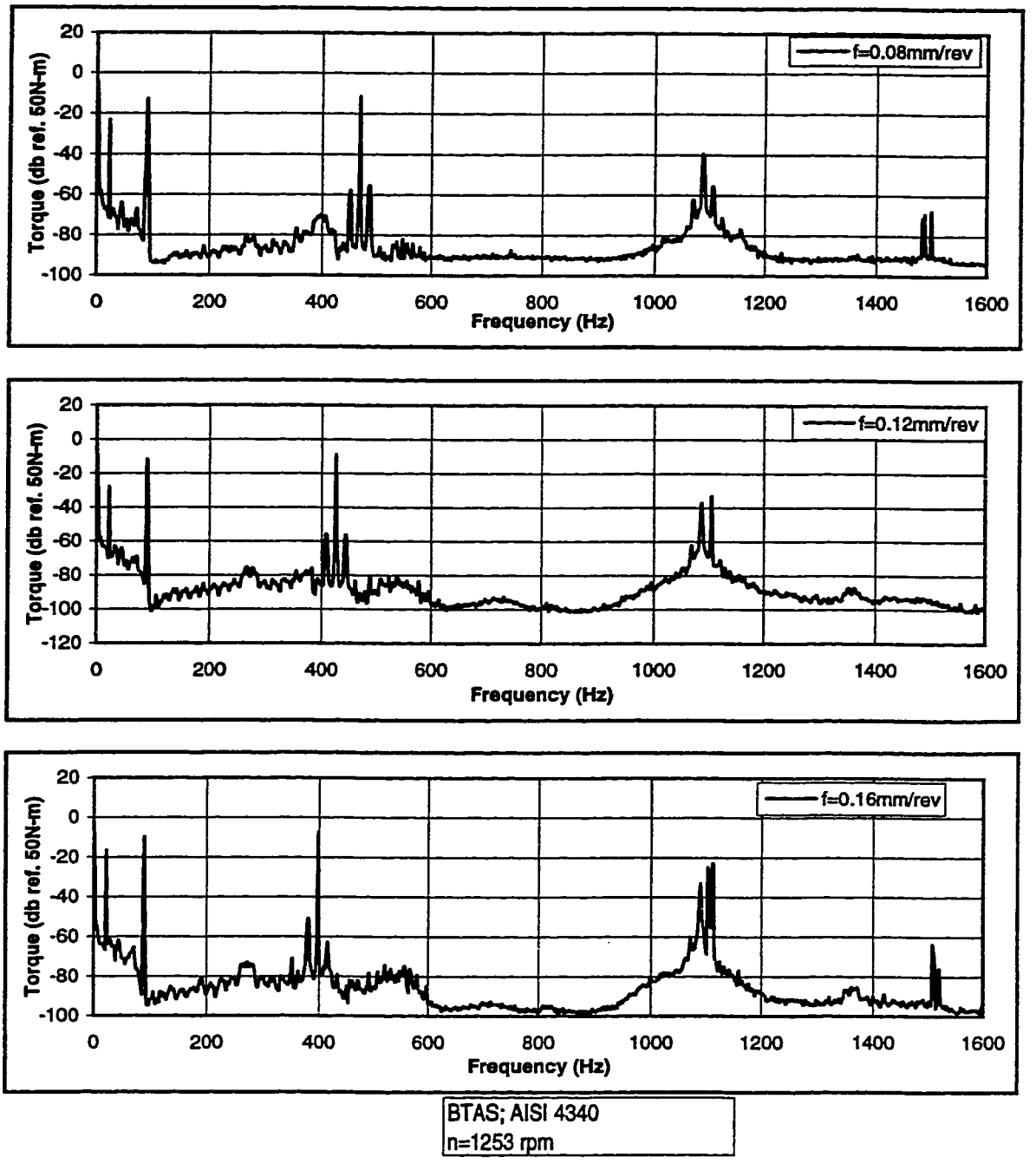

Figure 9.80: Autospectra of the cutting torque. Cutting conditions: workpiece, AISI 4340; tool, BTAS 1" inch diameter ; boring bar length, 2.0 m; spindle rotational speed n, 1253 rpm; misalignment, 15µm; cutting fluid flow rate, 80 l/min.

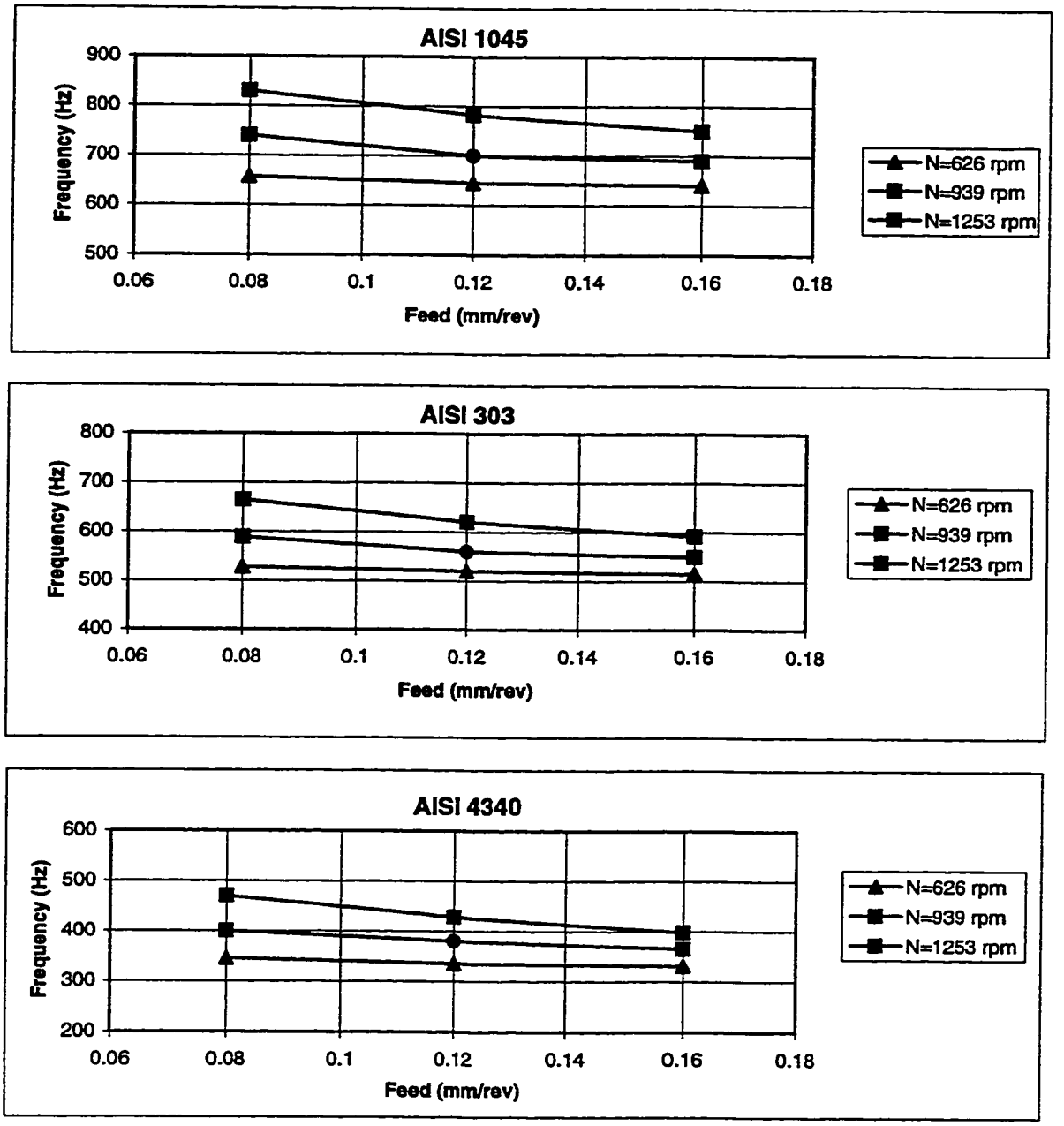

Figure 9.81: Effect of cutting feed on the cutting signatures. Cutting conditions: tool, BTAS and BTAH 1" inch diameter ; boring bar length, 2.0 m; misalignment, 15μm; cutting fluid flow rate, 80 l/min.

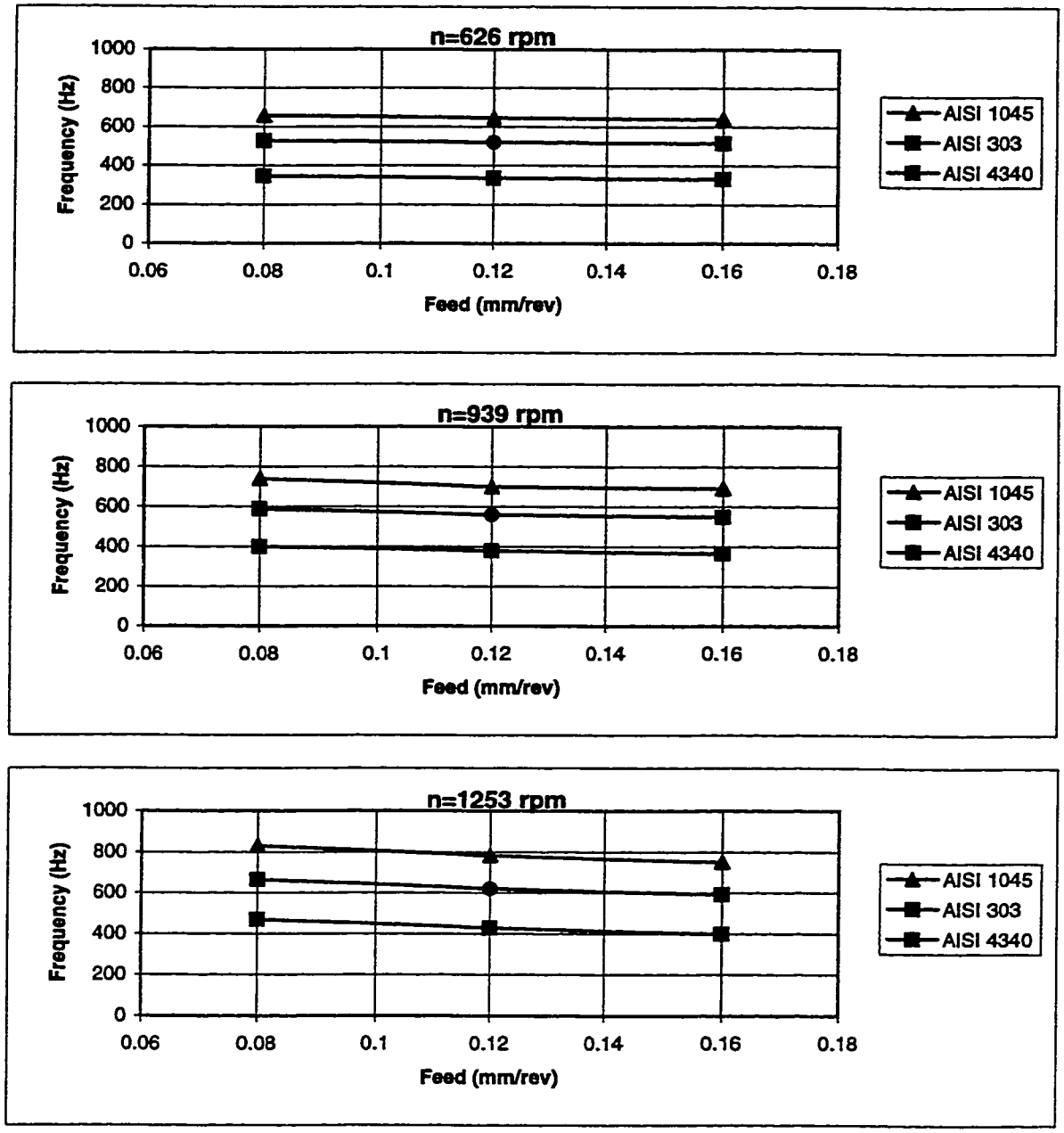

Figure 9.82: Effect of workpiece materials on the cutting signatures. Cutting conditions: tool, BTAS and BTAH 1" inch diameter ; boring bar length, 2.0 m; misalignment, 15μm; cutting fluid flow rate, 80 l/min.

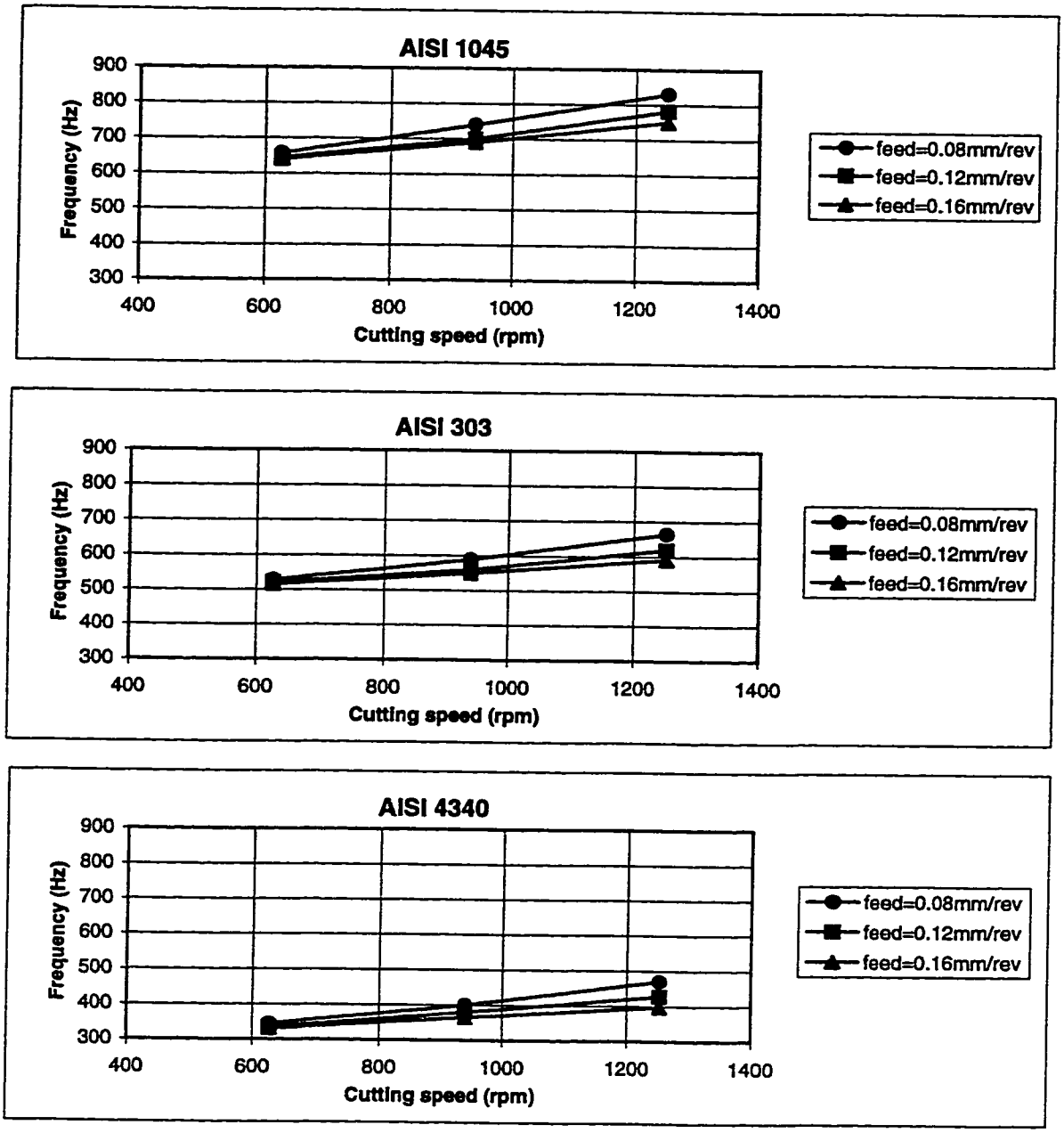

Figure 9.83: Effect of cutting speed on the cutting signatures. Cutting conditions: tool, BTAS and BTAH 1" inch diameter ; boring bar length, 2.0 m; misalignment, 15µm; cutting fluid flow rate, 80 l/min.

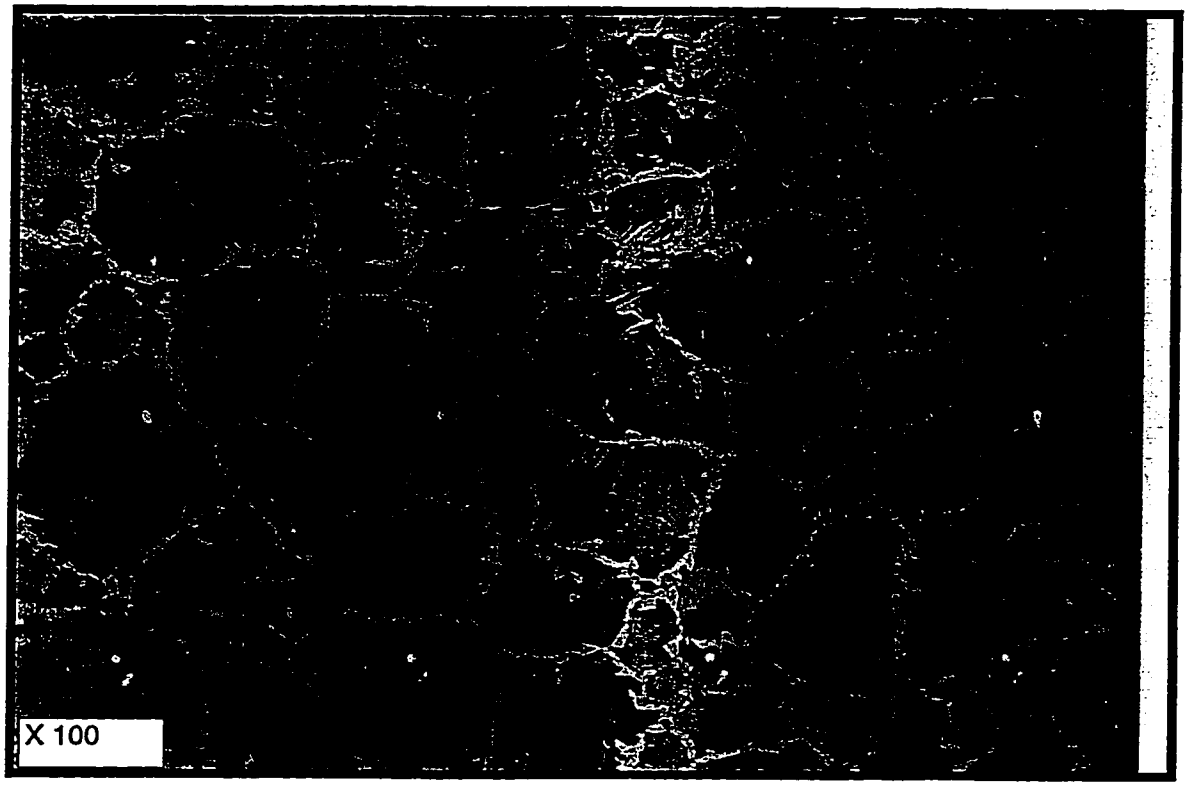

Figure 9.84: Microphotograph of the initial structure of AISI 1045 steel. (mag: 100 X). Etched with 10 mL Nital, 90 ml alcohol. Structure is mainly pearlite grain (gray) with a network of grain boundary ferrite (white).

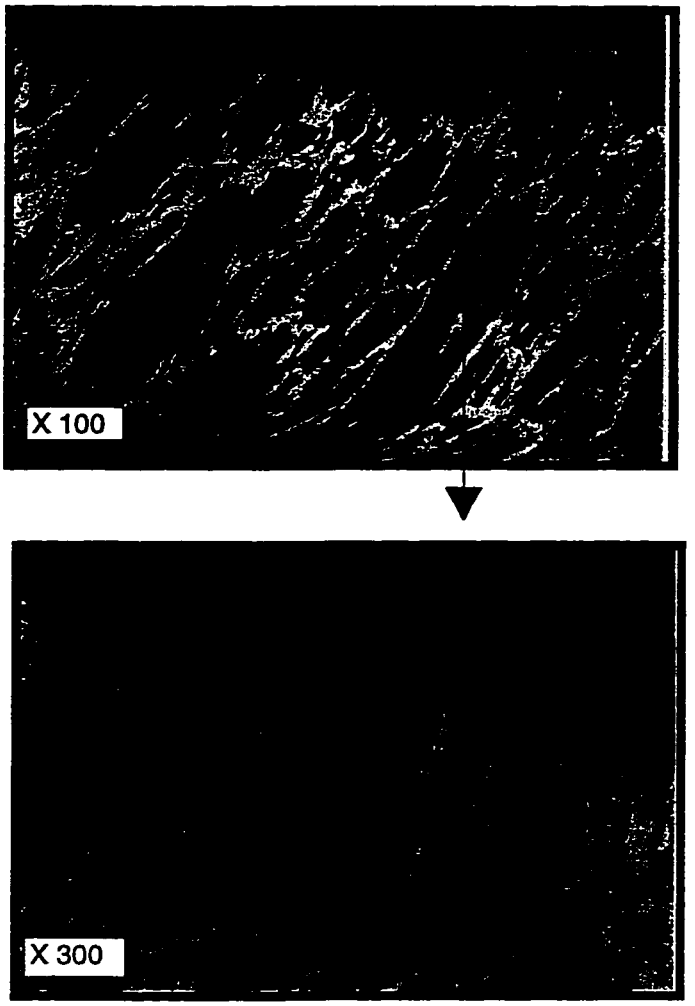

Figure 9.85: Microphotograph of a fully deformed chip of AISI 1045 steel. Cutting condition: tool (rake angle), 0.0; cutting speed v, 57.8 m/min; feed t, 0.2 mm/rev; width of cut b, 5.0 mm. Etched with 10 mL Nital, 90 ml alcohol. Structure reveals a series of sliplines one following another and the grains are elongated in the direction of the deformation.

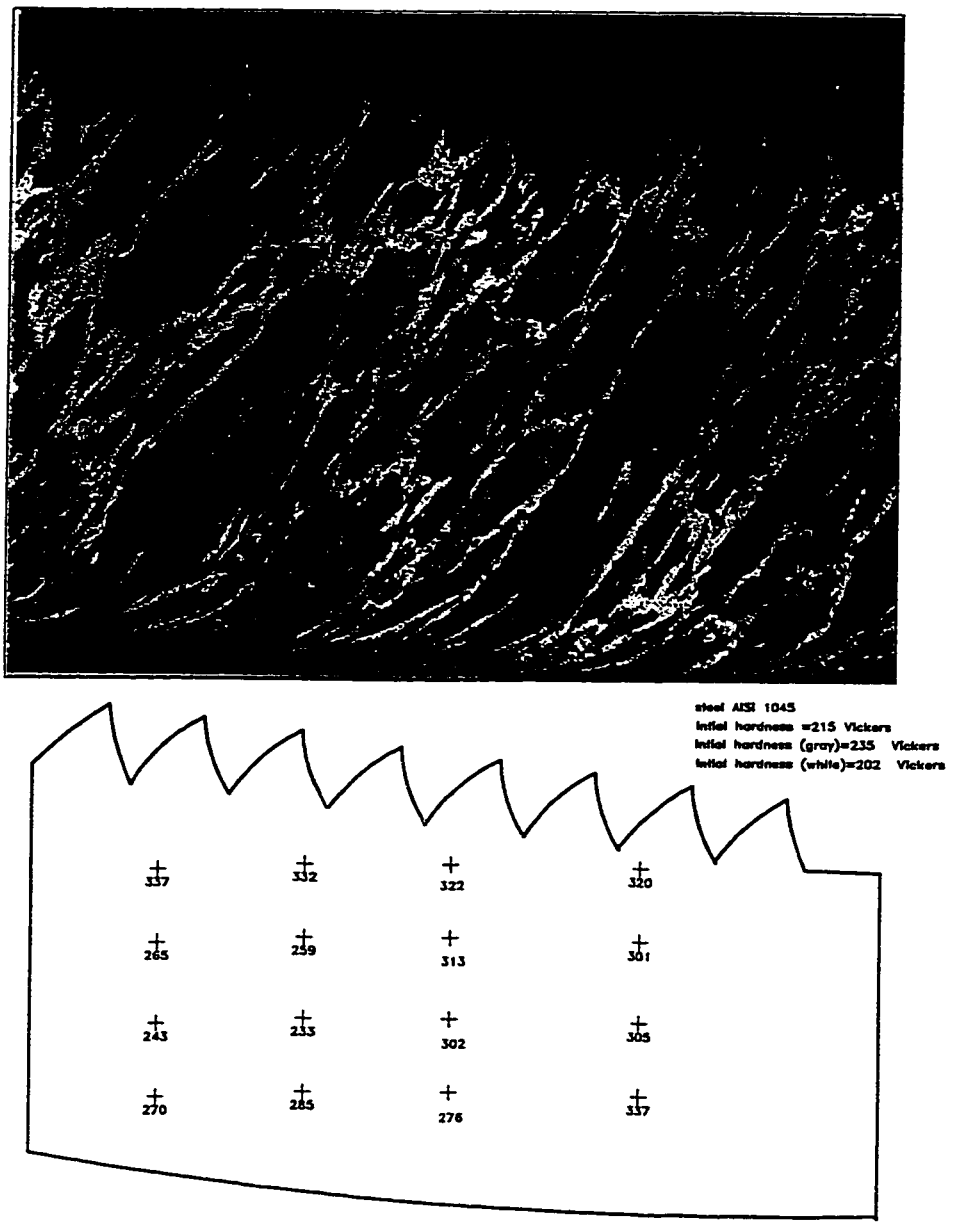

Figure 9.86: Microhardness distribution (Vickers) in a fully deformed chip of AISI 1045 steel. Cutting condition: tool (rake angle), 0.0; cutting speed v, 57.8 m/min; feed t, 0.2 mm/rev; width of cut b, 5.0 mm.

Figure 9.87: Microphotograph of the initial structure of AISI 303 stainless steel (mag: 400 X). Etched with 40 mL hydrofluoric (HF), 20 mL Nitric acid (HNO3), 40 mL glecren. Structure is a matrix of austenite grains bound an intermetallic stringer-type inclusions.

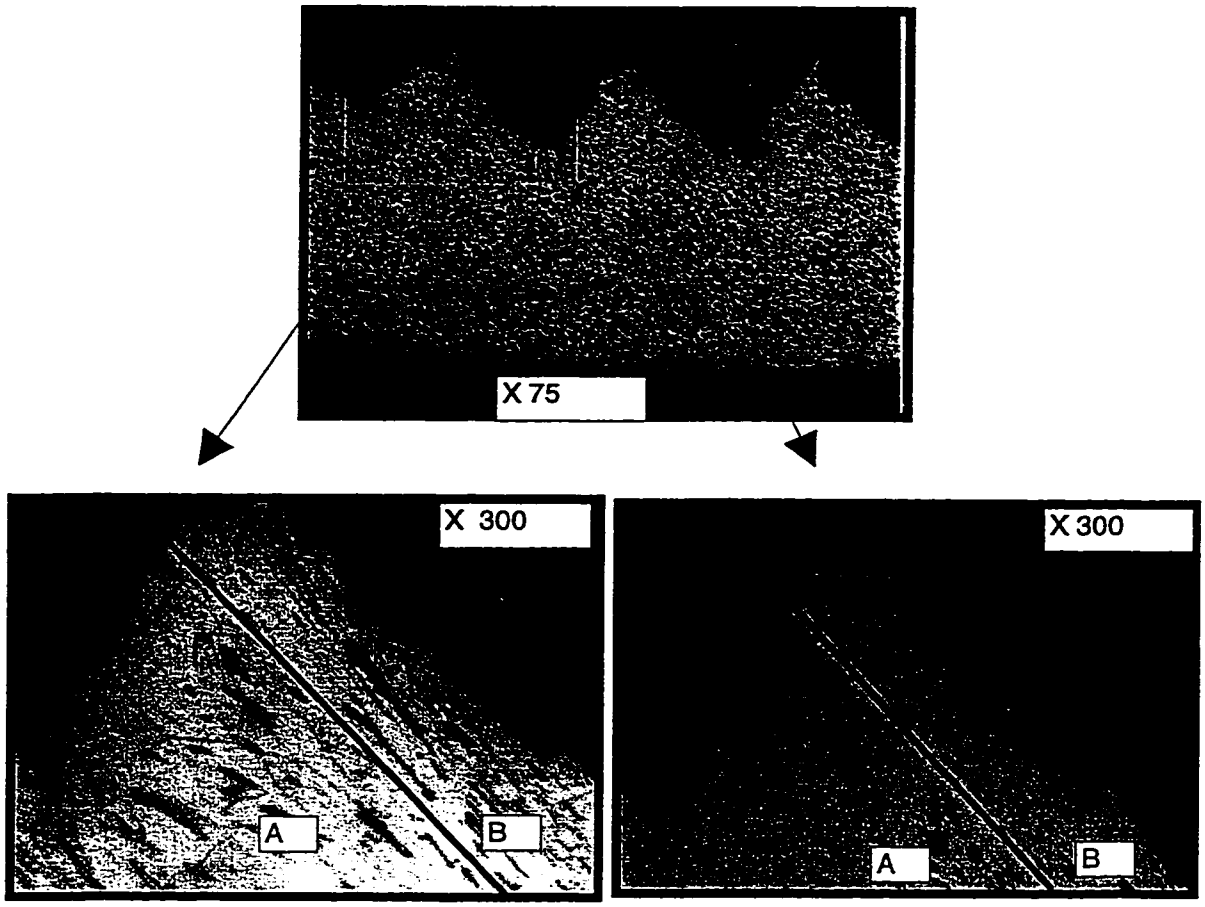

Figure 9.88: Microphotograph of fully deformed chip of AISI 303 stainless steel. Cutting condition: tool (rake angle), 0.0; cutting speed v, 57.8 m/min; feed t, 0.2 mm/rev; width of cut b, 5.0 mm. Etched with 40 mL hydrofluoric (HF), 20 mL Nitric acid (HNO3), 40 mL glecren.

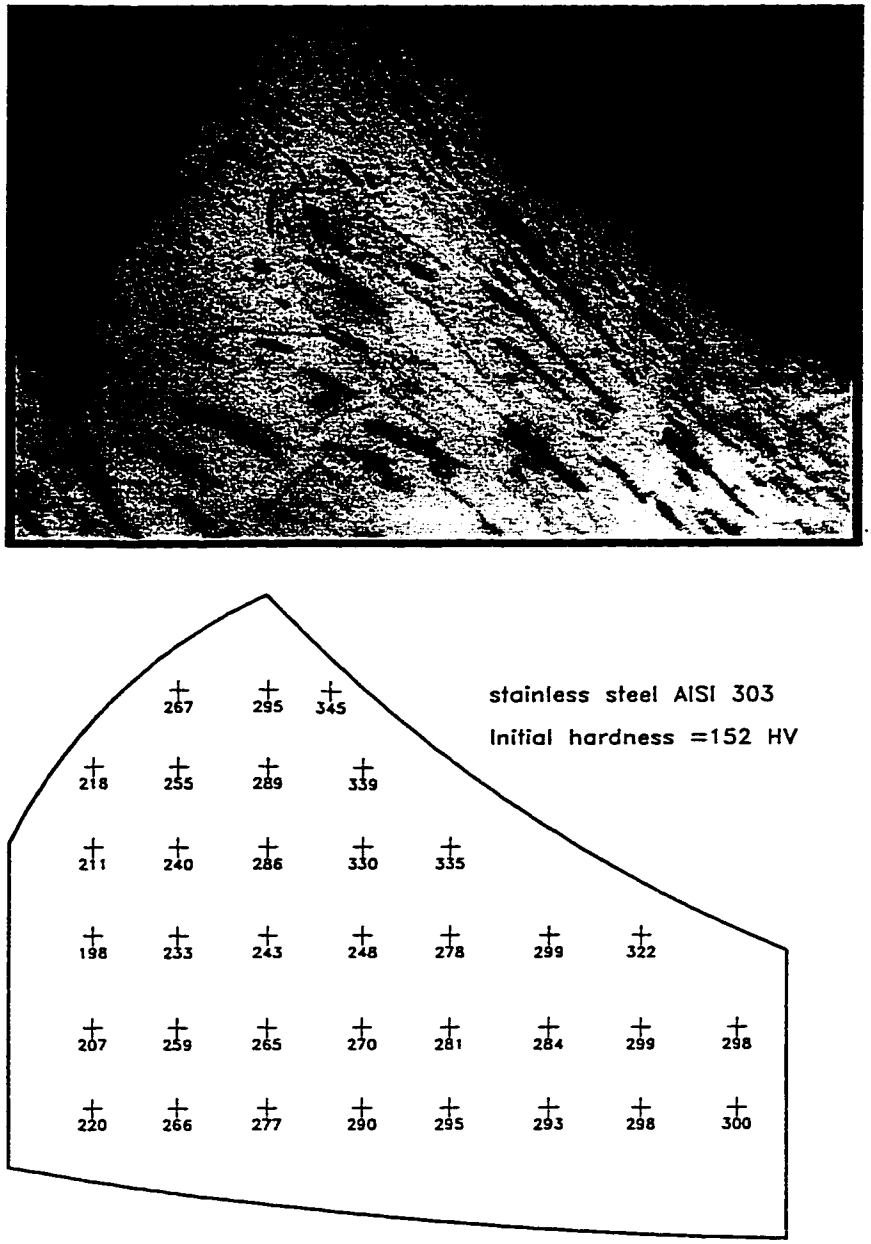

Figure 9.89: Microhardness distribution (Vickers) in a fully deformed chip of AISI 303 steel. Cutting condition: tool (rake angle), 0.0; cutting speed v, 57.8 m/min; feed t, 0.2 mm/rev; width of cut b, 5.0 mm.

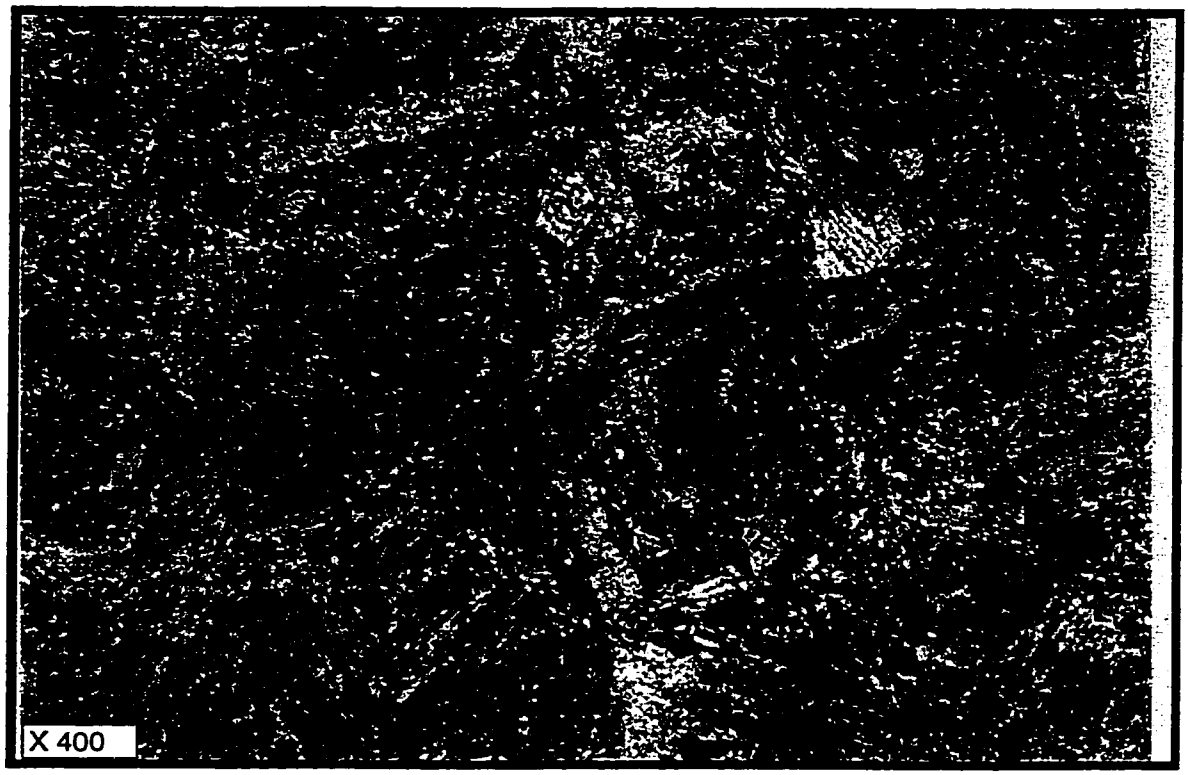

Figure 9.90: Microphotograph of the initial structure of AISI 4340 steel (mag: 400 X). Etched with 10 mL Nital, 90 ml alcohol. Structure is tempered martensite.

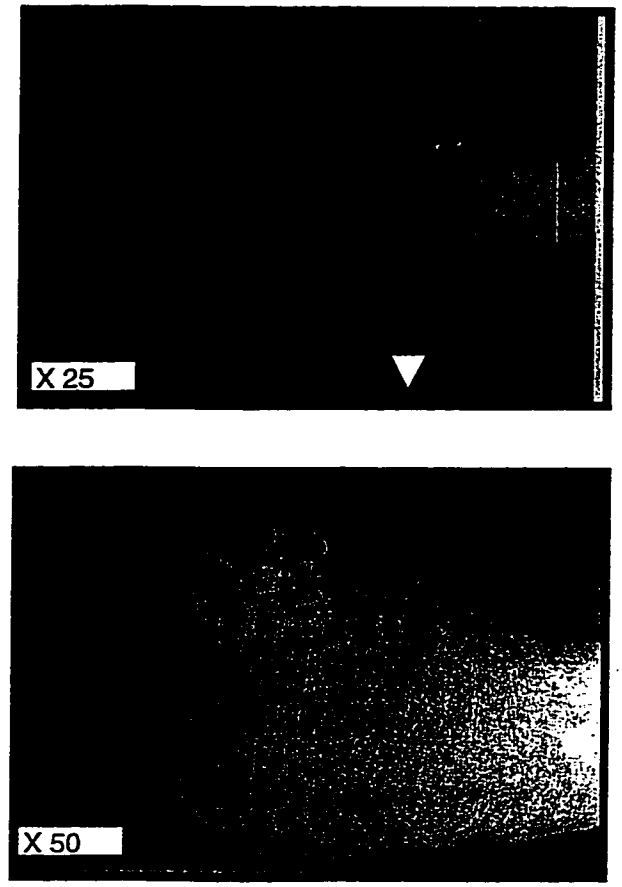

Figure 9.91: Microphotograph of a fully deformed chip AISI 4340 steel (mag: 50 X). Cutting condition: tool (rake angle), 0.0; cutting speed v, 57.8 m/min; feed t, 0.2 mm/rev; width of cut b, 5.0 mm. Etched with 10 mL Nital, 90 ml alcohol.

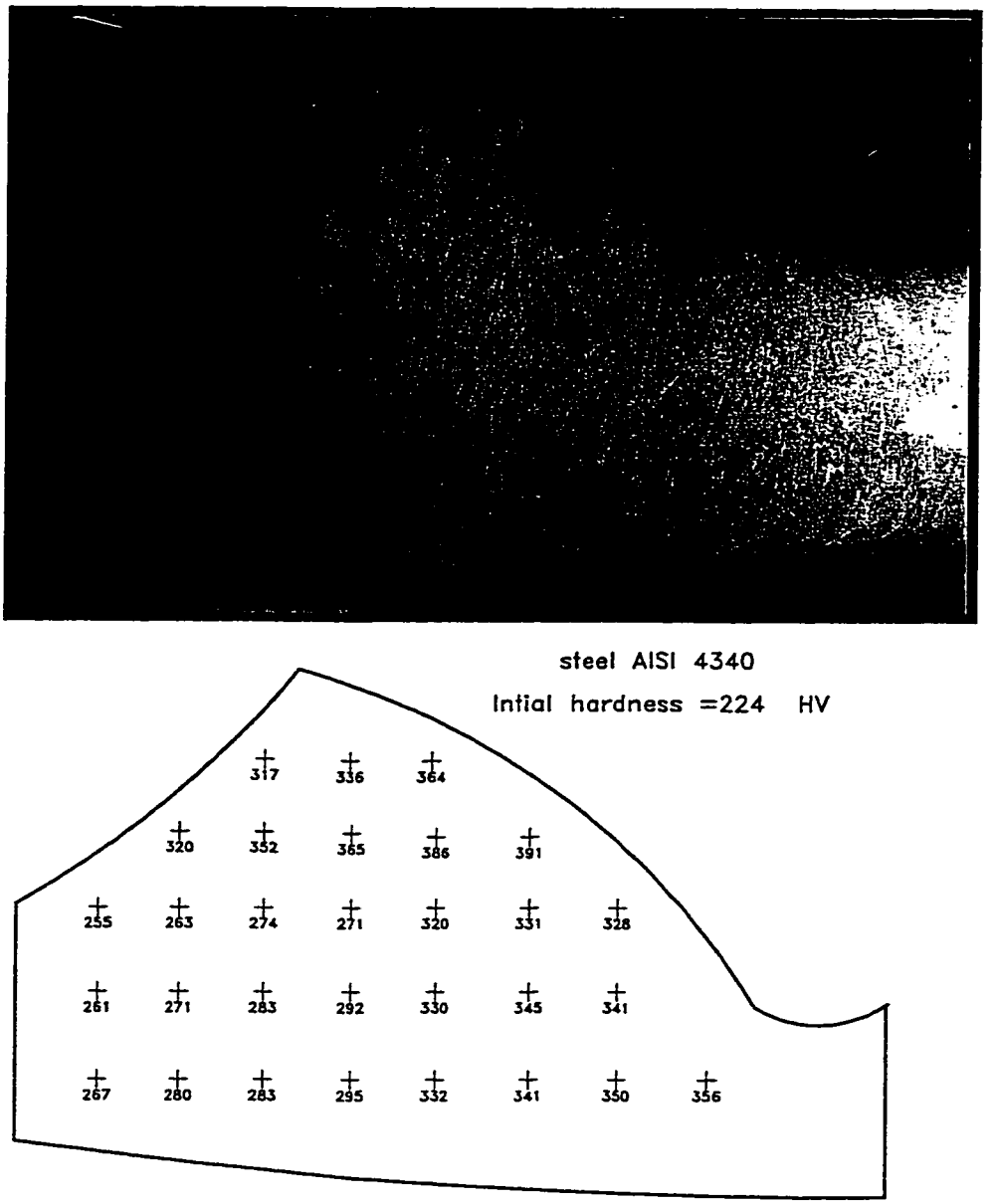

Figure 9.92: Microhardness distribution (Vickers) in a fully deformed chip of AISI 4340 steel. Cutting condition: tool (rake angle) , 0.0; cutting speed v, 57.8 m/min; feed t, 0.2 mm/rev; width of cut b, 5.0 mm.

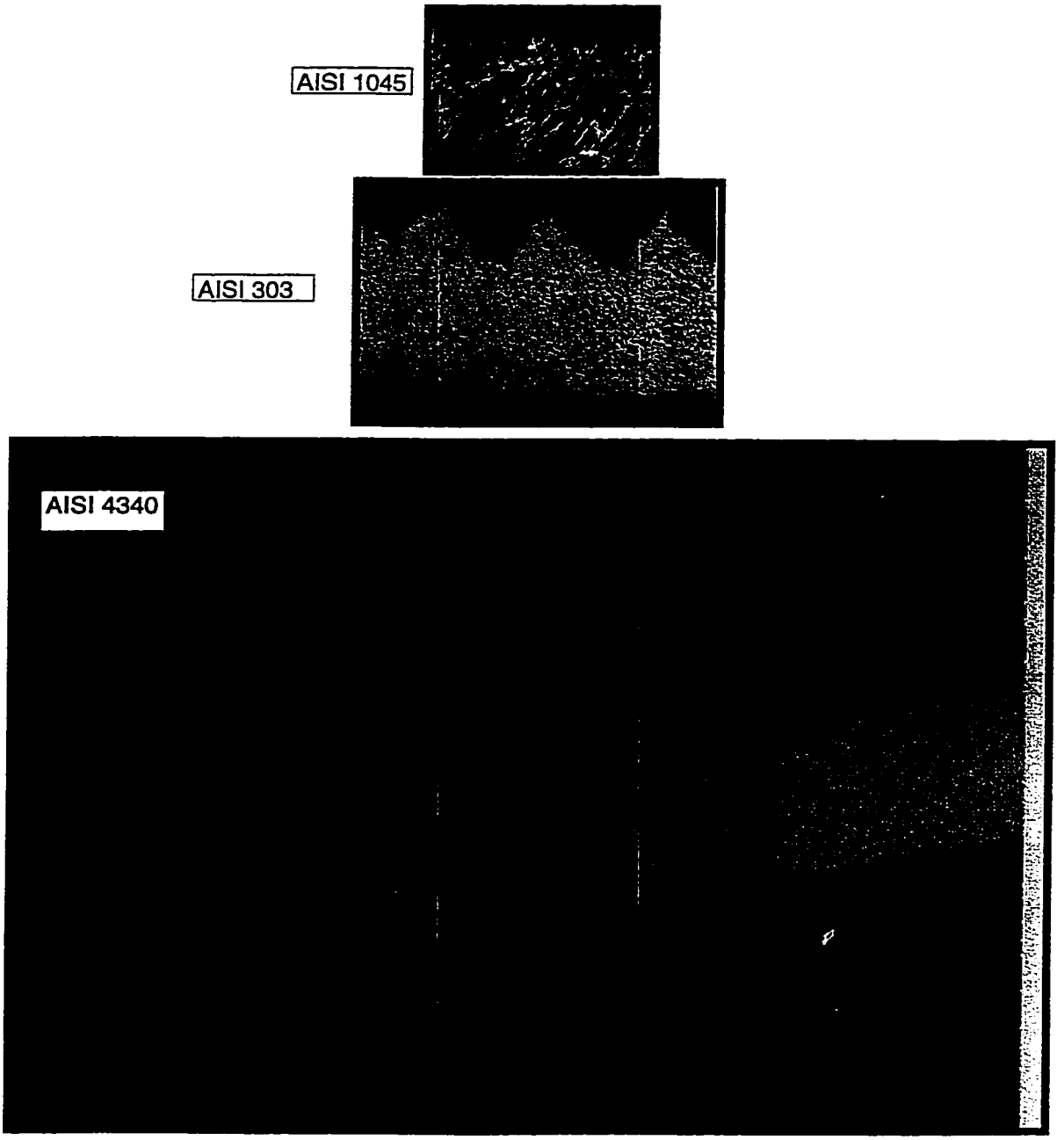

Figure 9.93: Copmarison between the microphotographs of the fully deformed chip of AISI 1045, AISI 303 and AISI 4340 steels(mag : 50). Cutting condition: tool (rake angle), 0.0; cutting speed v, 57.8 m/min; feed t, 0.2 mm/rev; width of cut b, 5.0 mm.

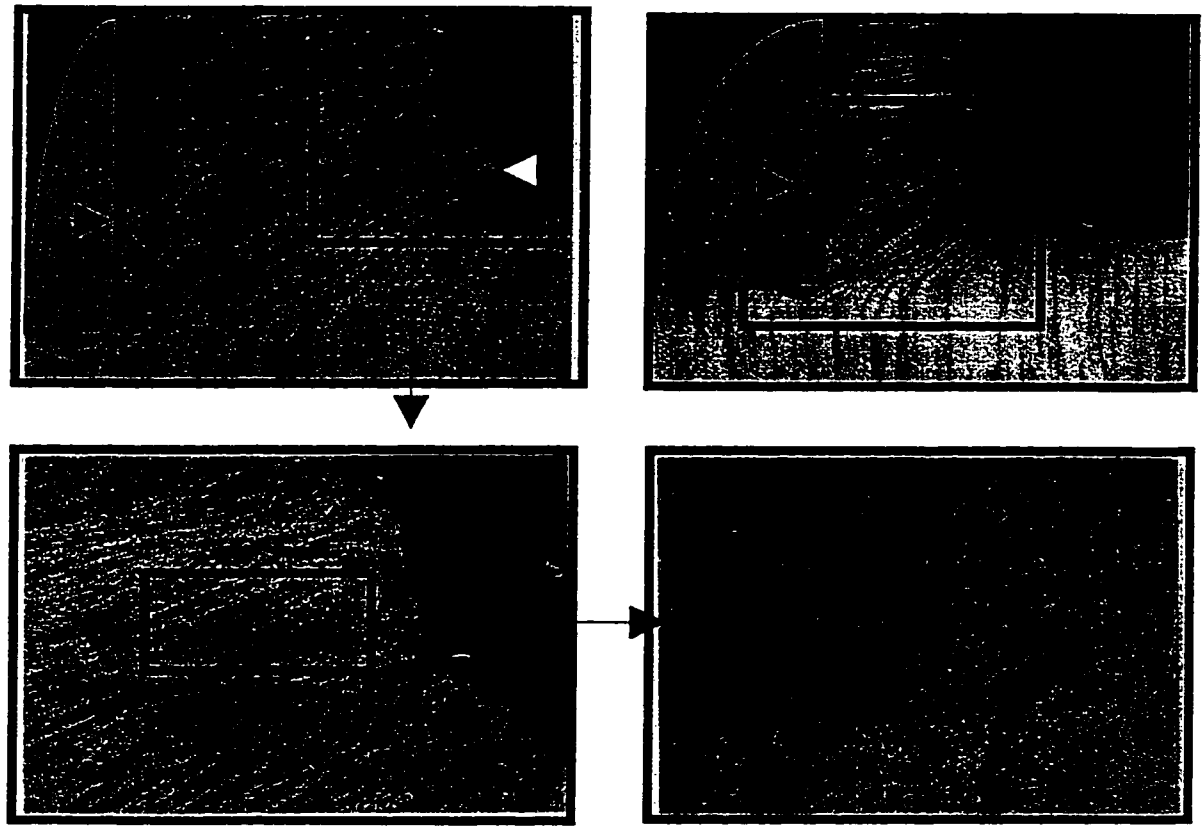

Figure 9.94: Microphotographs of partially formed chip. Cutting condition: workpiece, AISI 4340; tool , BTAH 1" inch diameter; spindle rotational speed n, 1000rpm; feed t, 0.1 mm/rev; Etched with 10 mL Nital, 90 ml alcohol.

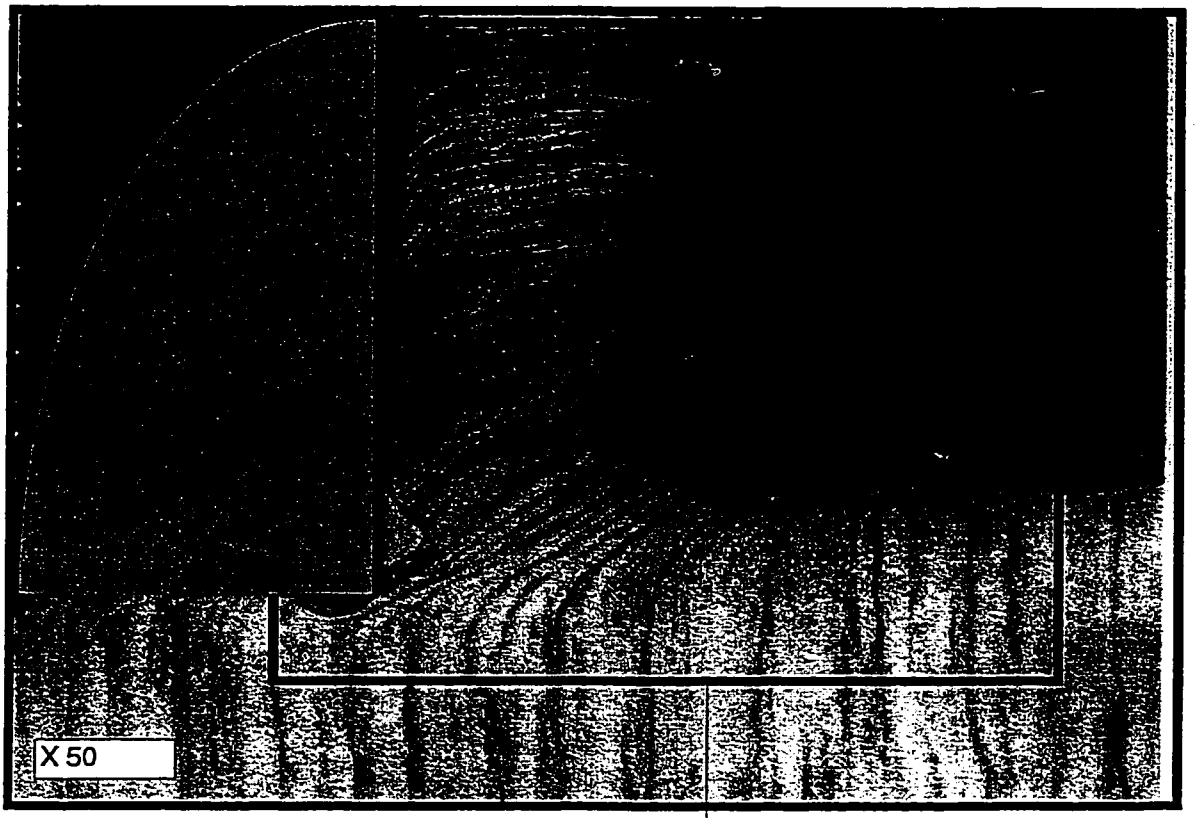

Figure 9.95: Microphotographs of partially formed chip (mag: 50X). Cutting condition: workpiece, AISI 4340; tool , BTAH 1" inch diameter; spindle rotational speed n, 1000rpm; feed t, 0.1 mm/rev; Etched with 10 mL Nital, 90 ml alcohol.

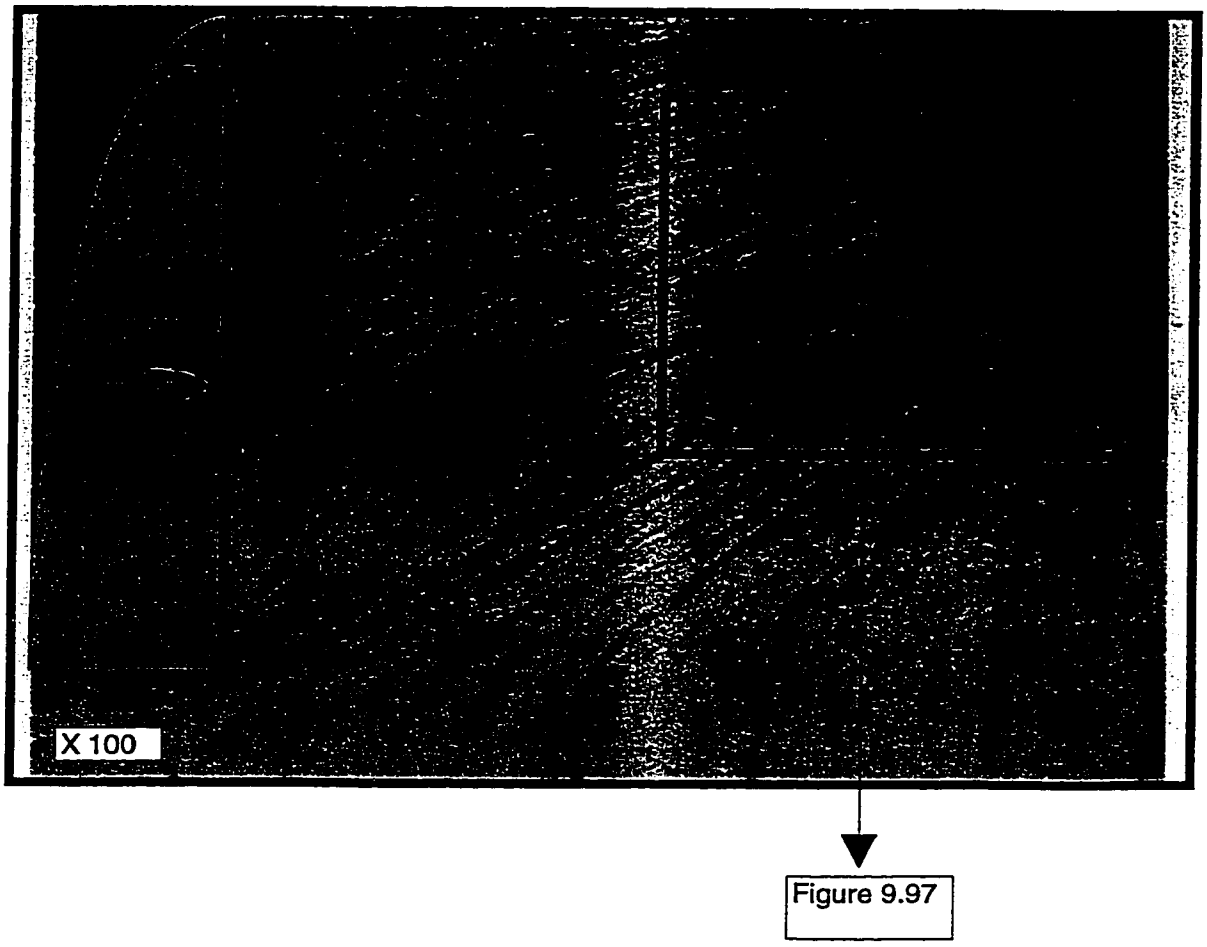

Figure 9.96: Microphotographs of partially formed chip (mag: 100X). Cutting condition: workpiece, AISI 4340; tool , BTAH 1" inch diameter; spindle rotational speed n, 1000rpm; feed t, 0.1 mm/rev; Etched with 10 mL Nital, 90 ml alcohol.

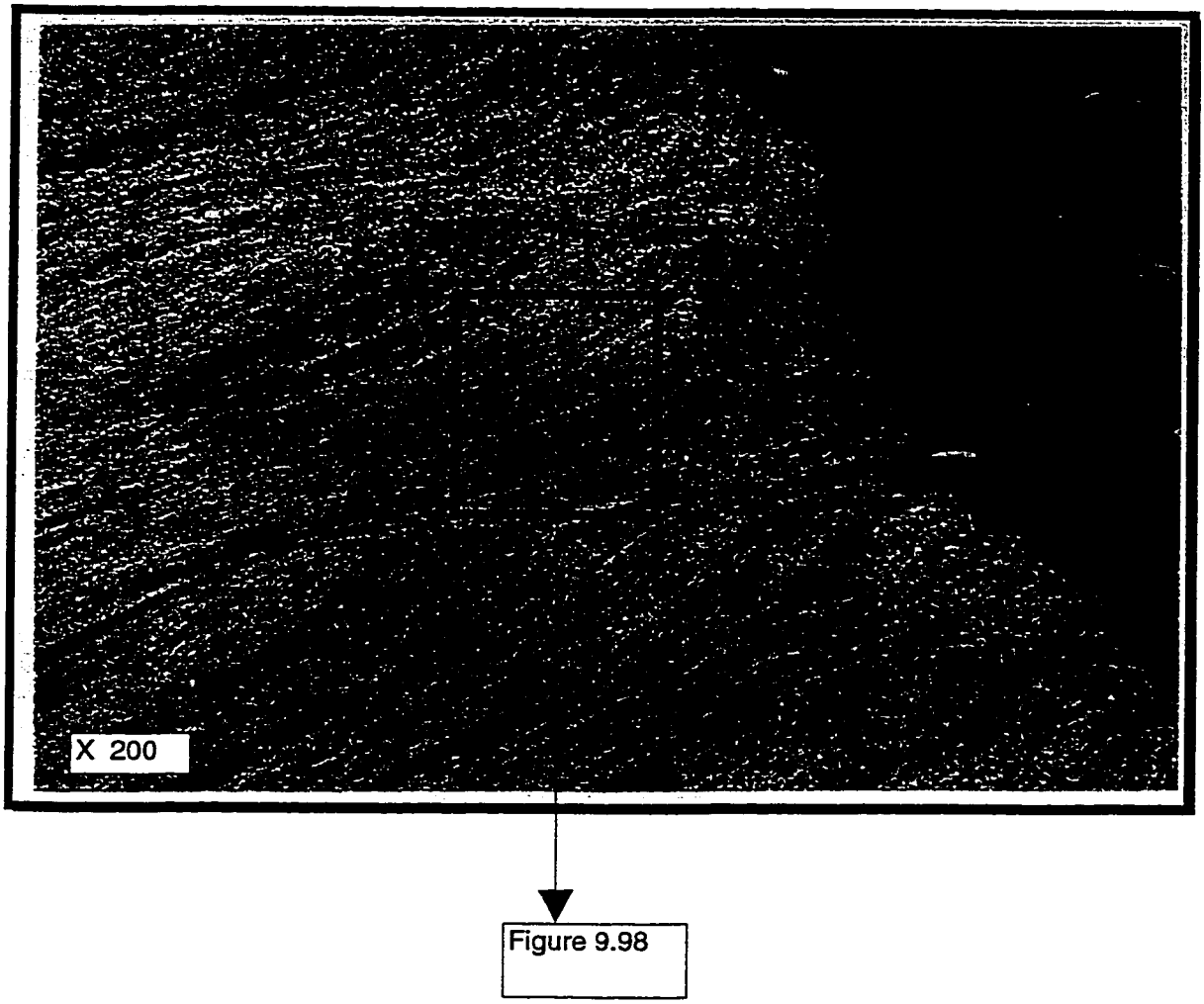

Figure 9.97: Microphotographs of partially formed chip (mag: 200X). Cutting condition: workpiece, AISI 4340; tool , BTAH 1" inch diameter; spindle rotational speed n, 1000rpm; feed t, 0.1 mm/rev; Etched with 10 mL Nital, 90 ml alcohol.

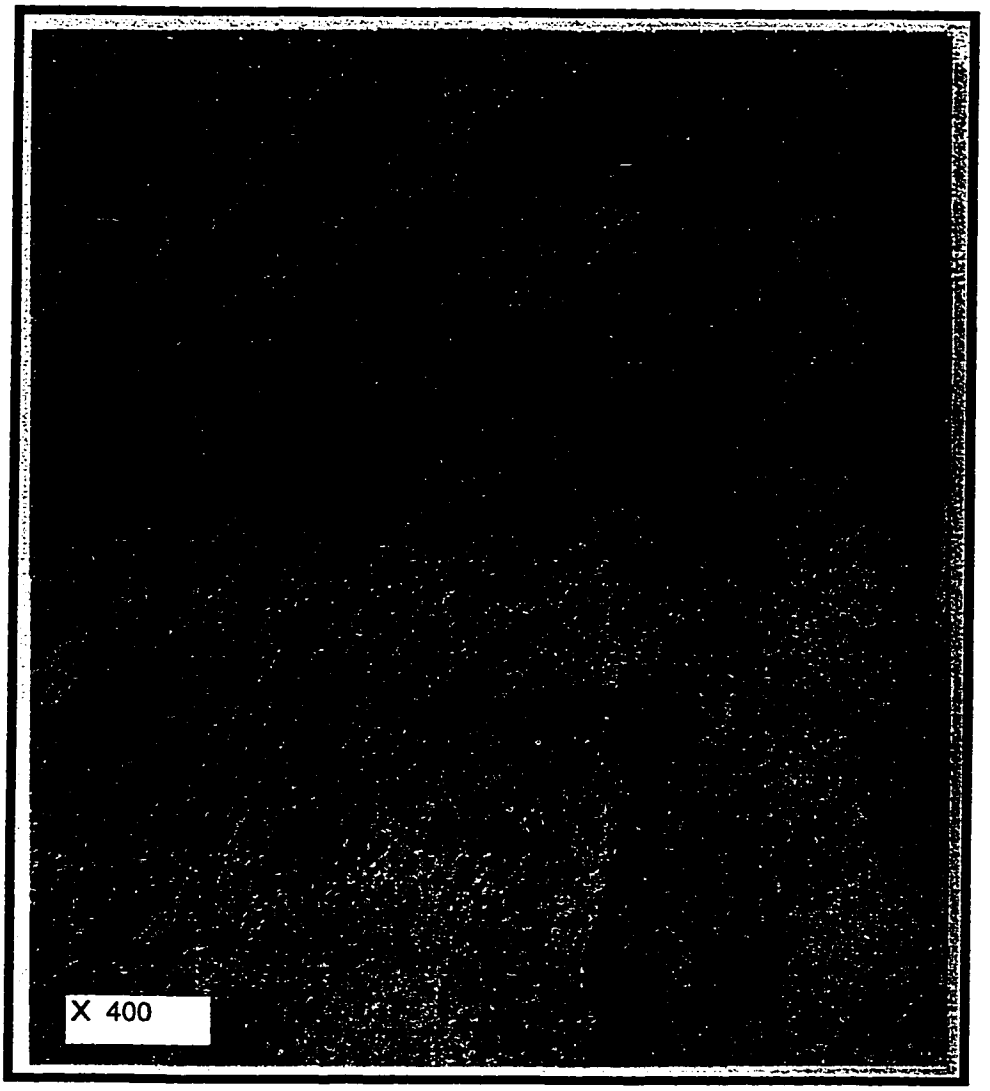

Figure 9.98: Microphotographs of partially formed chip (mag: 400X). Cutting condition: workpiece, AISI 4340; tool , BTAH 1" inch diameter; spindle rotational speed n, 1000rpm; feed t, 0.1 mm/rev; Etched with 10 mL Nital, 90 ml alcohol.

10

CONCLUSIONS AND RECOMMENDATIONS FOR FUTURE WORK

10.1 CONCLUSIONS

A new model of chip formation has been developed. This model is not limited by the most assumptions usually made to build the single shear plane, flow region and parallel sided shear zone models and in the same time capable of relating the cutting forces, tool-workpiece and temperature to the cutting speed, feed, tool geometry and properties of the workpiece material. The proposed model involves the formulation of the shear zone model with parallel boundaries. It has been defined by applying the mechanics of continuum to the analysis in

the chip formation zone. The analysis yields the following conclusions:

a. Two families of straight slip-lines constitute the deformation zone in metal cutting: one family is parallel and another is perpendicular to the straight upper boundary of the zone.

b. The well-known equation for the chip compression ratio is a form of the mass conservation principle.

c. As a results of the consideration of slip-line structure of the shear zone combined with the boundary conditions, a new feature of velocity diagram is constructed.

d. The discontinuity of the tangential velocity (the component of the cutting speed which is parallel to the boundary of the shear zone) during the transformation of a deformed fragment from the workpiece into the chip is attributed to the shear plane model phenomenon in the cutting process. In practice, the shear zone always has a certain width along which a continuous velocity is maintained. Therefore, the acceleration, strain and strain-rate in the shear zone with parallel boundaries are not uniformly distributed as thought before. The final true shear strain depends upon neither the zone's width, nor the power of non-uniform distribution of strain, but is entirely defined by the values of the discontinuity of the tangential and normal velocity components.

Thermomechanical model of the work-material resistance to cutting defines the ratio of the flow shear stress (in the shear zone and in the plastic zone along the tool rake face)

to the ultimate tensile stress as a linear function of cutting temperature. Based on this , a model for the cutting force components is proposed. To avoid the determination of the friction angle, the computation of the tangential force acting on the tool face is formulated.

The proposed model have been used to calculate the dynamic cutting forces in orthogonal cutting. The cutting system was modeled using a single degree-of freedom dynamic system where the variations of the cutting forces are represented by their total differentials. This study shows that the shear zone with parallel boundaries accommodates the dynamic variations in cutting conditions.

The analysis of the axial force and torque measurements reveals that the torque and axial force are stationary deterministic in nature.

This study shows that fluctuation of the cutting forces is a result of chip segmentation and not the cause of it. It also reveals the effect of material and cutting conditions on the cutting signatures that have never been considered as a factor in the previous studies of the cutting dynamics.

A new methodology has been established to align the machine such that the misalignment between the tool and the workpiece is minimized to make sure that the measured forces are not affected by this effect. A low cost laser-camera based system has been designed and build to achieve this goal.

The effect of misalignment on the cutting process has been investigated. The study shows that the misalignment affects the result dramatically. To test this effect on the forces measured, the cutting tool has been deliberately misaligned. The misalignment values have been measured using the laser-camera based system and the forces have been recorded using

using the FFT Analyzer. The study shows that increased the misalignment causes increase in the steady-state axial cutting force and cutting torque. The study also shows effect of misalignment on the axial dynamic cutting force and cutting torque; the misalignment effect shows up as a series of different amplitude harmonics.

The morphology study supports the theoretical finding of the parallel shear zone model with parallel boundaries. The study reveals that the shear zone is composed of two regions. The first region is termed as the "wide region" where the tangential velocity v_x changes at a small rate. The second region is termed as the "narrow region " where the tangential velocity v_x changes at a high rate.

10.2 RECOMMENDATIONS FOR FUTURE WORK

One may consider the present work as step toward a predictive theory of metal cutting. It is, therefore, reasonable to point out the issues that would be necessary to address to advance such a model and to further use it further as a powerful tool in the process planning practice. Here are the issues to focus on:

1. Exact deformation state causing chip formation is yet to be identified using the proposed velocity diagram through determining the state of stress in the deformation zone. As shown and discussed, the deformation zone is not simple shearing as it is believed. A good starting point might be to account for the bending moment in the deformation zone which in combination with the shear stress in the deformation zone causes chip formation (Astakhov, 1997b). The main question to answer is the ratio of bending and shear stress in the deformation zone that is sufficient to trigger

chip formation. If this ratio is a material constant then a novel approach to optimize the cutting process may be in sight.

2. Finite element analysis of the stress and strain distribution in the deformation zone could be conducted using the defined state of stress and deformation. As a result, the cutting forces may be determined for different cutting conditions. To accomplish the job, however, the thermomechanical behavior of workpiece material in cutting should be known.

3. To find the exact thermomechanical behavior of workpiece material in cutting, the physics of plastic deformation should by employed. The stress-strain conditions associated with cutting should be determined precisely.

4. Combining the known thermomechanical behavior of workpiece material in deformation with defined state of stress in the deformation zone, it might be possible to predict machinability of engineering material as the first stage. The further research would be toward improving machinability on the basis of the proper selection of process parameters which affect state of stress. By optimizing these parameters the minimum energy consumption and maximum process economy can be achieved.

5. The defined state of stress in the deformation zone might be considered as the first phase toward controllability of the cutting process. Since this state of stress can be altered by the process parameters and by the tool geometry two principal ways to improve the cutting process may be feasible. The first is to optimize the geometry of the cutting tool to achieve any desirable state of stress in the deformation zone in

order to cut a given material with minimum energy consumed. The second is to vary the process parameters over the machining cycle; it might be possible to maintain the desired state of stress in the machining zone over this cycle.

6. The defined state of stress in the deformation zone may be extended to define the state of stress in the partially formed chip. Having this state of stress defined, one might select a particular chipbreaker just to increase the chip bending in a particular direction to break the chip with minimum additional effort. Actually, the whole chip formation process might be designed to achieve this objective.

7. To achieve all these objectives, the following caution should be undertaken. The experimental results obtained by different research teams should be compatible. A special set of standards on the experimental methodologies used in metal cutting should be set through professional associations as ASME, CIRP, etc.

It seems, metal cutting is just at the beginning of its renaissance and its full capabilities are to be discovered.

REFERENCES

1. Adolfsson C. and Stahl J.E., 1995, "Cutting Force Model for Multi-Toothed Cutting Processes and Force Measuring Equipment for Face Milling," *Int. J. Mach. Tools Manufact.* Vol. 35, No. 12, p. 1715-1728.
2. Ahn, T. Y., Ehman, K. F. and Wu, M. S., 1985, "Cutting Dynamics Identification by Dynamic Data System, Modeling Approach," *ASME Journal of Engineering for Industry*, Vol. 107, p. 91-94.
3. Albrech P.t, 1962, *Trans. Am. Soc. Mech. Engrs* ,B 84, p. 405 .
4. Albrecht P., 1960a, "New Development in the Theory of the Metal Cutting Process: Part I.. The Ploughing Process in Metal Cutting," *ASME Journal of Engineering for Industry*, Vol. 83, p. 348.
5. Albrecht P., 1960b, "New Development in the Theory of the Metal Cutting Process: Part II. The Theory of Chip Formation," *ASME Journal of Engineering for Industry*, Vol. 83, p. 557.
6. American Society of Metals, 1979 , *Metals Handbook*, 9th Ed., Vol. 2,
7. Armarego, E. J. A., Jawahir, L. S., and Ostafiev, V. K., 1996, Working Paper, STC

'C', Working Group "Modeling of Machining Operations". CIRP, Paris, France.

8. Armarego, E. J., 1996," Predictive modeling of machine operations - a means of bridging the gap between theory and practice," *CSME Forum SCGM "Manufacturing Science and Engineering*," Hamilton , Canada, p. 18.
9. Armarege E. J. And Brown R. H., 1969, "The Machining of Metals, " Prentice Hall.
10. Astakhov, V.P., "System Approach in Metal Cutting," *Journal of Material Processing Technology,* to be published in 1998)
11. Astakhov, V. P., Shvets, S. V. and Osman, M. O. M., 1997a, " Chip structure classification based on mechanism of its formation, *J. of Materials Processing Technology*, 71, 247,
12. Astakhov, V. P., Shvets, S. V. and Osman, M. O. M., 1997b, " The Bending Moment as A cause of Chip Formation in Metal Cutting," *Proceedings ASME Symposium IMECE-97, 1977, November 16-21*, Dallas, Texas, USA.
13. Astakhov, V.P., and Osman, M.O.M., 1996, "An Analytical Evaluation of the Cutting Forces in Self-piloting Drilling Using the Model of Shear Zone with Parallel Boundaries. Part 1: Theory," *International Journal of Machine Tools & Manufacture*, Vol. 36, No. 11, p.1187-1200.
14. Astakhov V. P., 1994, "A Methodology for the Experimental Force Determination in Self-piloting Drilling," *Metallorezuchi Stanky*, (In Russian) Vol. 43, p. 40-49.
15. Astakhov V. P., 1983, "Method of Determination of the Chip Compression Ratio," *Patent No. 1004012 (USSR).*
16. Bagchi, A., 1983, "Technical Note on Wright's Paper : Predicting the Shear Plane Angle in Machining from Work Material Strain-hardening Characteristics," *ASME Journal of Engineering for Industry*, Vol. 105, p. 129-131.
17. Bendat, J.s., and Piersol, A.g., 1980, "Engineering Applications of Correlation and Spectral analysis," *John Wiley*, New York.
18. Bendat, J. S., and Piersol, A. G.,1971, "Random Data: Analysis and Measurement Procedures," *Wiley Inter Science.*
19. Bendat, J.S., and Piersol, A.G., 1966, "Measurement And Analysis Of Random

Data", *Wiley Inter Science.*

20. Bhattacharyya, A. and Ham I. , 1969, " Design of Cutting Tool Use of Metal Cutting Theory", *ASTM.*
21. Bobrov, V., 1984, "Metal Cutting", *Moscow: Mashinostrostroenie*, (In Russian).
22. Boothroyd, G., 1963, " Temperatures in Orthogonal Metal Cutting," *Proc. Inst. Mech. Eng.*, Vol. 177, p. 789-802.
23. Boothroyd, G. and Knight, W. A., 1989, " Fundamentals of Machining and Machine Tools, " *New York*
24. Bridgman, P. W., 1943 , "On Torsion Combined with Compression," *Journal of Applied Physics*, Vol. 14, p. 273.
25. Bridgman, P. W., 1937, Flow Phenomena in Heavily Stressed Metals, " *Journal of Applied Physics*, Vol. 8, p. 329.
26. Chandrashekhar, S., Osman, M.O.M., and Sankar, T.S., 1985, "An Experimental Investigation for the Stochastic Modeling of the Resultant Force System in BTA Deep-Hole machining," *International Journal of Production Research*, Vol.23, No. 4, 657-673.
27. Chandrashekhar, S., 1984, " An Analytical and Experimental stochastic modeling of the resultant force system in BTA Deep hole machining and its influences on the dynamic of machine tool workpiece system," *Concordia University*, Ph.D. thesis.
28. Childs, T.H., 1980,"Elastic Effects in Metal Cutting Chip Formation," *Int. J. Mech. Sci.*, Vol. 22, p. 457.
29. Das, K. and Tobias S. A., 1967, " The Relation Between The Static and the Dynamic Cutting of Metals," *Int. J. Mach. Tool Des. Res.*, Vol. 7, p. 63-89.
30. Das, S. A., 1965, Ph.d Thesis, *University of Birmingham.*
31. Del Taglia, A., and Tani, G., 1982, "A Method for Measuring Cutting Forces in Boring Operation", *Int. J. of Mac. Tool Des. Res.*, Vol. 22, No. 1, p. 23.
32. Devries M. F., 1970, "Review of Metal Cutting Theory," *Society of Manufacturing Engineer* Technical Paper Mr 70-142.
33. Dewhurst, P., 1978, "On the Non-uniqueness of the Machining Process," *Proc. R.*

Soc. London. A. 360, p. 587.

34. Dieter, G.e., 1986,"Mechanical Metallurgy,"3ed. Ed., Mcgraw-Hill Publishing Company, New York

35. Doyle, E. D., Horne, J. G. and Tabor, D., 1979," Frictional Interactions Between Chip and Rake Face in Continuous Chip Formation," *Proc. R. Soc.* , London, Vol. 366, p. 173.

36. Eggleston, D.M., Herzog, R. N. and Thomsen E.G., 1959," Observations on the Angle Relationships in Metal Cutting," *ASME Journal of Engineering for Industry*, Vol. 81, p. 263.

37. Elbestawi, M.A., Papazafiriou, T. A., and Du, R. X., 1991, "In-Process Monitoring of Tool Wear in Milling Using Cutting Force Signature," *Int. J. Mach. Tools Manufac.* Vol. 31, No. 1, p. 55-73.

38. El-Wardany, T.I., Gao, D, and Elbestawi, M.A., 1996, "Tool Condition Monitoring in Drilling Using Vibration Structure Analysis," *Int.J.Mach. Tools Manufact.* Vol. 36, No 6, 687-711.

39. Ernst H., 1951, "Fundamental Aspects of Metal Cutting and Cutting Fluid Action," *Annals of the New York Academy of Sciences*, Vol. 53, p. 936.

40. Ernst H. And Merchant M. E., 1941, "Chip Formation, Friction and High Quality Machined Surfaces, in the Surface Treatment of Metals," *American Society of Metals*, Vol. 29, p. 299.

41. Fenton, R. G. and Oxley, P. L., 1970,"Mechanics of Orthogonal Machining: Predicting Chip Geometry, Cutting Forces, Etc. from Work Material Properties and Cutting Conditions," *Proc. R. Soc.*, London, Vol. 184, p. 927.

42. Finnie I., 1956, "Review of the Metal Cutting Analyses of the past Hundred Years,"*Mech. Engineering.*, Vol. 78, No. 8, p. 715.

43. Frazao, J., Chandrashekhar, S., Osman, M.O.M., and Sankar T.S., 1986, "On the Design and Development of a New BTA Tool to Increase Productivity and Workpiece Accuracy in Deep Hole Machining," *The International Journal of Advanced Manufacturing Technology*, Vol. 1, No. 4, p.3-23.

44. Fredental, I. and Geiringer X., 1962, "Mathematical Theories of Inelastic Solids ". Moscow

45. Fujii, H. , Marui, E. and Ema, S., 1986a, "Whirling Vibration In Drilling. Part 1: Cause of Vibration And Role of Chisel Edge,"*ASME Journal of Engineering for Industry*., Vol. 108, P. 157-162.

46. Fujii, H. , Marui, E. and Ema, S. , 1986b," Whirling Vibration In Drilling Part 2: Influence of Drill,"*ASME Journal of Engineering for Industry*, Vol. 108, p. 157-162.

47. Gessesse, Y. B., "1990, Stability of BTA Deep Hole Machining Process," MASc Thesis, *Concordia University*, Montreal.

48. Goriani, V. I. and Kobayashi, S., 1967, "Strain and Strain-rate Distributions in Orthogonal Metal Cutting," *Annals of CIRP*, Vol. XV, p. 425.

49. Griffiths, B. J., 1982, " An Investigation into the Role of the Burnishing Pads in the Deep Hole Machining Process," *Ph.D. Thesis, Dept. of Production Technology*, Brunel University.

50. Griffiths, B. J., 1977,"An Introduction to Deep Hole Drilling and Boring," *Proceedings of the Second International Conference on Deep Hole Drilling and Boring, Burnel University*, Germany

51. Griffths, B.J., 1973, "The Measurement of Thrust and Torque in Deep-hole Boring", *Symposium Brunel University*, Germany.

52. Griffths, B.J., 1973, "The Machining Action During Deep-hole Boring and the Resultant Hole Force and Force System", *Proc. Second Int. Con. on Prod. Res.*.

53. Hayajneh M., Osman M. O. M. and Latinovic V. N., 1997a, "A Study of Wave-removing Cutting Process Using a Model of Shear Zone with Parallel Boundaries", *Proceedings ASME Symposium IMECE-97, 1977, November 16-21*, Dallas, Texas, USA.

54. Hayajneh M. T., Astakhov V.P., and Osman M.O.M., 1997b, "An Analytical Evaluation of the Cutting Forces in Orthogonal Cutting Using the dynamic Model of Shear Zone with Parallel Boundaries," *J. of Materials Processing Technology*, (in print, 1997) to be published in October 1998.

55. Hayajneh M. T., Astakhov V. and Osman M.O, 1996," A Novel Approach to the Mechanics of Chip Formation Using Shear Zone Model with Parallel Boundaries," *Proceedings CSME Forum SCGM 1996, 13th Symposium on Engineering Application of Mechanics Manufacturing Science and Engineering*, McMaster University, Canada.

56. Horne, J.G., Wright, P. K. and Bagchi, 1981, "A Study of Built-up-edge Formation Using Transparent Cutting Tools," *9th North American Research Conference Proceedings*, p. 223.

57. Hsu, T.C., 1966, "A Study of the Normal and Shear Stresses on a Cutting Tool," *ASME Journal of Engineering for Industry*, Vol. 88, p. 51.

58. Huang, H., Went, C. and Chen, C., 1994," Prediction of Thrust and Torque for Multifaced Drills ," *ASME Journal of Engineering for Industry*, Vol. 116, p. 1-7.

59. Jawahir, I. S. and van Luttervelt, C. A., 1993,"Recent developments in chip control research and applications," *CIRP Annals,* Vol. 42, p. 659

60. Johnson, W., Sowerby, R. and Venter, R. D., 1982, "Plane-strain Slip-line Fields for Metal-Deformation Process", *Pergamon*, Oxford.

61. Kececloglu D., 1960, "Shear-zone Size, Compressive Stress, and Shear Strain in Metal Cutting and Their Effect on Mean Shear-flow Stress," *ASME Journal of Engineering for Industry*, Vol. 82, p. 79-86.

62. Kececioglu, D., 1958, "Shear-Zone Temperature in Metal Cutting and its Effect on Shear Flow Stress," *Transactions of ASME, Series B, Journal of Engineering for Industry*, Vol. 80, p. 541-546.

63. Klamecki B. E. and Kim S., 1988, "On the Plane Stress to the Plane Strain Transition Across the Shear Zone in the Metal Cutting ," *ASME Journal of Engineering for Industry* , Vol. 104, p. 322-325.

64. Kistler, Piezo-instrumentation Kistler, "2-component Load Washer (Fz, Mz) Type 9065," *Nr. 6.9065 de.*

65. Kobayshi M. And Kawata K. ,1967,"Effects Of The Curvature Of Work Surface On Metal Cutting," *Annals Of The CIRP,* Vol. XV, p. 393-403

66. Kobayashi S. And Shabaik A., 1964, "Chip Formation With Varying Under Chip Thickness At Very Slow Speed," *ASME Journal Of Engineering For Industry*, p.389-394.

67. Kobayashi, S., Herzog, R. B., Eggieston, D. M. and Thomsen, E. G., 1960, "A Critical Comparison of Metal Cutting Theories with New-experimental Data," *ASME Journal of Engineering for Industry*, Vol. 82, p. 337

68. Kobayashi, S. and Thomsen, E., 1959, "Some Observations of the Shearing Process in Metal Cutting," *Trans. Amer. Soc. Mech. Engineering., Series B, Journal of Engineering for Industry*, Vol. 81, p. 251.

69. Kudo, H., 1965, "Some New Slip-line Solutions for Two-dimensional Steady-state Machining," *Int. J. Mech. Sci.*, p. 43.

70. Kushner, V. S. , 1982, "Thermomechanical Approach in Metal Cutting," Irkutsk University Pabl. Ltd, (In Russian).

71. Kufarev G., 1970, " Chip Formation and High Quality Machined Surfaces under Conditions of Oblique ", (In Russian) Frunz: Mechtep.

72. Latinovic V. , 1978," An Investigation of the Theoretical and Design Aspects of Unsymmetrical Multi-Cutting Action in Deep-Hole Machining," Ph.D. thesis, Concordia University, Montreal.

73. Lee, L.C., Lee, K.S., and Gan, C.S., 1989, "On the Correlation Between Dynamic Cutting Force and Tool Wear," *Int. J. Mach. Tools Manufact.*, Vol. 29, No. 3, p. 295-303.

74. Lee E. H., and Shaffer B. W., 1951, "the Theory of Plasticity Applied to the Problem of Machining," *Trans ASME Journal of Applied Mechanics*, Vol. 18,, p. 405-413.

75. Lee S.J. and Kapoor S.G., 1986, "Cutting Process Dynamics Simulation for Machine Tool Structure Design,"*ASME Journal of Engineering for Industry*, Vol. 108, p. 68-74.

76. Liu, C.R. and Barash, M.M., 1976, "The Mechanical State of the Sublayer of a Surface Generated by Chip Removal Process, Part 1: Cutting with a Sharp Tool," *ASME Journal of Engineering for Industry*, Vol. 98, P. 1192.

77. Manyindo B. and Oxley P. L. , 1986," Modeling the Catastrophic Shear Type of Chip when Machining Stainless Steel," Proceedings Inst. Mech. Eng., Vol. 200, p. 349-358.

78. Marui, E. , Kato, S., Hashimoto, M. and Yamada, T., 1988a, "The Mechanism Of Chatter Vibration System: Dynamic Vibration In A Spindle-workpiece Part 1– properties Of Self-excited Chatter Vibration In Spindle-working System," *ASME Journal of Engineering for Industry*, Vol. 110, p. 236-242.

79. Marui, E., Kato, S., Hashimoto, M, and Yamada, T., 1988b, "The Mechanism of Chatter Vibration in a Spindle-Workpiece System: Part 2-Characteristics of Dynamic Cutting Force and Vibration Energy,"*ASME Journal of Engineering for Industry*, Vol. 110, p. 242-247.

80. Marui, E. , Kato, S., Hashimoto, M. and Yamada, T., 1988c, "The Mechanism Of Chatter Vibration System: Dynamic Vibration In A Spindle-workpiece Part 3– analytical Considerations," *ASME Journal of Engineering for Industry*, Vol. 110, p. 242-247.

81. Merchant M. E., 1945, " Mechanics of the Metal Cutting Process. I. Orthogonal Cutting and a Type Chip; Plasticity Conditions in Orthogonal Cutting,' *Journal of Applied Physics*, Vol. 16, p. 267, and p. 318-324.

82. Merchant M. E., 1944, "Basic Mechanics of Cutting Process," *Journal of Applied Physics*, Vol. 11, p. 168-175.

83. Nakayama K. and Tamra K., 1964, " Hardness Test of Chip," Bulletin of the Faculty of Eng., Yokohama National Unversity, Japan, Vol. 13, p.17.

84. Nigm M. M. and Sadek M. M., 1977,"Experimental Investigation of the Characteristics of Dynamic Cutting Process,"*ASME Journal of Engineering for Industry*, p. 410-418.

85. Nigm M. M.,Sadek M. M. And Tobias S. A., 1977a, "Dimensional Analysis of the Steady State Orthogonal Cutting Process," *Int. J. Mach. Tool Des. Res.*, Vol. 17, p. 1-18.

86. Nigm M. M. , Sadek M. M. And. Tobias S. A, 1977b, "Determination Of Dynamic

Cutting Coefficients From Steady State Cutting Data," *Int. J. Mach. Tool Des. Res.*, Vol. 17, p. 19-37.

87. Okushima, K., and Hitomi, K., 1961, "An Analysis of the Mechanism of Orthogonal Cutting and its Application to Discontinuous Chip Formation, "*ASME Journal of Engineering for Industry*, p. 545-556.

88. Osman, M.O.M., and Sankar, T.S., 1972, "Short-time Acceptance Test for Machine Tools Based on the Random Nature of the Cutting Forces",*ASME Journal of Engineering for Industry*, Vol. 94, No. 4, P.1020.

89. Osman, M.O. Sankar, T.S. and G.D. Xistris, 1974, "Measurement and Analysis of Random Cutting Forces in Single Point Machining" Presented in the 20th International Instrumentation Symposium, May 21-23, 1974 , Albequerque, New Mwxico, ISA, 1974 p. 259-264.

90. Oxley P. L. and Welsh M. J., 1963 " Calculation the Shear Angle in Orthogonal Metal Cutting from Fundamental Stress, Strain, Strain-Rate Properties of the Work Material," Proceeding 4th International Machine Tool design and Research Conference, Pergaman, Oxford, p. 73-86.

91. Oxley P. L., 1989, "Mechanics of Machining - An analytical Approach to Assessing Machinability", *John Wiley & Sons*, New York.

92. Poletica M., 1976, "Contact Loads along the Cutting Surfaces of Tools," *Moscow:mashinostrostroenie*, (In Russian)

93. Palmer, W.b. and Oxley, P.L., 1959, "Mechanics of Orthogonal Machining," *Proc. Instr. Mech. Engrs.*,Vol. 173, P. 623.

94. Peters, J.,1976, "Dynamic Analysis Of Machine Tools Using Complex Modal Methol", *Annals CIRP*, Vo.. 25, No. 1, p. 257.

95. Pfleghar, F., 1977, "Guidelines for Deep Hole Tool Design," *WT Zeitschrift fuer Industrielle Fertigung*, 67, p. 211-218, (in German).

96. Pugh, H. D., 1958,"Mechanics of Cutting Process," *Proc. Ime Conf. Tech. Eng. Manufacture*, London, P. 237.

97. Randall, R. B., 1987, " Frequency Analysis ," K. Larsen & Son, Clostrup, Denmark.

98. Rostoker, W. and Dvorak, J. R,1977, "Interpretation of Metallographic Structures," *2nd. Ed., Academic Press*, New York.

99. Rubenstein C. , 1972, "An Analysis Of Dynamic Cutting When A Plane Surface :Is Cut With An Oscillating Tool -I: General Equations," *Int. J. Mach. Tool Des. Res.*, Vol. 12, p. 179-191.

100. Rubenstein C. , 1972, "An Analysis of Dynamic Cutting when A Plane Surface :is Cut With An Oscillating Tool," *Int. J. Mach. Tool Des. Res.*, Vol. 12, p. 249.

101. Ramalingam S., Desai P. V. and Kim K., 1981, 1981, "On the Determination of the Domain of Plasticity Associated with a Plastic Free Boundary and its Application to the Machining Problem," *9th North American Research Conference Proceedings*, p. 334.

102. Roth, R.N., and Oxley P.L., 1972, "Slip-line Analysis for Orthogonal Machining Based upon Experimental Flow Fields," *J. Mech. Engr. Sci.*, Vol. 14, p. 85 .

103. Rozenberg, A., 1956, " Elements of Metal Cutting Process", (In Russian) *Mashgiz-Moscow.*

104. Sakuma, K., Taguchi, K., and Katsuki, A.,1981, "Self Guiding Action Of Deep-hole Drilling Tools", *Annals CIRP,* Vol. 30, No. 1, p. 311

105. Sakuma, K., Taguchi, K., And Katsuki, A., 1980a, "Study On Deep-hole Drilling With Solid Boring Tool The Burnishing Action of Guide Pads and Their Influence On Hole Accuracies", *Bull. Of The JSME*, Vol. 23, No. 185, p. 121.

106. Sakuma, K., Taguchi, K., And Katsuki, A., 1980b, "Study On Deep-hole Boring By A Bta System Solid Boring Tool-behaviour of Tool and Its Effects On The Profile of The Machined Hole", *Bull. of The Jspe*, Vol. 14, No. 3, p. 143.

107. Sankar, T.S., and Osman, M.O., 1975, "Profile Characterization Of Manufactured Surfaces Using Random Function Excursion Technique Part I: Theory,"*ASME Journal of Engineering for Industry.*, Vol. 97, p. 190.

108. Scrutton, R., 1968, "The Geometry of the Shear Zone in Metal Cutting," *ASME Journal of Engineering for Industry*, p. 420-424.

109. Shaw, M. C., 1984," Metal Cutting Principles, "Clarendon Press, Oxford,.

110. Shaw, M. C. and Finnie I., 1955, "The Shear Stress in Metal Cutting," *ASME*, Vol. 77, P. 115-125.

111. Song, X., 1995, "Strain-Hardening and Thermal-Softening Effects on Shear Angle Prediction: New Model Development and Validation,"*ASME Journal of Engineering for Industry*, Vol. 117, p.28-32.

112. Stevenson R. and Stephenson D.A., 1995, "The Mechanical Behaviour of Zinc During Machining," *ASME Journal of Engineering for Industry*, Vol. 117, p. 172-178.

113. Strenkowski, J.S. and Moon, K.J., 1990, "Finite Element Prediction of Chip Geometry and Tool/Workpiece Temperatures Distributions in Orthogonal Metal Cutting," *ASME Journal of Engineering for Industry*, Vol. 112, p. 313-318.

114. Sun, P., Chang, Y.K., Wang, T.C., and Lui, P.t.,1982 "A Simple and Practical Piezo-electric Shank Type Dynamometer", *Int. J. of Mach. Tool Des. Res.*, Vol. 22, No. 2, p. 111.

115. Spaans C., 1972, " A Treatise on the Streamlines and the Stress, Strain Rate Distributions, and on Stability in the Primary Shear Zone in Metal Cutting ", *ASME Journal of Engineering for Industry*, 94, p. 690-696.

116. Steed W. E. , 1987 ,"Chip Removal Simulation to Predict Part Error and Vibration," *Proc. ASME Conf. Computers in Engineering*, Vol. II, p. 447-455.

117. Stephenson, D.A. and Agapionu, J.S. ,1997, "Metal Cutting Theory and Practice,"*Marcel Dekker, Inc.*, Ney York.

118. Stevenson,. M. G. and Oxley, P. L., 1969-1970, '' An Experimental Investigation of the Influence of Speed and Scale on the Strain-rate in a Zone of Intense Plastic Deformation,'' *Proc. Inst. Mech. Engineering*, Vol.184, P. 561-576.

119. The, J., 1975, "The Quadratic Curve and the Trajectory in the Shear Zone in Metal Cutting," *ASME Journal of Engineering for Industry.*, p.1105-1111.

120. Thangaraj, A. And Wright, P.K., 1988, "Computer-assisted Prediction of Drill-failure Using In-process Measurements of Thrust Force," *ASME Journal of Engineering for Industry*, Vol. 110, p.192-200.

121. Thomsen, E.g.,1966, "Applications of the Mechanics of Plastic Deformation to Metal Cutting," *Annals of the CIRP.*, Vol. XIV, p. 113.

122. Trent, E., 1991, "Metal Cutting," *Butterworth-* Heinemann.

123. Usui, E. and Hoshi K., 1963,"Slip-line Field in Metal Machining Which Involve Centered Fans," *Internation Production Engineering Research Conference Proceedings*, (Pittsburgh), p. 61.

124. Wright P. K. ,1982, "Prediction the Shear Plane Angle in Machining from Work Material Strain-hardening Characteristics," *ASME Journal of Engineering for Industry*, Vol. 104, p. 285-292.

125. Wright P.k., Bagchi A. and Chow J. G., 1982,"Influence of Friction on the Shear Plane Angie in Machining," *10th North American Research Conference Proceedings*, p. 255.

126. Wright, P.K.,1981, "Frictional Interactions in Machining: Comparisons Between Transparent Sapphire and Steel Cutting Tools," *Metals Technology*, Vol. 8, p. 150.

127. Wu D. W., 1989, "A New Approach of Formulating the Transfer Function for the Dynamic Cutting Processes," *ASME Journal of Engineering for Industry*, Vol. 111, p. 37-47.

128. Wu, D. W., 1988, "Comprehensive Dynamic Cutting Force Model and its Application to Wave-removing Processes," *ASME Journal of Engineering for Industry*, Vol. 110, p. 153-161.

129. Wu, D. W., 1986, "Governing Equations of The Shear Angle Oscillation In Dynamic Orthogonal Cutting,"*ASME Journal of Engineering for Industry* ,Vol. 108,, p. 280-287.

130. Wu, D. W and. Liu, C. R., 1985a, "An Analytical Model Of Cutting Dynamics Part 1: Model Building," *ASME Journal of Engineering for Industry* , Vol. 107, p. 107-111.

131. Wu, D. W and. Liu, C. R. ,1985b, "An Analytical Model of Cutting Dynamics Part 2 : Verification ," *ASME Journal of Engineering for Industry*, Vol. 107, p. 107-111.

132. Yamamoto, A., Nakamura S., Toyama K. and Kawamura I, 1979, "Proposal of

Stresses Distribution Models on Rake Surface in Orthogonal Cutting,"*J. of Precision Engr.*, Vol 45, p. 90.

133. Zhang G.M. and Kapoor S.G., 1987, "Dynamic Modeling and Analysis of the Boring Machine System,"*ASME Journal of Engineering for Industry*, Vol. 109, p. 219-226

134. Zorev N. N., 1966, " Metal Cutting Mechanics," Pergamon.